

IMPACT OF CLIMATE AND CATCHMENT DYNAMICS ON RUNOFF GENERATION

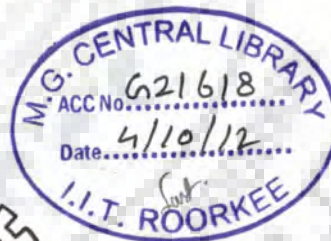
A THESIS

*Submitted in partial fulfilment of the
requirements for the award of the degree*

of
DOCTOR OF PHILOSOPHY
in
HYDROLOGY

by

NEGASH WAGESHO AMENCHO



DEPARTMENT OF HYDROLOGY
INDIAN INSTITUTE OF TECHNOLOGY ROORKEE
ROORKEE-247 667 (INDIA)

JUNE, 2012

©INDIAN INSTITUTE OF TECHNOLOGY ROORKEE, ROORKEE-2012
ALL RIGHTS RESERVED



INDIAN INSTITUTE OF TECHNOLOGY ROORKEE ROORKEE

CANDIDATE'S DECLARATION

I hereby certify that the work which is being presented in the thesis entitled **"IMPACT OF CLIMATE AND CATCHMENT DYNAMICS ON RUNOFF GENERATION"** in partial fulfilment of the requirements for the award of the degree of **DOCTOR OF PHILOSOPHY** and submitted in the Department of Hydrology, Indian Institute of Technology Roorkee, Roorkee, is an authentic record of my own work carried out during a period from July, 2009 to June, 2012 under the supervision of **Dr. M. K. Jain**, Assistant Professor and **Dr. N. K. Goel**, Professor, Department of Hydrology, Indian Institute of Technology Roorkee, Roorkee.

The matter presented in this Thesis has not been submitted by me for the award of any other degree of this or any other Institute.

(Negash Wagesho Amencho)

This is to certify that the above statement made by the candidate is correct to the best of our knowledge.

(N. K. GOEL)
Supervisor

(M. K. JAIN)
Supervisor

Date: June 7, 2012

The Ph.D. Viva-Voce Examination of **Mr. Negash Wagesho Amencho**, Research Scholar, has been held on June 28, 2012.....

Signature of Supervisors
Signature of Chairman SRC
Signature of External Examiner
Head of the Deptt./Chairman ODC
28/6/12

The Sub-Saharan region of Africa has been challenged by natural and man-made stresses extending from flood and prolonged drought to poor economic and institutional developments. Ethiopia, situated in the horn of Africa and its economy dominantly based on agriculture, is becoming a victim of such global challenges. The Rift Valley lakes and rivers system of Ethiopia has undergone major changes in recent past. Agricultural, water supply, and hydropower sectors are affected by variable climate patterns. The impact of changing climate condition is more profound in semi-arid regions of Rift Valley lakes basin where competition for water is immense. Quantitative assessment of the impacts of climate and catchment dynamics on runoff generation in the basin is vital.

In the present study, an attempt has been made to explore the impact of climate change and catchment dynamics on runoff generation in the Rift Valley lakes basin of Ethiopia. The broad objectives of the present study are:

- i. Investigation of the spatial and temporal variability of annual and seasonal rainfall over Ethiopia,
- ii. Identification of non-stationarity and reasons of non-stationarity in hydro-climatic datasets in the Rift Valley lakes basin of Ethiopia using short and long-term time dependence analysis,
- iii. Assessment of the impacts of topographic, weather and catchment input parameters on runoff generation using Soil and Water Assessment Tool,
- iv. Analysis of the impacts of climate change on runoff generation using coupled atmospheric-ocean Global Climate Model (GCM) outputs for current and future climatic conditions under varied greenhouse gas emission scenarios,
- v. Evaluation of the impacts of temporal land use/land cover dynamics on runoff generation using distributed hydrologic model.

Spatial and temporal rainfall variability analysis covers entire Ethiopia whereas investigation of non-stationarity in hydroclimatic variables is confined to Rift Valley lakes basin of Ethiopia. Assessment of the impacts of catchment and weather input parameters, GCM outputs under varied greenhouse gas emission scenario and land use dynamics on runoff generation are limited to Bilate (5330 km²) and Hare (166.5 km²) watersheds. Specific

methodologies applied to achieve the intended objectives and major findings from the analysis are summarized as follows.

Spatial and temporal variability of annual and seasonal rainfall over Ethiopia

Monthly gridded rainfall data of 50 years (1951-2000) at 0.5° latitude x 0.5° longitude resolution covering entire Ethiopia was acquired from Global Precipitation and Climate Center (GPCC) and its validity for subsequent analysis is examined against nearby observed series. Trends in seasonal, annual and maximum 30-days extreme rainfall over Ethiopia are investigated using Mann-Kendall and Theil-Sen's slope estimator approaches. Spatial coherence of annual rainfall among contiguous rainfall grid points is examined for possible spatial similarity across the country applying Moran's spatial autocorrelation model. The association of Atlantic Multidecadal Oscillation index over Ethiopian rainfall pattern is also explored through statistical analysis.

The main summer season and annual rainfall exhibit significant decreasing trend in northern, north-western and western part of Ethiopia. In most other parts of the country (approximately 77% of geographical coverage), the annual rainfall series remained without significant trend for the second half of 20th century. Based on the Moran's spatial analysis, annual rainfall for the total sampling points (381 grid stations) is divided into four zones of annual rainfall spatial similarity. Regions with high annual and seasonal rainfall distribution exhibit high indices of temporal (r_1 and r_2) and spatial (Moran index) autocorrelation coefficients. Atlantic Multidecadal Oscillation and annual rainfall indices over the last half century reveal modestly good correlation in the northern region whereas the association is weakly developed in other parts of the country.

Investigation of non-stationarity in hydroclimatic variables

Statistical analysis of short and long-term persistence in hydro-climatic variables such as rainfall, stream flow and lake level to detect possible time-trends over the historical period is undertaken. Mann-Kendall trend detection method, Theil and Sen's slope estimator, Hurst's coefficient, Spectral and Wavelet analysis approaches are applied to identify trends and periodic signals in hydro-climatic variables. Temporal land use/cover information and nearby Indian Ocean SST anomalies are further examined to study their association to hydro-climatic fluctuations.

Despite less statistically significant trend in seasonal and annual rainfall events and number of rainy days within the catchment, streamflow and lake level have showed significant increasing trend for more than 75 percent of events investigated. This observed non-stationarity is variable across hydro-climatic elements that could likely be attributed to the combined effect of global climatic variability on local climate and altered catchment condition over the years. The estimated Hurst's coefficient (H) is greater than 0.5 for all events of streamflow and lake level, which suggests a likely evidence of long term persistence in hydrologic variables.

The deterministic cyclic components of streamflow are legitimately represented as discrete finite Fourier series. The variance explained by the first two harmonics exceeds 96 percent in most cases and the monthly flows are approximated by the first two harmonics. Trend analysis carried out on various model combinations of discrete wavelet decomposed signals detected the prevailing trends in hydrologic variables efficiently. The average stations total rainfall is better correlated to summer season (June-September) SST whereas the association becomes weak for annual average SST.

Impact of terrain, weather and catchment input parameters on runoff generation

The impact of terrain, weather and catchment input parameters on runoff is assessed using process oriented Soil and Water Assessment Tool. The limitations of 30m resolution Advanced Spaceborne Thermal Emission and Reflection Radiometer (ASTER) and 90m resolution Shuttle Radar Topography Mission (SRTM) DEM in watershed delineation are explored. Sensitivity of catchment input parameters while simulating runoff at Bilate and Hare watersheds is investigated and the most sensitive parameters are identified.

Contrary to 90m SRTM DEM, the 30m ASTER DEM resulted in spurious flow accumulation path that subsequently reduced the watershed area by 29% and affected other basin parameters at Hare watershed. Soil and Water Assessment Tool effectively captured the underlying hydrologic processes while simulating runoff at both watersheds. The simulated annual water yield is within $\pm 3.4\%$ error to the observed series. Initial curve number for average soil moisture condition, deep aquifer fraction, minimum water depth in the shallow aquifer for flow and available soil water holding capacity parameters are found to either attenuate or accentuate the resulting runoff more significantly than other parameters in the watersheds.

Simulating present and future runoff using Global Climate Model outputs

The impact of large-scale atmospheric-ocean variables on local-scale hydrology is investigated through Global Climate Model (GCM) outputs under different greenhouse gas emission scenarios. Downscaled and subsequently bias corrected GCM outputs are applied to simulate present and future runoff at Bilate and Hare watersheds of Rift Valley lakes basin of Ethiopia. Future implications of extreme precipitation and runoff events are discussed from GCMs outputs for varied greenhouse gas emission scenarios.

Large-scale GCM outputs are obtained from BCCR-BCM2.0 of Norway and CSIRO MK3.0 of Australia GCMs and subsequently reduced to local-scale weather variables (temperature and precipitation) using station weather data. Since GCMs are operating at coarser scales, the statistical downscaling model (SDSM) is employed to reduce large-scale atmospheric variables to local level weather condition. The statistical downscaling model, followed by bias correction, effectively reproduced the current climate (1990-1999) weather variables. Statistically downscaled and subsequently bias corrected daily temperature and precipitation variables are used to simulate runoff for present and two future (A1B and A2) greenhouse gas emission scenarios at Bilate and Hare watersheds. Simulated future runoff events are characterized by increased extreme events that ultimately resulted in increase in the gross annual runoff volume from the watersheds. The simulated runoff varies from -4% to 18 % at Hare watershed and is within the range of -4 % and 14 % at Bilate watershed. Simulated average annual water yield shows slight variation between GCMs. It lies within ± 10 % at Bilate basin and ranges from -17% to 12% at Hare basin. Future water resources planning and management could likely be affected by such variability and hence existing design methods could expand their scope to account for these extreme events.

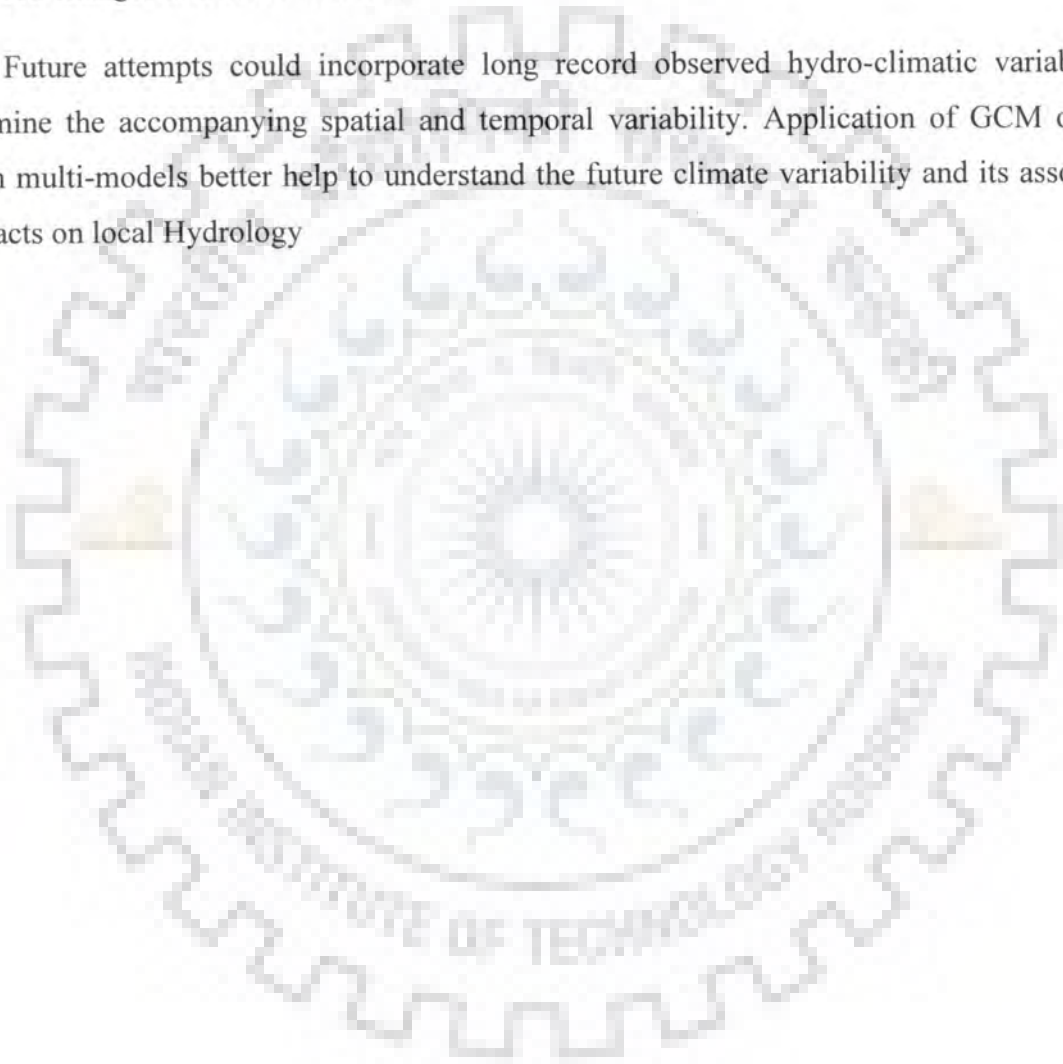
Impact of temporal land use/land cover dynamics on runoff generation

Temporally varying (1976/1986/2000) Satellite image acquired from landsat satellite system is processed and land use/cover classes are identified. Runoff is generated using SWAT model for temporally varying land use /land cover conditions and the ensuing results of land use dynamics on runoff is discussed. Statistical trend test is also applied to detect the unexplained natural climate variability.

Joint analysis of watershed modeling for temporally varying land use/land cover condition and statistical time-trend analysis of streamflow is undertaken to explore the

impact of altered land use/land cover condition on runoff generation at two watersheds. The method detected the underlying variability efficiently. The percentage of forest cover declined substantially at Bilate and Hare watersheds during 1976/2000 analysis period. The simulated surface runoff component increases progressively since 1970s. Percentage annual surface runoff varies from 10 to 23% at Bilate and 16% to over twofold at Hare watersheds. The increasing trend of observed daily maximum flow at Alaba Kulito and slightly raised slope of rainfall-runoff double mass curve since 1992 supports the attribution of climate induced changes at Bilate catchment.

Future attempts could incorporate long record observed hydro-climatic variables to examine the accompanying spatial and temporal variability. Application of GCM outputs from multi-models better help to understand the future climate variability and its associated impacts on local Hydrology



ACKNOWLEDGEMENTS

At the outset, I would like to express my profound sense of gratitude and indebtedness to my academic supervisors Dr. N. K. Goel, Professor, and Dr. M. K. Jain, Assistant Professor, Dept. of Hydrology, IIT Roorkee, for their meticulous guidance, invaluable suggestions and constant encouragement throughout the course of the present study that helped me gain fundamental knowledge and strengthened my research methodology. I have been deeply influenced by their resounding insight, novel teaching ability and a caring and humane personality. I enjoyed the great academic freedom they have offered to me to pursue independent work.

I take this opportunity to thank the Ministry of Education of the Federal Democratic Republic of Ethiopia for granting me financial assistance to pursue my Ph.D. study through my parent Institute, Arba Minch University. Institutions and organizations (Ministry of Water Resources, National Meteorological Service Agency, Ministry of Agriculture of Ethiopia and the Regional Meteorological Agency, SNNPR, Hawassa) cooperated while accessing valuable data for present study are highly acknowledged. My sincere thanks are due to Dr. Tarekegn Tadesse, the Former President and Dr. Yosef Birru, President, Arba Minch University for their useful arrangements and supports to spare my field duty during data collection.

All the needful services offered to me from Dept. of Hydrology during my study period are highly acknowledged. Besides my research study, I have got a wide range of exposure to involve myself in multidisciplinary projects and short courses both as project team member and course assistant. The financial support, as project assistantship, obtained from Dept. of Hydrology through Professor N. K. Goel during this period is worth mentioning.

I would like to express my gratitude to Dr. M. Perumal, Professor and Head, Dept. of Hydrology, Dr. B. S. Mathur, Former Professor, Dr. Himanshu Joshi, Dr. D. K. Srivastava, Dr. D. C. Singhal, Dr. Ranvir Singh and Dr. D. S. Arya, Faculty members of Dept. of Hydrology.

It is my great pleasure to acknowledge the unreserved academic support obtained from Dr. Manohar Arora, Scientist, National Institute of Hydrology, Roorkee.

I am also thankful to all supporting staff members of Dept. of Hydrology, for their valuable supports during the course of my study. My warm thanks are due to Ms. Asmita, Research Scholar, Mr. Neeraj Sharma, Ms. Khushbu, Ms. Priya, Project Assistants and Mr. Bhanesh, Laboratory Assistant, Dept. of Hydrology for their valuable supports in many ways and welcoming gesture throughout. I am very much grateful to all research scholars and graduate students of Dept. of Hydrology for their encouragement and companionship during my research study period and stay at Roorkee.

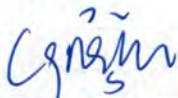
It gives me an immense pleasure to thank all Ethiopian and foreign students residing at Khosla International House, IIT Roorkee, with whom I have savoured the very delightful moments and tasted the bitterness of life as well. My thanks also go to residents and staff members of Khosla International House for their uninterrupted services.

There are many friends and people whom have been constantly encouraging me during the last couples of years. It is highly gratifying to thank them all at this juncture. My warm thanks are due to my colleagues Mr. Samuel Dagalo and Mr. Teferi Labisso of Arba Minch University for their keen interest in bearing very great responsibility on my behalf. The support and services provided by Dr. Kassa Tadele, Arba Minch University, Mr. Gezahegn Wajebo, Water Resources Development Bureau of SNNPR, Mr. Bekele Tolossa and Mr. Yared, colleagues at Arba Minch University, during my study period are greatly acknowledged.

I express my deep sense of heartily gratitude to my beloved parents who bore, raised and taught me. Their inspirational thoughts and blessings are always with me. From my soul, I extend my indebtedness to my siblings and family members (Mrs. Damenech, M., Mrs. Woinitu, H., Mr. Batissa, W., Mrs. Zerfinesh, W., Mrs. Birtukan, S., Mr. Mega, B., Mr. Teshome, B., Mr. Terefe, T. and my younger siblings) for their unflagging encouragement throughout my journey. Their motivation and true sense of emotional and moral support strengthened me while I was combating against my study over the last three years.

Above all, thanks to God Almighty who has made all this possible! Amen!

Place: Roorkee


Negash Wagesho A.

Date : 07-06-12

TABLE OF CONTENTS

CANDIDATE'S DECLARATION	i
ABSTRACT	iii
ACKNOWLEDGEMENTS	ix
TABLE OF CONTENTS	xi
LIST OF FIGURES	xvii
LIST OF TABLES	xxiii
ABBREVIATIONS AND ACRONYMS	xxiv
CHAPTER 1 INTRODUCTION	1
1.1 GENERAL	1
1.2 OBJECTIVES OF THE STUDY	3
1.3 ORGANIZATION OF CONTENTS OF THE THESIS	4
CHAPTER 2 TEMPORAL AND SPATIAL VARIABILITY OF ANNUAL AND SEASONAL RAINFALL OVER ETHIOPIA	7
2.1 GENERAL	7
2.2 OVERVIEW OF RAINFALL VARIABILITY OVER ETHIOPIA	7
2.3 TEMPORAL AND SPATIAL VARIABILITY ANALYSIS METHODS	9
2.4 THE STUDY AREA	11
2.5 DATA USED AND METHODOLOGY	11
2.5.1 Data Used and Preliminary Data Analysis	11
2.5.2 Spatio-Temporal Variability of Rainfall	14
2.5.2.1 Spatial Distribution of Annual & Seasonal Rainfall	14
2.5.2.2 Temporal Dependence of Rainfall	17
2.5.2.3 Trend Analysis of Annual and Seasonal Rainfall	18
2.6 RESULTS AND DISCUSSION	21
2.6.1 Autocorrelation	21
2.6.2 Spatial Variability of Rainfall	22

2.6.3 Trends in Rainfall	26
2.6.4 Atlantic Multidecadal Oscillation (AMO) Signal and Rainfall	33
2.7 CONCLUSIONS	34
CHAPTER 3 INVESTIGATION OF NON-STATIONARITY IN HYDRO-CLIMATIC VARIABLES IN THE RIFT VALLEY LAKES BASIN OF ETHIOPIA	39
3.1 INTRODUCTION	39
3.2 SHORT AND LONG TERM TIME DEPENDENCE IN HYDRO-CLIMATIC VARIABLES	41
3.3 STUDY AREA AND DATA USED	44
3.3.1 The Study Area	44
3.3.2 Hydro-climatic Data	45
3.3.3 Land Use/Land Cover Data	46
3.4 STATISTICAL TEST METHODS	47
3.4.1 Autocorrelation	47
3.4.2 Von Neumann Ratio Test	48
3.4.3 Mann-Kendall (MK) Trend Test	49
3.4.4 Theil-Sen Trend Slope Estimator	50
3.4.5 Spectral Analysis	51
3.4.6 Wavelet Transform	52
3.4.7 Long Term Persistence in Streamflow	54
3.5 RESULTS AND DISCUSSION	56
3.5.1 Time Dependence of Hydro-climatic Variables	56
3.5.2 Streamflow Spectral Analysis	64
3.5.3 Wavelet Analysis	66
3.5.4 Long Range Dependence	72
3.5.5 Association of Sea Surface Temperature (SST) to Rainfall	74
3.5.6 Land Use Dynamics: A potential Implication to Streamflow Trends	75
3.6 CONCLUSIONS	80

CHAPTER 4 CATCHMENT HYDROLOGIC MODELLING USING SOIL AND WATER ASSESSMENT TOOL	83
4.1 GENERAL	83
4.2 THE NEED FOR HYDROLOGIC MODELLING IN THE STUDY WATERSHEDS	83
4.3 DESCRIPTION OF THE SWAT MODEL	86
4.4 MODEL SENSITIVITY AND UNCERTAINTY ANALYSIS	92
4.5 MODEL PERFORMANCE EVALUATION TECHNIQUES	94
4.6 DESCRIPTION OF THE STUDY AREA	96
4.7 ACQUISITION AND PRELIMINARY PROCESSING OF DATA FOR SWAT MODEL	98
4.7.1 Topographical Data	98
4.7.2 Soil and Land Use Data	98
4.7.3 Hydro-meteorological Data	99
4.8 WATERSHED DELINEATION AND SWAT MODEL SETUP	106
4.8.1 Watershed Delineation	106
4.8.2 Model Setup	106
4.9 RESULTS AND DISCUSSION	107
4.9.1 DEMs and Limitations of Watershed Delineation Algorithms	107
4.9.2 Model Sensitivity Analysis	112
4.9.3 Model Calibration and Validation	114
4.9.4 Groundwater (Baseflow) Contribution	121
4.9.5 Simulated Total Water Yield of the Watersheds	122
4.9.6 Manual Input-Output Sensitivity Analysis	124
4.10 CONCLUSIONS	126

CHAPTER 5	DOWNSCALING GLOBAL CLIMATE MODEL OUTPUTS AND ASSESSMENT OF CLIMATE CHANGE IMPACTS ON RUNOFF GENERATION	129
5.1	GENERAL	129
5.2	OVERVIEW OF GLOBAL CLIMATE CHANGE	130
5.3	HISTORICAL EVIDENCES OF CLIMATE VARIABILITY OVER ETHIOPIA	131
5.4	WATERSHED MODELLING IN PURSUIT OF CHANGING CLIMATE AND CATCHMENT CONDITIONS	133
5.5	DOWNSCALING GCM OUTPUTS	136
5.6	STUDY AREA AND CLIMATE DATASETS	138
5.6.1	The Study Area	138
5.6.2	Climate Datasets	138
5.7	METHODS USED	143
5.7.1	Temperature Downscaling	144
5.7.2	Precipitation Downscaling and Bias Correction	146
5.8	SIMULATION OF RUNOFF FOR CURRENT AND FUTURE CLIMATE	148
5.9	RESULTS AND DISCUSSION	148
5.9.1	Statistical Downscaling Model	148
5.9.2	Precipitation Bias Correction	149
5.9.3	Dry-/Wet-Spell Analysis	153
5.9.4	Extreme Temperature and Precipitation Events	154
5.9.5	Runoff Generated	155
5.10	CONCLUSIONS	162
CHAPTER 6	IMPACT OF CATCHMENT DYNAMICS ON RUNOFF GENERATION	165
6.1	GENERAL	165
6.2	OVERVIEW OF IMPACT OF CATCHMENT DYNAMICS ON TOTAL WATER YIELD OF A WATERSHED	165
6.3	THE STUDY AREA	167
6.4	DATA USED AND METHODOLOGY	167

6.4.1 Data Used	167
6.4.2 Temporal Land Use/Land Cover Conditions	169
6.4.3 Watershed Modelling Under Changing Land Use/Land Cover Conditions	170
6.4.4 Land Use/Land Cover Change and Streamflow Trend	171
6.5 RESULTS AND DISCUSSION	172
6.5.1 Land Use/Land Cover Dynamics in the Study Watersheds During 1973-2000	172
6.5.2 Land Use/Land Cover Dynamics and Hydrologic Modelling	176
6.5.3 Streamflow Trend Analysis	179
6.6 CONCLUSIONS	183
CHAPTER 7 CONCLUSIONS AND SCOPE FOR FUTURE WORK	185
7.1 GENERAL	185
7.2 MAJOR FINDINGS OF THE STUDY	185
7.3 LIMITATIONS OF THE STUDY AND SCOPE FOR FURTHER WORK	188
REFERENCES AND BIBLIOGRAPHY	189

LIST OF FIGURES

FIGURE No.	DESCRIPTION	PAGE
2.1	Study area (location map of Ethiopia) and 0.5° latitude x 0.5° longitude spatial resolution monthly precipitation grid points used for analysis	12
2.2	Mean annual rainfall distribution at 200 mm contour interval overlaid on elevation grid map (a). Mean seasonal rainfall pattern where the country is categorized into two regions based on main summer (region-I) and spring/summer (region-II) rainfall distribution (b)	12
2.3	Partial plot of correlogram of significant positive lag-one autocorrelation coefficient for annual rainfall series. The upper and lower boundaries of the correlogram are plotted as dashed line. Grid coordinates (longitude, latitude) are given on top right corner of each figure	23
2.4	Time dependent (lag-1, lag-2 and lag-3) distribution of annual rainfall series presented as figure (a), (b) and (C)	24
2.5	Distribution of local Moran index for (a) annual (b) summer main rainy season (July- September) and (c) Spring/Summer (April – October) season rainfall	25
2.6	North-South and East-West transects considered for annual rainfall spatial variability analysis.	26
2.7	Box plots of percentile (lower bound, 25, 75 and upper bound) mean annual precipitation at various segments of grid points traversing linearly through specified latitude/longitude	27
2.8	Spatial distribution of lowest bound, 25, 75 and upper bound percentile annual rainfall of Ethiopia averaged over the time period 1951-2000.	29
2.9	Regions showing significant trend of annual rainfall series (1951-2000) with mean annual rainfall contour overlaid. (a) MK-test at $\alpha = 5\%$, (b) MK-test at $\alpha = 10\%$, (c) MK pre-whitened test at $\alpha = 5\%$, (d) MK-Pre-whitened at $\alpha = 10\%$	30
2.10	Map of regions showing significant trend of seasonal rainfall series (1951-2000); (a) MK-test at $\alpha = 5\%$, (b) MK-test at $\alpha = 10\%$, (c) MK pre-whitened test at $\alpha = 5\%$, (d) MK pre-whitened at $\alpha = 10\%$	32

2.11	A 10-year running average of standardized annual rainfall (smooth line) superimposed over AMO index (dashed line). Precipitation grid locations are given with numbers and corresponding compass directions (NW=North-West, NE= North-East, C= central, S = South, NC=North-Central)	35
2.12	Correlation coefficient (partial) between standardized annual rainfall and AMO index at specified grid locations (NW=North-West, NE= North-East, C= central, S = South, NC=North-Central)	37
3.1	Map of Rift Valley lakes basin showing study catchments, observed and gridded rainfall location points	45
3.2	Empirical and theoretical correlogram (K in years) of dependent hydrologic processes: (a) Bilate river at Alaba Kulito (b) Tikur Wuha river at Dato Village (c) Hare river (d) Hawassa lake level	59
3.3	Spectral density of monthly runoff of (a) Bilate river at Alaba Kulito (b) Hare river (c) Tikur Wuha river at Dato village and (d) Hawassa lake level. The 95 percent confidence bound is depicted as broken line plot	65
3.4	Correlogram of monthly hydrologic series (a) Bilate river at Alaba Kulito (b) Hare river (c) Tikur Wuha river at Dato village and (d) Hawassa lake level. The smooth curve is theoretical correlogram of AR (1) process	65
3.5	Monthly streamflow and lake level fitted to finite Fourier series for the first two harmonics: (a) Bilate at Alaba Kulito (b) Hare river (C) Tikur Wuha at Dato village and (d) Hawassa lake level	66
3.6	Wavelet decomposition of monthly lake level at Hawassa lake during 1980-2007	67
3.7	Original and Daubechies denoised signal of monthly lake level (a) and Tikur Wuha streamflow (b). The smooth line is a denoised signal using db-4 level - 5	68
3.8	Original and Daubechies denoised signal of annual average lake level (a) and Tikur Wuha (b) streamflow. The smooth line is a denoised signal using db-4	68
3.9	Standardized original and discrete wavelet decomposed signals plot of Tikur Wuha stream flow (left panel) and Hawassa lake level (right panel)	69
3.10	Continuous wavelet spectrum for Hawassa lake level (a), stream flow of Tikur wuha at Dato village (b), streamflow of Bilate at Alaba Kulito (c), and streamflow of Hare at Arba Minch (d)	73

3.11	Annual Average sea surface temperature anomaly based on 1982-2010 average at 0 ^o -10 ^o N and 45 ^o -65 ^o E region	74
3.12	Standardized SST (°C) and average annual rainfall (mm) at Rift Valley lakes basin	75
3.13	Association of annual rainfall to June-September (a) and annual average (b) SST	75
3.14	Temporal land use/cover distribution at Hawassa lake catchment	77
3.15	Temporal land use/cover distribution at Bilate catchment	78
4.1	Schematic representation of methodology employed in the study	86
4.2	Location and watersheds map of the study area: Bilate (1) and Hare (2) watersheds	97
4.3	Soil map at Bilate (a) and Hare (b) watersheds	100
4.4	Land use map at Bilate (a) and Hare (b) watersheds	101
4.5	Land slope map at Bilate (a) and Hare (b) watersheds	102
4.6	Rainfall double mass curve analysis for selected stations	104
4.7	Annual rainfall plots for selected stations in the study basin	105
4.8	Probability distribution fitted to annual rainfall series at selected stations	105
4.9	SRTM-90m and 30m ASTER DEM data generated watershed boundary and flow path at Hare watershed	108
4.10	ArcHydro and TOPAZ generated stream flow path (leftward red line) compared against Landsat image extracted stream (rightward blue line) at the lower foot of Bilate watershed	109
4.11	TOPAZ and ArcHydro delineated watershed and streams: Bilate (a) and Hare (b)	110
4.12	ArcSWAT delineated watershed characteristics at Bilate (a) and Hare (b) basins	111
4.13	Area-Elevation curve at Bilate and Hare basins	111
4.14	Parameter sensitivity ranking with (a) and without (b) observed discharge case at Bilate watershed	113
4.15	Parameter sensitivity ranking with (a) and without (b) observed discharge case at Hare watershed	113

4.16	Model Calibration for monthly Bilate river flow at Alaba Kulito	117
4.17	Model Calibration for monthly Hare river flow near Arba Minch area	117
4.18	Scatter plot of observed and simulated flow at Bilate (a) and Hare (b) river watersheds for calibration period	117
4.19	Simulated runoff during model validation phase at Bilate watershed	119
4.20	Simulated runoff during model validation phase at Hare watershed	119
4.21	Scatter plot of observed and simulated flow at Bilate (Fig. a) and Hare (Fig. b) watersheds for validation period	119
4.22	Plots of model calibration (a) and validation (b) for daily series at Bilate watershed	120
4.23	Plots of model calibration (a) and validation (b) for daily series at Hare watershed.	120
4.24	Baseflow contribution as percentage of annual total water yield at Bilate watershed during calibration (a) and validation (b) period	123
4.25	Baseflow contribution as percentage of annual total water yield at Hare watershed during calibration (a) and validation (b) period	123
4.26	Manual input-output sensitivity analysis result at Bilate watershed	125
4.27	Manual input-output sensitivity analysis result at Hare watershed	126
5.1	Preliminary model evaluation indices (RMSE and Scorr) between reanalysis temperature and precipitation gridded dataset covering entire Ethiopia and GCMs output during 1981-2000	141
5.2	Observed versus downscaled maximum temperature for BCM2.0 model at Alaba Kulito station	145
5.3	Quantile plots of observed and downscaled maximum temperature at Alaba Kulito for current (1990-1999) and future (2081-2090) climate condition	145
5.4	Quantile-Quantile plot of observed (at Alaba Kulito station) and raw GCMs outputs of maximum temperature for current (1990-1999) and future (2081-2090) climate scenarios	146
5.5	Average monthly future scenario (2081-2090) precipitation variability for two different GCM realizations. The observed station (Alaba Kulito) precipitation spans from 1990-1999	150

5.6	Linear and power transformed bias correction of precipitation for current climate condition for BCM2.0 (a) and MK3.0 (b) GCMs	151
5.7	Linear and power transformed precipitation bias corrections for A1B greenhouse gas emission scenario for two GCMs realizations	151
5.8	Linear and power transformed precipitation bias corrections for A2 greenhouse gas emission scenario for two GCMs realizations	152
5.9	Probability of exceedance of daily precipitation for current and future climate conditions for BCM2.0 (left panels) and MK3.0 (right panels) GCMs	153
5.10	Dry- and wet-spell lengths for future scenario precipitation predicted during 2081-2090 analysis period	154
5.11	Observed and simulated monthly runoff for current climate from two GCMs at Bilate (a) and Hare (b) watersheds	157
5.12	Runoff simulated for future climate scenario at Bilate (left panels) and Hare (right panels) from two GCMs	158
5.13	Average monthly runoff simulated for current and future climate (A1B and A2 scenarios) conditions at Bilate (left panels) and Hare (right panels) watersheds	159
5.14	Box plots of percentile (lowest, first quarter, median, third quarter and upper most) monthly runoff simulated for future climate scenarios at Bilate watershed	160
5.15	Box plots of percentile (lowest, first quarter, median, third quarter and upper most) monthly runoff simulated for future climate scenarios at Hare watershed. The smooth line a polynomial fitted into median values of simulated monthly flows over the analysis period	161
6.1	Reclassified land use/land cover classes for use in hydrologic modelling at Bilate watershed	174
6.2	Reclassified land use/land cover classes for use in hydrologic modelling at Hare watershed	174
6.3	Temporal variation of dominant land use/land cover proportion in the study watersheds	175
6.4	Simulated surface runoff component for different land use/land cover condition during the analysis period	177

6.5	Average monthly simulated surface rainfall-runoff relationship for different land use condition at Hare (left column) and Bilate (right column) watersheds	178
6.6	Average annual simulated surface runoff and rainfall relationship for three (1976, 1986 and 2000) land use/land cover conditions at Bilate (a) and Hare (b) watersheds	179
6.7	Simulated average monthly total water yield for three (1976, 1986, 2000) land use/land cover conditions at Bilate (a) and Hare (b) watersheds. The simulation is averaged for 1990-2009 at Bilate and 1990-2006 at Hare watersheds	179
6.8	Double mass curve analysis of observed runoff and rainfall at Alba Kulito (a) and Hare-near Arba Minch (b)	181
6.9	Flow Duration Curves (FDCs) for various segments of average monthly streamflow records of Bilate river at Alaba Kulito station	182



LIST OF TABLES

TABLE No.	DESCRIPTION	PAGE
2.1	Statistical test hypothesis cases	14
2.2	Significance of lag-one autocorrelation coefficient for annual rainfall series	21
2.3	Significance of lag-one autocorrelation coefficient for seasonal rainfall series	21
2.4	Moran's Index and corresponding test statistics for annual and seasonal rainfall series	24
2.5	Total number of grid points with significant trends at 5 and 10 percent significance level.	29
2.6	Annual rainfall trend test statistics for significant trends at $\alpha = 0.05$	31
3.1	Landsat images acquired and their respective characteristics	47
3.2	Autocorrelation test statistics for annual and seasonal observed rainfall series	57
3.3	Autocorrelation test statistics for annual and seasonal gridded rainfall series	58
3.4	Summary of r_1 , r_2 and r_3 significance test for original streamflow and lake level	58
3.5	Von Neumann ratio test statistic of streamflow and lake level	60
3.6	MK trend analysis for observed annual and seasonal rainfall series	61
3.7	MK trend test statistics for gridded annual and seasonal rainfall series	62
3.8	MK trend test for total number of rainy days of annual and seasonal-observed rainfall series	62
3.9	MK trend test statistics for annual and seasonal streamflow series	63
3.10	Theil-Sen's trend slope estimator and r_1 magnitude of streamflow before and after prewhitening	64
3.11	MK-trend analysis statistics and model efficiency of wavelet decomposed signals of Tikur Wuha and Hare streamflow	70
3.12	MK-trend analysis statistics and model efficiency of wavelet decomposed signals of Hawassa lake level and Bilate streamflow	71
3.13	Temporal land use/cover distribution at Bilate catchment	79
3.14	Temporal land use/cover distribution at Hawassa lake catchment	79

4.1	Land use/Cover distribution at Bilate and Hare watersheds in the year 2000	100
4.2	Meteorological stations near the study area	102
4.3	Rainfall statistical parameters at nearby stations to watershed outlets	103
4.4	Bilate and Hare watershed morphological parameters estimated at basin outlets	110
4.5	Initial model parameter ranges used for default simulation and mode of variation	116
4.6	Model efficiency and uncertainty indices during calibration and validation period	118
4.7	Annual model performance indices during calibration and validation period	118
4.8	Optimal model values after calibration at Bilate watershed	121
4.9	Optimal model values after calibration at Hare watershed	121
4.10	Average monthly (1992-1996) basin values during calibration period at Bilate watershed	123
4.11	Average monthly (1994-2000) basin values during calibration period at Hare basin	124
5.1	IPCC Forth Assessment Report (IPCC-FAR) approved climate models and respective atmospheric and oceanic resolutions	142
5.2	Simulated average runoff depths for different climate scenarios and corresponding percentage change with respect to observed series	162
6.1	Orthorectified landsat images used for land use/land cover classification	168
6.2	Details of hydro-meteorological dataset used for analysis	169
6.3	Areal coverage of reclassified land use /land cover condition for study watersheds	175
6.4	Trend analysis of annual and extreme daily streamflow series for the study watersheds	181

ABBREVIATIONS AND ACRONYMS

Abbreviations and acronyms having common meaning are defined here. Other locally used symbols are defined in the body of the Thesis during their first appearance.

AMO	Atlantic Multidecadal Oscillation
ANN	Artificial Neural Network
AOGCMs	Atmospheric Oceanic General Circulation Models
ASTER	Advanced Space-borne Thermal Emission and Reflection Radiometer
BCCR-BCM2.0	Bjerknes Centre for Climate Research-Bergen Climate Model Version2
CGIAR-CSI	Consultative Group on International Agricultural Research-consortium for Spatial Information
CIAT	Centro Internacional de Agricultura Tropical (International Center for Tropical Agriculture)
CMIP3	Coupled Model Intercomparison Project phase-3
CRU	Climate Research Unit
CSIRO-MK3.0	Common Wealth Scientific and Industrial Research Organization-Mark 3.0
DEM	Digital Elevation Model
ECHAM4/OPY3	European Center Hamburg 4/Ocean and Isopycnal model version 3
EM-DAT	Emergency Database
ENSO	El Niño–Southern Oscillation
ERDAS	Earth Resources Data Analysis System
FAO	Food and Agricultural Organization
FDCs	Flow Duration Curves
GCM	Global Climate (General Circulation) Models
GHCN	Global Historical Climatology Network
GPCC	Global Precipitation and Climate Center
GPCPV2.2	Global Precipitation Climatology Project Version 2.2
GTS	Global Telecommunication System
IHDM	Institute of Hydrology Distributed Model
ICRAF	International Center for Research in Agro-Forestry
IHDM	Institute of Hydrology Distributed Model

IPCC	Intergovernmental Panel on Climate Change
ITCZ	Inter-Tropical Convergence Zone
JAR-25	Japanese 25-year Reanalysis
LARS-WEGN	Long Ashton Research Station Weather Generator
MCM	Million Cubic Meter
MoWR	Ministry of Water Resources
MoFED	Ministry of Finance and Economic Development
NMSA	National Meteorological Service Agency
NOAA	National Oceanic and Atmospheric Administration
SDSM	Statistical Downscaling Model
SHE	Système Hydrologique Européen
SNNPR	Southern Nations, Nationalities and Peoples Republic
SRTM	Shuttle Radar Topography Mission
SST	Sea Surface Temperature
USDA-SCS	United States Department of Agriculture-Soil Conservation Service
SUFI-2	Sequential Uncertainty Fitting Version 2
SWAT	Soil and Water Assessment Tool
SWM	Stanford Watershed Modelling
TOPAZ	Topographical Parameterization
UN	United Nations
UNEP	United Nations Environmental Protection
WCRP's	World Climate Research Programs

1.1 GENERAL

The cognizance of impact of climate change and variability on our planet, and specifically on societal development, has got wide publicity among scientific community and governments since climate modelling tools have begun to emerge. The capability of climate models to simulate present and predict future climate condition has increased its application in addressing climate change implications (Marshall et al., 2011).

Climate change and variability due to either continuous seasonal astronomical pattern or inadvertent effects of man over earth-atmospheric continuum has significantly been affecting the hydrologic cycle. Varied precipitation in terms of frequency and intensity would result in more frequent events. Earth's surface temperature is fluctuating due to global climate change which is evident from increase in average air and sea surface temperature, melting of polar ice caps, rise in average global sea level and other associated changing aspects of our planet (Loaiciga et al., 1996; Singh and Kumar, 1997; Barnett et al., 2005; Steele-Dunne et al., 2008). Over the last one hundred years (1906-2005), global mean surface temperature has risen by $0.74^{\circ}\text{C} \pm 0.18^{\circ}\text{C}$. The rate of warming per decade in the last fifty years ($0.13^{\circ}\text{C} \pm 0.03^{\circ}\text{C}$) is nearly twice that over the last hundred years ($0.07^{\circ}\text{C} \pm 0.02^{\circ}\text{C}$) (IPCC, 2007a). However, in most cases, the effect of such changing climate and its variability on catchment hydrology is not well investigated. Water resources planning and management system is affected by this variability and associated uncertainties.

Due to rapid growth in world's population, the natural environment is under tremendous stress on account of various demands that ultimately influence the global water balance. The ever increasing need for food, fiber and shelter coupled with growing national economic interests aggravated land use dynamism. Anthropogenic induced land use/land cover changes have transformed one-third to one-fourth of ice-free surface of our planet (Vitousek, 1994; Vitousek et al., 1997). In most parts of the globe, significant area of pristine ecosystems with lush vegetation has been converted to other forms of land use/land cover management practices. Conversion of forest cover and dense naturally vegetated area to arable land (Angelsen, 1999;

Barbier, 2004) and cattle grazing field has significantly modified bulk water yield from the watersheds. Piao et al. (2007) argues that the land use change has been strongest in tropical regions and its contribution to global runoff outweighs that of climate change. On global scale, an average amount of 0.08 mm/year^2 increase in runoff is observed due to land use changes.

Shifts on onset of seasonal rainfall in some parts of the globe resulted in change in the hydrologic regime of the globe (Emanuel, 2005). Among the most severe natural disasters during the last century in Ethiopia, flood and drought accounts for major proportions (48 flood and 12 drought events) in terms of loss of life and associated damages to people and property (EM-DAT, 2010). The occurrence of frequent extreme precipitation and temperature events over the past signals key climate variability in the country and warns a future course of adaptive measures.

In addition to flood and drought, modification of fragile ecosystem in terms of deforestation, land degradation and sedimentation have become recurring facets of many watersheds. As per the world Food and Agricultural Organization (FAO) report of 2006, 30% of the world's land area only is estimated to be covered by forests with a gross deforestation rate of 12.9 million ha/yr. With some mitigation measures, the recent net global forest loss was reduced to 7.3 million ha/yr compared to 8.9 million ha/yr of the 1990s (IPCC, 2007b). Forest cover in Ethiopia declined phenomenally over the last century. The country's total forest cover was drastically fallen from 44% in 1885 to 4% in 1985 (McCann, 1997). This is mainly attributed to conversion of forest land into agricultural land, settlements, infrastructure developments and logging. Such noticeable man-induced land use/land cover dynamics substantially altered the hydrologic regime of the basins; by and large, affected the runoff process by modulating the storm response in the catchments.

The Earth's radiative energy balance due to anthropogenic influences markedly increased climate fluctuations. The atmospheric-ocean General Circulation Models provide credible estimates of such fluctuations for future climatic condition at continental scale. However, identifying impacts associated to continuous decadal climatic variability based on expected greenhouse gases emission scenario at small spatial scale is usually characterized by highly uncertain model results and requires significant attempt to approximate the reality.

Quantification of catchment responses under varying climate and catchment characteristics is required to address key water resources management problems. Stochastic

analysis of short and long term persistence in hydro-climatic variables such as stream flow and lake level to detect for possible time-trends over the historical period (Berndtsson et al., 2009; Ehsanzadeh ^{and Adamowski}, 2010; Burn et al., 2010) provides an insight about climatic variability. However, statistical trend analysis alone may not deal with a complete sense of complications arising from climate change. Joint use of such statistical time dependence analysis and hydrologic modelling may better help understand the response of catchment due to climatic and man-induced changes (Refsgaard et al., 1989). The natural fluctuation in hydrological variables caused by climatic and catchment conditions is detected by hydrologic models and the remaining unexplained variability is manipulated through statistical time-dependence analysis.

1.2 OBJECTIVES OF THE STUDY

Ethiopian Rift Valley system is part of the Great Rift Valley system of the world that extends from Syria in the north to Mozambique in the Eastern Africa with total length of about 6400 km. It is a fracture in the Earth's surface that widens over time due to Earth's tectonic forces forming an opposed dipping faults. Ethiopian Rift Valley lakes basin, covering a total area of approximately 52,500 km², is one amongst twelve major river basins of the country and accounts for 49% geographic area of the entire Rift Valley system (FAO, 1997). The basin, marked by its beautiful natural reservoirs and streams, is administratively shared between two Regional States (Oromia and Southern Nations, Nationalities and Peoples Republic (SNNPR)). Geomorphologically, the basin is characterized by lowland plateau and escarpments at both left and right ends extending from the central part of the country to Cewu Bahir bordering Kenya.

The impact of changing climate condition is more profound in semi-arid regions of the basin where competition for water is immense. Quantitative assessment of the impacts of climate and catchment dynamics on runoff generation in the basin is vital. Owing to limited data availability, little attempt has been made to understand the watershed dynamics of Ethiopian catchments in response to climate and land use change.

In view of the preceding major concerns, the study investigates the impact of climate change and catchment dynamics (land use/land cover changes) on runoff generation in the Rift Valley lakes basin of Ethiopia. To meet this goal, the research objectives are identified as follows.

- i. Investigation of the spatial and temporal variability of annual and seasonal rainfall over Ethiopia,
- ii. Identification of non-stationarity and reasons of non-stationarity in hydro-climatic variables using short and long-term time dependence analysis in Rift Valley lakes basin of Ethiopia,
- iii. Assessment of the impact of topographic, weather and catchment input parameters on runoff generation using Soil and Water Assessment Tool,
- iv. Analysis of the impact of climate change on runoff generation using coupled atmospheric-ocean Global Climate Model outputs for current and future climatic conditions under varied greenhouse gas emission scenarios,
- v. Evaluation of the impacts of temporal land use/land cover dynamics on runoff generation using distributed hydrologic model.

1.3 ORGANIZATION OF CONTENTS OF THE THESIS

The thesis is organized into seven major chapters. Chapter 1 presents introduction and objectives of the study.

Spatial and temporal variability of annual and seasonal rainfall over Ethiopia is investigated using trend detection approaches in Chapter 2. Association of Atlantic Multidecadal Oscillation (AMO) to Ethiopian annual and seasonal rainfall pattern is also examined in this Chapter.

Non-stationarity in hydro-climatic variables in the Rift Valley lakes basin of Ethiopia is investigated in chapter 3. Hydro-climatic variables such as rainfall, streamflow and lake levels for average and extreme events are investigated for possible long-term and short-term time dependence. Besides trend detection methods, spectral and wavelet analysis are utilized to examine the periodic behavior of streamflow and lake levels. Association of Sea Surface Temperature (SST) and temporal land use/land cover changes to prevailing temporal variability of hydro-climatic variables is also assessed.

Chapter 4 discusses the impact of weather and catchment input parameters on runoff using physically based distributed hydrologic modelling. Soil and Water Assessment Tool (SWAT) model is applied to two study watersheds in the Rift Valley lakes basin of Ethiopia to

characterize the ensuing effects of variable weather and catchment input parameters and on runoff.

Chapter 5 concentrates on investigation of impact of climate change on runoff generation. Climate change and key future signals of its variability are assessed using General Circulation Models (GCMs). Since GCMs are operating at coarser resolution, statistical downscaling model (SDSM) is applied to reduce large scale atmospheric variables into localized weather variables. Bias corrected daily precipitation and temperature variables are used to simulate runoff for current and future climate scenarios. The implication of changing climate condition on average and extreme future runoff magnitude is evaluated.

Chapter 6 deals with land use/land cover dynamics and associated impacts on runoff generation. Real-time land cover information acquired from landsat sensors is further processed to identify temporal land use/land cover condition in the study watersheds. Runoff is simulated for varied land use/land cover conditions using distributed hydrologic modelling. The behavior of simulated runoff is further investigated using statistical analysis of historical hydro-climatic datasets.

Conclusions drawn from the study and scope for further work are presented in Chapter 7.

TEMPORAL AND SPATIAL VARIABILITY OF ANNUAL AND SEASONAL RAINFALL OVER ETHIOPIA

2.1 GENERAL

In many parts of Ethiopia, failure of summer monsoon rainfall coupled with traditional farming practices notably reduced agricultural produce and aggravated poverty stricken economy of the nation over the last four decades. Impacts of climate variability and change are significantly felt in agriculture, water supply and hydropower sectors and adversely affecting the socioeconomic aspect of the livelihood. Assessing spatial and temporal variability of annual and seasonal rainfall over the country allows us to understand the impact of global climate system on regional weather pattern. Moreover, reliable knowledge of ecosystem resilience under variable precipitation condition can be obtained from temporal precipitation analysis so that future water resources planning and management accommodates commendable adaptive measures.

This chapter is devoted to identification of possible spatial and temporal trends in annual and seasonal rainfall variability over the country using statistical analysis. Secondly, short term persistence in annual and seasonal rainfall pattern is investigated and its statistical significance is examined. Finally, the coherence between North Atlantic Multidecadal Oscillation (AMO) and annual rainfall indices over the analysis window is assessed.

2.2 OVERVIEW OF RAINFALL VARIABILITY OVER ETHIOPIA

The inter-annual oscillation of Inter-Tropical Convergence Zone (ITCZ) and the influence of Indian monsoon cause variation in the wind flow patterns and determine the climate pattern over Ethiopia (Moron, 1998). ITCZ passes over Ethiopia twice a year and this migration alternately causes the onset and withdrawal of winds from north and south. Such periodic anomaly of winds as a result of ITCZ movement causes seasonal rainfall variability over the country. The south western, western and southern part of the country receives high (>1200 mm) mean annual rainfall. Mean annual rainfall magnitude decreases in the northern and eastern parts of the country that reaches below 400mm in some locale. Ethiopian main rainfall season follows both uni-modal (during June-September months when the ITCZ is to the northernmost)

and bi-modal (March-May and September-November) rainfall pattern (Gissila et al., 2004). The uni-modal rainfall pattern usually covers the northern part whereas bi-modal rainfall pattern is associated to southeastern and southern parts of the country.

Ethiopia has been ravaged by persistent drought of varying extent leading to social and economical ramification (Pankhurst, 1966; Degefu, 1987; Ntale and Gan, 2003). Rainfall anomalies in the form of extreme wet (1962–1966, 1979, 1998/1999, and 2006/07) and dry (1971–1973, 1984–1986, 1992, and 2002–2004) years substantially affected the agricultural sector (Jury, 2010).

The summer rainfall that accounts for major component (approximately 65-95 percent) of total annual rainfall over the country is governed by El Niño–Southern Oscillation (ENSO) and further enhanced by local climatic forcing (Korecha and Barnston, 2007). Main rainy season droughts in Ethiopia are likely associated to warm ENSO episodes (Seleshi and Demaree, 1995; Tsegay, 1998; Seleshi and Zanke, 2004). The low frequency fluctuation in North Atlantic Sea Surface Temperature (SST) described as North Atlantic Multidecadal Oscillation was signaled by both warm and cool phases over the last one and half-century. This synoptic scale signal affected the rainfall pattern of the globe exerting drought and hurricanes (Enfield et al., 2001; Uvo and Berndtsson, 2002; Trenberth and Shea, 2006) of variable magnitude with conspicuous effects in North Atlantic regions. Its impact is also characterized by detectable features in northern part of Ethiopia as well. The drop in Nile river level during 1970s and early 1980s appears to be related to a multi-year cool phase in the North Atlantic and a southward retreat of the near equatorial trough (Jury, 2010). Taye and Willems (2012) argue that changes that occur on the Pacific and Atlantic Oceans influence extreme rainfall and flow at the upper Blue Nile basin of Ethiopia. AMO shows strong and significant correlation to rainfall and streamflow during the dry season.

Rainfall trend analysis has drawn considerable attention of many climatologist and hydrologist since long back and being in use nowadays to trace the impact of climate variability and change due to natural and anthropogenic influences across the globe (Parthasarathy and Dhar, 1975; Partal and Kahya, 2006; Christensen et al., 2007; Trenberth et al., 2007; Kampata et al., 2008; Ghosh et al., 2009; Patra et al., 2012). In highly agrarian community like Ethiopia where the livelihood of the population and gross domestic product of the country is almost entirely dependent up on rain-fed agricultural production, analysis of precipitation pattern is of

paramount importance to cope up with damages associated to crop yield, animal breeding, power production and ecosystem management.

2.3 TEMPORAL AND SPATIAL VARIABILITY ANALYSIS METHODS

The complex interaction in land-atmosphere-ocean continuum yielding to varied climatic conditions could be approximated and evaluated through climatic variables such as precipitation, temperature and stream flow describing the process. Among others, investigation of precipitation pattern and its possible trends as function of spatial and temporal scale over the region provides valuable information for future water resources management. Moreover, it acts as a useful intermediate solution in deriving mitigation measures and evaluating ecosystem resilience towards such variability.

The weather conditions vary both spatially and temporally depending up on local orographic effects and large scale climate induced changes. The essence of accounting spatial variability of rainfall in watershed hydrologic modelling is manifold. Total water yield in the sub-watersheds could realistically be predicted provided that the spatial distribution of rainfall over the basin is known in advance. The influence of synoptic scale meteorological forcings and local orographic effects could be inferred from spatial rainfall pattern of a region. Moreover, it helps to bolster our knowledge of preliminary rainfall data analysis methods (such as storm transposition, filling missing data, etc) under limited data conditions.

Analysis of temporal variability of annual and seasonal rainfall pattern over historical observation period provides useful information about time dependence of rainfall events. On the basis such time-dependent patterns of rainfall events, present and future water resources management scenarios could be suggested. In this section, a brief review of the applications of spatial and temporal time series analysis tools is discussed in reference to available literature.

The spatial distribution of seasonal and annual rainfall pattern across the geographic locations is assessed using the spatial autocorrelation theory. The spatial autocorrelation method measures the similarity of a variable with respect to adjacent variable as a function of variable value and distance. Cliff and Ord (1981) provided detail mathematical model of spatial autocorrelation theory to capture the spatial variability of geographically dependent time series datasets. The basic notion of spatial autocorrelation is stated by Cliff and Ord as if the adjacent values are strongly related to each other, then there is strong spatial autocorrelation; if values

are simply arranged at random order over the surface, there should be no apparent spatial autocorrelation.

Grunsky and Agterberg (1991) presented an algorithm to analyse spatial association between multivariate datasets. The method computes auto-/cross correlation coefficients of a multivariate dataset to examine for possible spatial relationships. The developed model is successfully applied to geochemical datasets to study the spatial distribution.

Koenig (1999) discussed the application of spatial autocorrelation to study the spatial synchrony of ecological phenomena. He argued that the availability of long-term and large area datasets such as rainfall and temperature datasets acquired from Global Historical Climatology Network make possible to understand the underlying spatial pattern.

Cai and Wang (2006) used the Moran index (I) approach to quantify the topographic index in catchments derived from digital elevation models. The association of topographic index declines over increasing spatial extent.

The temporal variability of seasonal and annual rainfall pattern is investigated using short term persistence and time trend analysis. Giles and Flocas (1984) define persistence as a tendency of the successive values of a time series to remember their antecedent values and to be influenced by them. It is a correlational dependence of order k between each i^{th} element and the $(i-k)^{\text{th}}$ element of the series (Kendall, 1975). Such time-lagged dependence is measured using autocorrelation function. Time domain (autocorrelation) and frequency domain (spectral estimate) based tests can be applied to investigate persistence in time series. The time domain technique is applied to assess persistence in seasonal and annual rainfall pattern.

The non parametric, distribution-free trend test method of Mann and Kendall (Mann, 1945; Kendall, 1975) and its variants such as the modified Mann-Kendall trend test (Hamed and Rao, 1998; Rao et al., 2003) and the prewhitened Mann-Kendall test (Zhang et al., 2001, Cunderlik and Burn, 2004) used for autocorrelated series are widely used methods to detect non-stationarity in time series. The parametric regression coefficient approach (Matalas and Sankarasubramanian, 2003) is also applied in many hydrological time-trend analyses.

2.4 THE STUDY AREA

The study area covers the entire Ethiopia, situated approximately between 3⁰ to 15⁰N latitude and 33⁰E to 48⁰E longitude, with a total area of 1.13 million square kilometers (Fig. 2.1). The region is characterized by highly irregular topography in the central and northern highlands to lowland of the rift valley plain traversing from north-east to south-west with elevations ranging from around 110m below mean sea level in the Dallol Depression to 4,620m above mean sea level at Ras Dejen in the Simen mountain massif (Fig. 2.2a). The three major climatic zones of Ethiopia are tropical rainy climate characterized by dense forest and intense moisture content, temperate rainy climate and dry climate. Based on modified Koppen's climate classification of Ethiopia (Gonfa, 1996; Peel et al., 2007), the climatic zones are further subdivided into a total of nine categories to account for average local variability.

Monsoon rainfall distribution is highly erratic and unevenly distributed over the country. The monsoon rainy season is spatially varying in such a way that northern part of the country (as the rift system approximately describing the divide line) receives its substantial rainfall from June to October, however, the main monsoon rainy season ('Kiremt' season) is usually from July to September. Relatively low seasonal and annual rainfall distribution is prominent in south and south-eastern region of the country with highest rainfall magnitude in the months of April and slightly lower rainfall further extends to the month of October. Traditionally, this region mainly receives its highest rainfall both in 'Belg' (March-April-May) and 'Kiremt' seasons. Spatial distribution of mean annual and seasonal rainfall pattern is depicted in Fig. 2.2a and Fig. 2.2b respectively. Mean annual temperature varies from over 30 °C in lowlands to approximately 10 °C at very high altitudes.

2.5 DATA USED AND METHODOLOGY

2.5.1 Data Used and Preliminary Data Analysis

Data Used: Monthly gridded rainfall data at 0.5° latitude x 0.5° longitude resolution of 50 years (1951-2000) covering the entire Ethiopia is acquired from Global Precipitation and Climate Center (GPCC) under the framework of project Variability Analyses of Surface Climate Observations (<http://gpcc.dwd.de>). It is an updated and globally gridded precipitation estimate extracted from surface rain gauge observations with a minimum of 90 percent data availability over the years 1951-2000. The dataset is compiled in data centers (Food and Agricultural Organization (FAO) of United

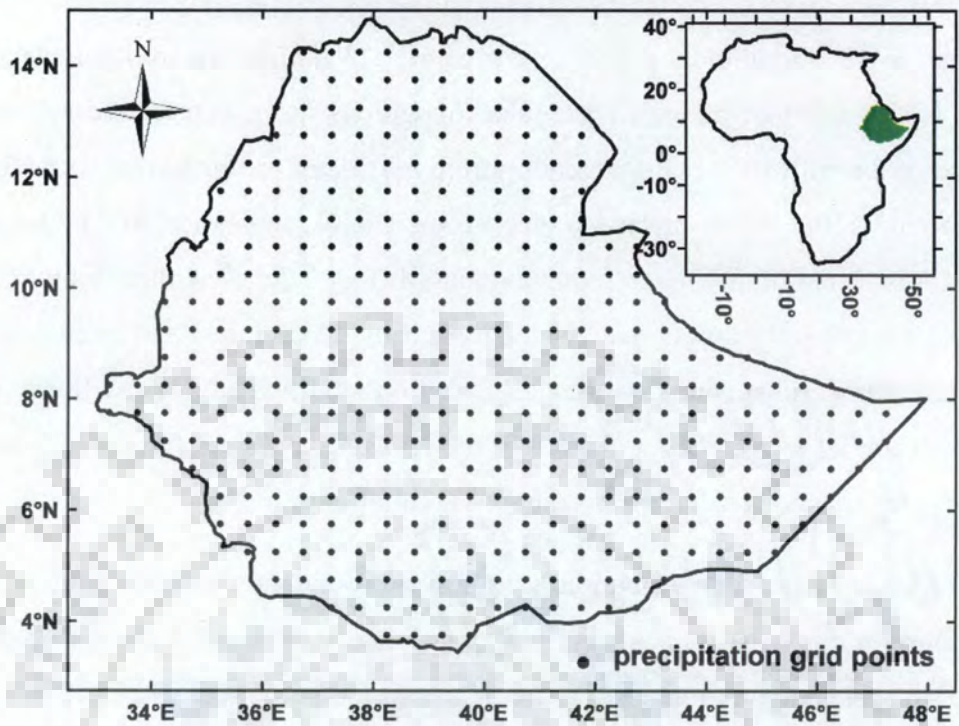


Fig. 2.1 Study area (location map of Ethiopia) and 0.5° latitude x 0.5° longitude spatial resolution monthly precipitation grid points used for analysis

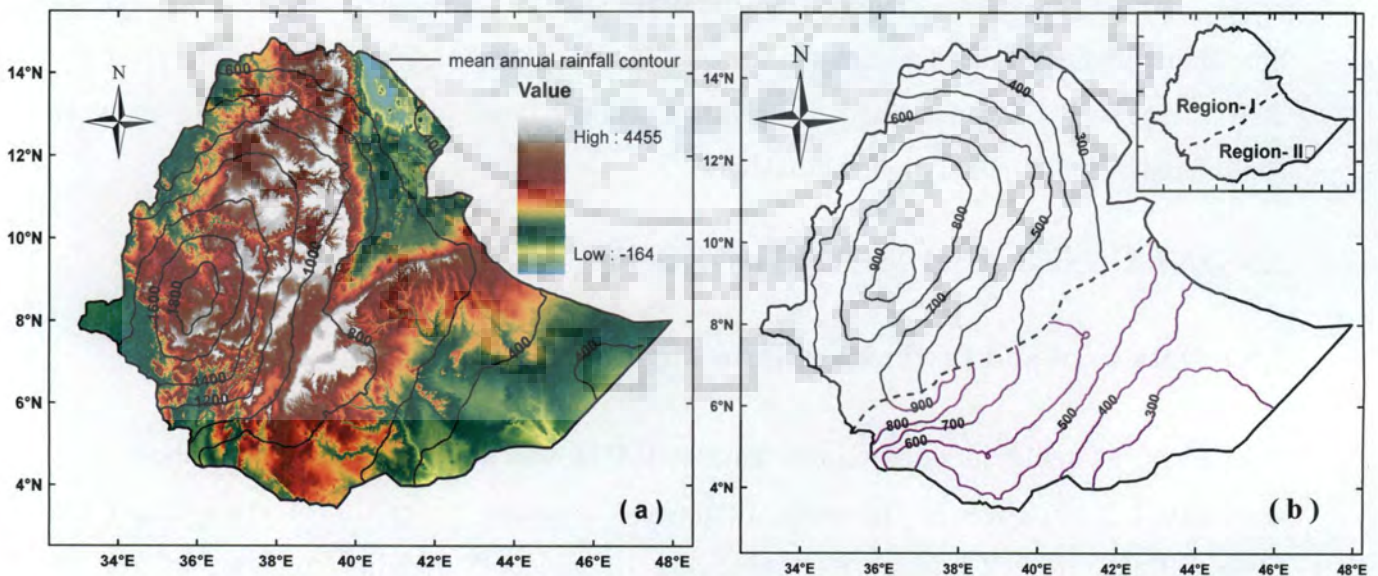


Fig. 2.2 Mean annual rainfall distribution at 200 mm contour interval overlaid on elevation grid map (a). Mean seasonal rainfall pattern where the country is categorized into two regions based on main summer (region-I) and spring/summer (region-II) rainfall distribution (b)

Nations, Climate Research Unit (CRU) and Global Historical Climatology Network (GHCN)) and data transferred via the Global Telecommunication System (GTS) (Adler et al., 2003; Beck et al., 2005). Beck et al. (2005) had undertaken a rigorous attempt in interpolating the precipitation data over the world to $0.5^{\circ} \times 0.5^{\circ}$ grid size using ordinary krigging that resulted in least interpolation error among other methods. A total of 381 precipitation grid points (Fig. 2.1) extracted from station data are considered for further statistical analysis. The total number of existing meteorological observatories in the country until 1999 exceeds 832 (Belete, 1999) with more monitoring stations being added henceforth. Gridded rainfall data is widely applied in various hydro-climatological analyses in different parts of the world (Rajeevan et al., 2006; Baigorria et al., 2007; Ghosh et al., 2009; Mair and Fares, 2010) and is advocated to be suitable for climate variability study. Jury (2010) applied a $0.5^{\circ} \times 0.5^{\circ}$ gridded precipitation data over a period of 1901-2007 from GPCC dataset to study decadal climate variability in Ethiopia. Observed rainfall data for selected stations of sufficient record length is obtained from National Meteorological Service Agency (NMSA) of Ethiopia to check the validity of gridded data through preliminary data analysis.

An unsmoothed and detrended AMO index data of Kaplan (1998) Sea Surface Temperature Version 2 (1948-2000) is acquired from National Oceanic and Atmospheric Administration (NOAA) dataset to investigate AMO-rainfall index. Digital elevation model with 90m resolution (Fig. 2.2a) is obtained from Consultative Group on International Agricultural Research-consortium for Spatial Information (CGIAR-CSI) center (<http://srtm.csi.cgiar.org/>) and further analyzed to identify surface elevation variability of the study area.

Preliminary Data Analysis: Prior to applying analytical evaluation, examining the quality of available data minimizes the errors that propagate throughout the analysis and eliminates potential bias in the final decision. Preliminary scrutiny of observed and gridded rainfall data in terms of time series plots, fitting probability distribution and checking for consistency has been made. Both observed and gridded rainfall series stem from similar distribution. Spatially close sets of observed and gridded rainfall series are characterized by statistically similar mean and standard deviation values.

Statistical Hypothesis Testing: Hypothesis testing represents a class of statistical decision making technique to extract information about a population from limited observations. McCuen (2003) summarizes procedures involved in statistical analysis of hypothesis testing as follows; formulating the hypothesis, selecting the appropriate statistical model that identifies the test statistic and its distribution, identifying the level of risk measured as significance level, computing an estimate of the test statistic from the sample data, obtaining the critical value of the test statistic which defines the region of rejection and finally comparing the computed test statistic with critical value to arrive at a conclusion based on the hypothesis. The null hypothesis is the logical antithesis of the notion that the investigator is seeking to prove while the alternative hypothesis is its exact opposite. Thus, throughout the sections the null hypothesis is represented by H_0 and its counterpart, alternative hypothesis as H_A .

The decision for most hypothesis test can be explained in terms of two tailed, one tailed lower or upper of the underlying problem statement. For parameter P tested against the standard value P_0 and S denoting the computed test statistic with S_c values of the variates associated to area described by α -term in respective tails are summarized (McCuen, 2003) in Table 2.1.

Table 2.1 Statistical test hypothesis cases

If H_A is	Then reject H_0 if	Test Case
$P \neq P_0$	$S > S_{\alpha/2}$ or $S < S_{1-\alpha/2}$	two tailed
$P < P_0$	$S < S_{1-\alpha}$	one tailed lower
$P > P_0$	$S > S_{1-\alpha}$	one tailed upper

Rejection of the null hypothesis does not mean that the alternative hypothesis is always true. The sampling procedure might have produced an extreme value by chance, though either this is very unlikely, or the extreme value of the test statistic might have occurred because the null hypothesis is false. The later has got statistical inference and often accepted in hydrology. Unless otherwise stated a two tailed problem case where region of rejection is on both sides has been applied in the subsequent sections.

2.5.2 Spatio-Temporal Variability of Rainfall

2.5.2.1 Spatial Distribution of Annual & Seasonal Rainfall

Climatic variables such as rainfall are highly influenced by local and synoptic scale meteorological forcings. Therefore, assessing the spatial variability of time series for observed

or extracted values of variables is highly demanded. Evaluation of feature similarity based on its location and unique attribute (eg. mean annual and seasonal rainfall magnitudes) assigned to it simultaneously provide sound technique to analyze whether there is a spatial relationship (similarity/dissimilarity) in the magnitudes of the variables over space or not.

The concept of variable similarity over space, variously known as spatial autocorrelation, was developed to capture the realm of regional behavior since the early 19th century, however, matured conceptual and mathematical model described as in spatial autocorrelation is to the credit of Cliff and Ord (1969;1973;1981). Since then the approach has received growing application in many literature to describe spatial autocorrelation (Koenig, 1999; Ping et al., 2004; Cai and Wang, 2006; Carl and Kuhn, 2007). The Cliff-Ord model herein after Moran's spatial autocorrelation (Moran, 1950) method where both location and its mean annual and seasonal rainfall magnitudes are simultaneously analyzed for possible spatial autocorrelation is used to examine spatial variability of annual and seasonal rainfall. The method compares the magnitude of a variable at a point to the magnitude at other points with explicit reference to location (Goodchild, 1986) in the given space domain and evaluates the association strength in terms of index. Finally, based on the estimated index at prescribed level of significance, spatial clustering or dispersion of regions is accomplished. Goodchild (1986) provides explanatory review of spatial analysis.

The Moran's (1950) test statistic, I of spatial autocorrelation in a vector of residual \hat{u} as summarized by Hepple (1991) as:

$$I = \left(\frac{n}{s} \right) \frac{\sum_{i=1}^n \sum_{j=1}^n \hat{u}_i \hat{u}_j w_{ij}}{\sum_{j=1}^n \hat{u}_j^2} = \left(\frac{n}{s} \right) \frac{\hat{u}' W \hat{u}}{\hat{u}' \hat{u}} \quad (2.1)$$

where \hat{u}_i is a residual value of variable at particular location i , \hat{u}_j is the residual value of variable at another locations; W is $n \times n$ matrix of spatial weight set denoting the strength of connection between regions or the weight indexing location of i relative to j ; n is number of elements and s being sum of all elements in the weights matrix. For raw standardized matrix, i.e., when raw elements are scaled to sum to unity, the value of s becomes equal to n . Omitting the scaling factor (n/s) without loss of generality, the test statistic becomes:

$$I = \frac{\hat{u}' W \hat{u}}{\hat{u}' \hat{u}} \quad (2.2)$$

Under the null hypothesis of no spatial autocorrelation, the statistic, I is normally distributed. Cliff and Ord developed the asymptotic distribution to the Moran's test statistic (Z_I) with regression residuals.

$$Z_I = \frac{I - E(I)}{\sqrt{\text{Var}(I)}} \quad (2.3)$$

where the expected value and variance assuming the error term follows the normal distribution. The distribution is critically dependent on the form of idempotent matrix M and hence the expected value and variance (Anselin, 1988; 1995) are given by:

$$E(I) = \left(\frac{n}{s}\right) \frac{[MW]^T}{n-k} \quad (2.4)$$

$$\text{Var}(I) = \frac{\left(\frac{n}{s}\right)^2 \{(MWMW')^T + [(MW)^T]^2 + [(MW)^T]^2\}}{(n-k)(n-k+2)} \quad (2.5)$$

where M is projection matrix equals to $1 - X(X'X)^{-1}X'$; W is weight matrix; k is the number of values in the empirical frequency distribution that are more extreme than the observed statistics. The spatial similarity of a single station to its proximity is described by Anselin's local Moran index as a function of mean annual rainfall and a Euclidian distance. Features sharing a common boundary such as adjacent grid points or contiguous polygons are analysed for similarity of values at spatial scale. Field Moran's index value is statistically evaluated using Z-score test where the test statistic follows normal distribution. Critical values of Z-score at 10 (5) and 1 percent significance level are ± 1.65 (± 1.96) and ± 2.58 respectively. The null hypothesis of the test statistic is that there is no spatial clustering of the values. The null hypothesis is rejected if Z-score lies beyond the critical level. In general, a Moran's Index value near +1 indicates clustering while an index value near -1 indicates dispersion. Local and global Moran's I are computed for respective precipitation locations to annual and seasonal rainfall and their spatial significance is evaluated.

Spatial distribution of rainfall influences the volume, peak and time to peak of runoff hydrograph in the catchment (Singh, 1997; Chaubey et al., 1999; Chaplot et al., 2005). The response of spatial variability is more pronounced when runoff is simulated from poorly networked station rainfall data in large catchments (Smith et al., 2004). Possible systematic pattern in spatial variability across the compass directions in the study area is demonstrated by estimating 25, 50, 75 and 100 percentile annual rainfall magnitudes throughout the grid points.

2.5.2.2 Temporal Dependence of Rainfall

The degree to which hydro-meteorological variables at any time t_i is dependent up on the value of preceding time in the domain of the sequence adequately represents the serial correlation, sometimes referred as autocorrelation. A tendency for a system to remain in the same state from one observation to the next described as persistence is associated to positive autocorrelation. Thus, evaluation of the statistical significance of such dependence in time series (Box and Jenkins, 1970; Salas et al., 1980) prior to development of stochastic models is a trustworthy approach. The significance of lag-one serial correlation coefficient for independent and identically distributed series can be computed using methods suggested by Anderson (1942) and latter by Kendall and Stuart (1968) that the distribution of r_k is approximated as:

$$N \left[\frac{-1}{n}, \frac{(n-2)^2}{n^2(n-1)} \right] \quad (2.6)$$

Hirsch et al. (1993) defined a test statistic, t , which follows a student's t -distribution with $n-2$ degree of freedom, to assess the significance of Pearson product moment correlation coefficient as:

$$t = r_1 \left(\frac{\sqrt{n-2}}{1-r_1^2} \right) \quad (2.7)$$

Presence of significant serial correlation in hydro-climatic time series affects subsequent trend test (von Storch and Navarra, 1999; Hamed and Rao, 1998; Yue et al., 2002) and need to be removed prior to trend analysis. To identify whether lag one serial coefficient is different from zero by sampling error or not, hypothesis testing for computed r_1 is carried out at prescribed level of significance. Thus, the significance of lag-one serial correlation coefficient is evaluated by Hirsch's approach and subsequently utilized to pre-whiten annual and seasonal series.

A serial correlation magnitude of lag k , r_k , is not significantly different from zero for random sequences, however, r_k value close to unity describes strong time dependence of the observations. The first-order autocorrelation coefficient is especially important because physical systems dependence on past values is likely to be strongest for the most recent past. Lags of higher order are used when the first order autocorrelation coefficient is not sufficiently enough to describe the serial dependence. A plot of set of autocorrelation coefficients of various lags known as correlogram has paramount importance in detecting randomness, short term correlation and stationarity of the sequence over the observation length (McCuen, 2003; Kottegoda, 1980). The presence of a secular trend in time series is associated to high serial

correlation magnitude in the correlogram for smaller lags and decreases slightly at higher lags. The upper and lower boundary of the correlogram test statistic, β (Anderson, 1942) for lag k serial dependence at α level of significance for N observations is given by:

$$\beta = \frac{-1}{N-k} \pm Z_{1-\alpha/2} \left(\frac{(N-k-1)^{0.5}}{N-k} \right) \quad (2.8)$$

The corresponding normal variate, $Z_{1-\alpha/2}$, is assumed to follow normal distribution and obtained from one side test hypothesis.

2.5.2.3 Trend Analysis of Annual and Seasonal Rainfall

Enough evidence exists to suggest that significant changes in trends of observed daily rainfall has been eminent over the second half of twentieth Century. Substantial change in heavy rainfall since late 1940's has been observed in Ethiopia (Easterling et al., 1999). Many early rainfall variability and trend analysis studies conducted in Ethiopia rely on either limited length of data or qualitative inference of changes from limited preliminary rainfall statistical analysis, however, recent rainfall variability studies (Segele and Lamb, 2005; Cheung et al., 2008) are worth mentioning. Segele and Lamb (2005) discussed variability on timing of onset and cessation of summer rainfall in Ethiopia. Cheung et al. (2008) conducted regression analysis of rainfall to examine for possible spatial and temporal variability. To the knowledge of the authors, no rigorous statistical trend analysis has been conducted covering the whole geographical area of the country with sufficient data length to demonstrate time evolution of rainfall. The significance of such variability should be verified through further statistical analysis with prescribed level of acceptance or rejection so that the resulting strength of statistical analysis could reflect the variability. In the present study, rainfall trend analysis is conducted covering entire geographical location based on 381 precipitation grid points of 50 years record length.

The distribution of time series has a significant effect on trend analysis and subsequent methods to be resorted. Hydro-climatic variables might exhibit a variable extent of probability distribution and hence either must be checked for distribution that fit the time series prior to assigning trend analysis or use distribution free trend test methods. Thus, application of trend detection methods that do not rely on the distribution of samples under consideration is advantageous. It ignores the complication arising in normality test as the distribution might fall in transition where the deviation from normality is difficult to identify. Even though a plethora

of trend detection approaches are being in use nowadays, the widely applicable Mann-Kendall (MK) trend test and Theil (1950) and Sen (1968) slope estimator methods are used in the present study. For easy reference, summary of statistical background of trend tests used in this thesis is presented herein after.

Mann-Kendall Test: The Mann-Kendall (Mann, 1945; Kendall, 1975) trend test is a rank based non-parametric test originally developed for non-correlated data. The Mann-Kendall test statistic (S) is computed as:

$$S = \sum_{i=1}^{n-1} \sum_{j=i+1}^n \text{sgn}(x_j - x_i) \quad (2.9)$$

where x_i and x_j are observations with $j > i$ and the sgn function is given by:

$$\text{sgn}(x_j - x_i) = \begin{cases} 1 & \text{if } x_j - x_i > 0 \\ 0 & \text{if } x_j - x_i = 0 \\ -1 & \text{if } x_j - x_i < 0 \end{cases} \quad (2.10)$$

For independent and identically distributed data with no tied elements (equal values) the expected value, $E(S)$ and the variance, $\text{Var}(S)$ of the distribution are:

$$E(S) = 0 \quad (2.11)$$

$$\text{Var}(S) = \frac{n(n-1)(2n+5)}{18} \quad (2.12)$$

If one or more data points are tied, the sample standard deviation is corrected to account for tied elements as:

$$\text{Var}(S) = \frac{n(n-1)(2n+5) - \sum_{i=1}^m t_i(i-1)(2i+5)}{18} \quad (2.13)$$

where t_i is the number of tied elements of extent i . For large sample size ($n \geq 10$), the standard normal test statistics,

$$Z_s = \begin{cases} \frac{S-1}{[\text{Var}(S)]^{0.5}} & \text{if } S > 0 \\ 0 & \text{if } S = 0 \\ \frac{S+1}{[\text{Var}(S)]^{0.5}} & \text{if } S < 0 \end{cases}$$

(2.14)

follows normal distribution (Kendall and Stuart, 1968). The measure of the probability of evidence against the null hypothesis (p-values) for each trend test can be obtained following Douglas et al. (2000) as:

$$P = 2[1 - \Phi(|Z_s|)]$$

(2.15)

where $\Phi(\cdot)$ denotes the cumulative distribution function of the standard normal variate represented by :

$$\frac{1}{\sqrt{2\pi}} \int_0^{|z|} e^{-t^2/2} dt$$

(2.16)

Kulkarni and von Storch (1995) and latter Yue et al. (2002) argue that presence of significant serial correlation in time series affects subsequent trend test. The Modified Mann-Kendall & pre-whitening approaches are commonly adopted techniques to account for the presence of serial correlation in time series that degrades the power of trend test methods. If r_1 is found significant, then the pre-whitened series is given as:

$$X_{t,pw} = x_{t-1} - r_1 * x_t$$

(2.17)

where x_t and x_{t-1} are original time series at time t and $t-1$ respectively with r_1 is lag one serial correlation coefficient. A contrasting idea is advocated by recent authors (Bayazit and Onoz, 2004; Hamed, 2009) that pre-whitening the time series either based on original data or applying detrended series for r_1 computation results in over or under estimation of r_1 and subsequent loss of apparent significance in the analysis. However, in this study owing to its computational ease, the pre-whitened series is subjected to MK trend test and number of significant trends is compared to that of trends in unfiltered series. Theil (1950) and Sen (1968) trend slope, herein after Sen's slope, b is estimated for significant trends to evaluate relative strength of MK trend test.

2.6 RESULTS AND DISCUSSION

2.6.1 Autocorrelation

Statistical significance test of annual and seasonal rainfall is conducted to assess short-term time dependence and to examine the influence of autocorrelation on subsequent trend analysis. From student's t-distribution for n-2 degree of freedom the corresponding p-value at 5 and 10 percent significance level is obtained and compared with estimated t-statistic. For sample size n= 50 with n-2 degree of freedom, the 5% and 10% p-values are 1.68 and 1.30 respectively. If the t-test value computed in eqn. (2.7) is less than the student's t-distribution mentioned at prescribed level of significance, then the lag-one autocorrelation is not significant and the variation is due to sampling error. Summary of t-test results for annual and seasonal (July-August for region-I and April-October for region-II) rainfall series is presented in Tables 2.2 and 2.3.

Table 2.2 Significance of lag-one autocorrelation coefficient for annual rainfall series

Significance level, α (%)	Total number of samples tested	Record length (years)	Number of Tests passed	Number of Tests failed
5%	381	50	88 (23)	293 (77)
10%	381	50	118 (31)	263 (69)

(.) indicates percentage of total sample

Table 2.3 Significance of lag-one autocorrelation coefficient for seasonal rainfall series

Significance level, α (%)	Total number of samples tested	Record length (years)	Number of Tests passed	Number of Tests failed
5	381	50	85 (22.3)	296 (77.7)
10	381	50	91 (23.4)	290 (76.6)

(.) indicates percentage of total sample

Among 381 observations, 23 percent found significant for lag-one autocorrelation for annual and seasonal series at 5 percent significance level. The level of serial dependence is almost similar in both annual and seasonal series. The autocorrelation coefficient of annual and seasonal series up to lag n/4 is further computed to build a correlogram. The upper and lower confidence interval of the correlogram is estimated using Anderson's approach described in

section 2.4.2.2. Partial plot of significant positive lag-1 autocorrelation coefficient is presented in Fig. 2.3. It has been observed from the correlogram that the serial dependence for annual series is high for the first two lags and asymptotically drops to zero. Substantial portion of western and north western part of the country is characterized by high first and second order lag coefficients whereas the serial interdependence diminishes as further moved to the eastern and southern regions. The mean annual rainfall series in such low serially correlated regions is dominated by independent and identically distributed terms i.e. the white noise case dominates. Limited portion of central and southern highlands also experience high lag-1 and lag-2 coefficients (Fig. 2.4).

2.6.2 Spatial Variability of Rainfall

The spatial variability of annual and seasonal rainfall is inspected applying the spatial similarity (spatial autocorrelation) analysis and percentile rainfall distribution over the region. Table 2.5 presents global and local Moran's index for annual and seasonal rainfall distribution over the years 1951-2000.

The Z-score statistics shows the spatial pattern of annual and seasonal rainfall is indicative of clustering at 10, 5 and 1 percent significance level. Regions with high annual and seasonal rainfall distribution exhibit high local Moran's index value. The annual rainfall is categorized into four distinct zones of spatial association, i.e., either clustering or dispersion (Fig. 2.5(a)). Zone-I (Moran's $I= 1.2- 4.1$), includes western land masses typical to its high annual and seasonal rainfall pattern (Western Oromiya, part of Gambela). High Moran's index value of zone-I is characteristic feature of high spatial similarity (clustering) of annual rainfall magnitude. Zone-II, ($I=1.0 -1.2$), low altitude of north-eastern (Afar) and substantial portion of eastern (Somali) region shows moderate spatial similarity. Zone-III ($I=0.3-0.9$) encompasses a small transition zone from high to low spatial similarity located in the western and eastern parts of the country. Zone-IV ($I < 0.1$) is a region of statistically insignificant spatial correlation (dispersion) includes rift valley floor and adjacent escarpments, substantial portion of central, northern & southern (Amhara, Southern Tigray, SNNPR and Oromiya) region. The spatial distribution of mean annual rainfall at one grid point to its contiguous grid points is highly erratic in this region. The seasonal rainfall follows a systematic pattern of spatial correlation both in northern and southern regions. It increases from the central region towards east and west corners in northern region (Fig. 2.5(b)) whereas decreases from west to east as in southern region (Fig. 2.5(c)).

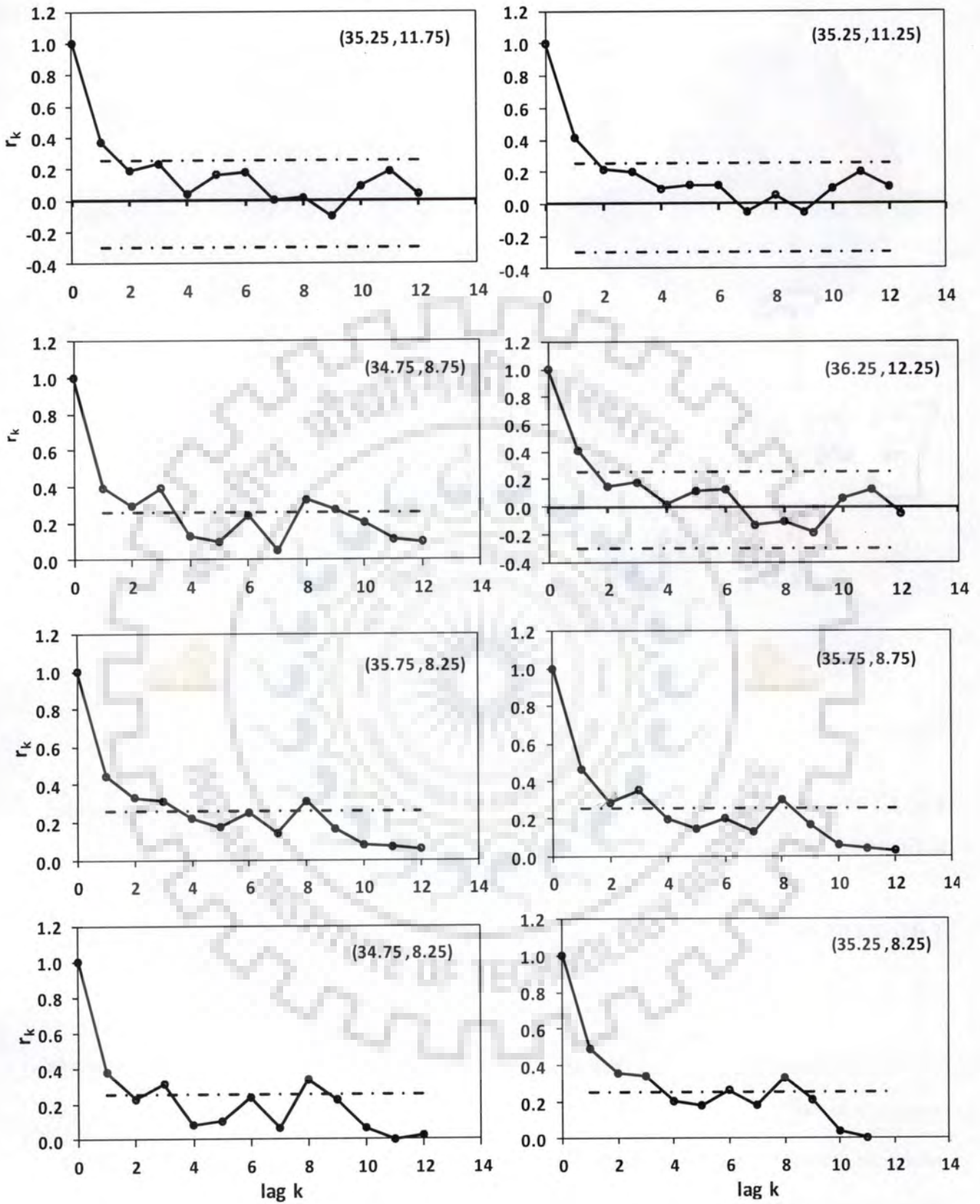


Fig. 2.3 Partial plot of correlogram of significant positive lag-one autocorrelation coefficient for annual rainfall series. The upper and lower boundaries of the correlogram are plotted as dashed line. Grid coordinates (longitude, latitude) are given on top right corner of each figure

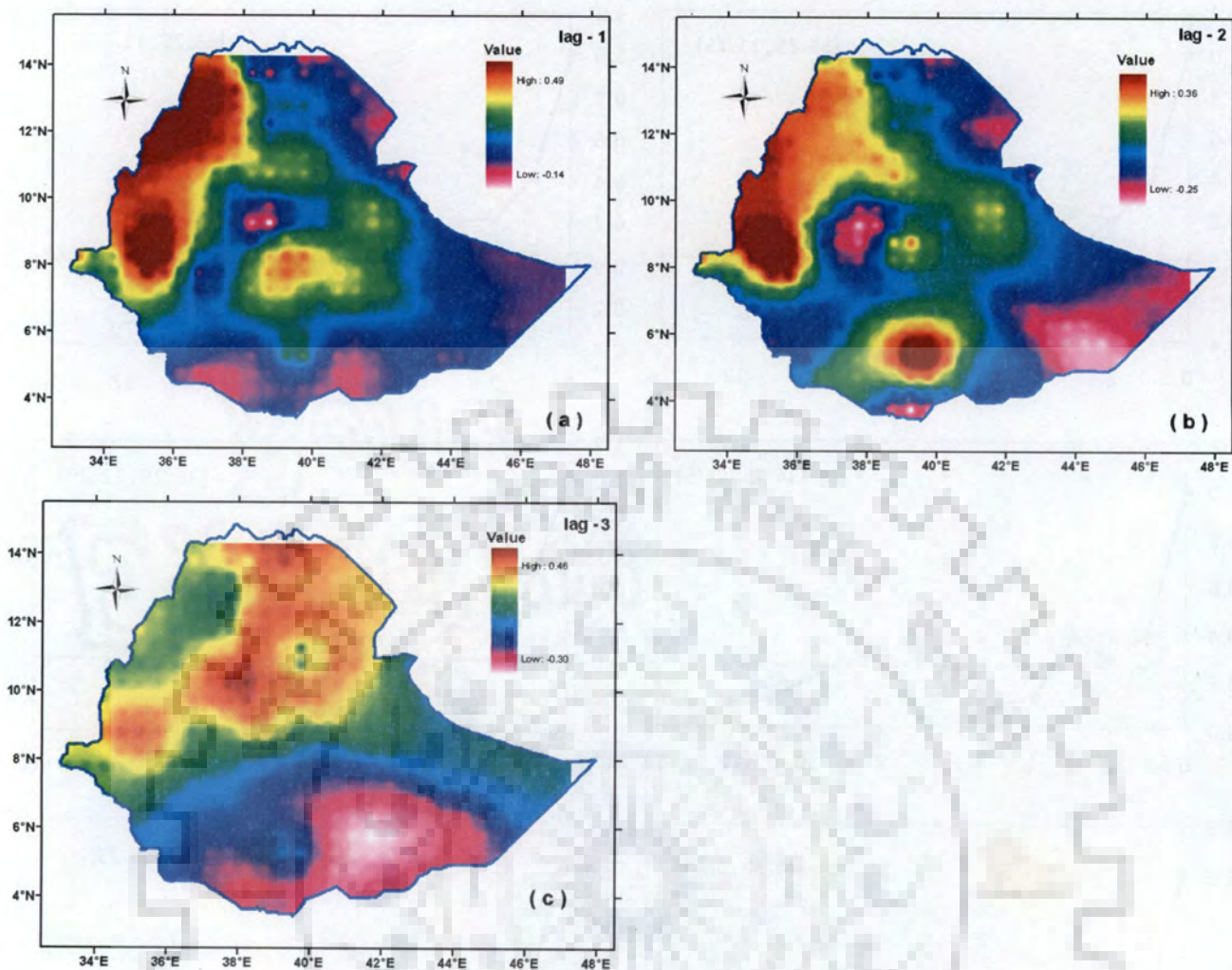


Fig. 2.4 Time dependent (lag-1, lag-2 and lag-3) distribution of annual rainfall series presented as figure (a), (b) and (C)

Table 2.4 Moran's Index and corresponding test statistics for annual and seasonal rainfall series

Parameter	Local *	Global	E (I)	Var (I)	Z- score
	Moran Index	Moran Index			
Annual Rainfall	(-) 0.077 - 4.16	0.71	-0.0026	0.0001	63.94
Monsoon Rainfall (region-I)	(-) 0.077 - 2.81	0.61	-0.0048	0.0003	37.57
Monsoon Rainfall (region-II)	(-) 0.18- 5.57	0.62	-0.0058	0.0004	32.56

* Local Moran index is given in ranges.

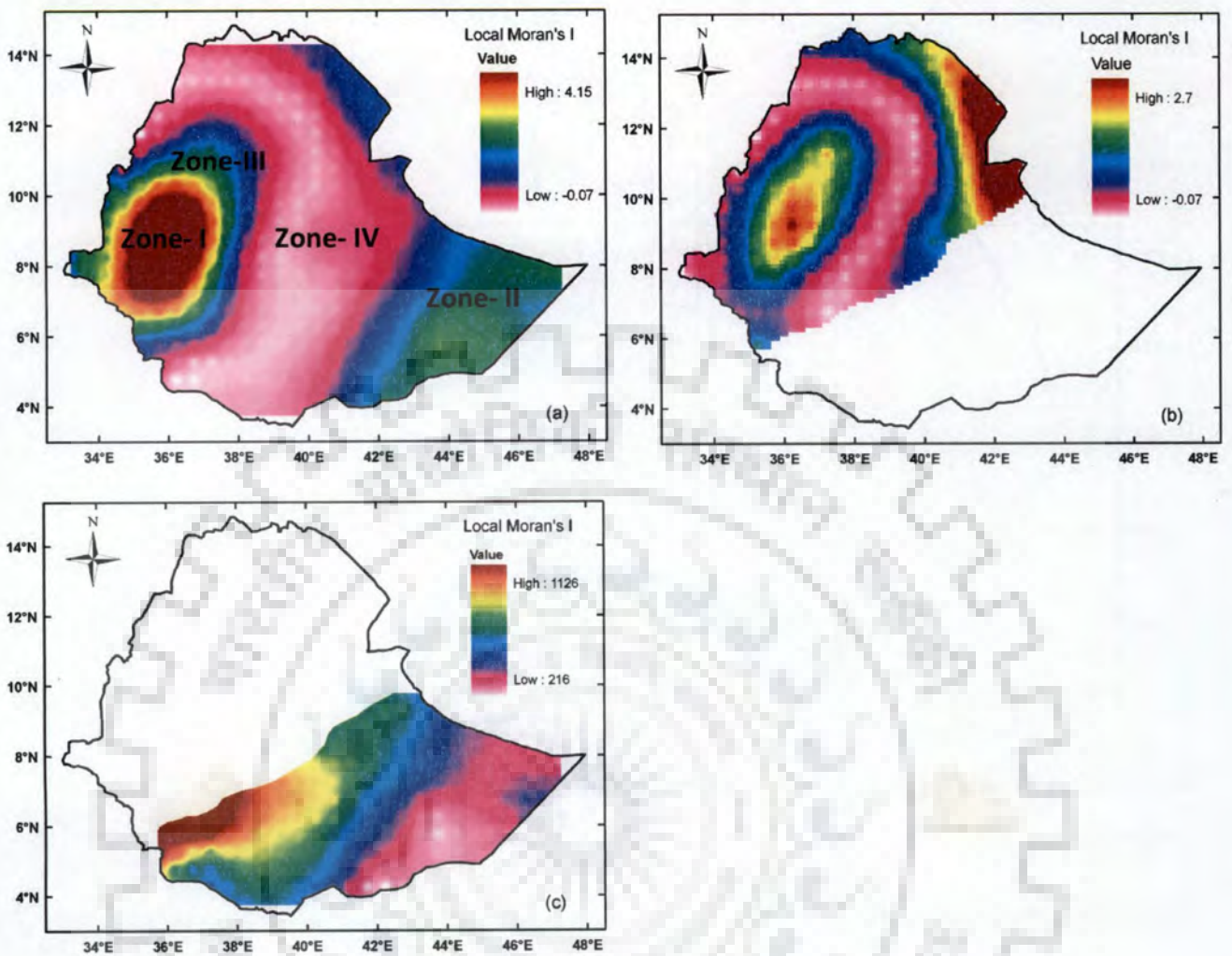


Fig. 2.5 Distribution of local Moran's index for (a) annual (b) summer main rainy season (July-September) and (c) Spring/Summer (April – October) season rainfall

Analysis of a long term multi-grid climatic data covering wide area could sometimes become very complex and liable to errors even under high computing ability. Thus, categorizing the data series into ranges in terms of percentiles to undertake subsequent analysis could minimize the potential threats and provide practical summary. The precipitation magnitude at each grid points for the analysis period is grouped as percentiles (lower, 0.25, 0.5, 0.75 and upper) and examined for spatial variability. The spatial variability of annual precipitation at various segments traversing from one end to the other over the country is discerned as box plots. Six combinations of north-south and west-east segments are selected to depict the spatial variability of mean annual precipitation over the country (Fig. 2.6). The corresponding box plots of mean annual precipitation along the transects are discerned in Fig.2.7. Trend line fitted to the median values of annual rainfall approves falling trend from west-to-east at all segments while

the north-south traverse has a falling trend in the eastern vertical segment. Finally, annual percentile distribution over the region is mapped as raster with rainfall contours overlaid (Fig. 2.8).

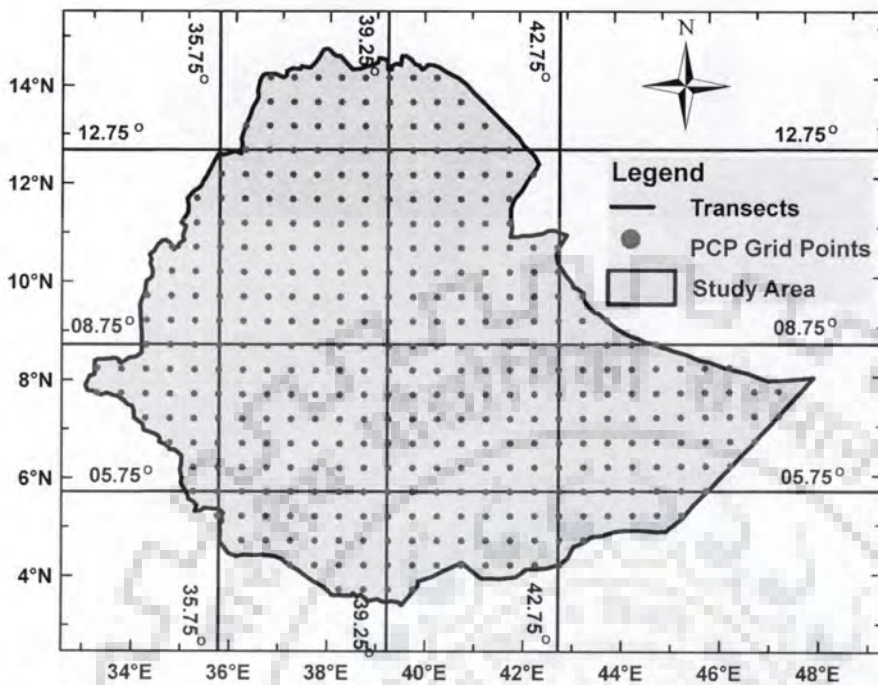


Fig. 2.6 North-South and East-West transects considered for annual rainfall spatial variability analysis

2.6.3 Trends in Rainfall

Annual, seasonal and annual maximum 30-days rainfall trend analysis is carried out by applying Mann-Kendal trend test for original and pre-whitened series. Mann-Kendall test statistics (S) and the probability that the null hypothesis could produce a sample as extreme as the observed events by chance represented as P-value are computed for annual, seasonal and maximum 30-days series and their significance is evaluated at 5 and 10 percent significance level. Total number of grid points characterized by significant increasing and decreasing trend at prescribed level of risk of rejection are listed in Table 5 and their respective geographical distribution is mapped as in Figs. 2.9 and 2.10. The Sen's slope estimator, b , and its minimum and maximum threshold for 95 percent confidence limit are estimated. The total number of significant trends identified by Sen's method is compared to that of MK test. Almost all samples identified as significant using MK trend test have maintained the same level of trend strength as in Sen's method. Added to this, natural series with significant r_1 is subjected to MK test after pre-whitening. As the size of test statistics is large enough, the summary of all test events is presented in Table 2.5. Detail

trend test statistics typical to annual rainfall series at 5 percent significance level is presented in Table 2.6.

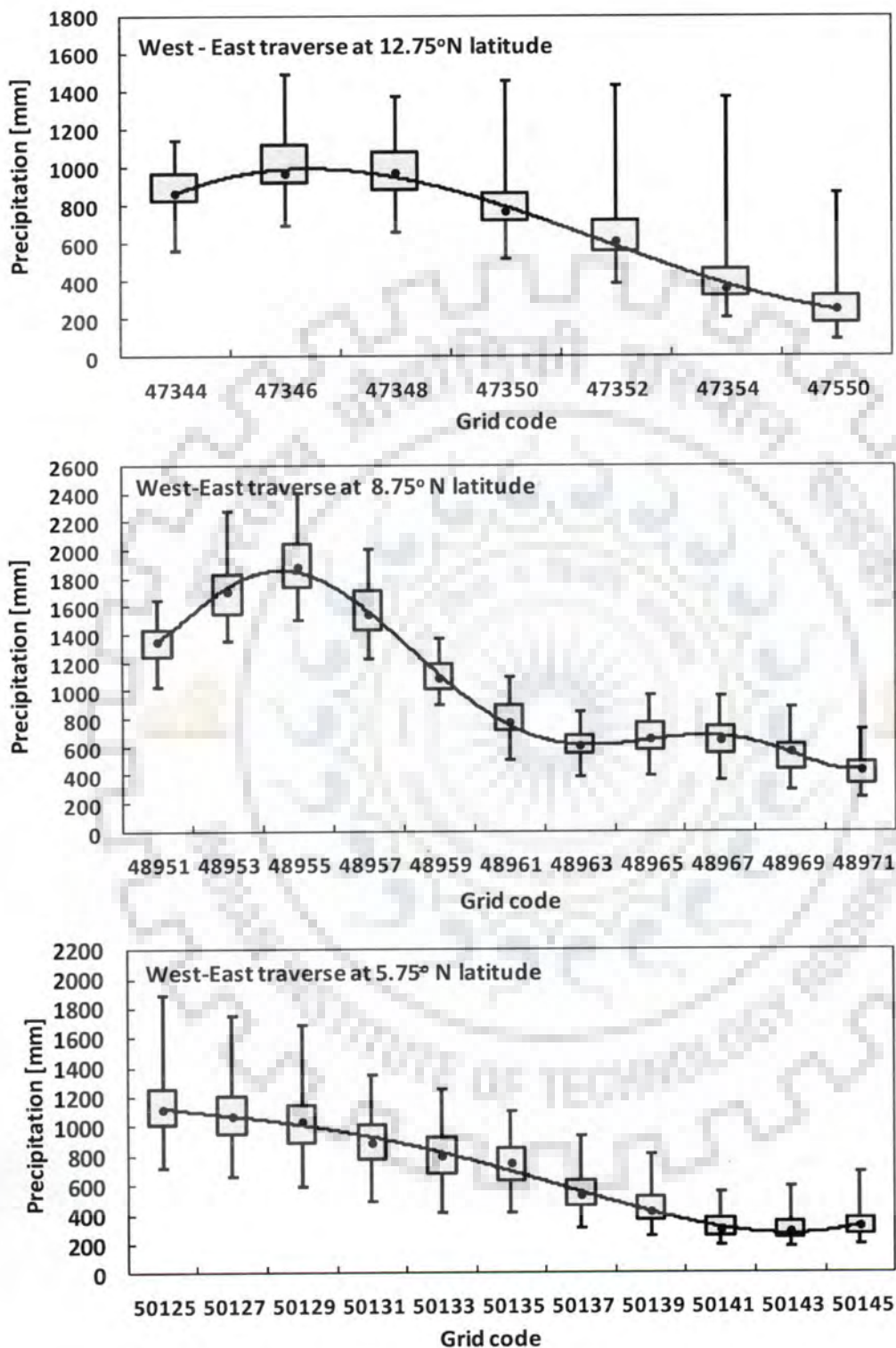


Fig. 2.7 Box plots of percentile (lower bound, 25, 75 and upper bound) mean annual precipitation at various segments of grid points traversing linearly through specified latitude/longitude

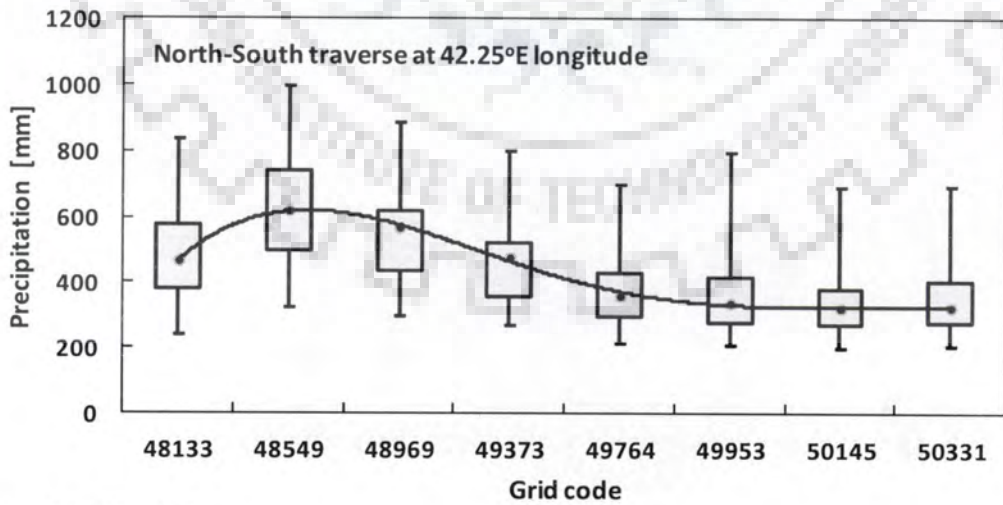
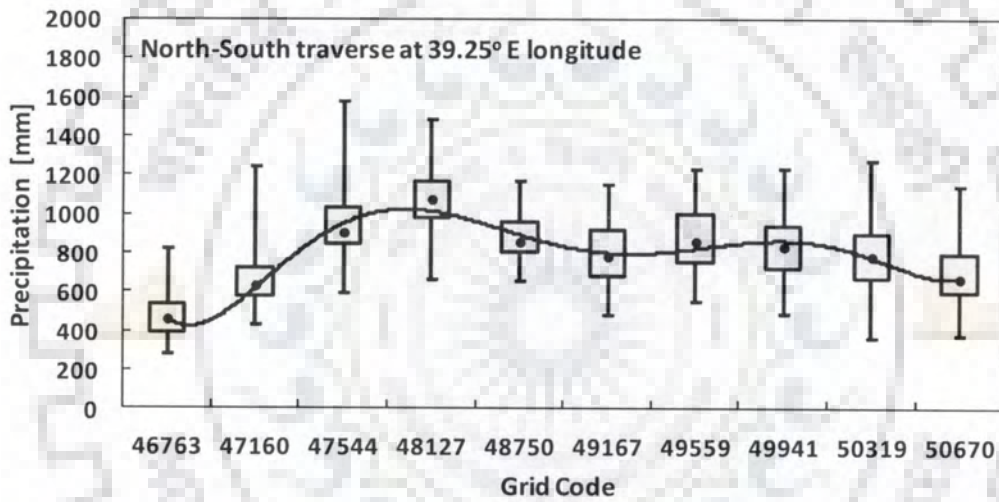
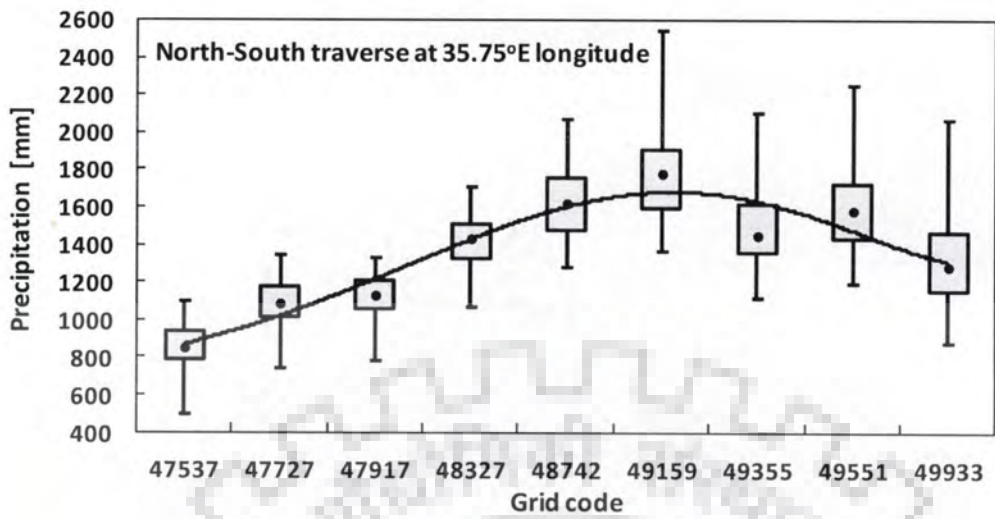


Fig. 2.7 Cont'd

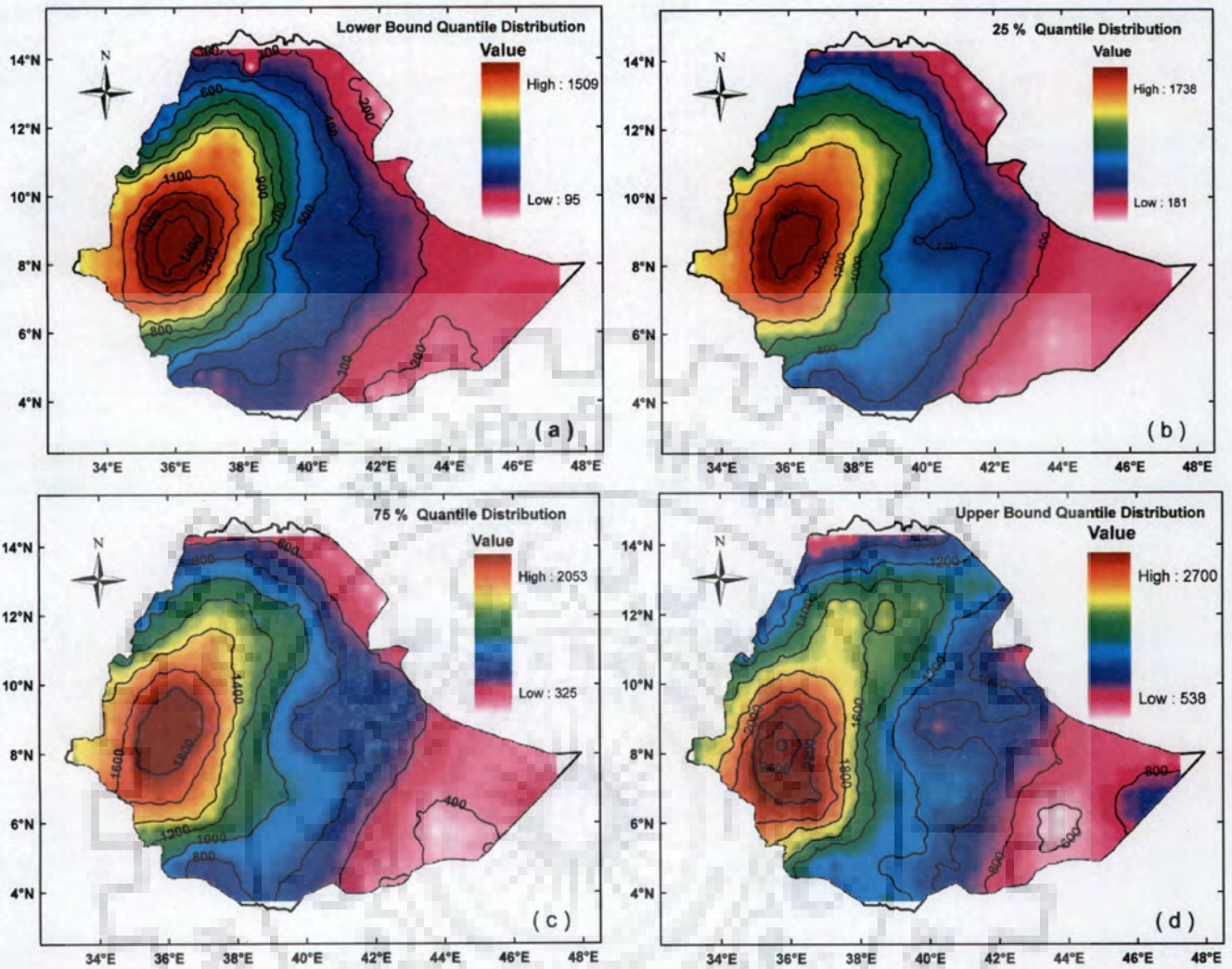


Fig. 2.8 Spatial distribution of lowest bound, 25, 75 and upper bound percentile annual rainfall of Ethiopia averaged over the time period 1951-2000

Table 2.5 Total number of grid points with significant trends at 5 and 10 percent significance level

Variables	MK Original				MK Pre-whitened			
	$\alpha=5\%$		$\alpha=10\%$		$\alpha=5\%$		$\alpha=10\%$	
	IT	DT	IT	DT	IT	DT	IT	DT
Annual rainfall	17	20	67	42	4	4	8	15
Seasonal rainfall	0	87	24	118	0	8	0	68
maximum 30-days	72	73	90	77	(-)	(-)	(-)	(-)
α =significance level	IT=increasing Trend				DT=Decreasing Trend			

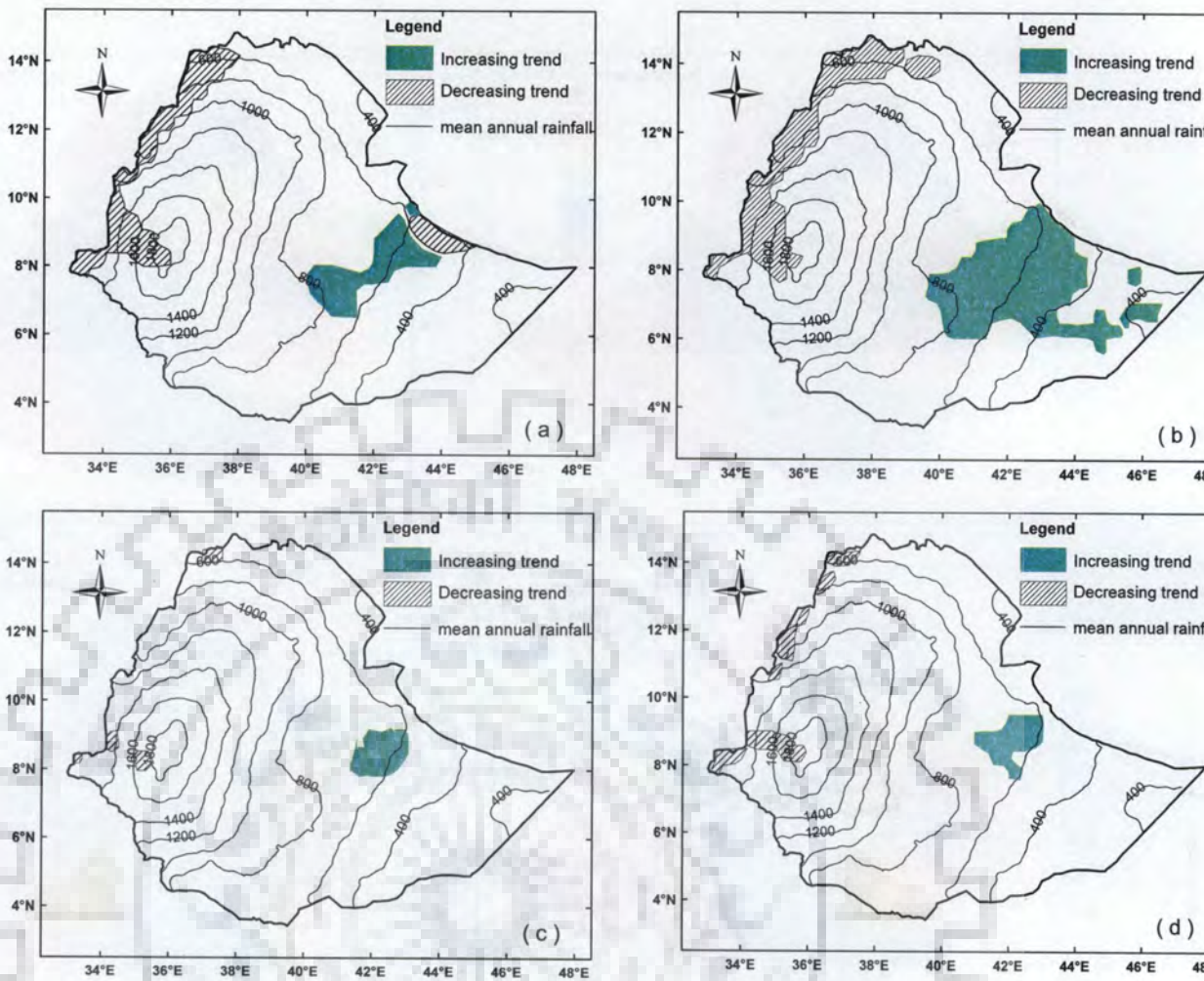


Fig. 2.9 Regions showing significant trend of annual rainfall series (1951-2000) with mean annual rainfall contour overlaid. (a) MK-test at $\alpha=5\%$, (b) MK-test at $\alpha=10\%$, (c) MK pre-whitened test at $\alpha=5\%$, (d) MK-Pre-whitened at $\alpha=10\%$

Limited portion of eastern part of the country shows increasing annual rainfall trend (Fig. 2.9) over the analysis period based on both MK original and pre-whitened test methods. However, MK original test at 10% significance level is an invariant resulting in increasing annual rainfall trend covering substantial part of eastern Ethiopia. Most part of the eastern and north eastern peripheries show significant decreasing annual rainfall trend, whereas all other parts of the country discern no significantly increasing or decreasing trends. Seasonal summer rainfall follows decreasing trends in most parts of the northern, north-western and north-eastern Ethiopia. An increasing seasonal rainfall trend is signaled at limited part of eastern (Somali and eastern Oromiya) region at 10 percent significance level for unfiltered series (Fig. 2.10).

Table 2.6 Annual rainfall trend test statistics for significant trends at $\alpha = 0.05$

Grid No.	Statistical parameters		MK	r_1 and its significance		Sen's slope and confidence limit			trend
	mean	std	P- values	r_1	significance	b	b_{95min}	b_{95max}	
48550	537.7	140.7	0.044	-0.006	†	2.31	0.08	5.32	I
48757	666.6	157.2	0.046	0.109	‡	3.18	0.13	6.42	I
48967	655.3	149.0	0.039	0.149	‡	3.33	0.20	6.38	I
48968	611.0	142.5	0.040	0.105	‡	3.22	0.24	5.89	I
49173	630.5	142.9	0.032	0.101	‡	3.40	0.39	5.97	I
49174	570.8	135.0	0.025	0.084	†	3.04	0.42	5.52	I
49175	508.7	125.8	0.036	0.055	†	2.50	0.17	5.11	I
49366	783.2	144.6	0.035	0.244	‡	2.86	0.19	5.64	I
49367	767.0	143.0	0.035	0.248	‡	2.33	0.12	5.67	I
49369	687.1	141.2	0.045	0.167	‡	2.63	0.14	5.68	I
49370	605.1	131.4	0.040	0.117	‡	2.57	0.13	5.60	I
49373	462.6	124.2	0.048	0.020	†	2.29	0.00	4.84	I
49561	818.0	153.8	0.046	0.173	‡	3.19	0.03	6.42	I
49562	794.0	148.7	0.034	0.226	‡	3.13	0.23	5.99	I
49563	729.6	142.4	0.027	0.206	‡	2.72	0.34	5.36	I
49756	804.3	157.3	0.049	0.131	‡	3.33	0.12	6.73	I
49757	682.1	138.3	0.036	0.144	‡	2.67	0.22	5.50	I
46758	439.3	73.8	0.017	0.285	‡	-1.47	-3.04	-0.37	D
46759	473.1	76.5	0.012	0.331	‡	-1.70	-3.20	-0.42	D
46760	496.3	90.1	0.028	0.161	‡	-1.68	-4.04	-0.26	D
46958	624.6	91.0	0.013	0.364	‡	-1.73	-3.89	-0.40	D
46959	703.7	103.9	0.020	0.385	‡	-1.96	-4.23	-0.26	D
47154	736.5	104.7	0.020	0.380	‡	-2.06	-4.40	-0.31	D
47155	808.5	119.6	0.049	0.416	‡	-2.00	-4.49	0.00	D
47344	887.8	128.2	0.036	0.414	‡	-2.43	-5.33	-0.15	D
47537	858.6	128.1	0.040	0.378	‡	-2.64	-5.32	-0.05	D
47725	798.5	110.2	0.030	0.371	‡	-2.60	-4.72	-0.31	D
47916	956.2	110.6	0.018	0.413	‡	-2.44	-4.81	-0.55	D
48118	952.7	108.6	0.035	0.390	‡	-2.36	-4.77	-0.17	D
48532	1213.0	140.3	0.050	0.324	‡	-2.90	-5.85	0.00	D
48740	1320.1	149.7	0.030	0.309	‡	-3.75	-6.17	-0.35	D
48741	1438.7	162.3	0.040	0.335	‡	-3.45	-7.03	-0.18	D
49155	1223.3	145.8	0.004	0.287	‡	-3.90	-6.90	-1.16	D
49156	1314.6	158.5	0.026	0.179	‡	-3.46	-6.47	-0.55	D
49159	1798.7	267.2	0.012	0.491	‡	-5.52	-10.27	-1.18	D
49160	1929.3	278.9	0.040	0.445	‡	-5.00	-10.34	-0.32	D
49352	1203.4	154.5	0.032	0.198	‡	-3.43	-6.20	-0.32	D

‡ = r_1 significant at $\alpha = 0.05$ † = r_1 NOT significant at $\alpha = 0.05$ I = Increasing trend D = Decreasing trend

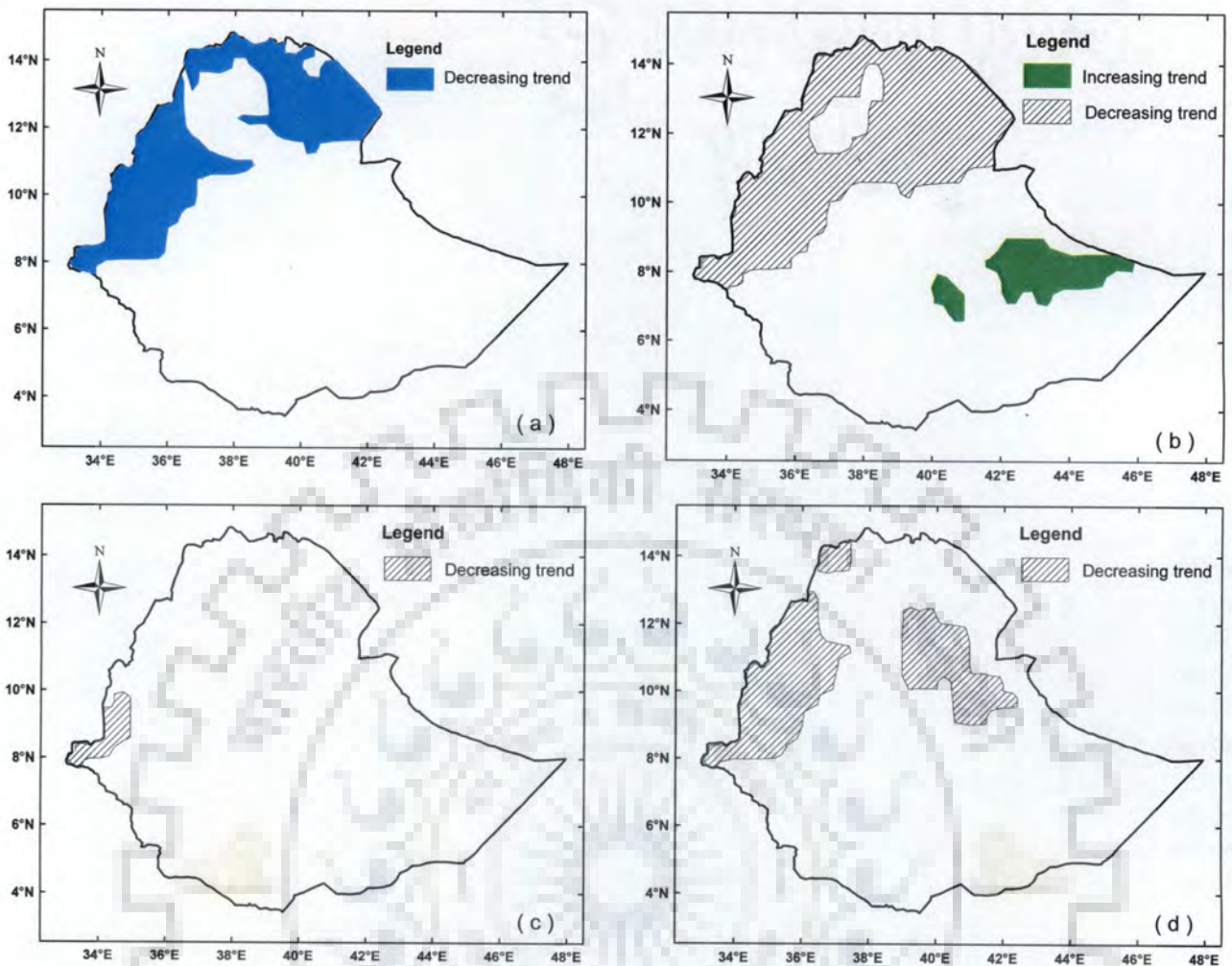


Fig. 2.10 Map of regions showing significant trend of seasonal rainfall series (1951-2000); (a) MK-test at $\alpha = 5\%$, (b) MK-test at $\alpha = 10\%$, (c) MK pre-whitened test at $\alpha = 5\%$, (d) MK pre-whitened at $\alpha = 10\%$

A noticeable fall in number of grid points detected as significant trends (increasing or decreasing) is observed due to pre-whitening. Most precipitation grid points captured as increasing or decreasing trend when original series is subjected to MK-test, fail to show similar trends for pre-whitened series. Fig. 2.9 and Fig. 2.10 show the area covered by significant trends using both methods. The percentage area covered by significant annual rainfall trends dropped to 27.3 and 21.7 percent at 5 and 10 percent significance level respectively when pre-whitened series is subjected to trend analysis. Similar reduction (9.1 and 47.2 percent) is evident for seasonal series at 5 and 10 percent significance level respectively. It is observed that pre-whitening eliminates some of the actual trend components from the time series and should be applied cautiously in trend detection. This is in agreement with discussions by Hamed (2009) addressing the adverse effects of pre-whitening when true trend exists in the time series. The

mutual influence between significant autocorrelation and associated trends in time series is also addressed with suggestive remedial techniques in the literature (Kulkarni and von Storch, 1995; Hamed and Rao 1998; Douglas et al., 2000; Yue et al., 2002).

Trends in extreme events are essential to study the impact of global climate change over regional climatic variability whereby present and future water resources planning and management sector extracts key information for sustainable resource utilization. Even though interpolation to finer grids could have some influence (such as generating outliers) in the distribution of extreme events over the region, trends in maximum 30-days rainfall events are examined without omitting the outliers. Contrary to substantial portion of northern and western regions of the country, the south-eastern regions show increasing trend of maximum 30-days rainfall. Severe drought years (1983-1984, 1987-1988 and 1990-1992) described as a period of significantly below 50 years average annual rainfall due to failure of main rainy season are identified from gridded rainfall dataset. The warm ENSO episodes documented in literature (Pankhurst, 1966; Quinn and Neal, 1987; Degefu, 1987; Tsegay, 1998) conforms to similar time span of the drought years, however, the cause-effect relationship between drought years and warm ENSO episodes requires further investigation and is not covered under present work.

2.6.4 Atlantic Multidecadal Oscillation (AMO) Signal and Rainfall

Understanding the effect of SST on regional rainfall pattern requires full investigation of dominating perturbations caused by global oceans such as north and south AMO, Indian Ocean modulation and Pacific Decadal Oscillation (Folland et al., 1986). In the present context, our investigation is limited to statistical analysis of AMO and rainfall index for possible association.

The association of AMO warm and ensuing cool phase to average annual rainfall is investigated by plotting AMO index computed from low-pass filtered area average sea surface temperature over North Atlantic region (Enfield et al., 2001) and time coinciding standardized annual rainfall over 1951-2000. A 10 year running average of standardized annual rainfall is superimposed onto the AMO index and the correlation coefficient between AMO and annual rainfall index is examined. It has been observed that the annual rainfall pattern in the northern half of the region (above 9°25' latitude) including Blue Nile basin follows a modestly good correlation ($R^2=0.55 - 0.83$) to AMO index where the warm AMO phases (1951-1965 and 1996-2000) are associated to above average annual rainfall in the region (Fig. 2.11). However, a noticeable diminution in correlation ($R^2 = 0.01 - 1.0$) is reflected in the southern region (below

9°25' latitude). The results from present analysis are in agreement with previous studies (Segele and Lamb, 2005; Jury, 2010; Taye and Willems, 2012). Fig. 2.12 shows partial correlation coefficient between AMO and rainfall index over the analysis window. Diverse pattern of fluctuation in wetter and drier years is ascertained from the plot of standardized decadal running average of annual rainfall, i.e., above and below long term average rainfall oscillates with a period of 10-28 years across the country. The associated perturbation of AMO on Ethiopian rainfall cannot be discounted as the north and central part of the country contiguous to the eastern part of Sahel region shows modestly strong AMO-rainfall correlation. However, the association is very weak to rainfall grid points in the southern part of the country. The warm (1951-1965 and 1996-2000) and cool (1966-1995) phases of AMO are well associated to the above and below average rainfall index respectively in northern latitudes of the country whereas a contrasting case is eminent in the southern latitudes.

2.7 CONCLUSIONS

Characterization of seasonal and interannual spatial and temporal variability of rainfall in a changing climate is vital attempt to assess climate induced changes and suggest adequate future water resources management strategies. Trends in seasonal, annual and maximum 30-days extreme rainfall over Ethiopia are investigated. Spatial coherence of annual rainfall among contiguous rainfall grid points is examined for possible spatial similarity across the country. Furthermore, correlation between time coinciding north Atlantic Multidecadal Oscillation (AMO) index and annual rainfall variability is examined to understand the underlying coherence.

Main summer season (July - September) and annual rainfall exhibit significant decreasing trend in northern, north-western and western part of the country whereas very limited portion of eastern blocks, bounded by 7°-9°N latitude and 43°- 45°E longitude, show increasing annual and seasonal (April-October) rainfall trend. In most other parts of the country (approximately 77% of geographical coverage) the annual rainfall series remained without significant trend for the second half of 20th century (Figs. 2.9 and 2.10). This is in agreement with Mwale et al. (2004) arguing that East Africa suffered a consistent decrease in the September–October–November rainfall from 1962 to 1997 and climate trend analysis of Kenya (Fact Sheet-2010) that suggests the unlikely increase of summer rainfall for the region for the

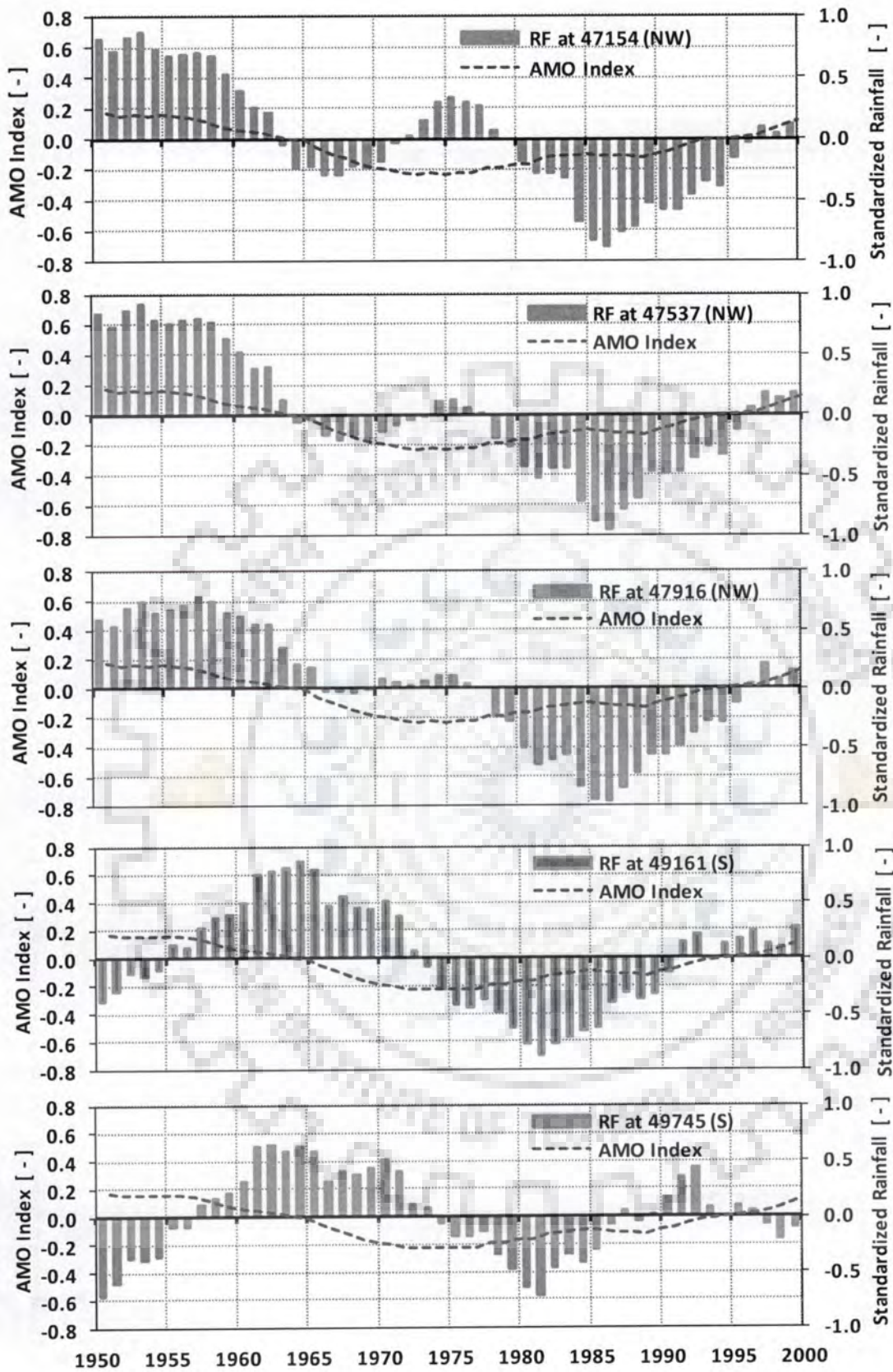


Fig. 2.11 A 10-year running average of standardized annual rainfall (smooth line) superimposed over AMO index (dashed line). Precipitation grid locations are given with numbers and corresponding compass directions (NW=North-West, NE= North-East, C= central, S = South, NC=North-Central)

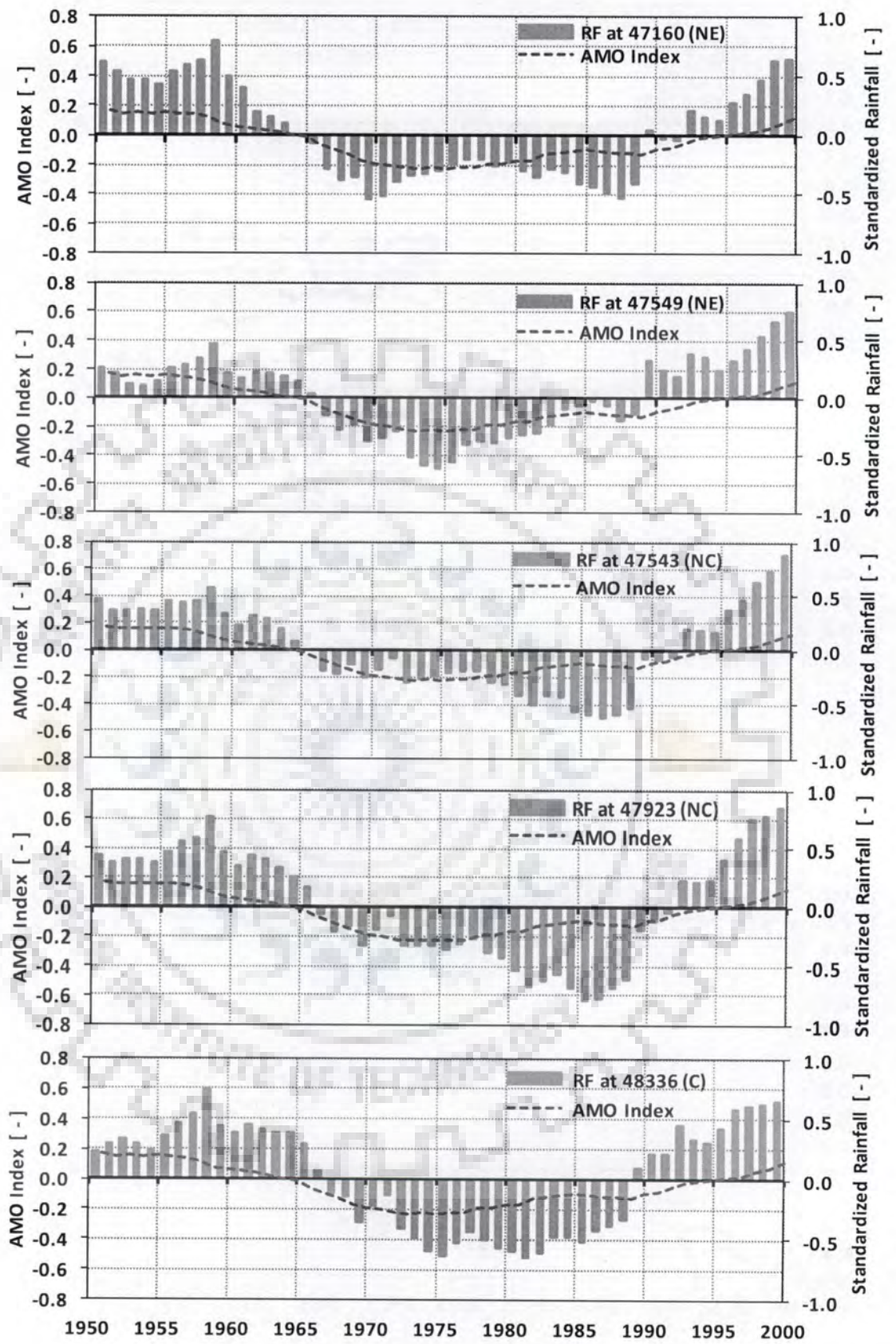


Fig. 2.11 Cont'd

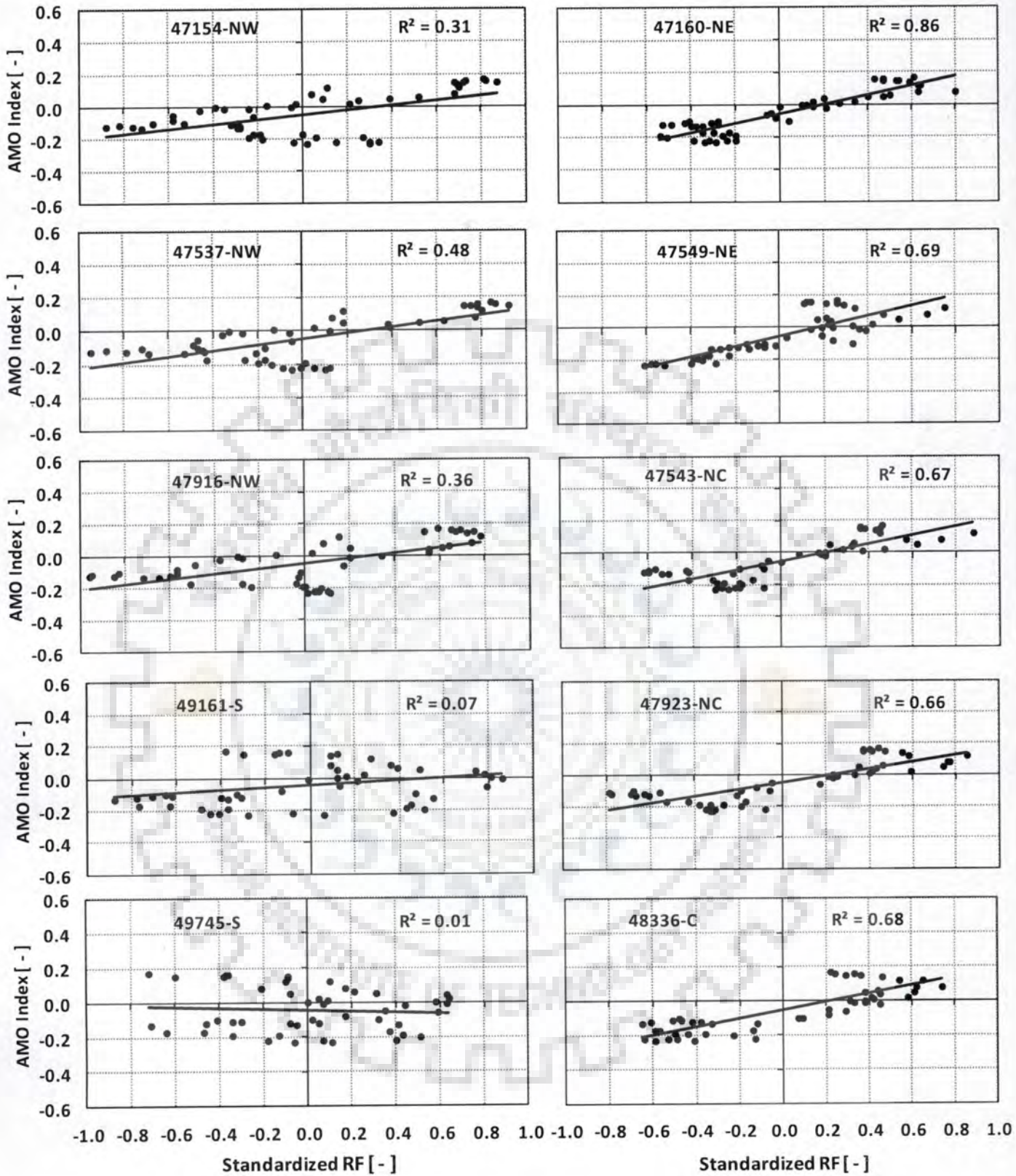
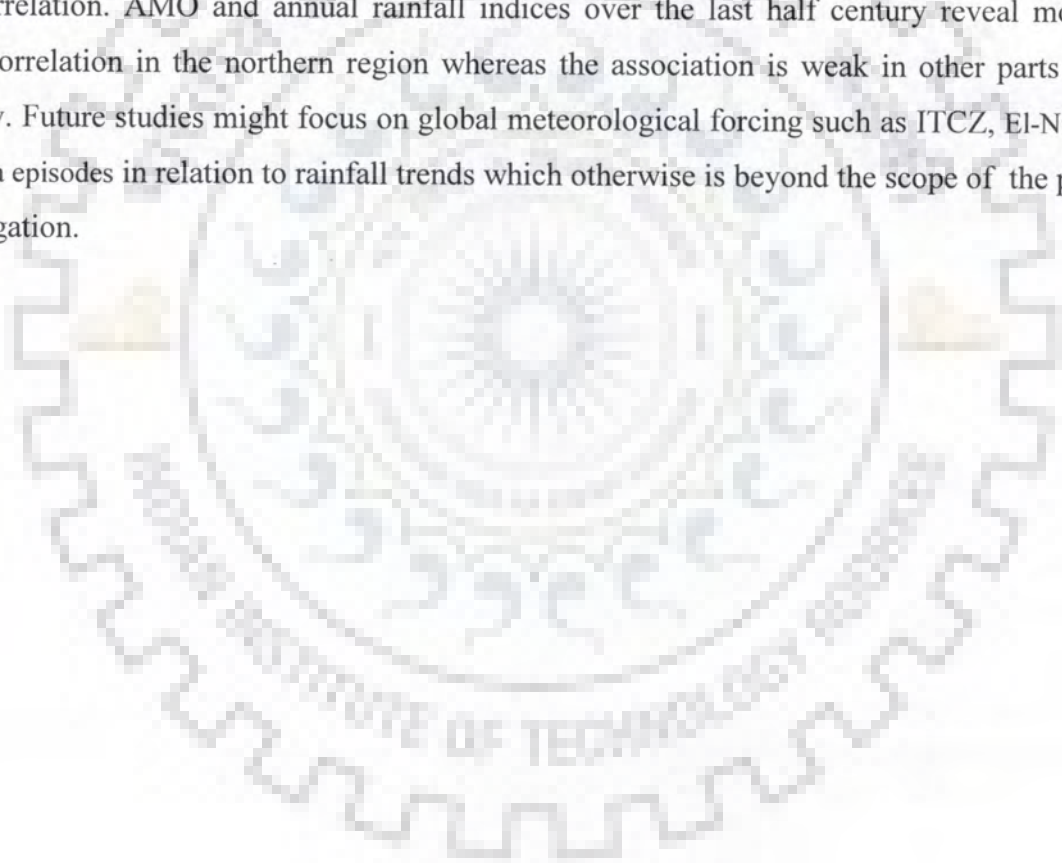


Fig. 2.12 Correlation coefficient (partial) between standardized annual rainfall and AMO index at specified grid locations (NW=North-West, NE= North-East, C= central, S = South, NC=North-Central)

observed series. Moreda and Bauwens (1998) also observed a declining mean annual and summer rainfall over four consecutive decades since 1951 in the upper Awash basin of Ethiopia. However, IPCC (2007a) Fourth Assessment Report argues that the projected (21st Century) mean annual rainfall trend is likely to be increasing in East Africa.

Regions with moderately high to high rainfall (western and north western regions) are characterized by high positive lag-one and lag-two serial correlation whereas the serial dependence diminishes as further moved to east and south. Based on the Moran's spatial analysis, annual rainfall for the total sampling points (381 grid stations) is divided into four zones of annual rainfall spatial autocorrelation. Regions with high annual and seasonal rainfall distribution exhibit high indices of temporal (r_1 and r_2) and spatial (Moran index) autocorrelation. AMO and annual rainfall indices over the last half century reveal modestly good correlation in the northern region whereas the association is weak in other parts of the country. Future studies might focus on global meteorological forcing such as ITCZ, El-Nino and La-Nina episodes in relation to rainfall trends which otherwise is beyond the scope of the present investigation.



INVESTIGATION OF NON-STATIONARITY IN HYDRO-CLIMATIC VARIABLES IN THE RIFT VALLEY LAKES BASIN OF ETHIOPIA

3.1 INTRODUCTION

Hydro-climatic variables are under constant dynamism over time and space domain and are subjected to trends and periodic components. The hydrologic variability could be attributed to either a single or combined effect of (1) natural climatic variability and change (cyclical astronomical behaviour, volcanic eruption and oceanic circulation) and (2) anthropogenic effects (increased greenhouse gases content, catchment wise man-induced disturbances) (McGuffie and Henderson-Sellers, 2005).

Many early time series models, both statistical and empirical, are based on the fundamental assumption of stationary model parameters (Box and Jenkins, 1970) and rely on notion that past is representative of the future. However, the hydrologic model parameters do not remain constant and, as a matter of fact, require continuous revision to mimic the dynamic environment as a result of global climatic change and man-induced disturbances in the watersheds. Underpinned by various climate models, such approximation requires further improvement to account for non-stationarity (Leclerc and Ouarda, 2007; Wilby, 2007; Vaze et al., 2010). More vividly, prominent researchers of recent days (Milly et al., 2008) have stressfully asserted that the fundamental assumption of stationarity is undermined by climate change and as a result future water supply, demand and risk assessment are highly affected by such variability.

To develop stochastic model presumably representing the non-stationary behavior of time series, firstly existence of non-stationarity in time series should be investigated and secondly the most probable reason for such nonstationarity should be identified. In most of the studies reported in literature, only the first aspect, i.e investigation of nonstationarity in hydro-climatic variables, is widely endeavoured. The second aspect, i.e whether the nonstationarity is due to climate change and/or catchment changes is seldom attempted. In light of this,

simultaneous analysis of both hydro-climatic variables and land use dynamics is required. In the present study both of these aspects are investigated for watersheds from Rift Valley lakes basin of Ethiopia.

The behavior of some transitory or hidden hydrologic processes could not be easily captured by a single time series model due to intrinsic model deficiency. The hydrologic behavior that could not be captured by one stochastic model due to such inherent model deficiency could be made easy through other approaches. Therefore, application of multiple hydrologic time series models (Refsgaard et al., 1989; Lorup et al., 1998; McCuen, 2003) to detect the prevailing long and short term changes in hydro-climatic variables increases the confidence to adequately explain the behaviour of time evolution of hydro-climatic series.

Recent studies (Boer et al., 1992; Dore, 2005) strongly argue that global reallocation of precipitation and streamflow is a realistic signature of climate change though regional and local variability is more pronounced (Markgraf et al., 2000). Constantly increasing demand of water use for various purposes and intense rural land use operation to feed the ever growing population substantially altered the flow regimes in eastern parts of Africa (Koutsouris et al., 2010). The effect of frequent rainfall anomalies and associated variation in flow volume has become more pronounced in rain-fed agriculture and hydropower sector (Ziervogel et al., 2008; Conway and Schipper, 2011). Added to such anomalies, man-induced catchment modification aggravated the alteration of flow regime, however, the latter is not well perceived by many.

The Rift Valley lakes basin of Ethiopia has undergone a major land use change in the past, and such alterations remain vivid nowadays too, affecting the hydrology and ecology of the basin. Hawassa lake, one among Ethiopian central Rift Valley lakes, is known for its beautiful scenery and exotic aquatic life. Foreshadowed by disquieting future climate condition, growing demand of available water for agricultural and water supply purposes raised the apprehension for sustainability. Similar environmental pressures are also practical in other watersheds of economic interest in the Rift Valley basin where the use of available water resources for irrigation is becoming crucial for rural livelihood. Well motivated by environmentally and ecologically fragile nature of the basin as a result of resource competition, provision of more realistic explanation about time evolution of streamflow, analysis of lake level and precipitation in relation to climate change and prevailing catchment dynamics at local level could help to render key information to water resources planners and end users. The

present study is aimed at investigation of non-stationarity and subsequent identification of possible reasons for such variability in hydro-climatic elements over various length of time.

3.2 SHORT AND LONG TERM TIME DEPENDENCE IN HYDRO-CLIMATIC VARIABLES

Historical hydro-climatic observations are composed of trends, shifts, periodicities and jumps as a result of natural and man-made influences within the climate and catchment system. The random nature of hydrologic variables makes the existing pattern very complex and hence it is difficult to model them deterministically. However, the uncertain part of the hydrologic process can be modelled stochastically having known priori information with some level of confidence. Therefore, the underlying behavior of time series can be traced by extracting dominant signals representative of the time evolution of the variables from past observations.

Siegel and Castellan (1988) describes the relative merits of parametric and non-parametric test statistics applicable to time series models. The parametric test approach usually assumes that the observation is drawn from homoscedastic and normally distributed population whereas the non-parametric test is a distribution-free method entirely based on the ordinals or signs of the observations rather than the scores. Even though parametric methods are robust, they are not successfully applied when the observation deviates from normality and the available dataset is limited to rankings rather than actual scores.

As water resources planning and management is highly influenced by random and uncertain physical processes, investigation of short and long-term persistence in hydro-climatic variables is useful to identify how the past knowledge is sufficient enough to understand the future behavior of a time series. The tendency of a system to remain in the same state from one observation to the other termed as persistence is a common phenomena in hydrologic time series. This is because most hydrological and geophysical processes are influenced by the carryover inertia that yields to the occurrence of other similar events. For example, the likelihood of rainy days to follow another rainy day is greater than to follow a dry day.

Malamud and Turcotte (1999) classify persistence in time series in terms of time-scale (short and long) and behavioural strength (weak and strong). If trend and periodic components of a time series are removed, the remaining behaviour is well described by the stochastic component. Virtually stochastic components are composed of statistical distribution of the

parameters and persistence that could be behaviourally weak, strong or of white noise. Autocorrelation, rescaled range analysis, spectral analysis and wavelet transformations are commonly used methods to detect persistence in time series.

Short-term persistence occurs when the effect of an observation on future event diminishes at short length of time whereas in long-term persistence the correlation between adjacent values in the long range is dominant. Short term persistence can be explained in terms of autocorrelation function where the successive observations exhibit similar informations. As time lag extends longer, the time dependence of the variables diminishes. However, in some hydrological datasets the observed dependence extends to large lags of infinite memory.

Hurst (1951) introduced a cumulative sum theory to analyze long range dependence of water in reservoir. In 1956, he further extended his study to the computation of adjusted rescaled range analysis and concluded that for purely random process the Hurst's coefficient (H) is equal to 0.5 whereas $H > 0.5$ for long memory processes. Mandelbrot and Wallis (1968) later came up with explanatory connotation of long-term persistence to the Biblical legend of 'Joseph Effect' in the Old Testament (*Behold, there come seven years of great plenty throughout all the land of Egypt; And there shall arise after them seven years of famine...*, Genesis 41: 29-30) to describe the long-term memory in time series. Since Hurst's first motivation, the long term memory notion has got growing attention in the area of economics, hydrometeorology and geophysical data analysis.

Climatic variables such as rainfall and temperature are highly influenced by synoptic scale influences and show certain level of variability on time-space domain. One of the hallmarks of time-trend analysis over the last couples of decades is to identify the non-stationary behavior of hydro-climatic time series in space-time domain emanating from variable natural and man-induced influences.

Many hydrologic time series events are composed of seasonal variability either in the short or long-term runs of the observation. The cyclic nature of a signal and its strength which collectively forms the spectrum of the signal could be explained by advanced periodic functions such as spectral and wavelet analyses.

Andreo et al. (2006) used spectral and wavelet methods to identify the distribution of periodicity in multiannual temperature, rainfall and groundwater outflow observations in

Iberian Peninsula. The observed multiannual periodic variations in south of Iberian Peninsula are attributed to climatic variations such as North Atlantic Multidecadal Oscillations. Almedeij and Al-Ruwaih (2006) applied unsmoothed spectral estimate (periodogram) approach to investigate the periodic pattern of groundwater fluctuations in residential province of Kuwait and associated the prevailing variations to Quasi-Biennial Oscillation in zonal wind.

Fourier transform based spectral analysis is limited to the frequency domain and does not provide the time-frequency distribution of a signal. The property that how the power of a signal changes over time is not captured by the conventional Fourier transform constructed from an infinite oscillating sine and cosine functions. Processes that involve stationary periodic behaviour, such as electronic signals in electrical engineering, can be described by the Fourier transform. However, hydrological processes usually involve a transient processes with varying frequency over time (Labat, 2005, Labat et al., 2005) and could not be adequately represented by the Fourier transform. To circumvent this limitation, a wavelet analysis that operates in frequency-time domain became appropriate mathematical tool.

Brillinger (1994) carried out the Haar wavelet analysis to examine abrupt anomalies in the mean river level of Nile at Aswan Dam of Egypt and Amazon at Manaus of Brazil. The river level change points were at the outset of twenty century (the time where low Aswan dam was built) for Nile river and around 1970 for Amazon river. Gaucherel (2002) used continuous wavelet transform to identify streamflow variability that is not well explained by standard times series models in French Guyana basins of South America. He detected a short March summer meteorological phenomena as a result of Atlantic Ocean influence in the continent. Labat et al. (2005) applied wavelet analysis method to investigate streamflow from different basins and climatic indices (Southern and North Atlantic Multidecadal Oscillations) variability. They identified different time-scale cycles extending from couples of months to three decades in streamflow and climatic indices.

Wavelet analysis is gaining momentum in recent years and became applicable to study temporal variability of environmental aspects such as hydrology and water quality monitoring (Kang and Lin, 2007; Koirala et al., 2010), flood forecasting (Adamowski, 2008), precipitation variability analysis (Partal and Kucuk, 2006) and wind velocity and temperature variability study (Bolzan and Vieira, 2006; Steel and Lange, 2007).

3.3 STUDY AREA AND DATA USED

3.3.1 The Study Area

The Rift Valley (RFV) lakes basin of Ethiopia (Fig. 3.1), situated in the horn of Africa, is known for its major natural and artificial lakes (Koka , Ziway , Langano ,Abiyata, Shala, Hawassa, Abaya, Chamo and Chew Bahir) of ecological interest and respective tributaries debouching into terminal pool. The RFV divides the country into two halves of northern and southern highlands of massive escarpments. Geographically the basin is located between $4^{\circ}24'29''$ to $8^{\circ}26'38''$ N latitude and $36^{\circ}35'45''$ to $39^{\circ}23'31''$ E longitude with sub-humid to moderate tropical semi-arid climatic condition. Three major sub-basins described by their main lake systems form the Rift Valley lakes basin of Ethiopia; the first sub-basin comprises lakes Ziway, Abiyata and Langano, the second is lake Awassa sub-basin and the third sub-basin encompasses the southern lakes of Abaya, Chamo and Chew Bahir. Annual and ephemeral streams contribute substantial amount of runoff to the terminal lakes.

Mean annual rainfall varies from 600 mm at extreme downstream to 1220 mm at uppermost western region of the basin. In the present study, lake level, streamflow and precipitation variability and land use dynamics investigation concentrate on three catchments of the RFV lakes basin. These include Hawassa Lake (1460 km^2), Bilate (5330 km^2) and Hare (166.5 km^2) catchments extending from middle to lower regions of the RFV lakes basin drainage system.

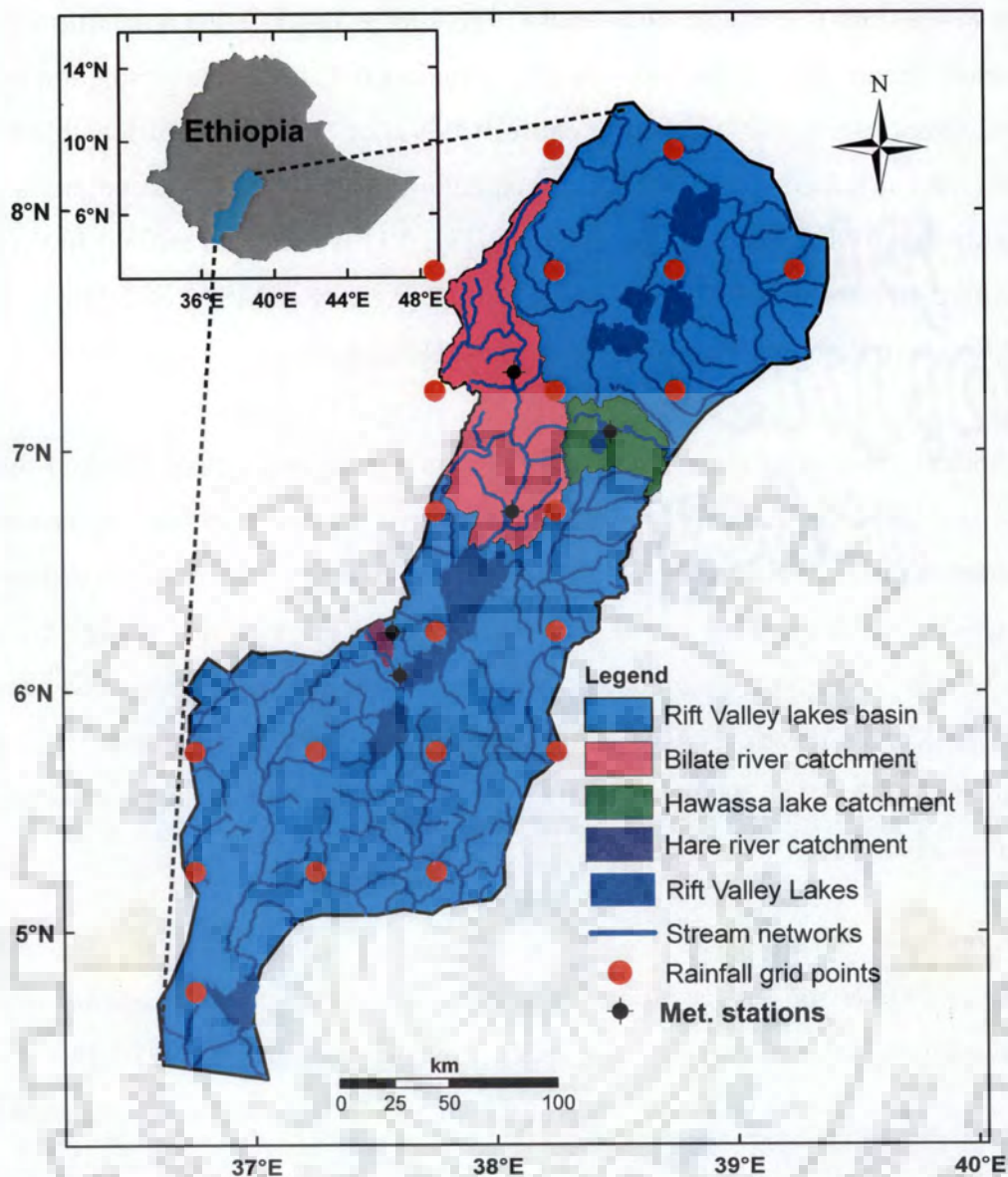


Fig. 3.1 Map of Rift Valley lakes basin showing study catchments, observed and gridded rainfall location points

3.3.2 Hydro-climatic Data

Hydro-climatic parameters used in the present investigation can be broadly categorized as streamflow, lake level and rainfall. Extreme and average streamflow records are used to better explain fluctuation in hydro-climatic variables; accordingly, mean annual, annual maximum and minimum daily streamflow and lake level records are utilized for subsequent analysis. Hydro-climatic variables of varying temporal and spatial extents are acquired from various organizations and online sources. Observed daily streamflow data are obtained from Ministry of Water Resources (MoWR), Ethiopia for the period of 27-38 years, i.e., Bilate

streamflow (1971-2005), Hawassa lake level (1970-2007), Tikur Wuha streamflow (1980-2007) and Hare streamflow (1980-2006). A 0.5° latitude x 0.5° longitude resolution gridded rainfall data (Beck et al., 2005) covering entire Rift Valley lakes basin of length 50 years (1951-2000) are acquired from Global Precipitation Data Center via online sources (<http://gpcc.dwd.de>). Observed daily rainfall data (Fig. 3.1) for selected stations in the study area is accessed from National Meteorological Service Agency (NMSA) of Ethiopia, Addis Ababa and Southern Region Meteorological Agency, Hawassa.

Historical observations and global rainfall data records are further checked for data consistency and gaps. As statistical models are sensitive to minor changes in time series, thorough examination of observed values in terms of time series plot, comparison with adjacent stations and regressing runoff over rainfall have been carried out to minimize systematic errors in observed magnitudes. Among available rainfall stations, five stations, namely; Alaba Kulito, Hawassa, Arba Minch Estate Farm and Chenchu each with record lengths extending from 1970-2009 and Bilate Estate Farm (1970-2003) are selected for time dependence analysis.

An optimally interpolated $1^{\circ} \times 1^{\circ}$ latitude and longitude monthly Sea Surface Temperature (SST) version-2 is acquired from Earth System Research Laboratory Physical Science Division (<http://www.esrl.noaa.gov/psd/>) (Reynolds and Smith, 1995). The Western Indian Ocean surface bound by 0° - 10° N latitude and 45° - 65° E longitude that could have influence on Ethiopian rainfall pattern has also been utilized in the subsequent analysis. SST data from 1982-2010 is used to examine its association to available observed rainfall in Rift Valley lakes basin of Ethiopia.

3.3.3 Land Use/Land Cover Data

Orthorectified four band multi-Spectral Scanner (MSS) Landsat-4, Thematic Mapper (TM) and seven band Enhanced Thematic Mapper Plus (ETM+) land cover images are acquired from Global Land Cover Facility archives (<http://glcf.umiacs.umd.edu/data/landsat>) and further classified using ERDAS Imagine 9.2 and ArcGIS 9.3 following vigorous standard image processing procedures. Table 3.1 summarizes the characteristics of raw satellite images utilized in the present study.

Table 3.1 Landsat images acquired and their respective characteristics

Area	ID	Sensor Type	Date acquired	Path/Row
Rift Valley Lakes Basin	029-736	MSS	Jan. 31, 1973	181/055
Rift Valley Lakes Basin	012-383	TM	Nov. 22, 1984	169/055
Rift Valley Lakes Basin	012-382	TM	Nov. 22, 1984	169/054
Rift Valley Lakes Basin	012-371	TM	Jan. 21, 1986	168/055
Rift Valley Lakes Basin	037- 657	ETM+	Nov. 26, 2000	169/054
Rift Valley Lakes Basin	037- 658	ETM+	Nov. 26, 2000	169/055
Rift Valley Lakes Basin	037- 883	ETM+	Feb. 5, 2000	168/055

3.4 STATISTICAL TEST METHODS

Persistence, a characteristic feature of fluctuation in weather and climatic elements where the rate of mixing is strong and eventually decreases as the time span between events of same order increases, has been analyzed using various statistical models in terms of trends and periodicities. The various statistical tests used in the present study are well mentioned in different literature; however, a brief statistical background is summarized in the subsequent sections.

3.4.1 Autocorrelation

Time dependence of successive values of a variable in a series is essential to assess randomness and identify possible time series model to represent the hydrologic process. The first few lags of autocorrelation function are of interest while examining for randomness, however, time lags up to one-fourth of the observations are usually utilized to assess time series model of a particular process. The significance of lag one serial correlation coefficient (r_1) could be evaluated applying the t-test statistics with n-2 degree of freedom (Hirsch et al., 1993; Chatfield , 1981) and normally distributed exact test for lag-one (Clarke,1973). An exact test for lag-one serial correlation coefficient (Clarke, 1973) assumes that r_1 is normally

distributed with $N \left[-\frac{1}{(n-1)}, \frac{(n-2)^2}{(n-1)^3} \right]$. The upper and lower range of the exact test for

lag-one serial correlation for n observations at $\alpha= 0.05$ significance level is given as:

$$-\frac{1}{n-1} \pm 1.96 \frac{(n-2)}{(n-3)^{3/2}} \quad (3.1)$$

If the computed first order autocorrelation coefficient lies outside the range given in eqn. (3.1), then it is likely that r_1 is significantly different from zero. In such cases the random walk case where successive values in the time series exhibit short term dependence dominates. However, if the lag-one serial coefficient is not statistically significant, then the sample events are the result of random process where the white noise situation prevails. Serial dependence of second and third order is examined for significance using Anderson's credibility bounds (Anderson, 1942) when statistical significance of lag-one correlation coefficient is not justifiable.

The upper and lower bounds of the correlogram test statistic, β (Anderson, 1942) for lag k serial dependence at α level of significance for n observations is given by:

$$\beta = -\frac{1}{n-k} \pm Z_{1-\alpha/2} \left(\frac{(n-k-1)^{0.5}}{n-k} \right) \quad (3.2)$$

where $Z_{1-\alpha/2}$ is independently and identically distributed normal variate.

3.4.2 Von Neumann Ratio Test

It is a non-parametric test for independence usually applied to time series of length approximately greater than thirty years. The test statistics (R) for a time series $Z(t)$ of length N with the null hypothesis of independence (von Neumann, 1941; Bartels, 1982) is approximated as:

$$R = \frac{N \sum_{t=1}^N (Z(t+1) - Z(t))^2}{(N-1) \sum_{t=1}^N (Z(t) - \bar{Z})^2} \quad (3.3)$$

with \bar{Z} being the mean of the series. The test statistics follows a normal distribution with mean and variance of $[2N/(N-1)]$ and $[4(N-2)/(N-1)^2]$ respectively. The standardized test statistic, C , is given by:

$$C = \frac{R - \frac{2N}{N-1}}{\left[\frac{4(N-2)}{(N-1)^2} \right]^{1/2}} \quad (3.4)$$

If $|C| > Z_{(1-\alpha/2)}$ where $Z_{(1-\alpha/2)}$ is the value of standard normal variate at $(1-\alpha/2)$ significance level, the null hypothesis that the series consists of independent observations is rejected.

3.4.3 Mann-Kendall (MK) Trend Test

The Mann-Kendall (Mann, 1945; Kendall, 1975) trend test is a distribution free non-parametric test originally developed for non-correlated data. Mann-Kendall family of trend tests are commonly used methods to detect monotonic trends in streamflow (Douglas, 2000; Kahya and Kalayci, 2004), precipitation (Xu et al., 2003; Partal and Kahya, 2006), temperature (Jhajharia and Singh, 2011), evaporation and evapotranspiration (Jhajharia et al., 2009; Dinpashoh et al., 2011; Jhajharia et al., 2012) time series. Statistical background of Mann-Kendall trend test is elaborated in section 2.4.4. Existence of possible step change in streamflow and lake level is also investigated using non parametric Mann-Whitney-Pettitt's (Pettitt, 1979) test. Details of test statistic can be referred from the author.

Presence of significant positive serial correlation in hydro-climatic time series affects subsequent trend test (Kulkarni and von Storch, 1995; Yue et al., 2002) and need to be removed prior to trend analysis. On the other hand, presence of significant trend also alters the magnitude of serial dependence. Such mutual influence between serial correlation and trend is discussed in Yue et al. (2002). To circumvent such mutual influence, Yue et al. (2002) suggests pre-whitening the time series followed by detrending and finally blending the pre-whitened series with deterministic trend component. Trend analysis could be carried out on final blended time series (X^C) which significantly reduces the effect of serial correlation on trend detection.

Yue et al. (2002) summarizes the following steps to detect significant trend under serially correlated time series. The slope of a trend line, b is identified and its statistical significance is examined. If the slope of the trend line is different from zero, then the detrended series (X^{DET}) of the time series X_t is computed as:

$$X^{DET} = X_t - b*t \quad (3.5)$$

with t being the time unit ($t = 1, 2, 3, \dots, N$). Secondly, Pre-whiten (X^{PW}) the detrended series using r_1 of the detrended series using

$$X^{PW} = X_t^{DET} - r_1*(X_{t-1})^{DET} \quad (3.6)$$

Thirdly, combine the pre-whitened series and deterministic trend component ($T=b*t$).

$$X^C = X^{PW} + b*t \quad (3.7)$$

3.4.4 Theil-Sen Trend Slope Estimator

The slope of trend line, b is estimated applying Theil (1950) and Sen (1968) referred herein after as Theil-Sen's approach. It is used to investigate the existence of trend and evaluate its strength (Gibbons et al., 2009), if any, compared to MK-trend test. Besides, the trend component of a series could be removed using slope of a trend line as in eqn. (3.5). Theil-Sen's trend slope estimator, Q , for N' number of data points is

$$Q = \frac{(X_j - X_i)}{(j - i)} \quad \text{for } j > i \quad (3.8)$$

Thus, the estimate of slope of trend line, b for equally spaced data points is given as:

$$b = \text{Median} \left[\frac{X_j - X_i}{j - i} \right] \quad \text{for } j > i \quad (3.9)$$

with X_i and X_j being data values at time i and j respectively. The trend slope identified in eqn. (3.9) should be tested for the null hypothesis of zero slope (no trends) by computing the confidence limits at prescribed significance level. The theoretical lower and upper confidence limits of Theil-Sen's trend slope are computed using the following relationship.

$$M_1 = \frac{N' - Z_{1-\alpha/2} * \sqrt{\text{Var}(S)}}{2} \quad (3.10)$$

$$M_2 = \frac{N' + Z_{1-\alpha/2} * \sqrt{\text{Var}(S)}}{2} \quad (3.11)$$

where N' being number of data pairs with $j > i$ and $Z_{1-\alpha/2}$ is the $(1-\alpha/2)$ value of the normal distribution. For two sided 95 percent ($\alpha = 0.05$) confidence limit the corresponding $Z_{1-\alpha/2}$ value is 1.96. The lower and upper confidence limits will be the $(M_1)^{\text{th}}$ and $(M_1+1)^{\text{th}}$ largest value of Q arranged in ascending order. If the $(M_1)^{\text{th}}$ value of Q is greater than zero, then the null hypothesis of no trend is rejected.

3.4.5 Spectral Analysis

The distribution of the variance of a process over frequency known as spectrum describes the frequency-dependent signals of a stochastic process. The sample raw spectral density function g_f for discrete series at any frequency f is estimated as:

$$g_f = 2 \left[1 + 2 \sum_{k=1}^m r_k \cos(2\pi f k) \right] \quad (3.12)$$

with r_k being the sample autocorrelation function and m is the maximum lag up to which r_k is computed. The maximum frequency that can be detected from the data points is 0.5 cycles per unit time. Accordingly, the frequency f at any harmonic number, k , is approximated as

$$f = \frac{0.5 * k}{m} \quad (3.13)$$

The spectral density function given by eqn. (3.14) is biased and not efficient. Therefore, the raw spectral estimated in eqn. (3.14) should be corrected to remove the bias using one of the following two methods. The first approach applies smoothing in the lag domain prior to estimation of the spectral density while the second method implements an equivalent smoothing technique in the frequency domain. The latter case has been applied in the spectral estimate of monthly streamflow series under consideration. An equivalent smoothing procedure to the Blackman and Tukey (1958) window is:

$$S_0 = \frac{1}{2}(g_0 + g_1) \quad (3.14)$$

$$S_k = \frac{1}{2}(g_k) + \frac{1}{4}(g_{k+1} + g_{k-1}) \quad \text{for } 0 < k < m \quad (3.15)$$

$$S_m = \frac{1}{2}(g_{m-1} + g_m) \quad \text{for } 0 < k < m \quad (3.16)$$

where g_0 and g_m corresponds to $f = 0$ and $f = 0.5$ respectively. The spectral estimate obtained from the above procedure usually has high and low spikes when plotted to harmonics and hence limiting the confidence interval (C.I) for further interpretation is required. The confidence interval is estimated from the chi-square distribution with ν - degree of freedom.

$$C.I = \frac{\nu \cdot \bar{S}_f}{\chi_{\nu(1-\alpha/2)}^2} < \gamma_f \leq \frac{\nu \cdot \bar{S}_f}{\chi_{\nu(\alpha/2)}^2} \quad (3.17)$$

$$\nu = \frac{2n}{m} - \frac{2}{3} \quad (3.18)$$

with \bar{S}_f being the average spectral estimate.

Periodic discrete hydrologic time series can appropriately be represented in terms of oscillating sine and cosine functions representative of the first few dominant harmonics. The finite Fourier series of a discrete time series X_t at finite number of time points, t_i ($i=1, 2, 3, \dots, n$) spaced equally can be described in terms of sine and cosine functions as:

$$X_t = \bar{X} + \sum_{m=1}^q a_m \cos(2\pi f_m t) + b_m \sin(2\pi f_m t) \quad (3.19)$$

with q being an integer function of $n/2$ and n is the maximum size of finite data points. The coefficients of the m^{th} harmonic a_m and b_m are given by:

$$a_m = \frac{2}{n} \sum_{t=1}^n X_t \cos(2\pi f_m t) \quad (3.20)$$

$$b_m = \frac{2}{n} \sum_{t=1}^n X_t \sin(2\pi f_m t) \quad (3.21)$$

with f_m being the m^{th} harmonic and is given as (m/n) for $m=1,2,3, \dots,q$.

3.4.6 Wavelet Transform

Hydro-climatic time series signals are composed of numerous transitory characteristics like trends, shifts and periodic components. In most cases, the conventional time series models fail to adequately isolate the dominant signal in time-frequency domain. The Short Fourier Transform (STFT) has been utilized to analyze the non-stationary behaviour of time series signal; however, it yields in constant resolution of signal at all frequencies. To overcome this problem, a wavelet transform that operates in multi-resolution mode by which different frequencies are analysed with different resolution became effective over the last couple of decade.

Partal and Kucuk (2006) applied Mann-Kendall test and wavelet based trend analysis to identify possible trends in annual precipitation at Marmara region of Turkey. The wavelet trend analysis documented as in Partal and Kucuk (2006) is the first appealing attempt of its kind to isolate the dominant periodic component that affects the precipitation trend. Wavelet transform is useful in extracting dominant time-frequency relationships by maintaining the energy of a signal pertaining to the original series. An explanatory set of documentation in wavelet analysis is presented in many literatures (Wang and Ding, 2003; Lau and Weng, 1995; Torrence and Compo, 1998; Labat, 2005), however, a concise theoretical background of wavelet transform is summarized herein to refresh the readers.

Wavelet transform decomposes a signal into a set of basis function called wavelets. The wavelets are generated from a single basic wavelet $\psi(t)$ called mother wavelet by scaling (dilation or compression) and translation as :

$$\psi_{\tau,s}(t) = s^{-1/2} \psi\left(\frac{t-\tau}{s}\right) \quad \tau, s \in \mathbb{R}, s \neq 0 \quad (3.22)$$

where $\psi_{\tau,s}(t)$ is a successive wavelet; s is a scaling (frequency) factor ; τ is shifting (time) factor and \mathbb{R} is the domain in real number.

For finite signal $f(t)$, the one dimensional successive wavelet transform of $f(t)$ is defined as ;

$$\Psi(\tau, s) = s^{-1/2} \int_{-\infty}^{\infty} f(t) \psi_{\tau,s}^*\left(\frac{t-\tau}{s}\right) dt \quad (3.23)$$

where $\psi_{\tau,s}^*(t)$ is a complex conjugate function of $\psi(t)$. In wavelet transform the translation parameter, τ is related to the location of the wavelet function as it is shifted to the signal. Thus, time information of the finite signal is obtained from translation parameter. The scaling parameter, s either compresses or dilates the signal. It is an absolute inverse of frequency and carries detail information associated to frequency domain. Many hydrologic time series data are characterized by hidden signals that provide subtle information during time series analysis. Under such circumstances dilating the signal (using large scales) provides detail information about the hidden signal. Large scales (low frequencies) last for entire duration of the signal and hence useful in capturing valuable information over the signal length. In contrast, small scales (high frequencies) compress the signals and are useful when global signal information is required.

In real applications successive wavelet signals are discrete and hence computing the wavelet coefficients at discrete points generates sufficient details. If scale and position are so selected based on power of two, the discrete wavelet transform has the form:

$$\Psi_{(m,n)} = s_o^{-m/2} \int_{-\infty}^{\infty} f(t) \psi^*\left(\frac{t - n\tau_o s_o^m}{s_o^m}\right) dt \quad (3.24)$$

and the analyzing wavelets are discretized as follows.

$$\Psi_{(m,n)} = s_0^{-m/2} \psi \left(\frac{t - n\tau_0 s_0^m}{s_0^m} \right) \quad (3.25)$$

where m and n are integers that control the scale and time factor; s_0 is specified fixed dilation step greater than 1 and τ_0 is location parameter. In eqn. (3.24) and eqn. (3.25) the scale and translation parameters are discretized as $s = s_0^m$ and $\tau = n\tau_0$ respectively. Mallat (1989) argues that for practical case, the power of two logarithmic scale (dyadic wavelet transform) is the simplest and efficient case.

For a discrete time series, $x(t)$ the discrete wavelet transform, $W_{m,n}$ for $s_0=2$ and $\tau_0 = 1$ is given as:

$$\Psi_{(m,n)} = 2^{-m/2} \int_{-\infty}^{\infty} f(t) \psi^*(2^{-m}t - n) dt \quad (3.26)$$

where scale, $s = 2^m$ and location, $\tau = 2^m.n$

The original signal $f(t)$ is obtained from inverse function of the wavelet transform. The inverse wavelet transform is given by:

$$f(t) = \frac{1}{C_\psi} \int_{-\infty}^{\infty} \int_{-\infty}^{\infty} \psi(\tau, s) \Psi_{\tau, s}(t) \frac{ds db}{s^2} \quad (3.27)$$

$$\text{where } C_\psi = 2\pi \int_{-\infty}^{\infty} \frac{|\psi(\omega)|^2}{|\omega|} d\omega < \infty \quad (3.28)$$

3.4.7 Long Term Persistence in Streamflow

Time series analysis for possible short and long term persistence over observation period has become a useful tool to assess the behavior of time evolution of various natural process and historical observations. Hydro-climatic observations such as rainfall and stream flow of today are highly associated to recent past. Such interdependence extends to large lags of infinite memory and hence examination of long term persistence in hydro-climatic variables helps in evaluating whether the time series is built up of random or autocorrelated events. The notion of long memory dependence in time series is pioneered to Hurst (1951). It has been an active area of thought since then and intensively utilized with slight modification in hydrology (Wallis and O'connell, 1973; Rao and Bhattacharya, 1999; Sakalauskienė, 2003;

Koutsoyiannis, 2003; Otache et al., 2008; Mielniczuk, 2007) to account for long range persistence.

Hurst (1951) developed the range statistic (R/S) approach to estimate long term dependence known as Hurst phenomenon. The adjusted range R_n^* is a difference of the maximum and minimum accumulated departures from the sample mean.

$$R_n^* = \max(0, S_1, S_2, S_3, \dots, S_n) - \min(0, S_1, S_2, S_3, \dots, S_n) \quad (3.29)$$

where S_i is cumulative departure and represented as

$$S_i = S_{i-1} + (x_i - \bar{x}) \quad (3.30)$$

with $S_0 = S_n = 0$; n is the size of sub-blocks used to compute rescaled range and $1 < i < n$. The adjusted rescaled range R_n^{**} is obtained by dividing the adjusted range R_n^* by standard deviation, S_n .

$$R_n^{**} = \frac{R_n^*}{S_n} \quad (3.31)$$

From multiple observations of hydrological, geophysical and economic indices data of various lengths, Hurst established an empirical relationship of the form:

$$R_n^{**} = \frac{R_n^*}{S_n} = an^H \quad (3.32)$$

where H is Hurst coefficient equal to 0.5 for purely random walk and $H > 0.5$ is evidence for persistence; the constant, a , is empirically fixed as 0.5 in Hurst's expression.

As Hurst's exponent applies to data sets that are derived from statistically self similar distribution, computation of rescaled range for sub-sequences of $n \leq N$ in the range of total samples (N) is employed. Rescaled range statistic (R/S) is computed for different blocks of data set within observation period where the minimum block length is approximately equal to 8 to 10. Log transformed rescaled range is computed for $n = N, N/2, N/4, \dots, 8$ block widths and average log (R/S) for each division is worked out. The Hurst coefficient, H , is estimated as best fit slope of averaged log (R/S) versus log (n) plot.

3.5 RESULTS AND DISCUSSION

3.5.1 Time Dependence of Hydro-climatic Variables

Correlogram analysis of observed seasonal (June-September and March- May) and annual rainfall series reveals that almost all positive r_1 , r_2 and r_3 values computed at $\alpha=0.05$ lie within 95 percent credibility bounds of the correlogram. This is further justified through exact test for lag-one autocorrelation coefficient. None of the positive first order autocorrelation coefficients found to be significant at $\alpha = 0.05$ (Table 3.2) and the second (r_1^2) and third (r_1^3) order theoretical autocorrelation coefficients are less than their corresponding empirical counterparts, r_2 and r_3 . This is indicative of propensity towards Markov linear type persistence in the series yet it is not statistically significant. The annual and 'Kerimet' (June-September) rainfall series show negative r_2 and r_3 magnitudes which is indicative of marked high frequency oscillation. Gridded rainfall for 21 grid points in the study area follows similar persistence pattern as that of observed series, however, few grid points (41966, 49363, 49558, 49364) in the north and north eastern parts of RFV lakes basin have shown significant r_1 for annual and June - September rainfall series.

Observed annual and seasonal rainfall series at all stations found to be statistical insignificant for the first three lags (Table 3.2). Four grid points out of 21 (19 % of total observations) of annual gridded rainfall are characterized by statistically significant r_1 whereas only two grid points found significant for June-September rainfall series at $\alpha = 0.05$ (Table 3.3). Rainfall series with significant r_1 are subjected to prewhitening before detecting for possible trends following the methods discussed in section 3.4.3.

Time dependence is further investigated using time-lag of various magnitudes and corresponding correlogram function for streamflow and lake level. Annual and extreme lake level events, maximum daily streamflow of Bilate and Hare, minimum daily streamflow of Hare and annual average streamflow of Tikur Wuha exhibit statistically significant lag-one where the red noise case dominates (Table 3.4 and Fig. 3.2). Detrending and subsequently pre-whitening the time series when there is no actual trend significantly reduced the magnitude of lag-1 serial correlation whereas detrending to remove the actual trend substantially increased the lag-1 serial dependence.

Table 3.2 Autocorrelation test statistics for annual and seasonal observed rainfall series

Parameters	r_1	r_2	r_3	Limit of exact test for r_1 at $\alpha = 0.5$	Anderson's credibility bound at $\alpha = 0.5$		
					r_1	r_2	r_3
Annual series							
Alaba Kulito	0.188	-0.270	-0.179	(-0.356, 0.305)	(-0.335,0.284)	(-0.340,0.287)	(-0.345,0.291)
Bilate Farm	0.209	-0.210	-0.206	(-0.394, 0.333)	(-0.366,0.306)	(-0.372,0.310)	(-0.379,0.314)
Hawassa	0.147	-0.332	-0.253	(-0.356, 0.305)	(-0.335,0.284)	(-0.340,0.287)	(-0.345,0.291)
Arba Minch Farm	0.164	-0.341	-0.214	(-0.356, 0.305)	(-0.335,0.284)	(-0.340,0.287)	(-0.345,0.291)
Chencha	0.184	-0.332	-0.268	(-0.368, 0.314)	(-0.345,0.291)	(-0.350,0.294)	(-0.355,0.298)
June - September series							
Alaba Kulito	0.188	-0.177	-0.035	(-0.356, 0.305)	(-0.335,0.284)	(-0.340,0.287)	(-0.345,0.291)
Bilate Farm	-0.092	0.192	0.002	(-0.394, 0.333)	(-0.366,0.306)	(-0.372,0.310)	(-0.379,0.314)
Hawassa	0.076	-0.109	-0.161	(-0.356, 0.305)	(-0.335,0.284)	(-0.340,0.287)	(-0.345,0.291)
Arba Minch Farm	0.089	-0.346	-0.051	(-0.356, 0.305)	(-0.335,0.284)	(-0.340,0.287)	(-0.345,0.291)
Chencha	-0.061	-0.052	0.030	(-0.368, 0.314)	(-0.345,0.291)	(-0.350,0.294)	(-0.355,0.298)
March - May series							
Alaba Kulito	-0.162	0.197	-0.019	(-0.356, 0.305)	(-0.335,0.284)	(-0.340,0.287)	(-0.345,0.291)
Bilate Farm	0.218	0.058	-0.404	(-0.394, 0.333)	(-0.366,0.306)	(-0.372,0.310)	(-0.379,0.314)
Hawassa	-0.074	0.119	-0.326	(-0.356, 0.305)	(-0.335,0.284)	(-0.340,0.287)	(-0.345,0.291)
Arba Minch Farm	-0.029	0.130	-0.233	(-0.356, 0.305)	(-0.335,0.284)	(-0.340,0.287)	(-0.345,0.291)
Chencha	0.122	-0.285	-0.337	(-0.368, 0.314)	(-0.345,0.291)	(-0.350,0.294)	(-0.355,0.298)



Table 3.3 Autocorrelation test statistics for annual and seasonal gridded rainfall series

Rainfall grid points	Annual series			June- September series			March- May series		
	Credability bound at $\alpha = 0.05$								
	$r_1 = (-0.420, 0.257)$			$r_2 = (-0.428, 0.259)$			$r_3 = (-0.437, 0.262)$		
	r_1	r_2	r_3	r_1	r_2	r_3	r_1	r_2	r_3
50128	0.043	-0.110	-0.057	0.123	-0.197	0.034	-0.206	0.161	-0.132
50314	0.004	-0.054	-0.083	0.116	-0.211	0.035	-0.163	0.152	-0.104
50494	-0.076	0.012	-0.113	0.106	-0.215	0.035	-0.163	0.152	-0.104
50129	0.026	-0.060	-0.100	0.157	-0.180	0.025	-0.129	0.105	-0.138
50315	-0.012	0.001	-0.147	0.143	-0.192	0.016	-0.168	0.128	-0.102
49361	0.090	-0.129	0.049	0.008	-0.059	0.112	-0.123	0.122	-0.078
49556	0.109	-0.091	0.017	0.061	-0.094	0.109	-0.202	-0.091	0.007
49750	0.115	-0.065	-0.018	0.182	-0.117	0.093	-0.221	-0.028	-0.024
49938	0.076	-0.023	-0.062	0.241	-0.101	0.063	-0.232	0.051	-0.056
50130	0.026	0.011	-0.099	0.215	-0.130	0.054	-0.198	0.082	-0.071
50316	-0.027	0.046	-0.144	0.163	-0.155	0.044	-0.155	0.107	-0.058
49165	0.140	-0.086	0.096	0.080	-0.113	0.152	-0.126	0.105	-0.041
49362	0.187	-0.108	0.013	0.130	-0.112	0.132	-0.200	-0.036	0.008
49557	0.200	-0.103	-0.035	0.179	-0.131	0.114	-0.195	-0.051	0.025
49751	0.157	-0.036	-0.059	0.239	-0.132	0.105	-0.209	-0.040	0.026
49939	0.087	-0.035	-0.077	0.256	-0.110	0.093	-0.224	0.034	-0.003
50131	0.022	0.070	-0.076	0.220	-0.138	0.101	-0.163	0.083	-0.027
49166	0.259	0.039	0.102	0.187	-0.059	0.172	-0.192	0.030	0.026
49363	0.275	-0.073	-0.017	0.226	-0.123	0.117	-0.191	-0.002	0.046
49558	0.258	-0.086	-0.086	0.290	-0.108	0.085	-0.188	-0.034	0.066
49364	0.308	-0.056	-0.039	0.265	-0.115	0.110	-0.175	0.010	0.059

Table 3.4 Summary of r_1 , r_2 and r_3 significance test for original streamflow and lake level

Parameters and gauge station code	r_1	r_2	r_3	Limit of exact test for r_1 at $\alpha = 0.5$	Anderson's credability bound at $\alpha = 0.5$		
					r_1	r_2	r_3
Annual series							
Bilate	0.032	-0.160	-0.252	(-0.387, 0.328)	(-0.361, 0.302)	(-0.366, 0.306)	(-0.372, 0.310)
Tikur Wuha \bar{r}	0.511	0.485	0.586	(-0.445, 0.371)	(-0.407, 0.333)	(-0.415, 0.338)	(-0.424, 0.344)
Hare	0.280	-0.245	-0.153	(-0.455, 0.378)	(-0.415, 0.338)	(-0.424, 0.344)	(-0.433, 0.350)
Hawassa lake level \bar{r}	0.846	0.631	0.550	(-0.357, 0.305)	(-0.345, 0.291)	(-0.350, 0.294)	(-0.355, 0.298)
Max. daily series							
Bilate \bar{r}	0.391	0.174	0.054	(-0.387, 0.328)	(-0.361, 0.302)	(-0.366, 0.306)	(-0.372, 0.310)
Tikur Wuha	-0.291	0.123	-0.253	(-0.445, 0.371)	(-0.407, 0.333)	(-0.415, 0.338)	(-0.424, 0.344)
Hare \bar{r}	0.456	-0.058	-0.002	(-0.455, 0.378)	(-0.415, 0.338)	(-0.424, 0.344)	(-0.433, 0.350)
Hawassa lake level \bar{r}	0.796	0.612	0.506	(-0.357, 0.305)	(-0.345, 0.291)	(-0.350, 0.294)	(-0.355, 0.298)
Min. daily series							
Bilate	0.061	0.168	0.277	(-0.387, 0.328)	(-0.361, 0.302)	(-0.366, 0.306)	(-0.372, 0.310)
Tikur Wuha	0.118	0.017	0.112	(-0.445, 0.371)	(-0.407, 0.333)	(-0.415, 0.338)	(-0.424, 0.344)
Hare \bar{r}	0.346	0.070	0.189	(-0.455, 0.378)	(-0.415, 0.338)	(-0.424, 0.344)	(-0.433, 0.350)
Hawassa lake level \bar{r}	0.831	0.601	0.491	(-0.357, 0.305)	(-0.345, 0.291)	(-0.350, 0.294)	(-0.355, 0.298)

\bar{r} = significant lag -one

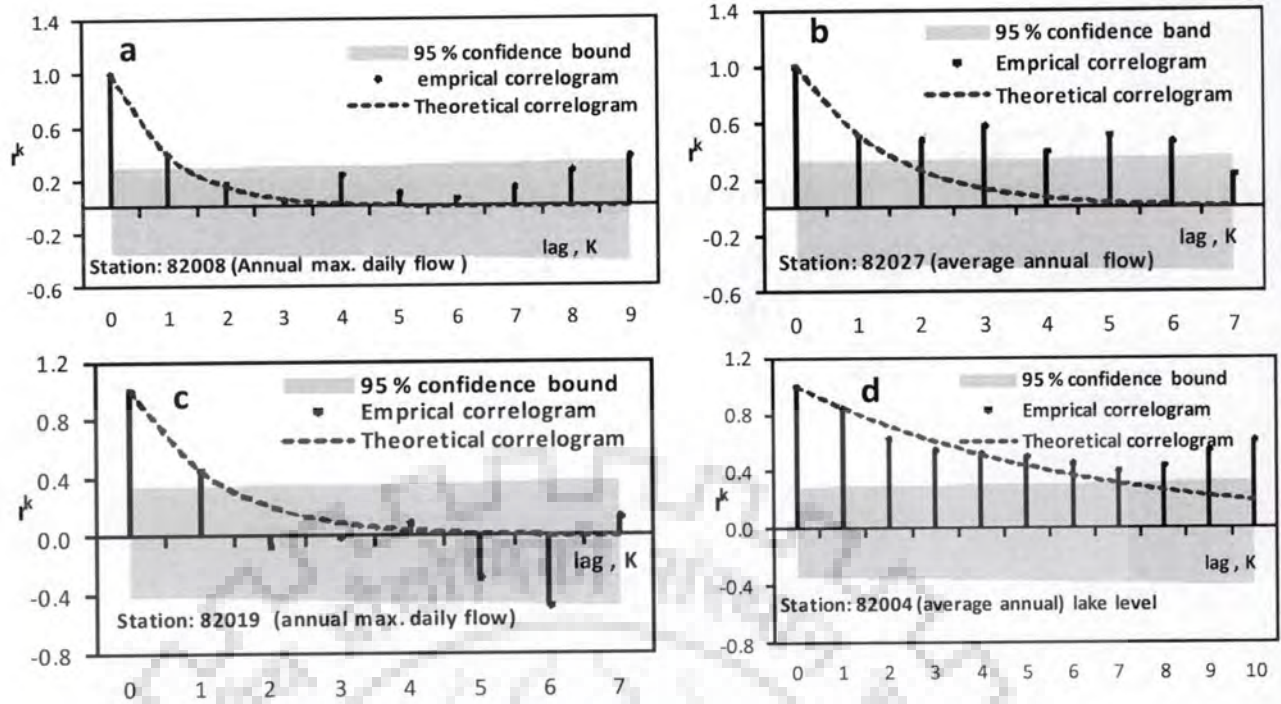


Fig. 3.2 Empirical and theoretical correlogram (K in years) of dependent hydrologic processes: (a) Bilate river at Alaba Kulito (b) Tikur Wuha river at Dato Village (c) Hare river (d) Hawassa lake level

Average annual, annual maximum and minimum daily streamflow and lake level at four gauging stations are also subjected to short term dependence analysis using Von Neumann ratio test. A total of 12 events of dependence tests are carried out to examine short term time dependence in hydro-climatic variables under investigation. Von Neumann test statistics, C , is evaluated with respect to prescribed significance level. In the present case, a 5 % significance level is considered and the corresponding value of $Z_{(1-\alpha/2)}$ is 1.96. If the computed test statistic (C) value is greater than the $Z_{(1-\alpha/2)}$ value, then the null hypothesis of independence is rejected. Annual and daily minimum flow of Bilate at Alba Kulito, maximum daily flow at Tikur Wuha and annual flow at Hare are characterized by random (white noise) cases at 5 % significance level. However, all other (approximately two-third of streamflow and lake level) events analyzed using Von Neumann ratio test have shown short term dependence (red noise case) in annual average and daily extreme events (Table 3.5). Apparently all events of Hawassa lake level and maximum daily flow at Alba Kulito (82008) and Hare (82019) are characterized by significant short term dependence.

Table 3.5 Von Neumann ratio test statistic of streamflow and lake level

Gauging Station / code /	Von Nueman test Parametrs	Annual flow	Maximum Daily Flow	Minimum Daily Flow
Bilate	R	1.946	1.203	1.94
at Alaba Kulito	E (R)	2.059	2.059	2.059
82008	Var (R)	0.114	0.114	0.114
	C	-0.293	-2.533	-0.353
	Statistical Significance	WN	RN	WN
Tikur Wuha	R	0.875	1.932	0.838
at Dato Village	E (R)	2.074	2.074	2.074
82027	Var (R)	0.143	0.143	0.143
	C	-3.175	-0.375	-3.272
	Statistical Significance	RN	WN	RN
Hare	R	1.461	1.112	1.292
at Arba Minch	E (R)	2.077	2.077	2.077
Bridge site	Var (R)	0.148	0.148	0.148
82019	C	-1.6	-2.509	-2.04
	Statistical Significance	WN	RN	RN
Hawassa	R	0.452	0.793	0.246
Lake level	E (R)	2.054	2.054	2.054
82004	Var (R)	0.105	0.105	0.105
	C	-4.941	-3.888	-5.575
	Statistical Significance	RN	RN	RN
RN= red noise , dependent case		WN= white noise , random case		

Annual and seasonal rainfall trend during the analysis period has been assessed using MK trend test and Theil-Sen's slope estimator. Observed and gridded annual and seasonal rainfall series found to exhibit insignificant trends at $\alpha = 0.05$ and 0.1 level of significance for most cases (Table 3.6 and 3.7). However, June-September rainfall at Alaba Kulito and Bilate Farm found to follow decreasing trend at $\alpha = 0.1$. Number of annual and seasonal rainy days (number of events with total daily rainfall magnitude $> 0.1\text{mm}$) was also subjected to trend analysis to observe the time variance of significant rainfall over the last four decades. The rainy days remain stable at 5 and 10 percent significance level for annual and seasonal rainfall series and no statistically significant trend is observed (Table 3.8). Streamflow in Rift Valley lakes basin varies seasonally and exhibits two distinct flow regimes; namely storm runoff and base flow. The dominant base flow regime usually begins in the month of November and extends to the end of May at Bilate and Tikur Wuha watersheds where as it extends from December to mid of March in lower Rift Valley lakes system. Annual average and extreme (annual minimum and maximum daily) runoff and lake level events for three different watersheds in the Rift Valley lakes basin are examined for a total of 16 independent variables to study periodic and monotonic time dependent behavior. Both MK trend test and Theil-Sen's slope estimator reveal

that about 75 percent of hydrologic variables tested for annual and seasonal series are characterized by increasing trends (Table 3.9 and Table 3.10). At similar significance level, the results obtained from Theil-Sen's trend slope estimator are at reasonable concordance to MK trend analysis method.

Table 3.6 MK trend analysis for observed annual and seasonal rainfall series

Rainfall stations	Statistical parameters		Original Mann-Kendall test			
	Mean	Std Dev.	S	Z	trend at	
	(mm)	(mm)			$\alpha=0.05$	$\alpha=0.1$
Annual series						
Hawassa	964.3	140.6	-32	0.358	NS	NS
Alaba Kulito	1016.4	195.9	-102	1.172	NS	NS
Bilate Farm	763.9	174.4	-99	1.447	NS	NS
Arba Minch Farm	871.9	180.5	72	0.822	NS	NS
Chencha	1258.0	256.1	61	0.749	NS	NS
June- September series						
Hawassa	469.3	101.1	-107	1.235	NS	NS
Alaba Kulito	461.6	122.5	-168	1.951	NS	D
Bilate Farm	321.1	106.5	-123	1.812	NS	D
Arba Minch Farm	261.7	104.7	-126	1.454	NS	NS
Chencha	426.2	128.7	7	0.075	NS	NS
March - May series						
Hawassa	298.8	82.5	16	0.174	NS	NS
Alaba Kulito	341.6	108.2	12	0.127	NS	NS
Bilate Farm	247.4	82.0	-21	0.294	NS	NS
Arba Minch Farm	343.8	91.7	14	0.151	NS	NS
Chencha	469.1	139.7	-19	0.225	NS	NS
NS = Not statistically significant			D = Decreasing trend			
S = Mann-Kendall test statistic			Z = Standard score			
For $\alpha = 0.05$ and $\alpha = 0.1$ the critical Z- values are 1.960 and 1.645 respectively.						

Table 3.7 MK trend test statistics for gridded annual and seasonal rainfall series

Grid code	Longitude (Decimal deg.)	Latitude (Decimal deg.)	Mean (mm)	Std. Dev. (mm)	Mann-Kendall test statistics					
					Annual series		June- September		March-May	
					S	Z	S	Z	S	Z
50128	36.75	5.75	1097	218	106	0.878	5	0.034	-104	0.861
50314	36.75	5.25	824	170	72	0.593	9	0.066	-129	1.071
50494	36.75	4.75	631	148	-43	0.352	-6	0.041	-159	1.323
50129	37.25	5.75	1053	211	98	0.812	62	0.510	-114	0.944
50315	37.25	5.25	781	164	57	0.469	60	0.493	-131	1.087
49361	37.75	7.75	1226	170	163	1.356	-29	0.234	109	0.904
49556	37.75	7.25	1189	191	177	1.472	9	0.066	64	0.527
49750	37.75	6.75	1145	210	183	1.522	55	0.349	13	0.100
49938	37.75	6.25	1057	210	160	1.332	77	0.636	-63	0.519
50130	37.75	5.75	982	201	123	1.022	108	0.895	-68	0.561
50316	37.75	5.25	850	181	77	0.636	-32	0.260	-96	0.794
49165	38.25	8.25	1020	139	106	0.878	-25	0.201	62	0.510
49362	38.25	7.75	1017	149	162	1.347	0	0.000	49	0.402
49557	38.25	7.25	1019	165	178	1.480	58	0.478	60	0.493
49751	38.25	6.75	1003	184	192	1.598	92	0.760	39	0.317
49939	38.25	6.25	969	197	168	1.398	92	0.760	-4	0.025
50131	38.25	5.75	916	191	165	1.372	122	1.013	-16	0.126
49166	38.75	8.25	882	147	74	0.611	-31	0.251	72	0.595
49363	38.75	7.75	901	150	161	1.338	3	0.016	59	0.485
49558	38.75	7.25	928	160	165	1.372	7	0.050	56	0.461
49364	39.25	7.75	847	152	172	1.429	-5	0.034	39	0.317

S= Mann-Kendall test statistic Z= Standard score
The critical Z-values are 1.96 and 1.645 at 5 and 10 % significance level respectively.

Table 3.8 MK trend test for total number of rainy days of annual and seasonal observed rainfall series

No. of rainy days events	Mann-Kendall test statistics		No. of rainy days trend at	
	S	Z	$\alpha = 0.05$	$\alpha = 0.10$
Alaba Kulito gauging station				
Annual rainfall	-32	0.937	NS	NS
June-September rainfall	12	0.333	NS	NS
March-May rainfall	-41	1.211	NS	NS
Arba Minch Farm gauging station				
Annual rainfall	112	1.518	NS	NS
June-September rainfall	12	0.15	NS	NS
March-May rainfall	80	1.083	NS	NS
Hawassa gauging station				
Annual rainfall	-34	1.001	NS	NS
June-September rainfall	35	1.034	NS	NS
March-May rainfall	-37	1.092	NS	NS
Critical Z-values			1.960	1.645
S = Mann-Kendall test statistic Z = Standard score NS = No statistically significant trend				

Table 3.9 MK trend test statistics for annual and seasonal streamflow series

S.No.	Parameters & Stations	Statistical Test Methods (at $\alpha = 0.05$)											
		Mann-Kendall original series				Mann-Kendall prewhitened series				Mann-Kendall seasonal series			
		τ	S	Z	Trend	τ	S	Z	Trend	τ	S	Z	Trend
Annual Series													
1	Bilate	0.082	49	0.676	NS	0.079	47	0.648	NS				
2	Tikur Wuha	0.566	214	3.910	+	0.519	196	4.418	+				
3	Hare	0.077	27	0.536	NS	0.100	35	0.701	NS				
4	Hawassa lake level	0.581	408	3.912	+	0.661	465	4.417	+				
Max. Daily Series													
5	Bilate	0.313	186	2.612	+	0.382	227	3.291	+				
6	Tikur Wuha	-0.149	-56	1.087	NS	-0.079	-30	0.568	NS				
7	Hare	-0.117	-41	0.826	NS	-0.164	-57	1.175	NS				
8	Hawassa lake level	0.540	379	3.901	+	0.616	433	3.291	+				
Min. Daily Series													
9	Bilate	0.335	197	2.807	+	0.358	213	3.090	+				
10	Tikur Wuha	0.506	191	3.7190	+	-0.127	-48	0.921	NS				
11	Hare	0.194	68	1.398	NS	0.268	94	1.943	NS				
12	Hawassa lake level	0.530	372	3.891	+	0.661	465	3.891	+				
Monthly Series													
13	Bilate									0.113	805	2.132	+
14	Tikur Wuha									0.357	1617	3.891	+
15	Hare									0.118	499	1.645	NS
16	Hawassa lake level									0.548	4621	3.891	+
Max. = Maximum , Min. = Minimum		Avg. = average				N = No statistically significant trend				.+ = Increasing trend			

Table 3.10 Theil-Sen's trend slope estimator and r_1 magnitude of streamflow before and after prewhitening

S.No.	Parameters & Stations	Serial correlation, r_1		Sen's Slope Estimator		
		Original series	DET-PWH Series	b	95 % Confidence bound	
					LCL	UCL
Annual Series						
1	Bilate	0.032	0.017	1.457	-2.639	4.925
2	Tikur Wuha	0.511	0.368	1.618	0.921	2.335
3	Hare	0.280	0.093	0.255	-0.651	1.287
4	Hawassa lake level	0.846	0.801	0.047	0.032	0.061
Max. Daily Series						
5	Bilate	0.391	0.462	0.897	0.254	1.756
6	Tikur Wuha	-0.291	0.083	-0.018	-0.039	0.017
7	Hare	0.456	0.2005	-0.061	-0.355	0.099
8	Hawassa lake level	0.796	0.694	0.047	0.03	0.062
Min. Daily Series						
9	Bilate	0.061	0.073	0.008	0.002	0.014
10	Tikur Wuha	0.118	-0.233	0.046	0.016	0.078
11	Hare	0.346	0.1993	0.018	-0.006	0.043
12	Hawassa lake level	0.831	0.723	0.046	0.03	0.060

DET-PWH=Detrended & Prewhitened LCL = Lower Confidence Limit UCL = Upper Confidence Limit

No persistent step change in streamflow and lake level is examined. Hawassa lake level and Tikur Wuha river exhibit a localized jump in year 1997/98 due to increased summer rainfall over the same period. The hydrologic variables recovered their monotonically increasing trend soon after such rainfall anomaly.

3.5.2 Streamflow Spectral Analysis

The spectrum of discrete time series is not entirely lying within the boundary of the confidence limits in all cases. Thus the monthly runoff is characterized by deterministic cyclic components represented as spikes in spectral density plot (Fig. 3.3). This is further evident from correlogram analysis of monthly series where the lag plot follows a systematic oscillation with known frequency of one cycle per year (Fig. 3.4). The deterministic cyclic components are represented as discrete Fourier series of time events. The percentage contribution to variance explained by the first two harmonics of streamflow and lake level data ranges from 88-98.3 in the watersheds investigated. The degree of association between observed and simulated hydrologic variables is further evaluated by computing various model efficiencies such as coefficient of determination (R^2), Root Mean Square Error (RMSE) and Nash-Sutcliffe (N-S) (Nash and Sutcliffe, 1970) model efficiency. The N-S and R^2 efficiency values appeared to be closer to unity with significantly small RMSE. Finite

Fourier series fitted to the first two harmonics of streamflow and lake level (Fig. 3.5) is at reasonable agreement to the observed series.

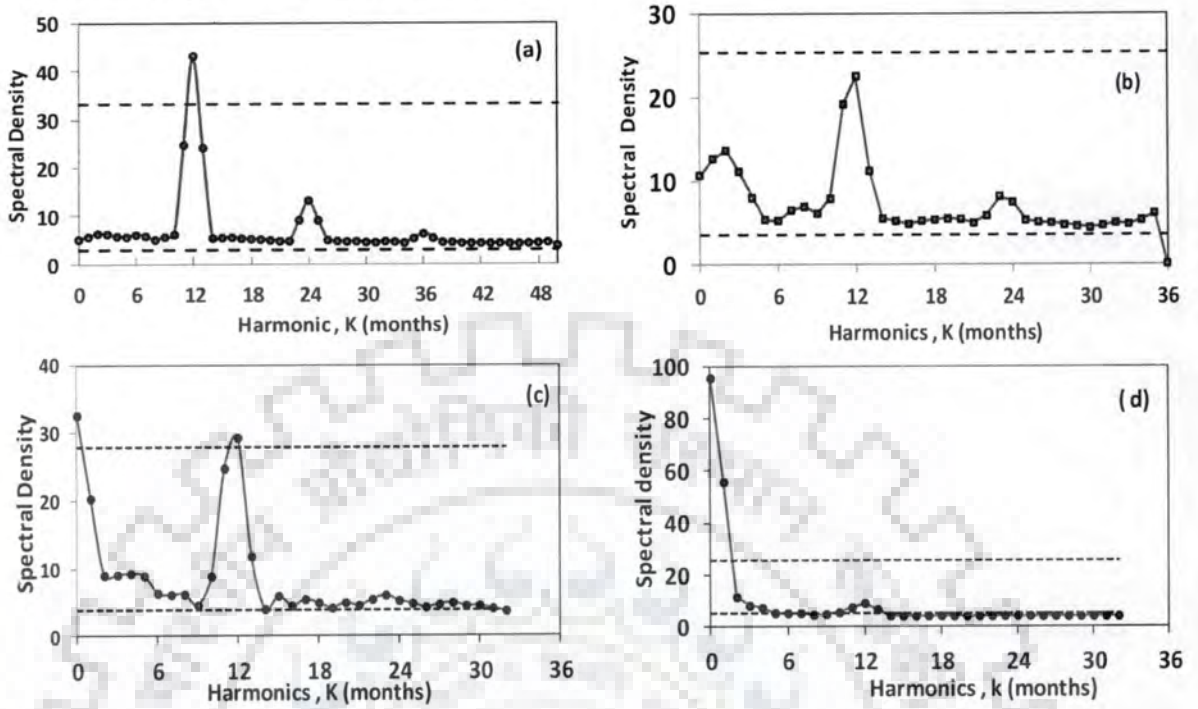


Fig. 3.3 Spectral density of monthly runoff of (a) Bilate river at Alaba Kulito (b) Hare river (c) Tikur Wuha river at Dato village and (d) Hawassa lake level. The 95 percent confidence bound is depicted as broken line plot

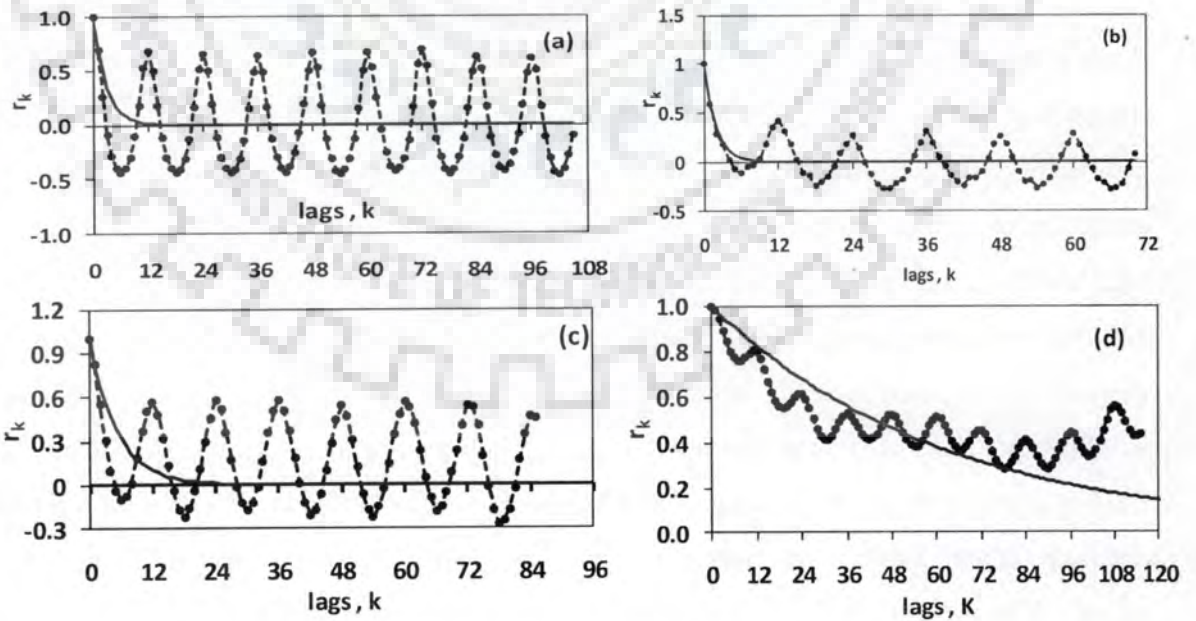


Fig. 3.4 Correlogram of monthly hydrologic series (a) Bilate river at Alaba Kulito (b) Hare river (c) Tikur Wuha river at Dato village and (d) Hawassa lake level. The smooth curve is theoretical correlogram of AR (1) process

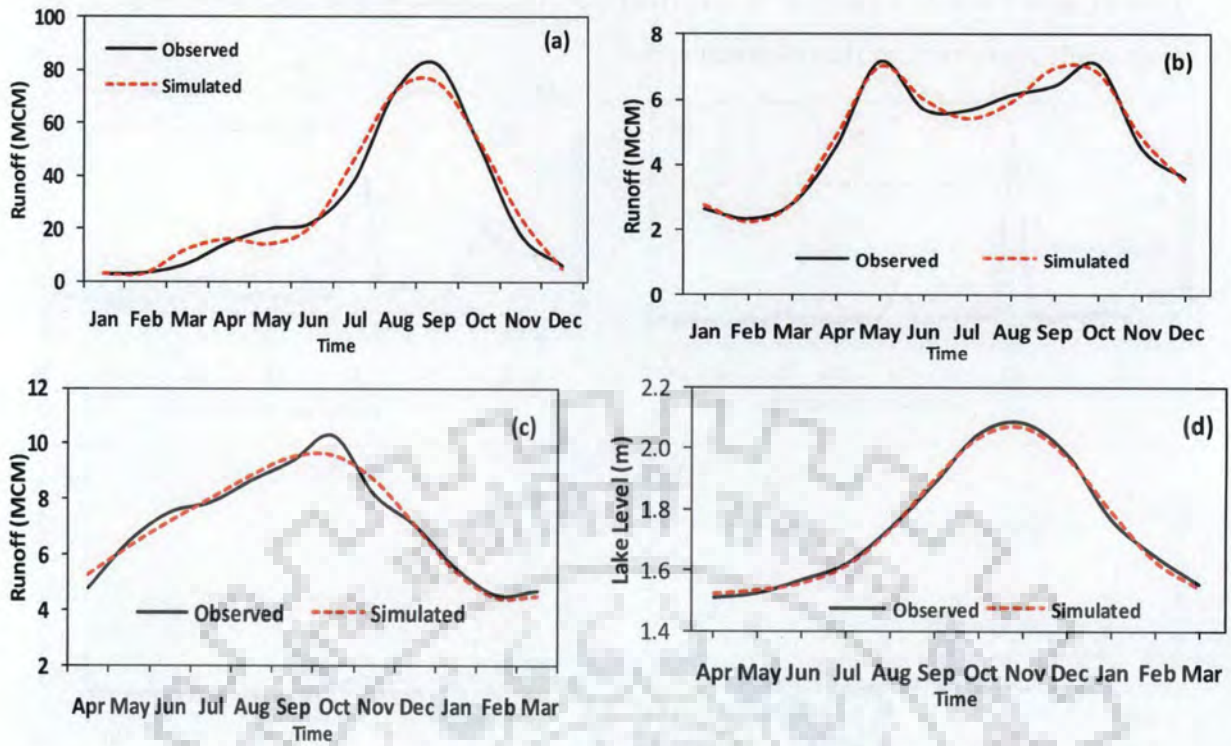


Fig. 3.5 Monthly streamflow and lake level fitted to finite Fourier series for the first two harmonics: (a) Bilate at Alaba Kulito (b) Hare river (C) Tikur Wuha at Dato village and (d) Hawassa lake level

3.5.3 Wavelet Analysis

Wavelet transform is carried out for monthly and annual lake level (Hawassa lake) and three streamflow (Bilate, Tikur Wuha and Hare) time series signals ranging from 1970-2007. The Daubechies wavelet transform is used to extract the dominant information with sufficient energy level of the signal. Annual and monthly original hydrologic series (streamflow and lake level) are decomposed into corresponding detail (2-year, 4-year, 8-year, 16-year and 32-year) and approximate signal components. Fig. 3.6 presents the detail and approximate wavelet decomposition result obtained from Daubachies-4 (db-4 at level 5) method for monthly lake level records at Hawassa. Compressing the original signal of annual lake level and Tikur Wuha streamflow using one of Daubechies wavelet family (db-4) with 5 levels of details removed most of the noises and preserved 98.24 % of the energy in the original signal. The wavelet coefficients are efficiently zeroed out through automatic threshold method. The denoised signal plot of monthly and annual Hawassa lake level and Tikur Wuha streamflow (Fig. 3.7 and Fig. 3.8) intuitively illustrates an increasing overall trend. This is further verified by statistical trend analysis of discrete wavelet (DW) decomposed hydrologic components.

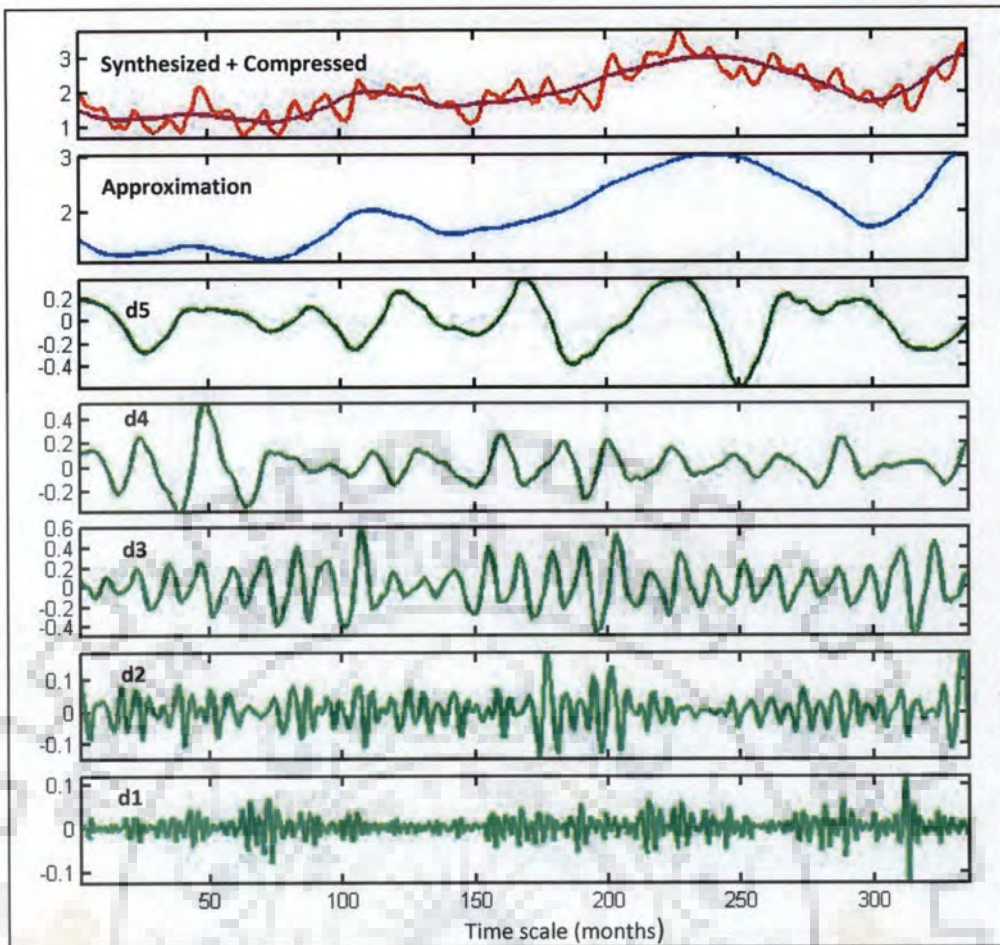


Fig. 3.6 Wavelet decomposition of monthly lake level at Hawassa lake during 1980-2007

Annual streamflow and lake level series are decomposed into corresponding detail and approximate discrete wavelet signals and are subjected to MK-trend analysis. Following the methods suggested by Partal and Kucuk (2006), the trend analysis is carried out for different model combinations of DW decomposed series. The effectiveness of wavelet decomposed series in identifying the underlying trends in original series is evaluated in terms of MK test statistics (Z -score). Total mean square error (MSE) and coefficient of determination (R^2) are used to examine how well the different model combinations of wavelet decomposed series have predicted the original series.

Fig. 3.9 presents standardized discrete wavelet decomposed signals of Tikur Wuha streamflow (1980-2007) and Hawassa lake level (1970-2007) using Daubechies algorithm. The contribution to total streamflow and lake level in each year is shown as a time series plot of the DW coefficients. For example, D1 indicates DW coefficients for 2-year mode; D2 shows DW coefficients for 4 -year mode and so on. Streamflow at Bilate and Hare rivers are also decomposed into similar detail and approximate signals, however, graphical display is not presented here.

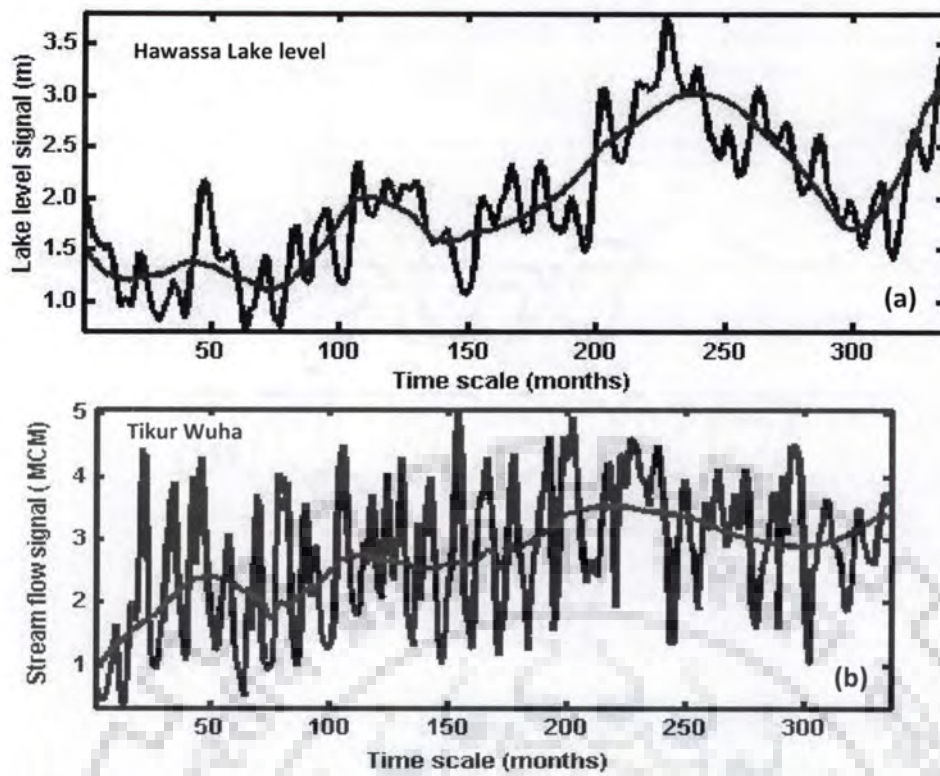


Fig. 3.7 Original and Daubechies denoised signal of monthly lake level (a) and Tikur Wuha streamflow (b). The smooth line is a denoised signal using db-4 level -5

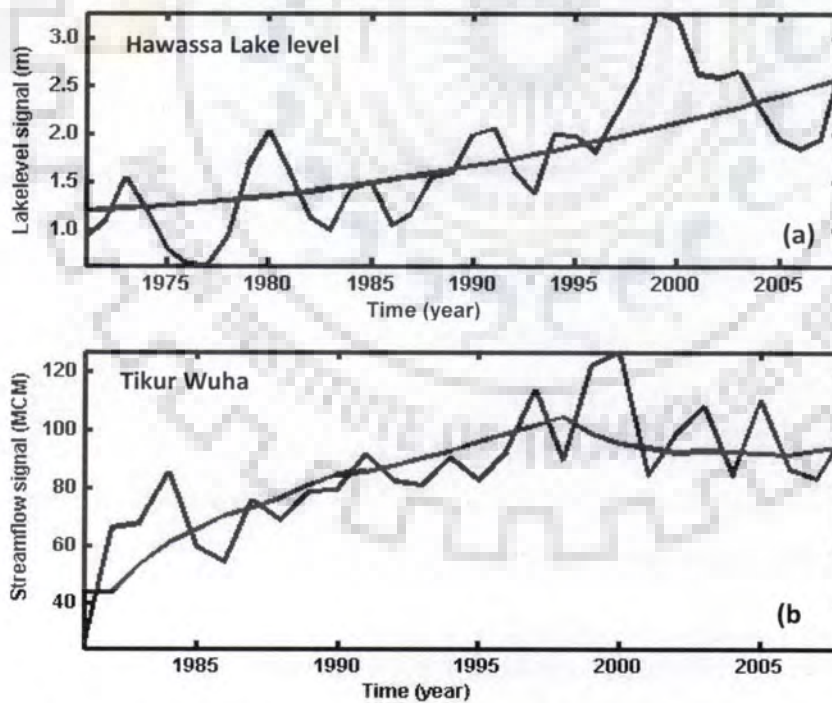


Fig. 3.8 Original and Daubechies denoised signal of annual average lake level (a) and Tikur Wuha (b) streamflow. The smooth line is a denoised signal using db-4

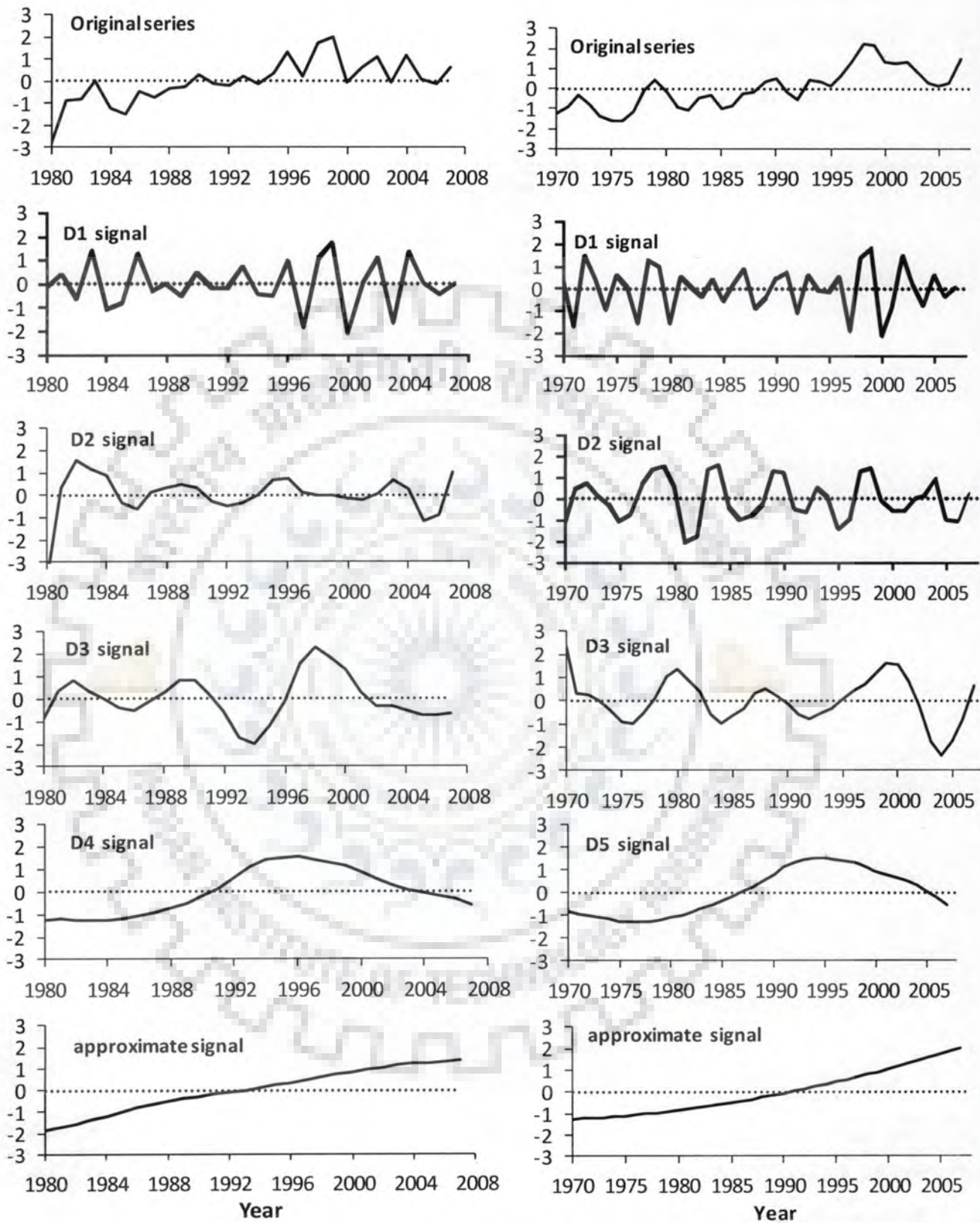


Fig. 3.9 Standardized original and discrete wavelet decomposed signals plot of Tikur Wuha stream flow (left panel) and Hawassa lake level (right panel)

Table 3.11 MK-trend analysis statistics and model efficiency of wavelet decomposed signals of Tikur Wuha and Hare streamflow

Model No.	Signal combinations	Tikur Wuha streamflow				Hare streamflow			
		MK- test statistics		Model efficiency		MK- test statistics		Model efficiency	
		S	Z	MSE	R ²	S	Z	MSE	R ²
1	Original series	214	4.21	-	-	26	0.52	-	-
2	D1 + approx.	197	3.87	0.30	0.71	71	1.46	0.64	0.44
3	D2 + approx.	294	5.79	0.38	0.65	24	0.48	0.11	0.89
4	D3 + approx.	255	5.02	0.42	0.61	139	2.88	1.17	0.15
5	D4 + approx.	246	4.84	0.44	0.60	72	1.48	1.19	0.15
6	D1 + D2 + approx.	177	3.48	0.14	0.86	69	1.42	0.28	0.73
7	D1 + D3 + approx.	175	3.44	0.19	0.81	91	1.88	0.45	0.59
8	D1 + D4 + approx.	412	4.17	0.18	0.82	38	0.77	0.46	0.58
9	D2 + D3 + approx.	208	4.09	0.33	0.69	69	1.42	0.66	0.43
10	D2 + D4 + approx.	238	4.68	0.28	0.73	45	0.92	0.68	0.42
11	D3 + D4 + approx.	252	4.96	0.34	0.68	53	1.08	0.90	0.28
12	D1 + D2 + D3 + approx.	165	3.24	0.09	0.91	53	1.08	0.13	0.87
13	D2 + D3 + D4 + approx.	224	4.41	0.23	0.77	47	0.96	0.49	0.56
14	D1 + D2 + D4 + approx.	208	4.09	0.44	0.77	27	0.52	0.14	0.86
15	D1 + D2 + D3 + D4 + approx.	214	4.21	0.00	1.00	26	0.52	0.00	1.00

Critical Z-value is **1.96** at 5 % significance level and **Bold** figures show significant values

Various combinations of wavelet decomposed signals are further investigated to identify statistically strong trends with higher model efficiency. Stream flow of Tikur Wuha and Hare are decomposed into four DW coefficients (D1 to D4) and an approximate signal whereas Hawassa lake level and Bilate streamflow series, with relatively long record periods, are decomposed into five DW coefficients (D1 to D5) and an approximate signal. For each hydrologic series a total of 15 to 30 signal combinations are identified and subjected time-trend analysis.

Tables 3.11 and 3.12 present the different model combinations and their respective time-trend analysis results. The tables also provide model efficiency of original series against various DW model combinations. All model combinations of annual average Tikur Wuha streamflow are characterized by increasing trends with acceptable model performance indices. The total MSE is low (0.0 to 0.44) and R² is lying between 0.60 and 1.0. Observed from trend statistics and model efficiency values, the combination of D1 signal found to reproduce the original signal efficiently (Table 3.11). It is only one (D3+approximate) model combination (6% of total models) that resulted in increasing trend of Hare

streamflow. However, these increasing trend model is characterized by poor model efficiency ($MSE = 1.17$ and $R^2 = 0.15$) and is an artifact of the actual trend. This permits us to conclude that the trend component of annual streamflow variable of Hare river is not statistically significant.

Table 3.12 MK-trend analysis statistics and model efficiency of wavelet decomposed signals of Hawassa lake level and Bilate streamflow

Model No.	Signal combinations	Hawassa lake level				Bilate streamflow			
		MK- test statistics		Model efficiency		MK- test statistics		Model efficiency	
		S	Z	MSE	R ²	S	Z	MSE	R ²
1	Original series	407	5.11	-	-	49	0.68	-	-
2	D1 + approx.	584	7.33	0.43	0.61	230	3.25	0.86	0.31
3	D2 + approx.	472	5.92	0.31	0.71	261	3.69	0.89	0.29
4	D3 + approx.	379	4.75	0.30	0.72	425	6.02	1.27	0.12
5	D4 + approx.	701	8.80	0.46	0.58	200	2.83	1.28	0.12
6	D5 + approx.	688	8.66	0.40	0.63	109	1.54	1.76	0.01
7	D1 + D2 + approx.	448	5.62	0.27	0.74	175	2.47	0.40	0.63
8	D1 + D3 + approx.	369	4.63	0.27	0.74	231	3.27	0.65	0.44
9	D1 + D4 + approx.	559	7.02	0.42	0.61	175	2.47	0.62	0.46
10	D1 + D5 + approx.	581	7.30	0.36	0.66	135	1.90	0.84	0.32
11	D2 + D3 + approx.	324	4.06	0.12	0.88	251	3.55	0.67	0.43
12	D2 + D4 + approx.	452	5.67	0.30	0.72	191	2.70	0.63	0.46
13	D2 + D5 + approx.	514	6.45	0.25	0.76	133	1.87	0.87	0.31
14	D3 + D4 + approx.	372	4.66	0.30	0.71	251	3.55	1.02	0.23
15	D3 + D5 + approx.	434	5.44	0.24	0.77	203	2.87	1.29	0.11
16	D4 + D5 + approx.	666	8.37	0.36	0.66	136	1.92	1.14	0.17
17	D1 + D2 + D3 + approx.	317	3.97	0.10	0.90	173	2.44	0.24	0.77
18	D1 + D2 + D4 + approx.	438	5.49	0.26	0.75	131	1.84	0.19	0.81
19	D1 + D2 + D5 + approx.	487	6.11	0.21	0.79	109	1.53	0.37	0.65
20	D1 + D3 + D5 + approx.	432	5.42	0.21	0.80	107	1.51	0.63	0.46
21	D1 + D3 + D4 + approx.	365	4.58	0.28	0.74	163	2.30	0.47	0.58
22	D2 + D3 + D4 + approx.	318	3.99	0.13	0.87	167	2.36	0.48	0.57
23	D2 + D4 + D5 + approx.	498	6.25	0.21	0.79	71	0.99	0.53	0.53
24	D3 + D4 + D5 + approx.	445	5.58	0.22	0.79	149	2.10	0.94	0.27
25	D1 + D2 + D3 + D4 + approx.	324	4.06	0.10	0.90	149	2.10	0.07	0.92
26	D1 + D3 + D4 + D5 + approx.	432	5.42	0.19	0.82	65	0.91	0.40	0.63
27	D2 + D3 + D4 + D5 + approx.	381	4.78	0.06	0.94	69	0.97	0.40	0.63
28	D1 + D2 + D4 + D5 + approx.	481	6.03	0.18	0.82	63	0.88	0.11	0.88
29	D1 + D2 + D3 + D5 + approx.	389	4.88	0.05	0.95	105	1.48	0.21	0.79
30	D1 + D2 + D3 + D4 + D5 + approx.	373	4.68	0.03	0.97	63	0.88	0.01	0.98

Critical Z-value is 1.96 at 5 % significance level ; approx. = approximate DW signal ; Bold figures show significant values

All model combinations of annual average lake level show increasing trends (Table 3.12). Model efficiency indices are at acceptable range in each case. Based on combined

performance criteria (statistically strong significant trend, lower MSE and higher R^2), model combinations with D3 signal perform better than others for Hawassa lake level. Model number 25 (D1+D2+D3+D5+approximate) found to show statistically strong trend with higher model efficiency for lake level data. About 53% of model combinations examined for Bilate streamflow reveals increasing trend based on the MK-trend statistic. Model efficiency in most cases is very low. Model numbers 7, 17, 21, 22 and 25 are modestly showing acceptable model efficiency indices (MSE= 0.07 to 0.48 and $R^2 = 0.57$ to 0.92). These statistically significant model combinations of Bilate streamflow include D1 signal. However, it should be noted that the original annual streamflow series of Bilate river does not show significant trends.

The annual average lake level observed during the years 1970-2007 is further analyzed for periodic behaviour using Morlet continuous wavelet transform. The dark yellow patches in Fig. 3.10 are well aligned to an 8-years time scale. This indicates that average annual lake level events are characterized by 8-year periodic signals. The wavelet transform of annual Tikur Wuha streamflow demonstrates a 4-years and 8-10 years periodicity (Fig. 3.10). Annual rainfall series (observed as well as gridded) does not show systematic periodic or monotonic trend components in most cases, however, a 4-years periodic signal is inferred from annual rainfall signal at Bilate basin during 1984-2000. The results obtained from wavelet analysis are in suitable agreement with previously discussed methods. The time-frequency relationships of the wavelet transform identified the occurrence of periodic signal that is not clearly captured by spectral analysis.

3.5.4 Long Range Dependence

Albeit limited length of available hydrological records, the adjusted rescaled range analysis (R/S) of Hurst has been applied to examine the long term dependence in stream flow and lake level. Both annual and monthly events of length varying from 27-456 are subjected to R/S analysis. Hurst coefficients, H , computed from annual series are 0.54, 0.68, 0.96 and 0.89 for Bilate, Hare, Tikur Wuha streamflows and Hawassa lake level respectively. Similarly, the monthly series yields an H estimate of 0.52, 0.89, 0.64 and 0.97 respectively. In all the subject matters examined Hurst's coefficient is greater than 0.5 and this is a likely evidence of long term persistence in hydrologic variables. Annual events of Tikur Wuha river ($H=0.96$) and Hawassa lake level ($H=0.89$) and monthly series of Hare river ($H=0.89$) and Hawassa lake level ($H=0.97$) are characterized by strong persistence. No random walk situation is examined from rescaled range analysis for monthly and annual series.

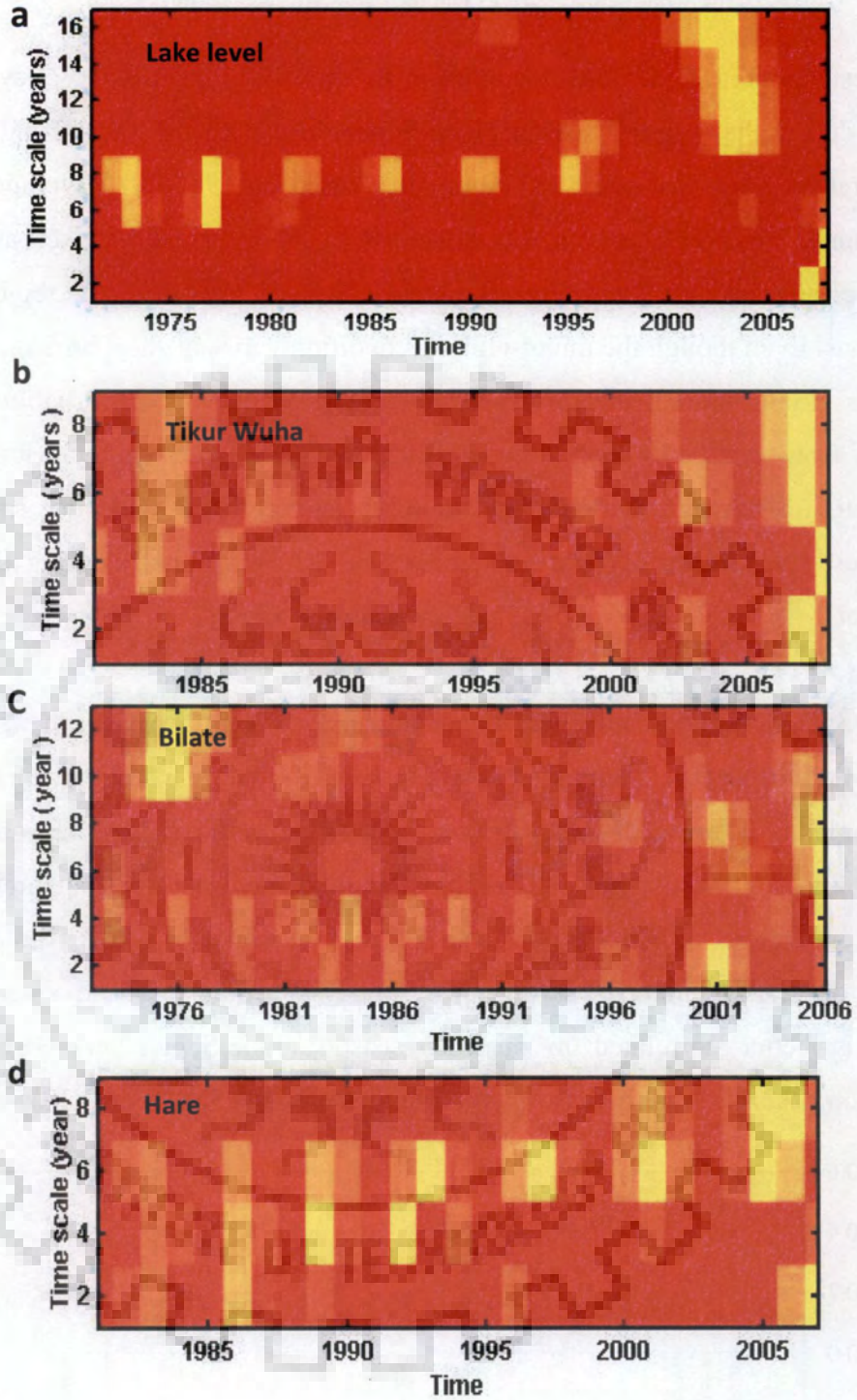


Fig. 3.10 Continuous wavelet spectrum for Hawassa lake level (a), stream flow of Tikur wuha at Dato village (b), streamflow of Bilate at Alaba Kulito (c) , and streamflow of Hare at Arba Minch (d)

3.5.5 Association of Sea Surface Temperature (SST) to Rainfall

The largest fraction of the annual rainfall in northern Ethiopian Rift Valley lakes basin is received during the summer season (June-September) with the second highest extending from March to May. Monthly SST anomalies based on 1982-2010 average SST data are first examined for likely systematic fluctuations. Secondly, annual as well as seasonal SST magnitudes are correlated with corresponding observed rainfall in the region for possible associations. Even though the micro-climate condition varies at short horizontal profiles due to various circumstances, the influence of large scale oceanic perturbation is distributed uniformly over the nearby land surface. Thus, to obtain a sub-regional view of prevailing association, an average stations total rainfall is correlated with the same span SST magnitudes. Association of June-September SST to total rainfall during the observation period is also accomplished to investigate for seasonal effects.

Positive SST anomalies with frequent signals are eminent over the last two decades (Fig. 3.11). Extreme wet years (1997-98 and 2006-07) are marked with increased positive SST anomalies whereas extreme dry years (1984-86 and 2002-04) are characterized by negative SST anomalies (Fig. 3.12). Even though there are such apparent associations between extreme rainfall magnitudes and SST, the frequency of above average total rainfall years to occur is relatively less during the analysis window. The average stations total rainfall is better correlated to summer season (June-September) SST whereas the association becomes weakly developed for annual average SST (Fig. 3.13).

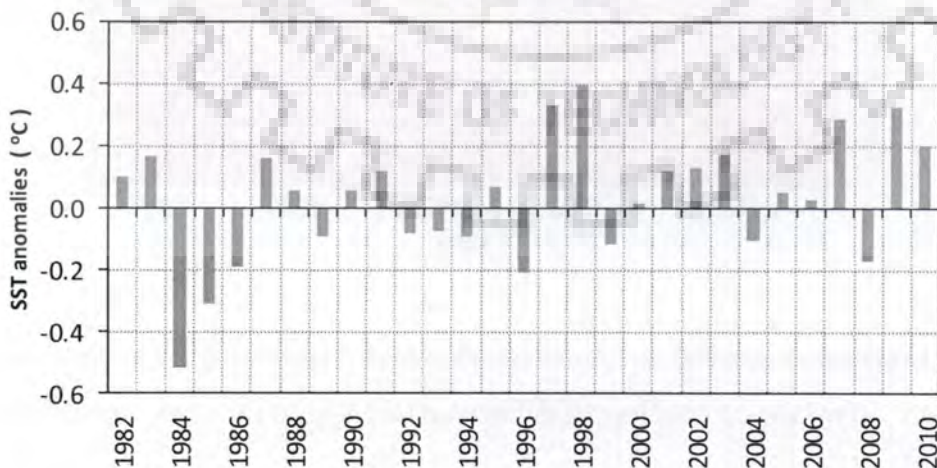


Fig. 3.11 Annual Average sea surface temperature anomaly based on 1982-2010 average at 0° - 10° N and 45° - 65° E region

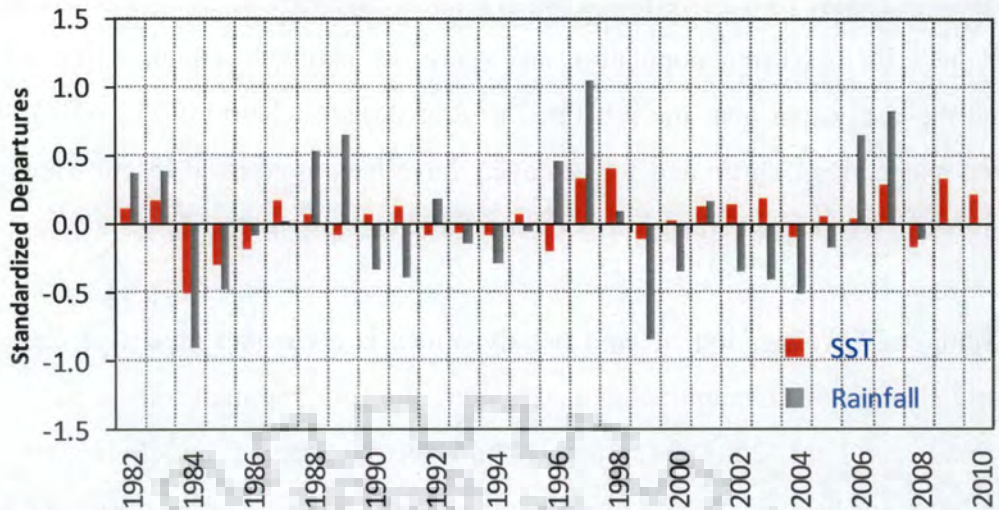


Fig. 3.12 Standardized SST ($^{\circ}\text{C}$) and average annual rainfall (mm) at Rift Valley lakes basin

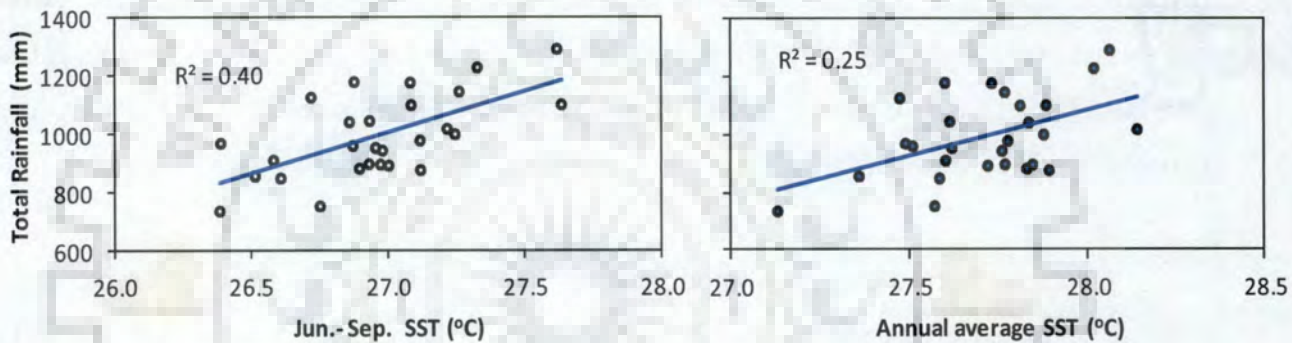


Fig. 3.13 Association of annual rainfall to June-September (a) and annual average (b) SST

3.5.6 Land Use Dynamics: A potential Implication to Streamflow Trends

Surface cover, soil physical properties and slope of terrain noticeably affect overland flow and material transport by limiting the infiltration rate. Land use /cover either attenuate or accentuate over land flow mechanism even under stationary climatic condition and hence it alters surface or subsurface flow regime. Conversion of forest area to agricultural land, urbanization, industrial development, cattle raising and local energy consumption results in modification of natural land cover. Such land use dynamics serve as a proxy data set to identify streamflow variability. Assessment of land use pattern over specified temporal scale provides useful information about the interaction between ecological process and streamflow.

As in most other parts of Ethiopia, major portion of Rift Valley lakes basin is dominated by agrarian community where crop production and animal breeding has become

the decisive mainstay of the livelihood. Such intense engagement on agricultural production to feed the ever increasing population and spare the national economy has substantially modified the ecosystem over the last three to four decades (Hurni et al., 2005). Immense land area under grass, shrub and forest cover have been converted to cultivated area and bare soil which by far aggravated surface runoff and erosion of top soil layer.

Temporal investigation of land use dynamics is a capable means of characterizing constantly changing catchment behavior affecting the flow regime (Seibert and McDonnell, 2010; Read and Lam, 2002). Temporal Multispectral Scanner and Enhanced Thematic Mapper plus land use/cover data acquired from global land cover data set for the years 1973, 1986 and 2000 are further processed and classified (Cermak et al., 1979) using ERDAS Imagine 9.2. The raw landsat image has been classified into 15 independent land use classes and subsequently merged to 7-8 dominant classes for ease of analysis (Fig. 3.14 and Fig. 3.15). Land use/cover status in the year 1973 is considered as a baseline for temporal land use variation.

Owing to intense catchment modification due to man-induced effects, the gross size of rural cultivated area and bare soil is increased by 23.1 and 15.8 percent at Bilate and Hawassa lake basin respectively. Eroded areas, unsuitable for crop production increased to 17 percent in 2000 compared to its baseline size of 7 percent at Bilate catchment. Percentage change in cultivated land and rural settlement area between 1973 and 2000 accounts for 64 and 50 at Bilate and Hawassa lake catchments respectively. Dense forest, open bush and wood land coverage decreased dramatically in both catchments. Both rural settlements and urban built-up area is increasing over the last 3-4 decades. The relative proportion of urban built-up area coverage in the watershed is very small. Therefore, direct influence of urbanization, either in attenuating or accentuating the runoff process is minimal at present context. The impacts of rural land use management operations (cultivation, overgrazing, timbering, deforestation as a result of local energy consumption) in the watershed are more significant and obvious than urbanization effects.

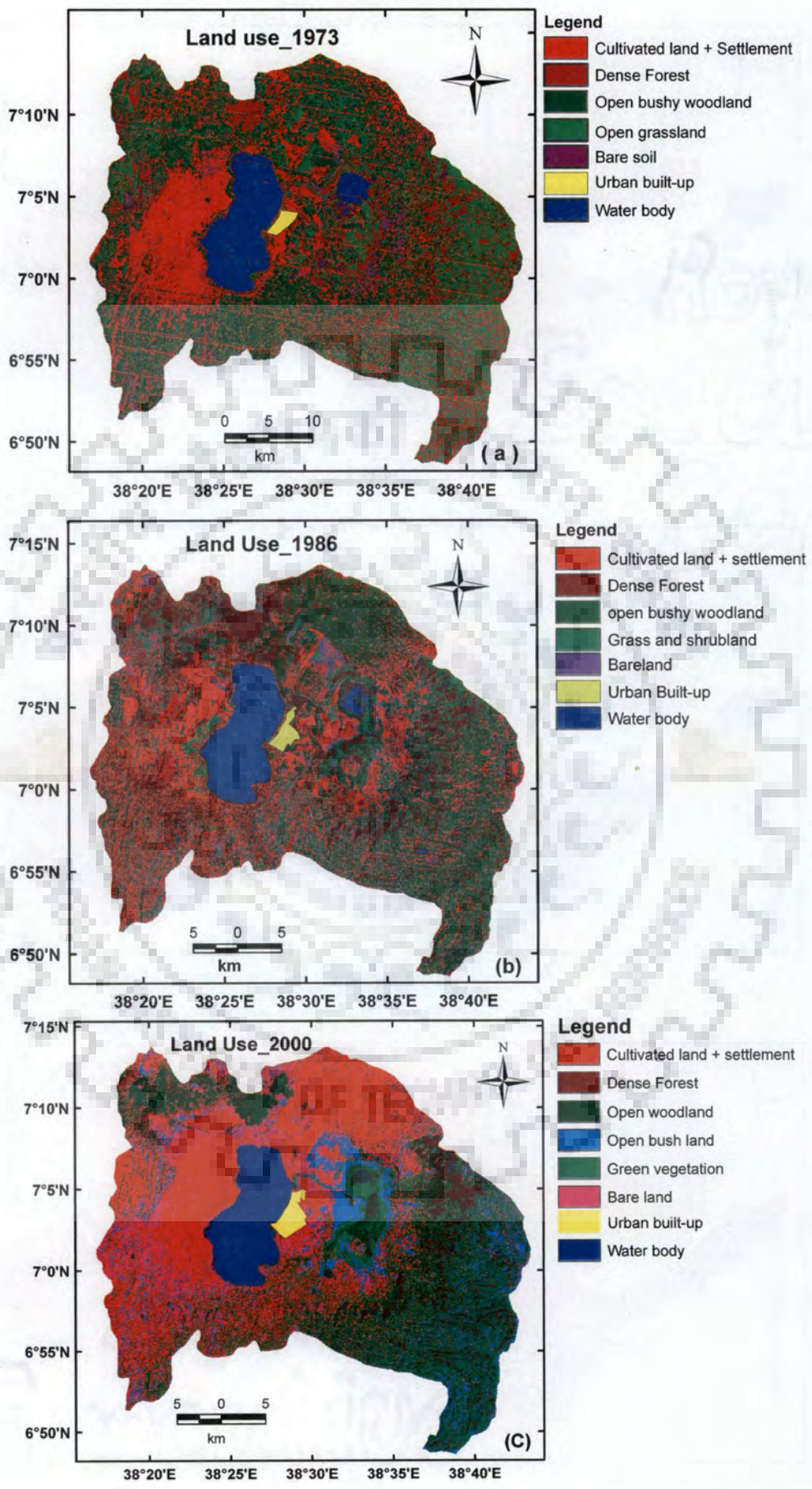


Fig. 3.14 Temporal land use/cover distribution at Hawassa lake catchment

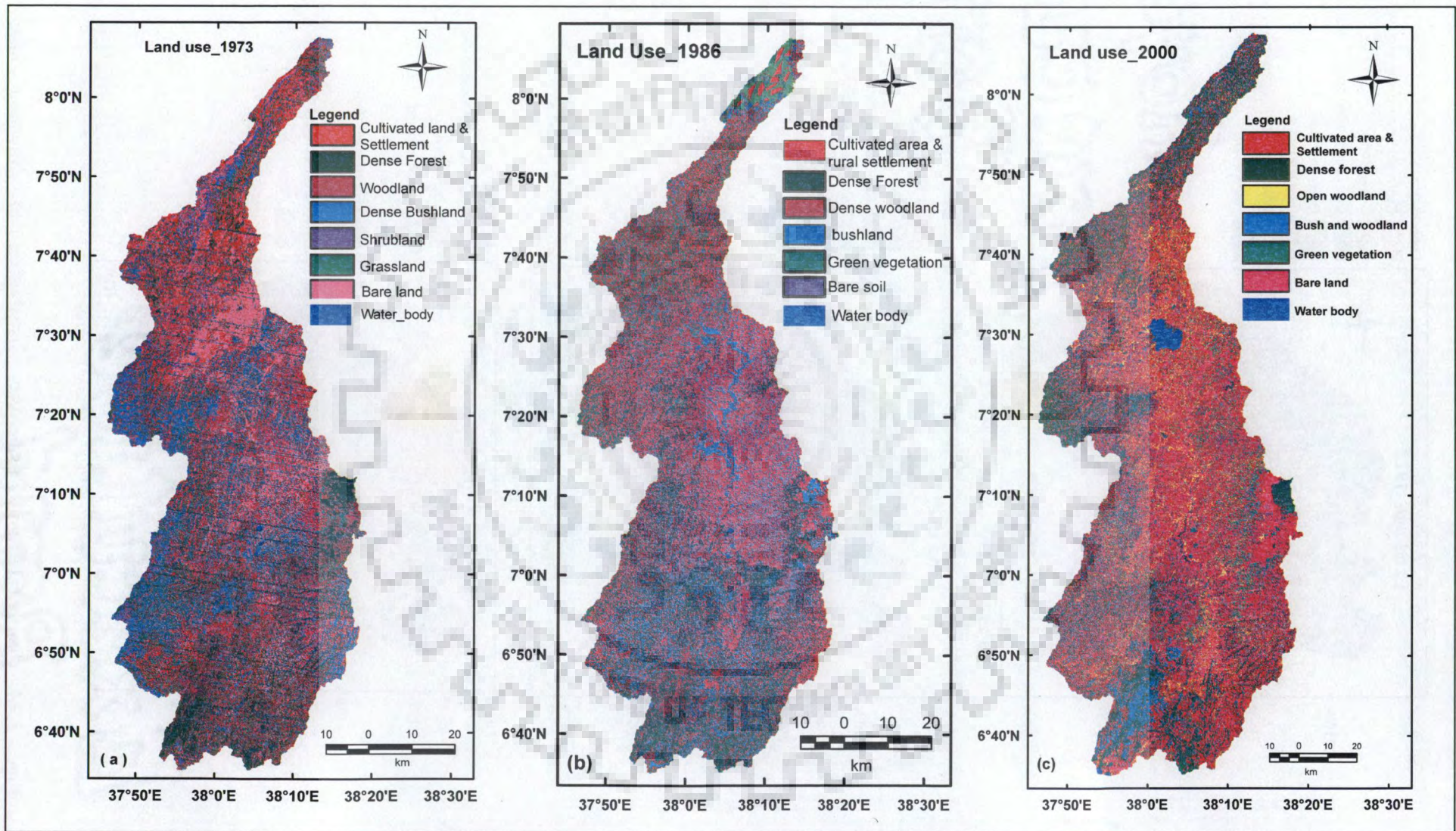


Fig. 3.15 Temporal land use/cover distribution at Bilate catchment

Table 3.13 Temporal land use/cover distribution at Bilate catchment

S.N	Land use class	1973		1986		2000		% land use change (1973/2000)
		Area (km ²)	% area	Area (km ²)	% Area	Area (km ²)	% Area	
1	Cultivated land and Settlement	1607.5	29.2	1828.3	33.3	2318.0	42.2	(+) 44.5
2	Dense Forest	659.5	12.0	871.9	15.9	440.0	8.0	(-) 33.3
3	Open Wood land	714.5	13.0	615.3	11.2	481.6	8.8	(-) 32.3
4	Bushland	975.5	17.7	820.1	14.9	570.5	10.4	(-) 41.2
5	Grassland and shrubland	1161.1	21.1	633.1	11.5	723.0	13.2	(-) 37.4
6	Bare soil	375.6	6.8	723.8	13.2	930.4	16.9	(+) 148.5
7	Water body	2.8	0.05	4.0	0.07	33	0.6	>> (+) 100
Total area		5496.5	100.0	5496.5	100.0	5496.5	100.0	

(+) = increment (-) = decrement

Table 3.14 Temporal land use/cover distribution at Hawassa lake catchment

S.N	Land use class	1973		1986		2000		% land use change (1973/2000)
		Area (km ²)	% area	Area (km ²)	% Area	Area (km ²)	% Area	
1	Cultivated land and Settlement	383.3	26.2	453.4	31.0	483.1	33.0	(+) 26.0
2	Dense Forest	180.5	12.3	165.5	11.3	80.1	5.5	(-) 55.3
3	Open bush and woodland	387.0	26.4	341.3	23.3	381.1	26.0	(-) 1.5
4	Grassland and vegetation	325.0	22.2	225.5	15.4	198.0	13.5	(-) 39.1
5	Urban built-up	5.2	0.4	7.5	0.5	10.8	0.7	(+) 75
6	Bare soil + slight cultivation	80.0	5.5	174.0	11.9	212.0	14.5	(+) 163.6
7	Gross water body	102.6	7.0	96.0	6.6	98.2	6.7	(-) 4.3
	*Cheleleka Lake (swampy area)	13.0	-	5.6	-	1.6	-	(-) 87.7
	*Hawassa Lake surface area	89.6	-	90.4	-	96.6	-	(+) 7.8
Total area		1463.0	99.9	1463.0		1463.0	100.0	

* = sub- classes of gross water body (+) = increment (-) = decrement

Gross water body in Lake Catchment found to decline in size which is further evidenced by almost drying small lake of Cheleleka and its adjoining swampy shores. The very striking phenomena of lake catchment is that the upstream swampy area gradually reduced its size over the past three decades, (13km^2 in 1973 to 1.6km^2 in 2000) and almost become abandoned, however, the main lake surface has increased by 7.8 percent compared to its coverage in 1973 (Table 4.13 and 4.14) . This might be attributed to highly modified catchment condition (encroachment of agricultural plot to swampy area, highly altered and unstable land use condition due to intense cultivation) aggravated overland flow. An important aspect of such land use alteration is further verified from increasing trend of Tikur Wuha flow and lake level over the analysis period.

3.6 CONCLUSIONS

Streamflow, lake level and rainfall events of various extents are subjected to short and long term time dependence analysis to investigate for possible fluctuations in hydro-climatic variables. Temporal land use/cover information and Sea Surface Temperature anomalies are further investigated to study their association to hydro-climatic variables.

Annual and seasonal rainfall events are characterized by statistically insignificant autocorrelation where successive time lagged events are weakly associated. Moreover, negative r_2 and r_3 which is indicative of high frequency oscillation in time series have become typical to most of observed annual and summer rainfall. MK-trend analysis for June-September rainfall at Alaba Kulito and Bilate Farm reveals decreasing trend over the observation period. Theil-Sen's trend slope estimator is in harmony with MK-trend test at similar level of confidence limit. Despite less statistically significant trend in seasonal and annual rainfall events and number of rainy days within the catchment, streamflow and lake level have showed significant increasing trend for more than 75 percent of events investigated. It is well observed from the study that observed non-stationarity is not linear over different hydro-climatic elements. This important phenomenon could likely be attributed to the combined effect of global climatic change and variability on local climate and altered catchment condition (reduction in forest cover, increase in cultivated area and expansion of eroded or bare soil) over the years. The decreasing trend of summer rainfall in Bilate catchment is a characteristic example of influence of global climate change in micro-climate. The long range dependence in hydrologic variables is examined using Hurst's coefficient. The estimated Hurst's coefficient (H) is greater than 0.5 for all events

of streamflow and lake level which suggests a likely evidence of long term persistence in hydrologic variables. Annual events of Tikur Wuha river ($H=0.96$) and Hawassa lake level ($H=0.89$) and monthly series of Hare river ($H=0.89$) and Hawassa lake level ($H=0.97$) are characterized by strong persistence. No random walk situation is examined from rescaled range analysis for monthly and annual series.

The deterministic cyclic components of streamflow are legitimately represented as discrete finite Fourier series. The variance explained by the first two harmonics exceeds 96 percent in most cases and the monthly flows are approximated by the first two harmonics. Observed and simulated monthly flows are analyzed for model efficiency using error coefficients and found to be in suitable harmony. The N-S and R^2 magnitude is greater than 0.97 with reasonably small RMSE. The wavelet transform is utilized to overcome the deficiency of Fourier transform in capturing time-frequency signal simultaneously. Annual rainfall series does not show systematic periodic or monotonic trend components in most cases, however, a 4-years periodic signal is inferred from annual rainfall data at Bilate basin during 1984-2000. Trend analysis carried out on various model combinations of discrete wavelet decomposed signals detected the prevailing trends in hydrologic variables efficiently. The predictive ability of different discrete wavelet combinations to reproduce the original signals is further verified using model efficiency indices. All model combinations of Hawassa lake level and Tikur Wuha streamflow are characterized by increasing trends with sufficiently acceptable model performance indices ($MSE = 0$ to 0.46 and $R^2 = 0.58$ to 1.0). Morlet continuous wavelet transform reveals that annual lake level events are characterized by 8-year periodic signals whereas Tikur Wuha streamflow follows a 4 and 8-10 years cycles.

Examined from SST anomalies over 1982-2010 analysis window, positive SST anomalies with frequent signals are eminent over the last two decades. Extreme wet years (1997-98 and 2006-07) are marked with increased positive SST anomalies whereas extreme dry years (1984-86 and 2002-04) are characterized by negative SST anomalies. Even though there are such apparent associations between extreme rainfall magnitudes and SST, the frequency of above average total rainfall years to occur is relatively less during the analysis window. The average stations total rainfall is better correlated to summer season (June-September) SST whereas the association becomes weakly developed for annual average SST. Conclusively, simultaneous analysis of catchment

dynamics and hydro-climatic variables using multiple time series models to detect non-stationarity eliminates potential biasness of ruling out the effect of catchment dynamics.



CATCHMENT HYDROLOGIC MODELLING USING SOIL AND WATER ASSESSMENT TOOL

4.1 GENERAL

Topographic, land use, soil and climatic parameters vary significantly over space and time in a watershed and the resulting model outputs such as runoff, sediment yield and nutrients load are affected by such variability. Capturing the watershed behavior at a very small possible spatial scale characterized by unique topographic, land cover and soil attributes known as hydrologic response units (HRUs) minimizes uncertainties generated during model simulation and calibration.

In this chapter, the impact of topographical, weather and catchment parameters on runoff generation is investigated. Concise review of watershed modelling, description of SWAT model and temporal and spatial input datasets pertinent to SWAT modelling are presented. Watershed delineation, runoff simulation, model parameter sensitivity analysis, calibration and validation phases are elaborated. Finally, based on results from subsequent analysis, conclusions are drawn.

4.2 THE NEED FOR HYDROLOGIC MODELLING IN THE STUDY WATERSHEDS

A plethora of deterministic hydrologic models (Abbott and Refsgaard, 1996; Beven, 2001), extending from empirical models such as unit hydrograph, regression methods and artificial neural network to physically based distributed hydrologic models like Syst'eme Hydrologique Europ'een (SHE) (Abbott et al., 1986a, 1986b), Institute of Hydrology Distributed Model (IHDM) (Beven et al., 1987) and Soil and Water Assessment Tools (SWAT) (Arnold et al., 1998) are in vogue owing to their suitability with respect to available data and problem under consideration. The application of SWAT model in runoff and sediment yield modelling (Chaplot, 2005; Tripathi et al., 2006; Schuol et al., 2008; Setegn et al., 2008; Srinivasan et al., 2010; Betrie et al., 2011; Oeurng et al., 2011), nutrient and

pollutant load prediction (Kannan, 2007; Galván, 2009) and climate change impact study (Wu and Johnston, 2007; Ficklin, 2009; Bae et al., 2009; Moradkhani et al., 2010; Sridhar and Nayak, 2010) has drawn significant attention of researchers over the past two decades due to its simplicity to address wide range of watershed problems at desired spatial and temporal scale.

In runoff simulation, peak and baseflow components are significantly affected by basin physiographic features, land use/cover condition, soil and groundwater parameters. Easily accessible gridded elevation data added to rapid enhancement of GIS interface to capture the realm of spatial information highly improved grid cell watershed modelling (Pandey et al., 2006). However, limitations in available Digital Elevation Models (DEMs) to extract valuable watershed features (Pryde et al., 2007; Bhang and Schwartz, 2008; Rahman et al., 2010) and limited ability of automated watershed delineation methods such as ArcHydro and Topographical Parameterization (TOPAZ) to accurately generate watershed parameters (Orlandini et al., 2003) are challenges besetting distributed hydrologic modelling.

Watershed parameters generated from grid-based DEMs data should well conform to the natural drainage pattern. Verifying the delineated watershed parameters against surrogate ground truths extracted from landsat data before employing hydrologic modelling minimizes errors. Thus, to represent the watershed behavior more accurately and increase confidence in predicting the output, model input parameters should be investigated thoroughly and their relative merit should be verified. Under rigorous definition of parameter ranges to resemble the watershed physical condition, modelers can substantially minimize the uncertainties. The magnitude of uncertainty could also be predicted at prescribed significance level that could help as a proxy tool for evaluating the accuracy of input variables.

As in most other developing countries, Ethiopian watersheds suffer from unreliable and inadequate hydrologic data that leads to loss of fidelity in obtaining valuable information for water resources management in the basin. The impact seems more profound in ungauged catchments where the broad catchment properties are forcibly represented as lumped parameters to estimate runoff and sediment yield.

To assess the impact of terrain, weather and catchment parameters on runoff generation, the Soil and Water Assessment Tool (SWAT 2005) is applied to two watersheds

of Rift Valley lakes basin of Ethiopia. Published research studies on runoff and sediment yield assessment using SWAT model in Ethiopia are limited to Blue Nile Basin (Setegn et al., 2008; Betrie et al., 2011) of Ethiopia.

Only limited attempt has been made in the past to apply process based continuous hydrologic models to study the combined effect of required input parameters on runoff generation in Rift valley lakes basins of Ethiopia. Bekele (2001) investigated water resources potential of Abaya-Chamo sub-basin of the lower Rift Valley basin using conceptual models. Tadele (2009) applied SWAT model to explore watershed responses to land use management practices in the Hare watershed.

In the present study an attempt has been made to explore the influence of Topographic parameters, weather variables and catchment characteristics on basin's water yield. The specific objectives of the study are (1) to explore the merits of two important watershed delineation methods (TOPAZ and ArcHydro) using 90m Shuttle Radar Topography Mission (SRTM) and 30m Advanced Space-borne Thermal Emission and Reflection Radiometer (ASTER) DEM data ; (2) to investigate the suitability of SWAT model to simulate runoff and (3) to assess the relative influence of basin and sub-basin parameters on runoff generation using two example watersheds operating under diverse climatic condition in the Rift Valley lakes basin. The schematic representation of methodology used in the present study is shown in Fig. 4.1.

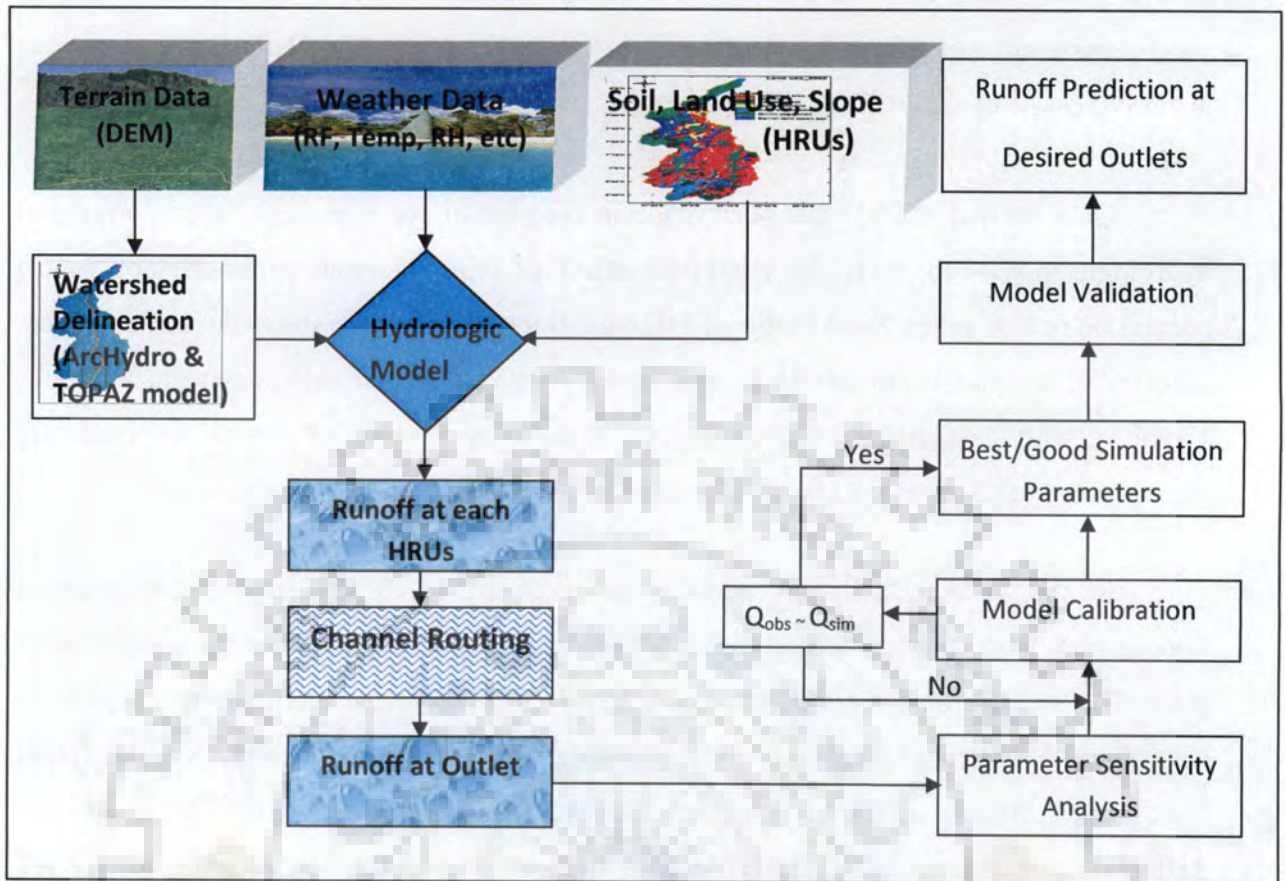


Fig. 4.1 Schematic representation of methodology employed in the study

4.3 DESCRIPTION OF THE SWAT MODEL

The hydrological component of SWAT model is based on the water balance equation that accounts for soil water content (SW), rainfall (R_i), surface runoff (Q_i), evapotranspiration (ET_i), amount of water entering the vadose zone from the soil profile ($W_{seep,i}$) and return flow (Q_{gw}). The equation is given by:

$$SW_t = SW_0 + \sum_{i=1}^t (R_i - Q_i - ET_i - W_{seep,i} - Q_{gw,i}) \quad (4.1)$$

Where SW_0 is the initial soil water available for plant uptake and is the difference between the initial soil water content and the permanent wilting point; SW_t is the final state soil water content; t is time in days and other parameters are as defined above in units of mm of water depth.

The SCS-CN (USDA-SCS, 1972) and Green-Ampt's soil moisture method (Green and Ampt, 1911) are two options available in ArcGIS interface based Soil and Water

Assessment Tool (SWAT-2005) to estimate runoff. In the present study the SCS-CN approach has been used as available weather data is limited to daily basis only. SCS-CN method identifies three CN values corresponding to dry, average and wet antecedent moisture conditions for subsequent estimation of direct runoff.

The Direct runoff is computed using SCS-CN method as:

$$Q_i = \frac{(P_i - I_a)^2}{(P_i - I_a + S)} \quad (4.2)$$

where Q_i is daily runoff; P_i is daily rainfall depth (mm); I_a is initial abstraction (mm) and include components such as interception, surface storage or pre-runoff infiltration amount and S being a retention parameter (mm). The retention parameter is a function of soil, land use, slope and soil water content parameters and approximated as a function of Curve Number (CN).

$$S = 25.4 \left(\frac{1000}{CN} - 10 \right) \quad (4.3)$$

Initial abstraction (I_a) is commonly approximated as 20% of maximum potential retention (S) and eqn. (4.2) is further simplified as:

$$Q_i = \frac{(P_i - 0.2 S)^2}{(P_i + 0.8 S)} \quad (4.4)$$

Once the curve number value for average soil moisture condition (CN_2) is identified, the corresponding CN values for dry (CN_1) and wet (CN_3) days are computed as:

$$CN_1 = CN_2 - \frac{20 * (100 - CN_2)}{(100 - CN_2 + \exp [2.533 - 0.0636 * (100 - CN_2)])} \quad (4.5)$$

$$CN_3 = CN_2 * \exp [0.00673 * (100 - CN_2)]$$

Peak runoff is estimated using rational method in which the time of concentration (time where the entire watershed area contributes to the outlet) is the sum of time of concentration for overland and channel flow. In this method, the rate of runoff increases until rainfall duration is equal to time of concentration and eventually decreases.

The rational formula is given as:

$$Q_{\text{peak}} = \frac{C i A_c}{3.6} \quad (4.6)$$

where Q_{peak} is peak runoff (m^3/s); C is runoff coefficient ; i is average rainfall intensity (mm/hr) during the time of concentration and A_C being sub-basin area (km^2). In SWAT model the amount of rainfall falling during the time of concentration is estimated as a fraction of daily rainfall occurring on specified day. The fraction ranges from one-twenty fourth of time of concentration for storms of uniform intensity to unity for short duration storms. The Overland flow time of concentration is computed as function of slope length and overland flow velocity.

$$t_{\text{ov}} = \frac{L_s}{3600 * V_{\text{ov}}} \quad (4.7)$$

Where t_{ov} is time of concentration (hrs); L_s is sub-basin slope length (m) and V_{ov} being overland flow velocity (m/s). Overland flow velocity (V_{ov}) is computed applying Manning's roughness equation for a unit width of channel section down the slope.

The Manning's equation is given as:

$$V = \frac{1}{n} R^{2/3} S^{1/2} \quad (4.8)$$

where V is flow velocity (m/s); R is hydraulic radius given as ratio of flow area and wetted perimeter (A/P_w); S is channel bed slope (m/m) and n being Manning's roughness coefficient. Draining areas that are not forming stream lines are generally treated as overland flow areas. A very thin layer of flow occurs on overland flow areas and the depth of flow is generally considered to be small and subsequently the wetted perimeter for overland flow is approximated by the width of the channel. Thus, overland flow velocity for unit width down slopping channel section will be:

$$V_{\text{ov}} = \frac{1}{n} \left(\frac{q}{V_{\text{ov}} P_w} \right)^{2/3} S^{1/2} \quad (4.9)$$

Simplifying eqn. (4.9) yields

$$V_{\text{ov}} = \frac{q^{2/5} S^{3/10}}{n^{3/5}} \quad (4.10)$$

where q is average overland flow rate (m^3/s). Assuming an average unit flow rate of 6.35 mm/hr (Neitsch et al., 2005), average overland flow velocity over entire slope length is given as:

$$V_{\text{ov}} = \frac{0.005 * L_s^{2/5} S^{3/10}}{n^{3/5}} \quad (4.11)$$

Substituting V_{ov} in eqn. (4.7) from eqn. (4.11), the time of concentration for overland flow becomes:

$$t_{ov} = \frac{L_s^{3/5} n^{3/5}}{18 * S^{3/10}} \quad (4.12)$$

The Manning's roughness coefficient for overland flow is dependent on the land management and cover condition.

The time of concentration for channel flow (t_{ch}) is computed using the following relation.

$$t_{ch} = \frac{0.62 * L * n^{3/4}}{A_C^{1/8} S_{ch}^{3/8}} \quad (4.13)$$

where t_{ch} is time of concentration for channel flow (hr) and L is the longest channel flow path (km); A_C is sub-basin area (km²) and S_{ch} is channel slope (m/m). Median size of bed material, channel irregularity, shape and size of the channel cross section, and surface cover are among few parameters influencing Manning's roughness coefficient for channel flow (Chow, 1959).

The total amount of surface runoff entering to the main channel includes the computed daily runoff and surface runoff amount lagged from previous days. The surface runoff lag coefficient (SURLAG) component accounts for the fraction of runoff allowed to enter a reach in a given day. Thus, the amount of surface runoff entering the main channel at day i ($Q_{s,i}$) is given by:

$$Q_{s,i} = (Q_{s,i} + Q_{lag,i-1}) \left[1 - \exp\left(\frac{-SURLAG}{t_c}\right) \right] \quad (4.14)$$

where $Q_{s,i}$ is surface runoff generated in the sub-basin in day i (mm); $Q_{lag, i-1}$ is surface runoff lagged from previous day (mm) and t_c is time of concentration (hrs). Appreciable amount of water is held in storage when the SURLAG value is smaller hence the runoff magnitude lagged from previous days would contribute substantial amount of runoff in the next days.

Transmission losses in SWAT model are estimated considering area of sub-basin, fraction of total sub-basin area contained in each HRUs, effective hydraulic conductivity, tributary channel width, length of longest flow path of tributary channel. Such transmission losses are expected to supplement moisture to the shallow aquifer.

The difference between the soil water content at permanent wilting point and field capacity termed as available soil water content is an essential component that limits the plant water uptake. Albeit both saturated and unsaturated flow take place within soil layer, SWAT simulates saturated flow directly assuming that the water is distributed uniformly within individual soil layer. The unsaturated flow governed by the difference in potential gradient of water in the soil layers usually moves in all directions and estimated indirectly from depth distribution of plant water uptake and soil water evaporation. Fraction of water in excess of field capacity moves down as percolation water. Percolation water moves down as long as the soil layer below is unsaturated and not frozen.

The potential water uptake by plants from soil surface in the root zone on a given day is estimated as:

$$W_{up,z} = \frac{E_t}{[1 - \exp(-\beta_w)]} \left[1 - \exp\left(-\beta_w * \frac{Z}{Z_r}\right) \right] \quad (4.15)$$

where $W_{up,z}$ is the potential water uptake from the soil surface at specified depth Z (mm); E_t is the maximum plant transpiration (mm); β_w is water distribution parameter; Z is depth from the soil surface and Z_r is the depth of root zone.

In SWAT, runoff generated from individual HRUs joins the respective stream path and routed through variable storage and Muskingum channel routing techniques while accounting for all possible losses in the channel. The variable storage routing method (Williams and Hann, 1973; Arnold et al., 1995) is employed in the present case. In Variable storage channel routing the travel time is computed as a simple linear function of volume of water in the channel and flow rate. The channel storage coefficient is estimated using travel time. Finally, the outflow volume will be the fraction of inflow volume into the reach and water stored in the reach. The fractional component is called the storage coefficient.

Expressing the continuity equation in terms of inflow and outflow rate at two defined time steps as:

$$\left(\frac{Q_{in,1} + Q_{in,2}}{2} \right) \Delta t - \left(\frac{Q_{out,1} + Q_{out,2}}{2} \right) \Delta t = V_{s,2} - V_{s,1} \quad (4.16)$$

where Q_{in} and Q_{out} are inflow and outflow rates (m^3/s) respectively, V_s is storage volume (m^3) and Δt is the time step (s). Subscripts 1 and 2 indicate the beginning and end of time steps.

The total travel time is computed as ratio of inflow volume and flow rate in the reach as:

$$T_{tr} = \frac{V_s}{Q_{out}} \quad (4.17)$$

where T_{tr} is travel time (s) and V_s is volume of water stored at any given time (m^3) and Q_{out} is corresponding outflow rate (m^3/s).

Re-arranging eqn. (4.16) we have,

$$\bar{Q}_{in} + \frac{V_{s,1}}{\Delta t} - \frac{Q_{out,1}}{2} = \frac{V_{s,2}}{\Delta t} + \frac{Q_{out,2}}{2} \quad (4.18)$$

where \bar{Q}_{in} is an average inflow rate (m^3/s).

Eliminating the storage volume from eqn. (4.18) by substituting eqn. (4.17) and further simplifying gives

$$Q_{out,2} = \left(\frac{2 \Delta t}{2 T_{tr} + \Delta t} \right) \bar{Q}_{in} + \left(1 - \frac{2 \Delta t}{2 T_{tr} + \Delta t} \right) Q_{out,1} \quad (4.19)$$

The term $\left(\frac{2 \Delta t}{2 T_{tr} + \Delta t} \right)$ is known as storage coefficient (SC). Expressing the flow rate in volume units and rearranging the eqn. (4.19) for V_{out} , yields

$$V_{out} = SC (V_{in} + V_{s,1}) \quad (4.20)$$

Transmission losses from the channel to the sub soil profile are eminent during dry periods. Effective hydraulic conductivity of the channel alluvium, flow travel time, wetted perimeter and channel length are parameters limiting transmission losses. Likewise, evaporation losses from reach are also computed as function of potential evapotranspiration, channel geometry (length and width) and fraction of time step in which water is moving in the reach. SWAT models the movement of water from bank storage to adjacent unsaturated zone to meet part of the evapotranspiration demand. The groundwater 'revap' coefficient (GW_REVAP.gw) for the HRU in the sub-basin accounts for such losses from bank storage.

Groundwater contribution to channel flow is modeled as shallow and deep aquifer in each sub-basin. SWAT considers the shallow aquifer contribution to the reach, however, the deep aquifer is assumed to contribute flow away from the watershed. The daily shallow aquifer water balance components are the inflow (antecedent shallow aquifer storage content

and recharge amount) and the outflow (base flow, 'revap' component to meet root zone water deficiency and amount removed from shallow aquifer by pumping). The base flow component for a steady state groundwater flow response to recharge is:

$$Q_{gw} = \frac{8000 * K_{sat}}{L_{gw}^2} * h_{WT} \quad (4.21)$$

where Q_{gw} is base flow to main channel (mm); K_{sat} is saturated hydraulic conductivity (mm/day); h_{WT} is water table height (m) and L_{gw} is distance from a sub-basin groundwater divide to main channel (m). The movement of water from the shallow aquifer to the overlying unsaturated zone represented as 'revap' is significant when the saturated zone is close to the surface and estimated as a fraction of the potential evapotranspiration. Evaporation is estimated using Penman-Monteith method as it uses more weather parameters influencing the evapotranspiration process.

4.4 MODEL SENSITIVITY AND UNCERTAINTY ANALYSIS

Uncertainties arising from assumptions considered during model development, input variables, model parameters and measured data need to be assessed. The sensitivity of model parameters to such uncertainties should be evaluated prior to fine tune model parameters. Defining model parameter values within physically permissible limits minimizes errors propagated during model calibration and validation. The sensitivity analysis techniques employed in SWAT 2005 model are summarized below.

The Latin Hypercube (LH) Sampling: The LH simulation uses a stratified sampling approach that is based on Monte Carlo simulation (Mckay, 1988). The stratified sampling techniques aids in materializing efficient output values over limited number of simulations. The LH approach subdivides the distribution of each parameter into N ranges each of which with a probability of occurrence equal to 1/N. Each range is sampled randomly once in the prescribed boundary. Finally, the model runs N times with the random combination of parameters.

One-Factor-At-a-Time (OAT) Sampling: The OAT method is designed to cover local to global sensitivity method (Morris, 1991). The local sensitivity analysis using OAT method is handled by changing one parameter at a time during the run and the change in output is ultimately attributed to the input parameter changed. Model output is evaluated in terms of

sum of square errors (SSQ) that matches observed and simulated outputs. OAT sampling appears to be widely used in SWAT modelling (van Griensven et al., 2001).

The LH-OAT Sampling: The LH-OAT sampling enjoys the benefit of LH sampling that ensures all parameters ranges are sampled applying OAT design that describes the change in output is uniquely attributed to particular input change. The method is robust in identifying sensitive parameters and for m intervals in LH and p number of parameters, a total of $m*(p+1)$ runs are required.

Sequential Uncertainty Fitting Version 2 (SUFI-2) Analysis: Sequential Uncertainty Fitting (Abbaspour, 2009) accounts for all sources of uncertainty associated to modelling. The strength of uncertainty analysis is measured by two important factors (P-factor and R-factor) in SUFI-2. The percentage of measured data bracketed by the 95 percent prediction uncertainty (95PPU) is described as P-factor. The 95PPU is measured at the lower 2.5% and upper 97.5% of the cumulative distribution function neglecting the 5% bad simulations. R-factor, the average thickness of the 95PPU band divided by the standard deviation of the measured data, is used to describe the cumulative uncertainty in the model. R-factor is determined from the expression:

$$R - \text{factor} = \frac{P - \text{factor}}{\sigma_x} = \frac{\frac{1}{n} \sum_{i=1}^n (X_U - X_L)_i}{\sigma_x} \quad (4.22)$$

where X_L and X_U are the 2.5th and 97.5th percentiles of the cumulative distribution of every simulated point respectively; σ_x is the standard deviation of measured variable x and n being the number of observed data points.

SUFI-2 begins with large parameter uncertainty with physically meaningful range so that the observed values are well bracketed by the 95PPU band and eventually decreases the size of uncertainty band over successive simulations. The P-factor values range between 0 and 100% while R-factor is lying between 0 and $+\infty$. P-factor value of 1 and R-factor value of 0 being an ideally optimal case where the simulated series exactly corresponding to the observed data.

4.5 MODEL PERFORMANCE EVALUATION TECHNIQUES

Watershed models are capable of simulating required output at desired location as a function of the input parameters. An ideal situation is where the model output is exactly equal to the observation values at every segment of the analysis window. Practically, simulated output is judged as acceptable if the predicted output is reasonably close to the observation. However, uncertainties associated to model input, assumptions considered in the model development, and uncertainty in observed values used for calibration and validation significantly affect the model performance. The uncertainties and assumptions are evaluated in terms of model efficiency indices. Some of commonly used model performance indices (Moriasi et al., 2007) applied for present analysis are discussed briefly in this section.

Nash-Sutcliffe Efficiency (NSE): NSE is a dimensionless index that compares residual variance to observed data variance (Nash and Sutcliffe, 1970). It is computed applying the following relationship.

$$NSE = 1 - \frac{\sum_{i=1}^n (Q_i^o - Q_i^s)^2}{\sum_{i=1}^n (Q_i^o - \bar{Q}^o)^2} \quad (4.23)$$

where Q_i^o is the i^{th} observation discharge ; Q_i^s is the i^{th} simulated discharge ; \bar{Q}^o is the mean of observed discharge and n being the total number of observations. The NSE values range from $-\infty$ to 1 with $NSE = 1$ being a perfect match of observed data to simulated one and is an ideal optimal value whereas $NSE = 0$ indicates that the model predictions are as accurate as the mean of the observed values. When the residual variance described by the nominator in eqn. (4.23) is larger than the data variance described as denominator, the observed mean is a better predictor than the model and under such circumstances NSE becomes negative. Generally, positive NSE values indicate acceptable level of performance whereas negative NSE values are judged as unacceptable. However, the NSE model alone does not adequately describe the model performance as poor models can give a high NSE value and vice-versa (Jain and Sudheer, 2008). Therefore it should be accompanied with other model efficiency performance tests.

Coefficient of Determination (R^2): Coefficient of determination describes the proportion of the variance in measured data explained by the model. R^2 ranges from 0 to 1 and values

greater than 0.5 shows acceptable level of model performance (Moriassi et al., 2007). Legates and McCabe (1999) argues that R^2 index is over sensitive to outliers and insensitive to proportionally increasing or decreasing model outputs with respect to observed values.

$$R^2 = \frac{\left[\sum_{i=1}^n (Q_i^o - \bar{Q}^o) (Q_i^s - \bar{Q}^s) \right]^2}{\sum_{i=1}^n (Q_i^o - \bar{Q}^o)^2 \sum_{i=1}^n (Q_i^s - \bar{Q}^s)^2} \quad (4.24)$$

where Q_i^o and Q_i^s are as defined in eqn. (23).

Modified Coefficient of Determination (bR^2): Modified Coefficient of determination index has the advantage over conventional R^2 in magnifying the sensitivity of coefficient of determination due to proportionally increasing or decreasing model outputs compared to observations. The slope of best fit straight line (b) of observed and simulated values is multiplied by R^2 and the resulting index is a reasonable estimate of model efficiency.

Percent Bias (PBIAS): Percent bias is a measure of the average departure of simulated data from the observed series. The optimum value of PBIAS is 0.0 with lower values indicate sufficiently reasonable model simulation (Gupta et al., 1999). The model underestimates bias when PBIAS is positive and overestimates when it is negative.

Percent bias is estimated applying the following relationship.

$$PBIAS = \left[\frac{\sum_{i=1}^n (Q_i^o - Q_i^s) * 100}{\sum_{i=1}^n Q_i^o} \right] \quad (4.25)$$

where Q_i^o and Q_i^s are as defined above.

Root mean square error–observations standard deviation Ratio (RSR): Lower values of Root Mean Square Errors (RMSE) are usually acceptable as better model performance is associated to lower RMSE. Singh et al. (2005) further extended the statistic RMSE to account for standard deviation of observed values and hence a standardized RMSE known as RSR is developed. RSR is a ratio of RMSE to standard deviation of observed values and includes the normalization factor. An optimal value of RSR is 0.0 and the lower values of RSR conform to better model performance.

Thus, RSR is computed using the statistics,

$$RSR = \frac{RMSE}{STDEV^{obs}} = \frac{\left[\sqrt{\sum_{i=1}^n (Q_i^o - Q_i^s)^2} \right]}{\left[\sqrt{\sum_{i=1}^n (Q_i^o - \bar{Q}^o)^2} \right]} \quad (4.26)$$

where $STDEV^{obs}$ is the standard deviation of observed discharges ; \bar{Q}^o is mean of observed discharges and all other terms are as defined above.

4.6 DESCRIPTION OF THE STUDY AREA

The study area encompasses Bilate and Hare watersheds of Rift Valley Lakes basin of Ethiopia (Figure 4.2).

Weira and Guder rivers emanating from the Silte and Butajira highlands are the two major perennial tributaries of Bilate river. Soon after the confluence of the two rivers, it is named as Bilate river and debouches into the terminal pool of Lake Abaya. Bilate watershed, with gross watershed area of 5330 km², stretches from an elevation of 3300 m at upstream highland to 1200 m downstream in the Rift Valley floor.

Bilate watershed is characterized by humid and semi-arid climatic conditions with bimodal rainfall pattern with major rainfall during the summer monsoon season. Mean annual rainfall observed at Alaba Kulito exceeds 1000 mm. The elevation of the watershed ranges from 3300 m at west of Butajira where Bilate river flowing down a ravine course to 1165 m at downstream outlet. Deforestation due to expansion of agricultural lands, cattle grazing and timbering substantially reduced the vegetation cover in the watershed. Series of deep gullies and massive bare soil pillars at upstream part of the watershed testifies its vulnerability to erosion hazard. The entire watershed practices a mixed cropping pattern where the lower foot of the watershed utilizes irrigation (approximately 1260 ha of government owned farm) to grow commercial crops such as tobacco and maize. Currently the demand for irrigation water is increasing and small scale communal and medium scale private investors are under urgent course of water demand.

Hare watershed (166.5 km² at the gauging outlet) is characterized by steep valleys at upstream mountainous highland and progressively stretches to flat fluvial plain until it joins the terminal lake Abaya. The lower plain area of the watershed is known for its intense

competition for irrigation water. The upstream highland region of the watershed experiences a humid climate with an average annual rainfall magnitude of 1250mm in contrast to 870mm of rainfall at Arba Minch region of the downstream sub-watershed area.

The upstream community of Hare basin is fully engaged on rain-fed cultivation and associated agricultural activities. The lower fluvial plains utilize communal based traditional and modern irrigation schemes to supplement rain-fed cultivation on nearly 2200 ha of land. Maize, sweet potato, banana, mango and cotton are among the major crops growing in the semi-arid irrigated watershed territory. Land resource competition as a result of growing number of population aggravated conversion of forest cover into agricultural plots and residential area. Household energy consumption is almost entirely based on wood biomass in the watershed and becomes another culprit to forest reduction.

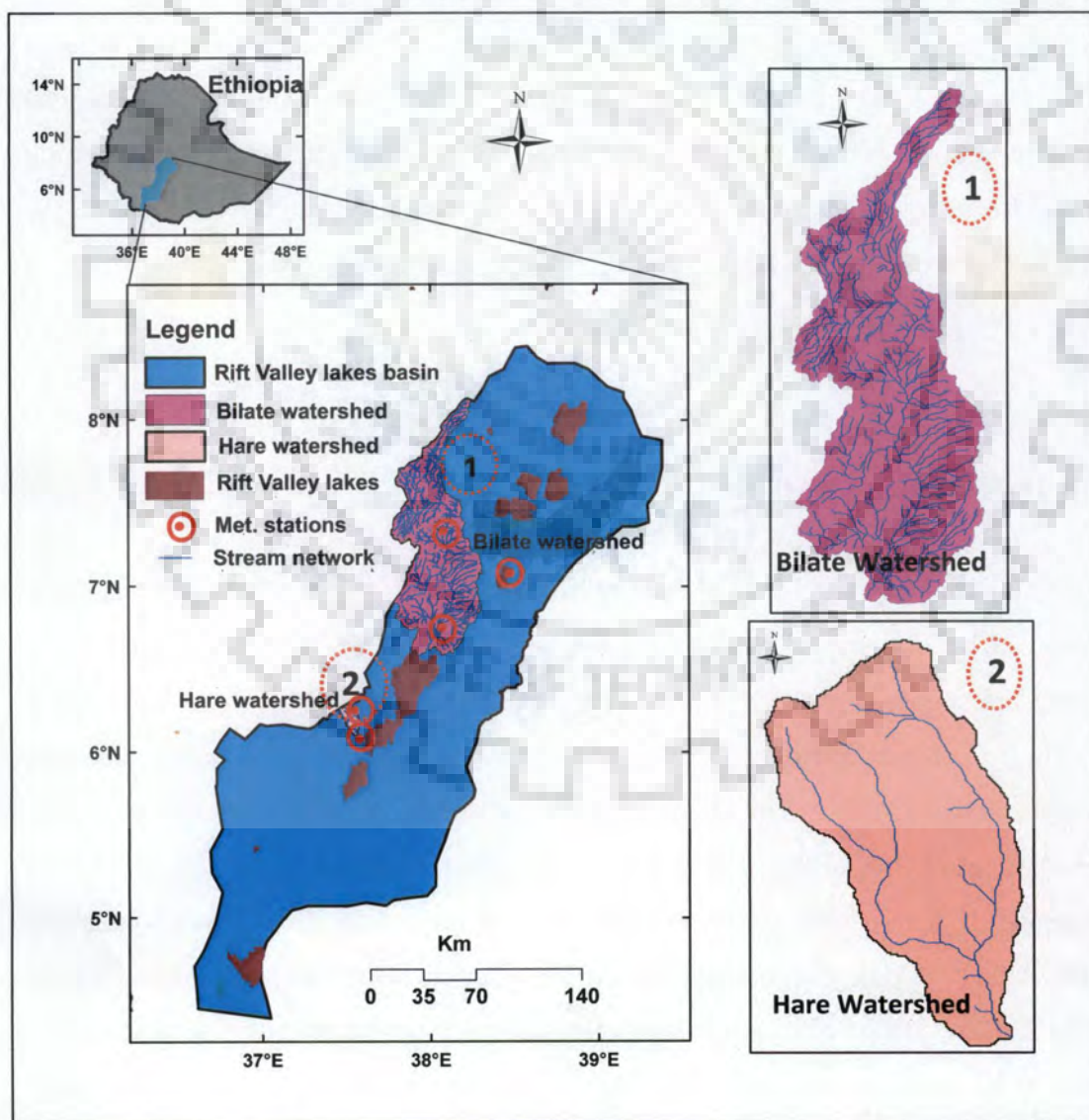


Fig. 4.2 Location and watersheds map of the study area: Bilate (1) and Hare (2) watersheds

4.7 ACQUISITION AND PRELIMINARY PROCESSING OF DATA FOR SWAT MODEL

It is not uncommon that most distributed hydrologic models are data intensive and adequate definition of spatial and temporal datasets is an essential preliminary step in application of these models for watershed modelling.

4.7.1 Topographical Data

Essential watershed morphologic parameters are computed from DEM data and subsequently utilized for watershed modelling. Elevation Model (DEM) is used to define flow direction, flow accumulation, stream network and eventually limits draining watershed area with respect to either predefined or model simulated outlet. An enhanced 90m x 90m longitudinal resolution processed Shuttle Radar Topographic Mission (SRTM) DEM data version 4.1 (Jarvis et al., 2008) is accessed from International Centre for Tropical Agriculture online source (<http://srtm.csi.cgiar.org>). A 30m Advanced Space-borne Thermal Emission and Reflection Radiometer (ASTER) data was acquired from Global Land Cover Facility online sources (www.landcover.org). To augment the raster digital data, a topographical map of scale 1:250,000 covering the study area was used in watershed delineation.

4.7.2 Soil and Land Use Data

Field scale definition of soil and land use parameters for large watershed is impractical. Soil classes organized by Ministry of Water Resources (MoWR) of Ethiopia from small scale FAO soil map are supplemented by basin-specific previous studies (Makin et al., 1975) in the region. The soil classes at Bilate and Hare basins are categorized into 9 and 4 dominant soil units respectively. The dominant soil units in Bilate watershed, as per FAO-90 soil class legend, are Vitric Andosols (28%), Chromic Luvisols (21.8%), Humic Nitisols (17.5%), Lithic Leptosols (12.6%), Mollic Andosols (3.7%) and remaining 1.3% covers other soil units. Humic Alisols (83%), Eutric Regosols (10%), Haphilic Ferralsols (5.8%) and Eutric Fluvisols (1.1%), are identified as major soil categories in Hare watershed. Respective soil physical properties such as maximum soil depth, soil hydraulic conductivity, soil water holding capacity, soil texture are defined for each soil units based on literature and previous site specific studies (Makin et al., 1975; Tadele, 2009).

Orthorectified four band multi-Spectral Scanner (MSS) LandSat-4 and seven band Enhanced Thematic Mapper Plus (ETM+) land cover images were acquired from Global Land Cover Facility online sources (<http://glcf.umiacs.umd.edu/data/landsat>). The landsat images were analysed using ERDAS imagine 9.2 and ArcGIS 9.3 following standard image processing procedures (Cermak et al., 1979; Gonzalez and Woods, 2002). Accordingly, land use/cover information for the year 2000 is extracted and major land use/cover units are identified. Table 4.1 provides the percentage area coverage of dominant land cover units in the study watersheds. Six (Bilate basin) and four (Hare basin) major land use classes are identified and latter converted to basic SWAT land use classes for initial model run; namely cultivated area (AGRL), range and bush land (RNGE), mixed green forest (FRST) and grassland (PAST). Reclassified soil, land use/cover and slope map for the study area is presented in Figs. 4.3, 4.4 and 4.5 respectively.

4.7.3 Hydro-meteorological Data

Climate data such as rainfall, temperature, wind speed and relative humidity were collected from Southern Nations Nationalities and Peoples Republic (SNNPR) meteorological department at Hawassa and National Meteorological Service Agency (NMSA) at Addis Ababa. Some of the meteorological stations located close to the study watersheds are mentioned in Table 4.2. SWAT model selects weather input data on the basis of proximity to the sub-watershed centeroid. Following the notion of station proximity to the watershed centeriod, five weather stations (Alaba Kulito , Bilate Farm, Hawassa, Arba Minch and Chench) with record length of 1990-2009 have been used for watershed modelling. Missing short length weather data values were filled up applying the weather generator (WXGN) option (Sharply and William, 1990) supplying monthly weather statistics as an input.

Observed daily stream flow data from single monitoring station at each watershed (Bilate and Hare) were obtained from Ministry of Water Resources (MoWR), Ethiopia for the analysis period. Preliminary rainfall-runoff analysis has been carried out to identify the reliability of gauge data.

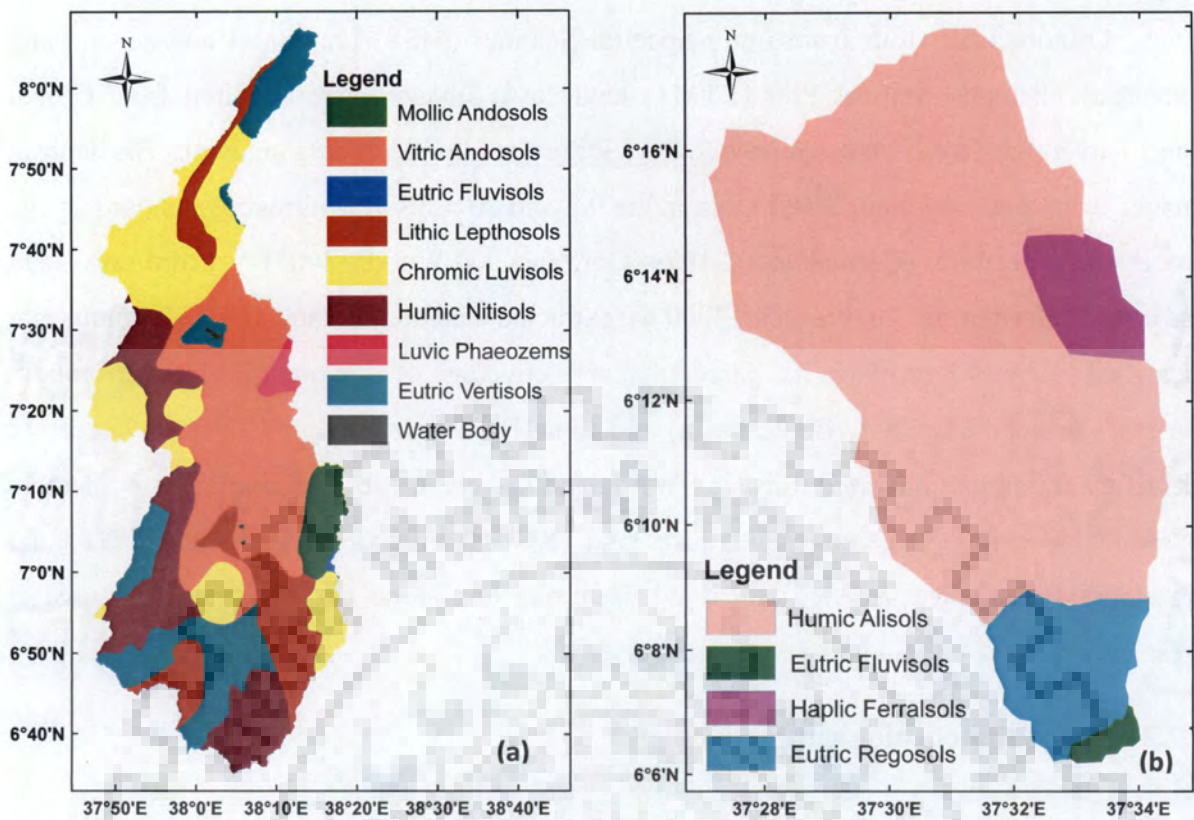


Fig. 4.3 Soil map at Bilate (a) and Hare (b) watersheds

Table 4.1 Land use/Cover distribution at Bilate and Hare watersheds in the year 2000

Land use/cover class	Land cover percentage of total Basin's area	
	Bilate basin	Hare basin*
Cultivated land and settlement area	42.2	53.2
Dense forest	8.0	28.0
Open bush and woodland	10.4	6.0
Grassland and green vegetation	13.2	12.6
Open Woodland	8.8	-
Barren land	16.9	-

* Dominant land use classes are considered

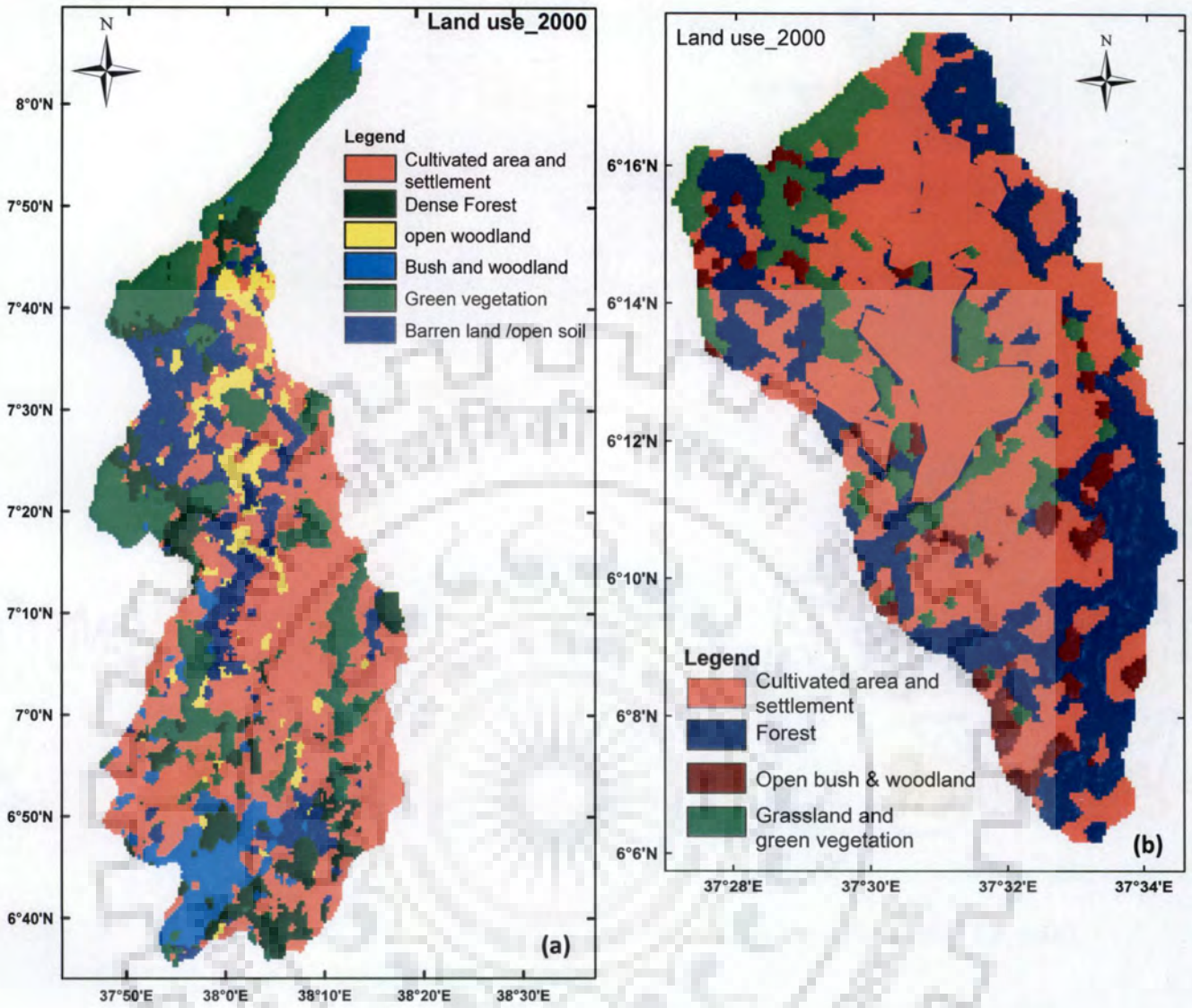


Fig. 4.4 Land use map at Bilate (a) and Hare (b) watersheds

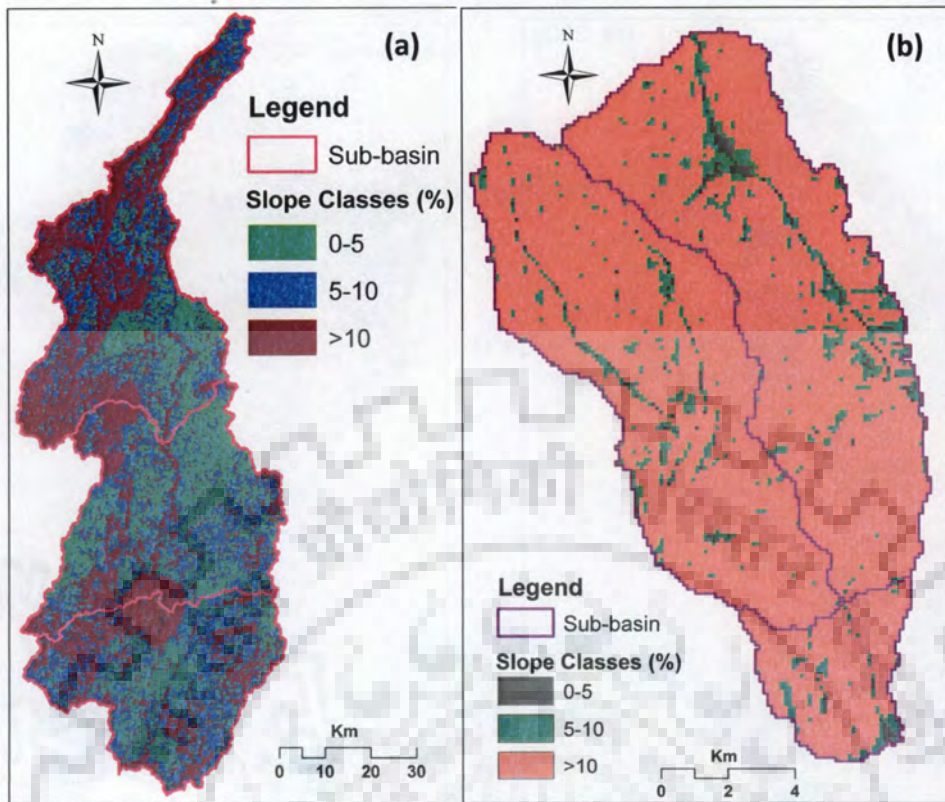


Fig. 4.5 Land slope map at Bilate (a) and Hare (b) watersheds

Table 4.2 Meteorological stations near the study area

Meteorological stations	Latitude (decimal degrees), N	Longitude (decimal degrees), E	Altitude (m)
Alaba Kulito	7.33	38.08	1750
Arba Minch Farm	6.08	37.58	1300
Bilate Farm	6.75	38.07	1300
Bilate Tena	6.40	38.05	1550
Boditi School	6.57	37.51	1860
Chencha	6.25	37.55	2680
Hawassa	7.08	38.48	1750
Hosaina	7.33	37.52	2200
Mirab Abaya	6.18	37.47	1260
Yirgalem	6.45	38.23	1735

At site and multi site rainfall analysis is carried out to identify consistency in the data series using double mass curve (Fig. 4.6) analysis and visual plots (Fig. 4.7). Kolmogorov-Simrnov (K-S) goodness-of-fit test for annual rainfall series confirms that annual rainfall

series at Alaba Kulito, Hawassa, Arba Minch and Chenchu are normally distributed (Fig. 4.8). Statistical parameters of annual rainfall series are summarized in Table 4.3 for four stations located in the watersheds.

Temperature variability and rainfall–runoff relationship in the watershed was also investigated for possible discrepancies in observed series. Long term average daily maximum temperature is observed during the months from January to April at Alaba kulito and Hawassa stations. It ranges from 28.5-31 degree Celsius with average minimum temperature of 10 degree Celsius in the months of November and December. The semi-arid climatic zone of lower Hare watershed is characterized by relatively higher daily maximum and minimum temperature during the same season. The average maximum temperature varies between 32 and 33 degree Celsius with minimum of 15 degree Celsius.

Table 4.3 Rainfall statistical parameters at nearby stations to watershed outlets

Rainfall station	Mean	Std. dev.	C_v	C_s	C_k	Percentiles			K-S Statistic	
						25%	50%	75%	D	$P_{crit.}$
Alaba Kulito	981.3	151.9	0.15	0.57	-0.72	864.9	953.5	1105.8	0.183	0.513
Arba Minch Farm	898.7	156.9	0.17	0.69	0.2	785.3	868.6	965.2	0.159	0.720
Chenchu	1298.5	339.9	0.26	1.22	3.33	1080.3	1269.6	1467.5	0.123	0.935
Hawassa	953.1	143.5	0.15	0.25	-0.72	841.7	924	1068.4	0.118	0.942

C_v =Coefficient of Variation , C_s =coefficient of Skewness , C_k =Coefficient of kurtosis , K-S =Kolmogorov-Simrnov

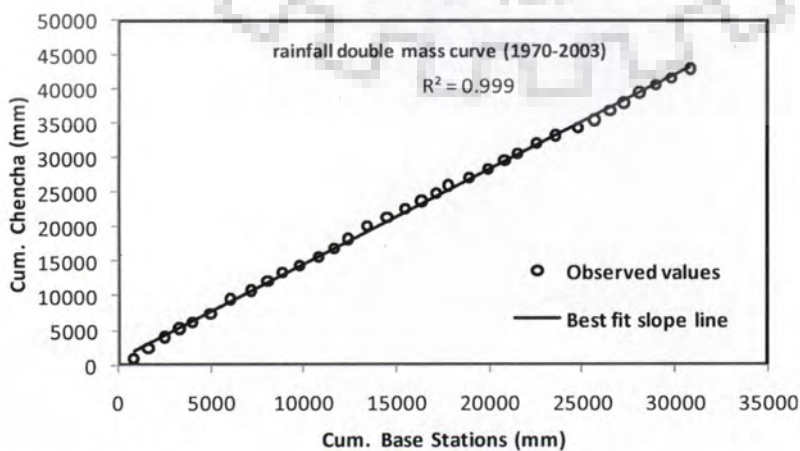
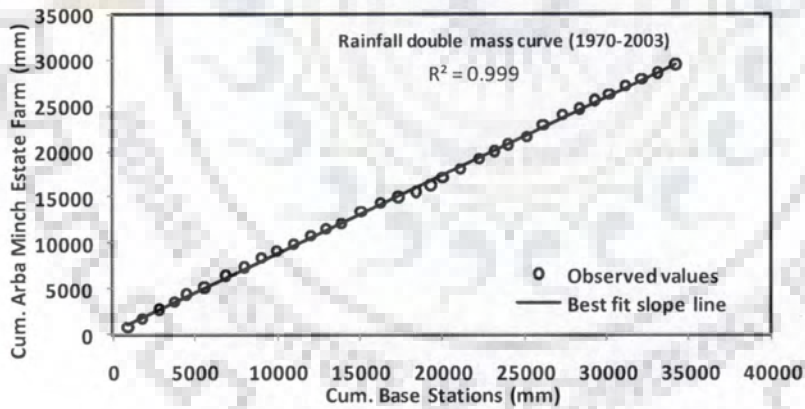
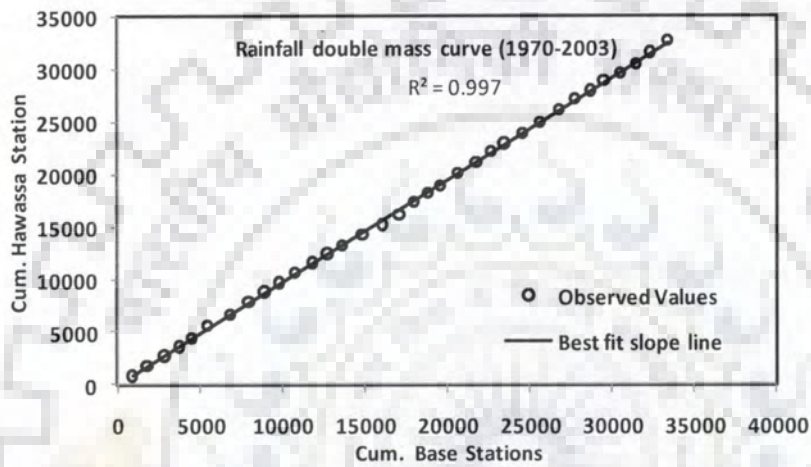
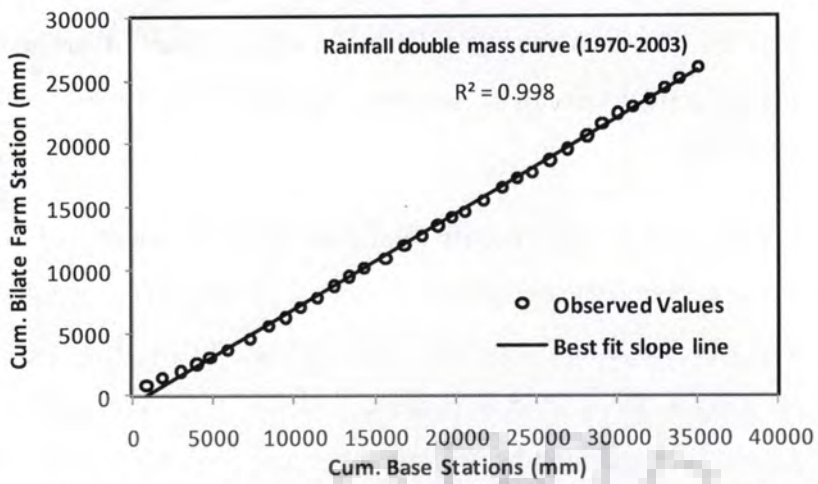


Fig. 4.6 Rainfall double mass curve analysis for selected stations

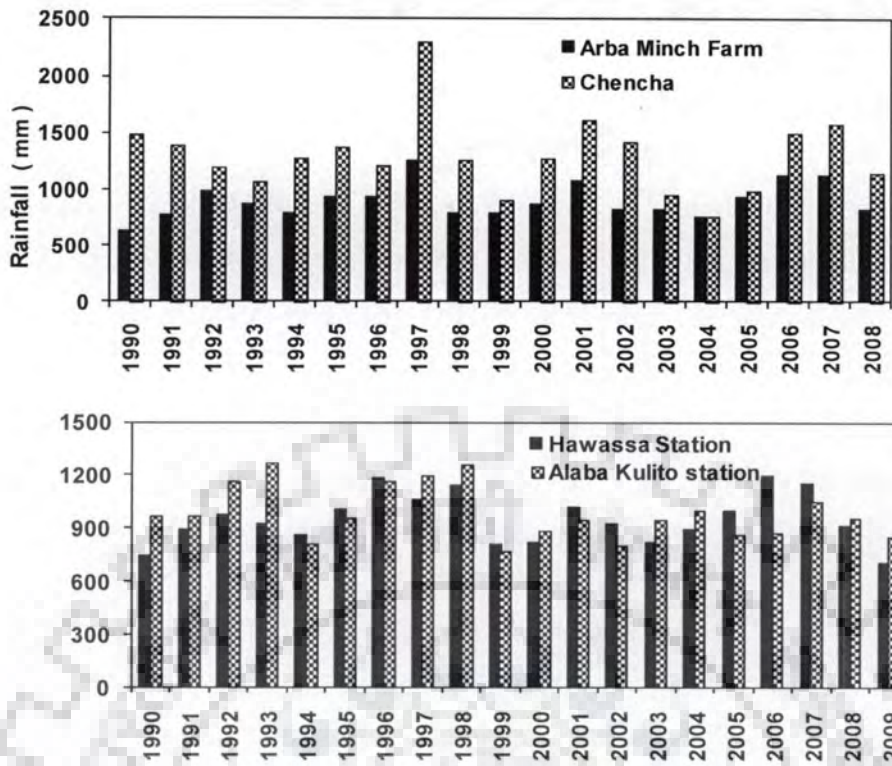


Fig. 4.7 Annual rainfall plots for selected stations in the study basin

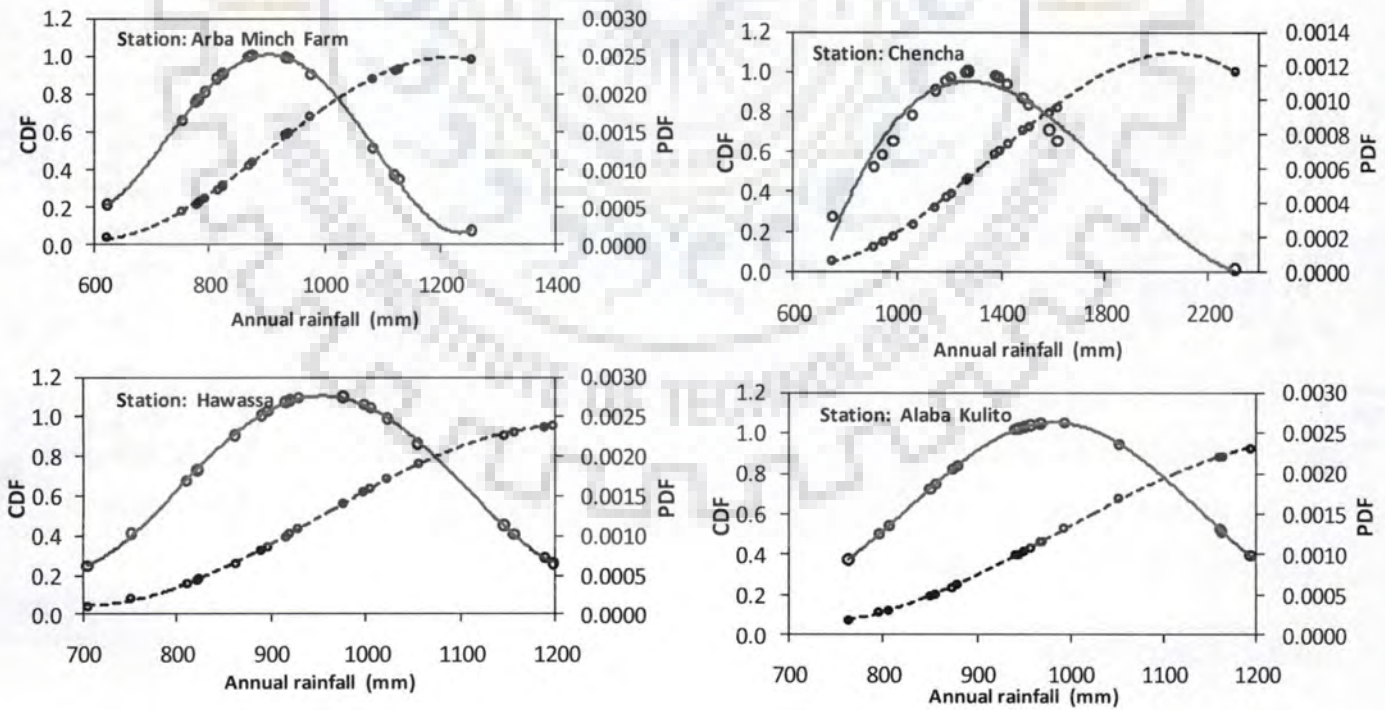


Fig. 4.8 Probability distribution fitted to annual rainfall series at selected stations

4.8 WATERSHED DELINEATION AND SWAT MODEL SETUP

4.8.1 Watershed Delineation

In the present study ArcHydro of ArcGIS/ArcSWAT and TOPAZ (Topographical Parameterization) (Garbrecht and Martz, 1997) of Watershed modelling System (WMS) are used to delineate the watersheds from 90m SRTM and 30m ASTER GDEM data. The delineated watershed boundary, stream network and main stream path are further verified using Landsat derived and Google Earth extracted stream and existing watershed map. Limitations of 90m SRTM and 30m ASTER DEM data in generating flow path and watershed boundary are explored using two example watersheds.

Both ArcHydro and TOPAZ watershed delineation tools utilize a deterministic eight-neighbour flow direction matrix (D8) algorithm (O'callaghan and Mark, 1984) in which each pixel discharges into one of its eight neighbours, separated by 45° from the nearest point, in the direction of the steepest descent. Sensitivity to DEMs, ability to produce spurious flow paths in flat terrain and failure to represent flow paths in convex slopes are commonly reported limitations of D8 approach (Gallant and Wilson, 1996; Tarboton, 1997; Martz and Garbrecht, 1998; Orlandini et al., 2003). Attempts have been made to minimize the problems encountered in the conventional D8 approach. The D8-TOPAZ algorithm (Garbrecht and Martz, 1997) overcomes some of the drawbacks encountered in D8 approach.

Spatially referenced and depression filled 90m and 30m DEM are subjected to step by step procedure of watershed delineation using ArcHydro and TOPAZ methods. The ArcHydro watershed delineation is based on the premises of systematically defined sub-basin outlets based on elevation data from DEM so that the user is either prompted to define the outlet or rely on automatically generated pour points as outlet. Stream networks and sub-basin boundary generated applying user defined "draining area" threshold requires further enhancement to produce seamless sub-watershed units.

4.8.2 Model Setup

Accuracy of the model output is judged by adequate assignment of land use and soil parameters. SWAT-2005 land use database contains approximately 102 land use properties and has a flexibility to include more land and soil databases. Slope classification up to 5 different slope class ranges is also possible. On the premise of this, the land use, soil and

slope units are reclassified based on the respective dominant properties. The required soil, land use and slope data are overlaid and a unique combination of these parameters called hydrologic response units (HRUs) are identified. HRUs threshold values for land use, soil and slope class is selected as percentage over sub-basin (10%), land use (15%) and soil (15%) respectively. For example, if the land use unit covers at least 10% of the sub-basin area, then it is assigned a land use class whereas the land use unit that covers less than 10% of the sub-basin area is proportionally spread over other dominant land use classes. Following similar notion, 15% threshold value is assigned for soil and slope units. A total of 56 HRUs at Bilate and 14 HRUs at Hare watersheds are identified. Observed daily weather data from nearby stations and station location parameters are supplied to the model as input parameters. Associated soil, land use, groundwater, management, crop, basin and HRUs parameters are edited to suit the prevailing watersheds behaviour.

4.9 RESULTS AND DISCUSSION

4.9.1 DEMs and Limitations of Watershed Delineation Algorithms

A rigorous attempt has been made to analyze the effect of different resolution Digital Elevation Model data while generating watershed morphological parameters. Watershed area, flow accumulation path and stream networks are generated by two automated water delineation approaches (ArcHydro and TOPAZ) from 90m SRTM and 30m ASTER DEM and subsequently evaluated for their performance.

It has been observed that the 30m ASTER DEM data generated spurious flow accumulation area at Hare watershed, as sketched by dark solid arrows, in the eastward direction that drains away from the watershed boundary and joins the adjoining watershed. A maximum Euclidean distance of 1.86 km flow accumulation and subsequent stream path offset is observed. Such deviation in flow path resulted in reduction of 29.2 % in actual watershed area (Fig. 4.9). The longest flow path generated from 90m and 30m DEM is compared and an offset in terms of Euclidean distance for 147 points is summarized. An average offset of 0.162 km with standard deviation of 0.375km is observed. The stream path and basin boundary generated from 90m SRTM data using ArcHydro and TOPAZ methods are at reasonable agreement.

The observed difference in area between the two automated watershed delineation methods are 1.14km^2 at Hare and 0.6km^2 at Bilate watersheds. The density of stream network, in both cases, is proportional to draining area threshold. Both TOPAZ and ArcSWAT fail to capture the actual flow path accurately in flat terrain of Bilate basin. The main stream flow path deviates from surrogate Landsat (acquired for the year 2000) and Google Earth (2005/2006 image) extracted main stream path by an average distance of 7.5 km in west-east direction for a total stream length of 30km at the lower foot (Fig. 4.10). Fig. 4.11 presents ArcHydro and Topaz generated watershed boundary and stream network compared against Google Earth map extracted stream path.

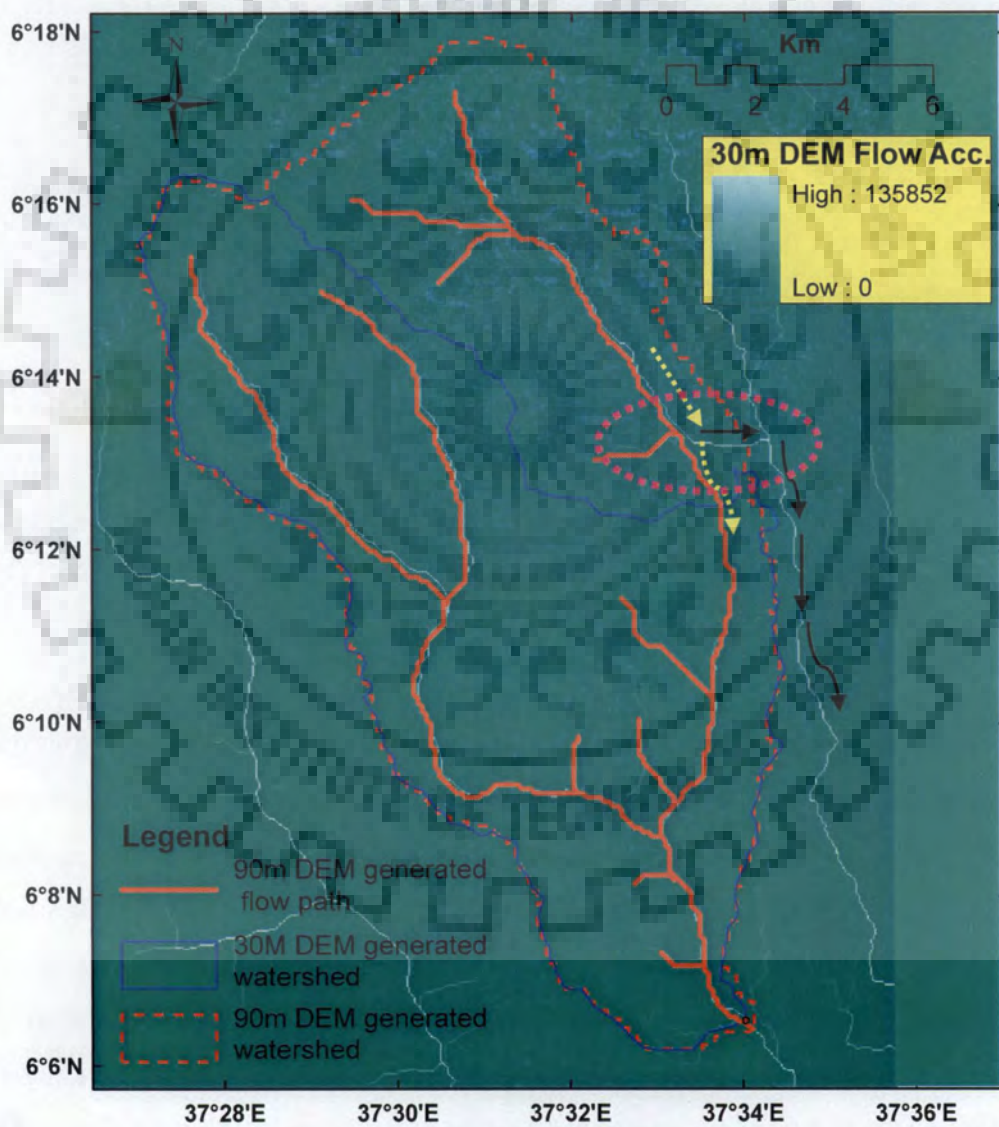


Fig. 4.9 SRTM-90m and 30m ASTER DEM data generated watershed boundary and flow path at Hare watershed

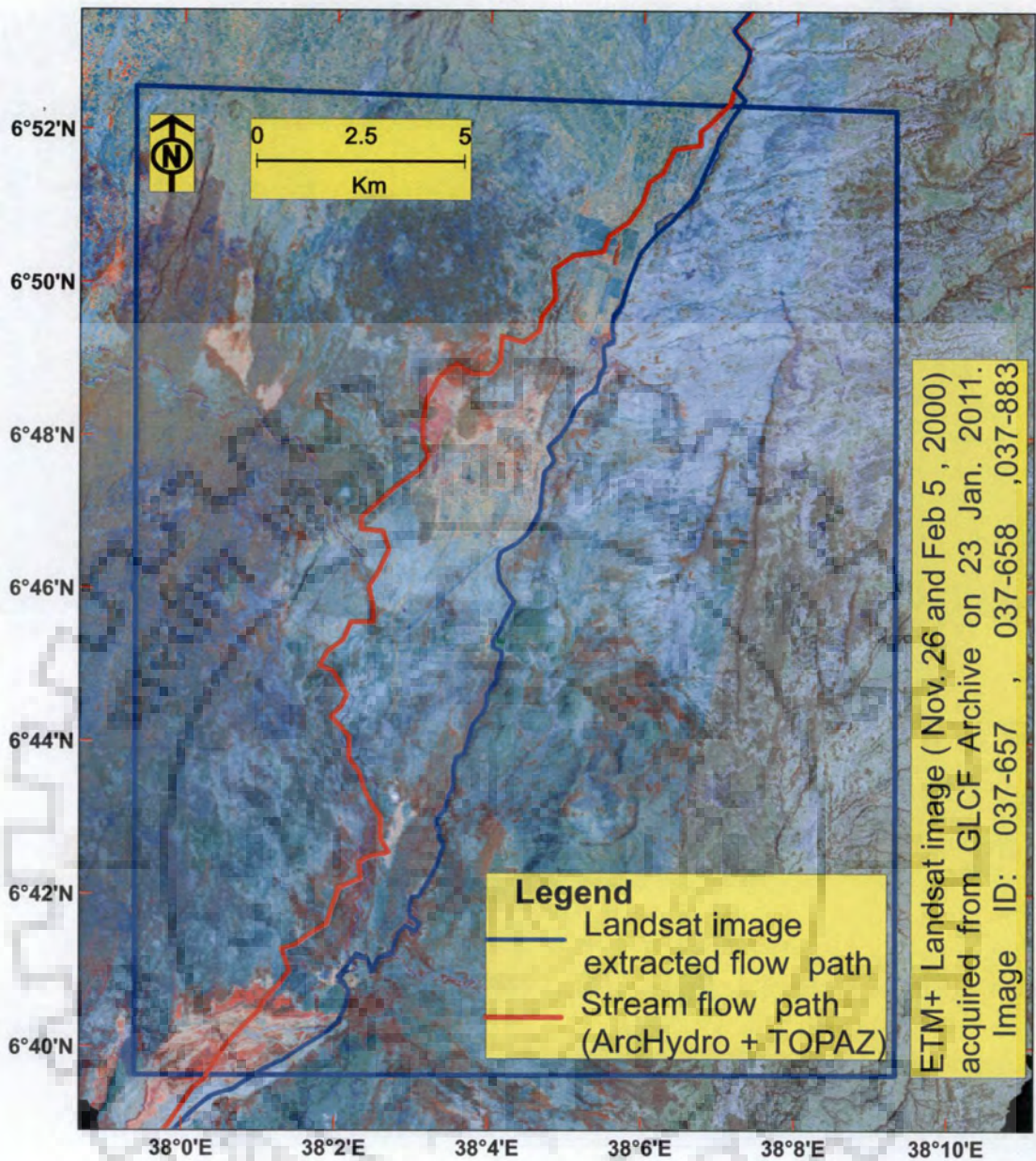


Fig. 4.10 ArcHydro and TOPAZ generated stream flow path (leftward red line) compared against Landsat image extracted stream (rightward blue line) at the lower foot of Bilate watershed

ArcHydro generated basin parameters from 90m SRTM DEM are utilized for subsequent watershed modelling. Accordingly, both Bilate and Hare watersheds are divided into three sub-basins each based on the location of monitoring stations, outlets and average basin slope (Fig. 4.12). Computed watershed geo-morphological parameters are summarized in Table 4.4.

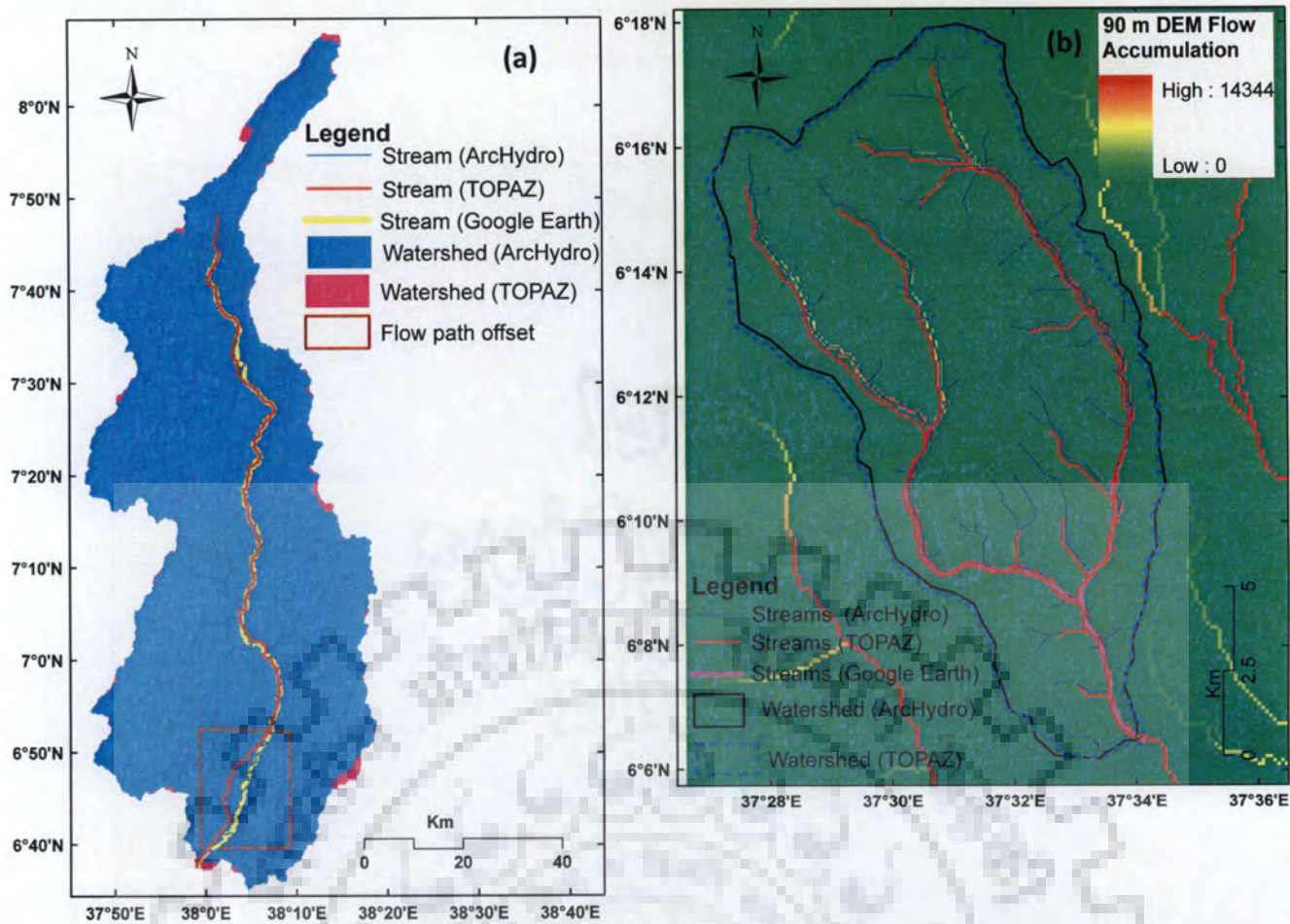


Fig. 4.11 TOPAZ and ArcHydro delineated watershed and streams: Bilate (a) and Hare (b)

Table 4.4 Bilate and Hare watershed morphological parameters estimated at basin outlets

Basin Parameters	Bilate basin	Hare basin
Basin area (km ²)	5302.2	166.5
Basin slope (m/m)	0.1	0.3
Basin length (km)	168.4	21.9
Basin perimeter (km)	664.9	77.4
Shape factor [-]	5.4	2.9
Sinuosity factor [-]	1.3	1.2
Mean basin elevation (m)	1924.0	2561.7
Maximum flow distance (km)	222.2	26.8
Maximum flow slope (m/m)	0.0	0.1
maximum stream length (km)	220.2	25.4
maximum stream slope (m/m)	0.0	0.1
Distance from centroid to stream (km)	1.5	0.9

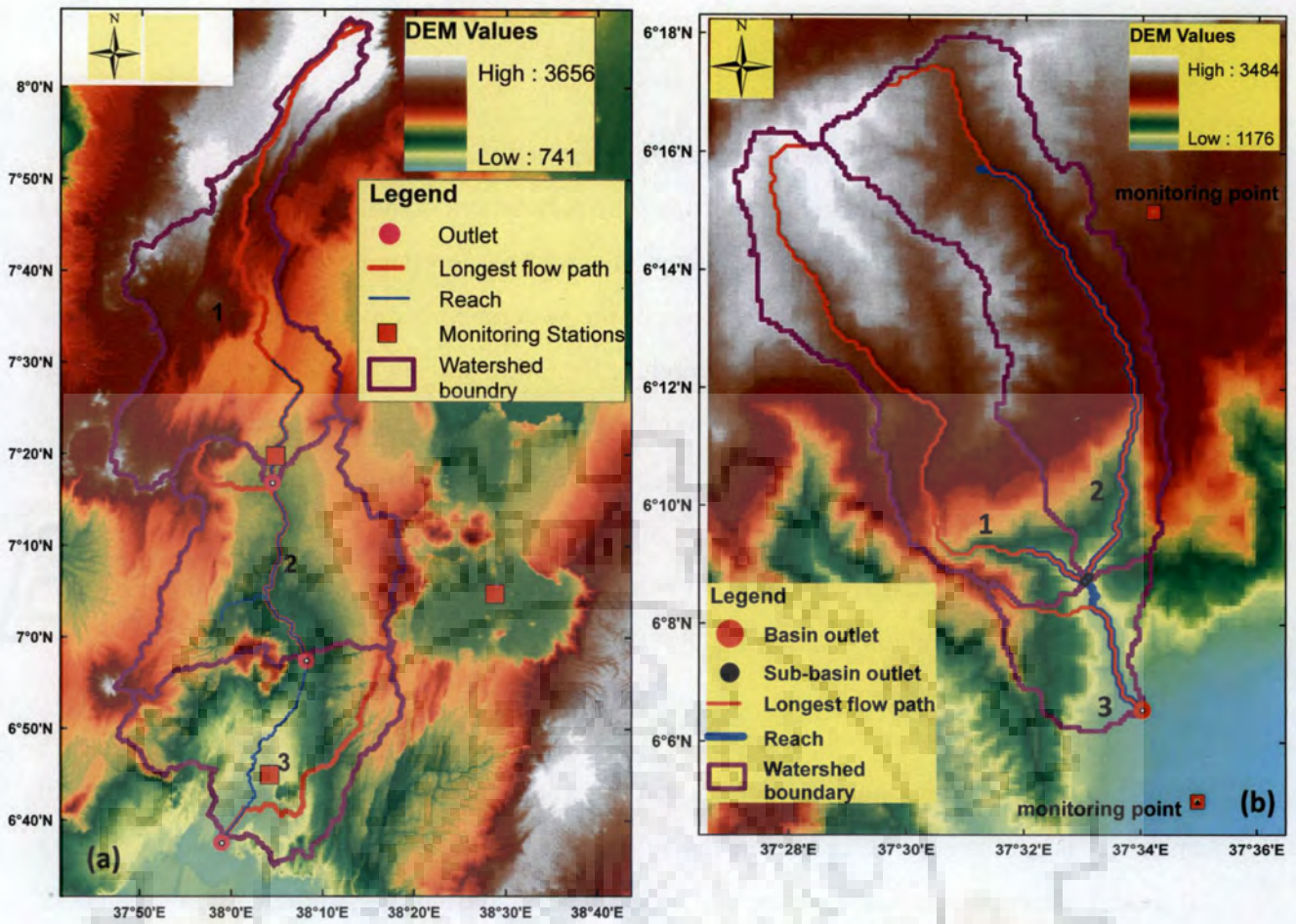


Fig. 4.12 ArcSWAT delineated watershed characteristics at Bilate (a) and Hare (b) basins

Elevation is varying in the watersheds approximately from 741m to 3656m above mean sea level. The cumulative area below a given elevation is computed to identify elevation-area relationship in both basins. It is observed that cumulative area increases sharply as elevation increases at Hare basin, whereas the increase in area under a given elevation is moderate and becomes constant at higher elevations at Bilate basin (Fig. 4.13).

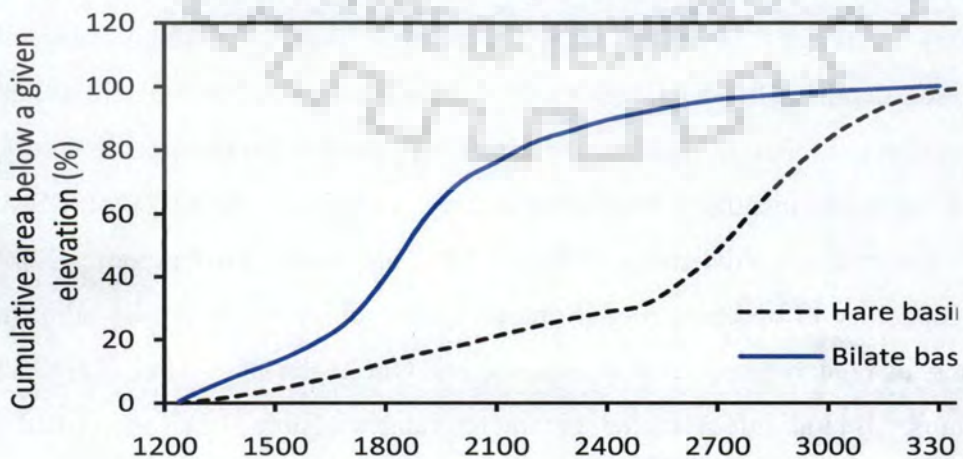


Fig. 4.13 Area-Elevation curve at Bilate and Hare basins

4.9.2 Model Sensitivity Analysis

Catchment dynamics and climatic conditions pertinent to the region alters soil, land use, groundwater and other watershed properties. The parameters do not remain stable throughout the analysis period. Such model parameter uncertainties propagate during model run and affect the final output. Therefore, to represent the watershed behavior realistically, sensitive parameters should be identified prior to model calibration and such parameters are fine-tuned over physically meaningful bound. Model sensitivity analysis is carried out for flow parameters using with and without observed discharge. Twenty flow parameters are identified as runoff influencing variables and an $(n+1)*P$ number of iteration is made to evaluate the degree of sensitivity where n being the total number of parameters ($n=20$) and P the width of Latin Hypercube sampling ($P=10$).

The OAT-LH sampling index statistics (maximum, mean, median and minimum) are derived from sensitivity analysis model run for each model parameter and the degree of sensitivity is evaluated. The mean sensitivity index is utilized to rank the parameters. Among 20 model parameters affecting runoff, 13 parameters at Bilate basin and 10 parameters at Hare basin were found more sensitive based on the mean sensitivity index of the OAT-LH sampling (Fig. 4.14 and Fig. 4.15). These are deep aquifer percolation fraction (RCHRG_DP.gw), threshold water depth in the shallow aquifer for flow (GWQMN.gw), groundwater 'revap' coefficient (GW_REVAP.gw), baseflow alpha factor (ALPHA_BF.gw), initial SCS curve number for average moisture condition (CN2.mgt), soil evaporation compensation factor (ESCO.hru), threshold water depth in the shallow aquifer for re-evaporation (REVAPMN.gw), maximum potential leaf area index (BLAI.crop.dat), maximum canopy storage (CANMX.hru), available water holding capacity (SOL_AWC.sol), soil depth (SOL_Z.sol), saturated hydraulic conductivity (SOL_K.sol) and average slope steepness (SLOP.hru). Finally, the identified sensitive parameters are used for model calibration using Sequential Uncertainty Fitting Version 2 (SUFI-2) of SWAT Calibration and Uncertainty Prediction (SWATCUP) algorithm (Abbaspour, 2009). SWATCUP has capability to optimize model output against observed values by adjusting sensitive parameters using combined Latin Hypercube and One-factor-at-A-Time (LH-OAT) sampling algorithms. Default initial model parameter ranges (Table 4.5) prescribed in SWAT model are used for initial model run using SUFI-2 calibration and uncertainty analysis module.

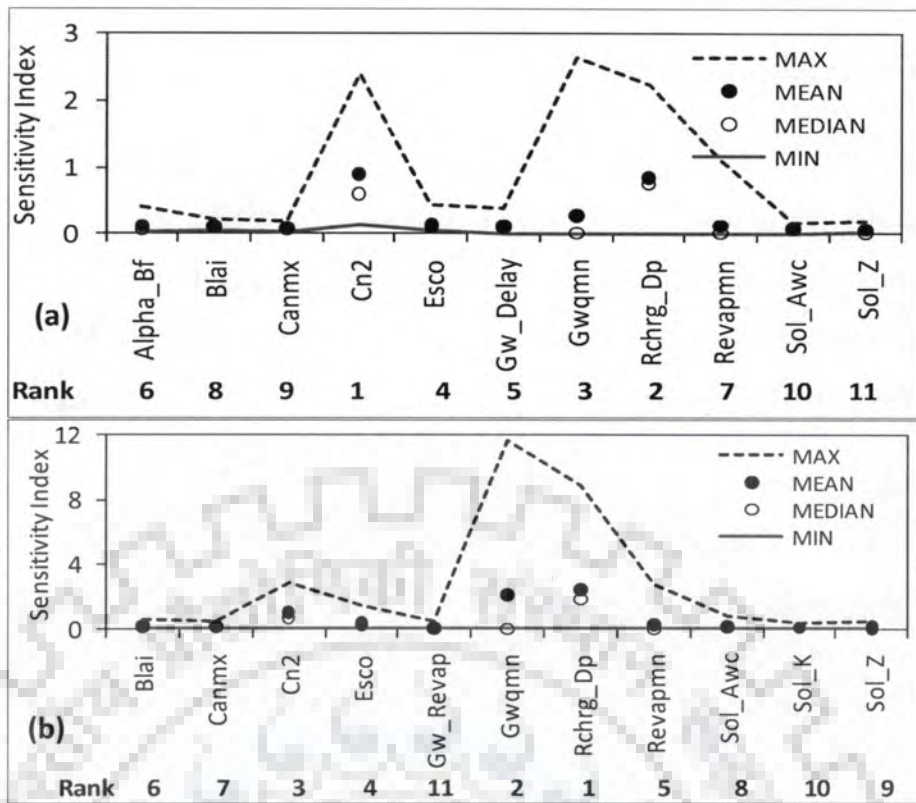


Fig. 4.14 Parameter sensitivity ranking with (a) and without (b) observed discharge case at Bilate watershed

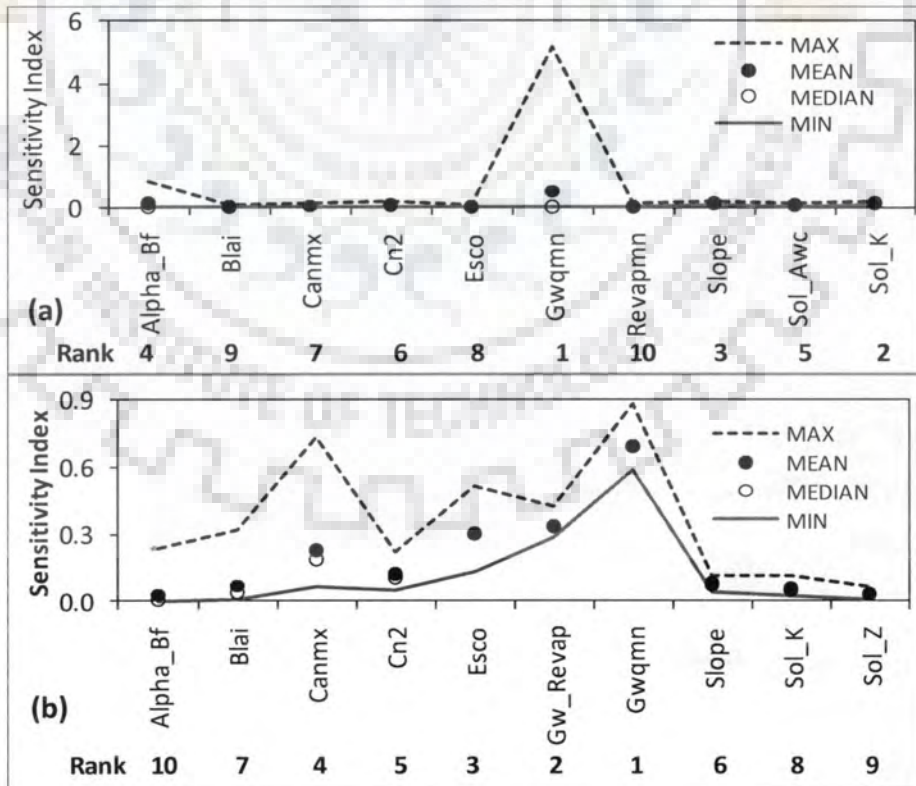


Fig. 4.15 Parameter sensitivity ranking with (a) and without (b) observed discharge case at Hare watershed

4.9.3 Model Calibration and Validation

The initial model simulation is carried out using default simulation parameter values introduced during data preparation. Manual calibration is followed by automated calibration option of SUFI-2 algorithm of SWAT-calibration and uncertainty program. Manual calibration reduced uncertainties in the input parameters slightly and permissible limits for automated calibration are identified.

Model “warm up” period of 2-4 years is used to train initial model simulation period. Successive iterations are conducted using SUFI-2 by renewing the parameter values for the next iteration until it converges. The calibrated model parameters are used to simulate runoff for validation period of non-overlapping time span. Model calibration period from 1992-1996 at Bilate basin and 1995-2000 at Hare basin are selected to account for model training phase, presence of wet and dry years during the calibration period and availability of reliable observed stream flow data for calibration. Similarly, a validation period of 1998-2002 and 2003-2006 is utilized at Bilate and Hare watershed respectively.

It is observed that SWAT model simulates runoff at both basins with sufficiently acceptable model efficiency in the watersheds. The Nash-Sutcliffe Efficiency (NSE) and Coefficient of determination (R^2) indices computed for monthly series are greater than 85% for calibration period in both watersheds. The percent bias (PBIAS) during calibration period is equivalent to 9% at both watersheds. The RMSE-standard deviation ratio (RSR) is close to zero in all cases. 82% and 80% of measured data is bracketed by the 95 percent prediction uncertainty (95PPU) at Bilate and Hare watersheds respectively. Model efficiency indices also show modestly good performance for daily simulated and observed series at both watersheds. The NSE ranges from 0.68 to 0.88 and R^2 lies between 0.70 and 0.89. The overall model performance indices during calibration period are at reasonably good concordance to their calibration counterparts at both watersheds.

The results of model calibration and validation are presented as plots of monthly and daily series. The monthly plots account for entire period of model calibration and validation phases whereas partial plots of calibration and validation phases for daily series are portrayed. (Fig. 4.16 to Fig. 4.23). Model efficiency and uncertainty magnitudes during calibration and validation period are summarized in Tables 4.6 and 4.7. After calibration and subsequent validation is arrived at acceptable level, final model parameter values are

estimated following three mode of variation i.e., adding the new value to the initial model run, replacing the original value or multiplying the original value by a relative change. This model parameter values are specific to particular sub-basin utilized during simulation. The optimal model parameter values estimated after calibration period at Bilate and Hare watersheds are presented in Table 4.8 and 4.9 respectively.



Table 4.5 Initial model parameter ranges used for default simulation and mode of variation

S.No.	Lower bound	Upper Bound	* Parameter change option	HRUs Coverage	Parameters	Parameter Description
1	0	1	1	2001	Alpha_Bf	Baseflow alpha-factor [days]
2	0	1	1	2001	Blai	Maximum potential leaf area index [-]
3	0	10	1	2001	Canmx	Maximum canopy storage [mm]
4	0	150	1	2001	Ch_K2	Channel effective hydraulic conductivity [mm/hr]
5	0	1	1	2001	Ch_N2	Manning's n-value for main channel [-]
6	-25	25	3	2001	Cn2	Initial SCS CN for average soil moisture condition [-]
7	0	1	1	2001	Epc0	Plant uptake compensation factor [-]
8	0	1	1	2001	Esco	Soil evaporation Compensation factor [-]
9	-10	10	2	2001	Gw_Delay	Groundwater delay [days]
10	-0.036	0.036	2	2001	Gw_Revap	Groundwater 'revap' coefficient [-]
11	1000	1000	2	2001	Gwqmn	Threshold water depth in the shallow aquifer for flow [mm]
12	-100	100	2	2001	Revapmn	Threshold water depth in the shallow aquifer for 'revap' [mm]
13	-25	25	3	2001	Slope	Average slope steepness [m/m]
14	-25	25	3	2001	Slsbbsn	Average slope length [m]
15	-25	25	3	2001	Sol_Al0	Moist soil Albedo [-]
16	-25	25	3	2001	Sol_Awc	Available water capacity (mm H ₂ O/mm soil)
17	-25	25	3	2001	Sol_K	Saturated hydraulic conductivity [mm/hr]
18	-25	25	3	2001	Sol_Z	soil depth [mm]
19	0	10	1	0	Surlag**	Surface runoff lag time [days]
20	0	1	1	2001	Rchrg_Dp	Deep aquifer percolation fraction [-]
* 1 = replace by value , 2 = add values , 3 = multiply by a relative change						2001 implies parameter value change is meant for all HRUs
**Surlag is a basin parameter whereas all others in the list are sub-basin parameters						

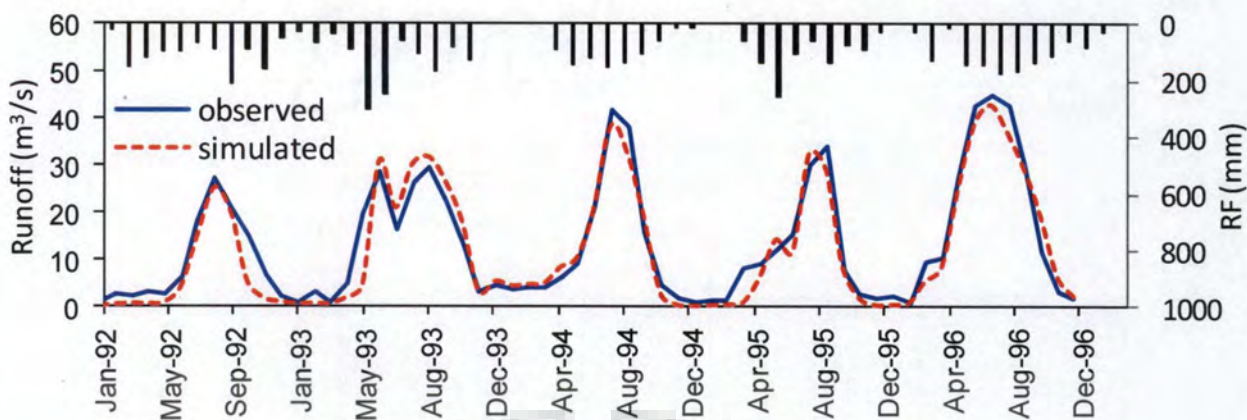


Fig. 4.16 Model Calibration for monthly Bilate river flow at Alaba Kulito

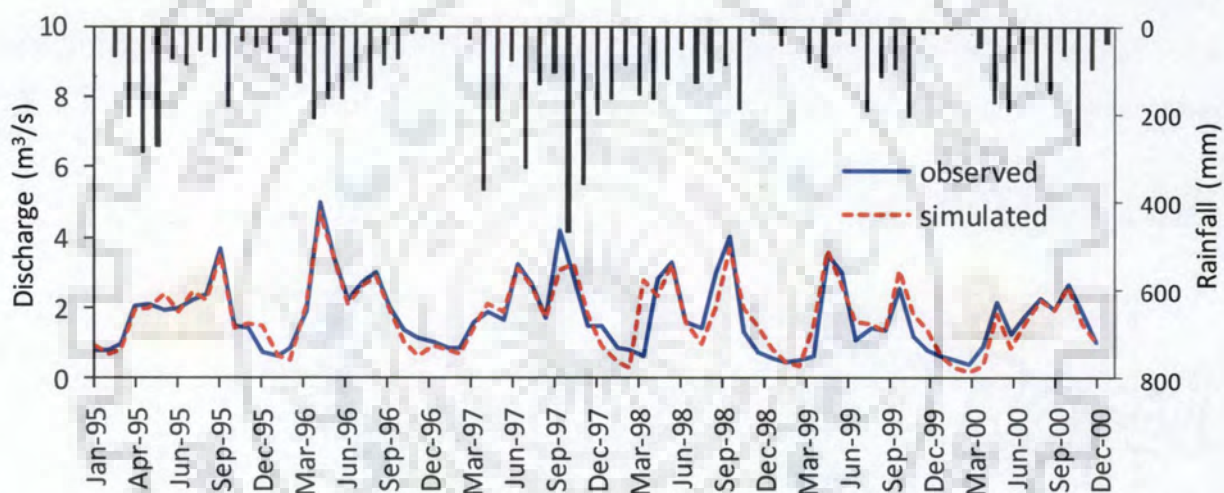


Fig. 4.17 Model Calibration for monthly Hare river flow near Arba Minch area

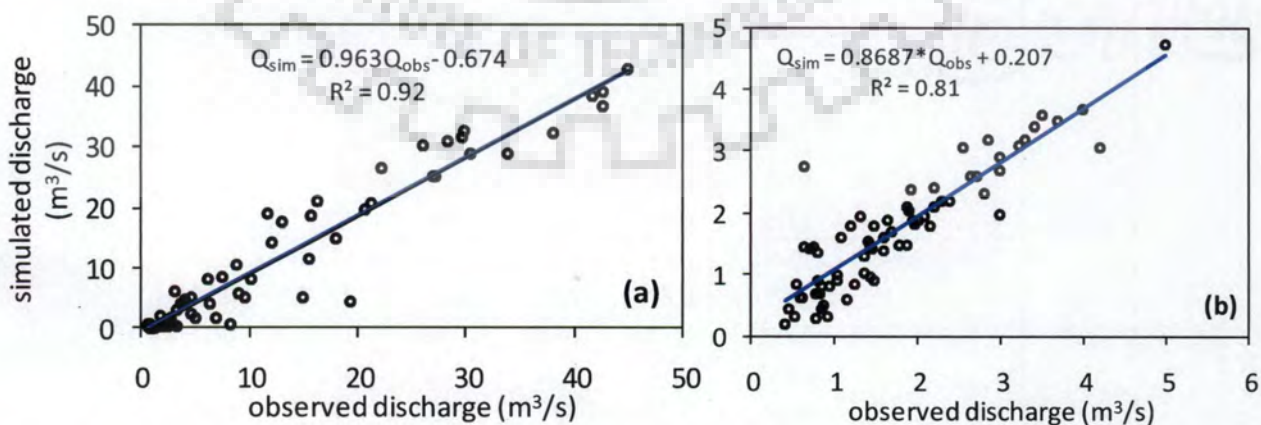


Fig. 4.18 Scatter plot of observed and simulated flow at Bilate (a) and Hare (b) river watersheds for calibration period

Table 4.6 Model efficiency and uncertainty indices during calibration and validation period

Model efficiency indices	Bilate basin		Hare-basin	
	Calibration	Validation	Calibration	Validation
	(1995-2000)	(2003-2006)	(1994-2000)	(2003-2006)
R ²	0.92	0.82	0.88	0.81
bR ²	0.89	0.78	0.71	0.86
NSE	0.91	0.79	0.87	0.96
RSR	0.09	0.21	0.19	0.32
p-factor	0.82	0.78	0.81	0.78
r-factor	0.72	0.88	1.40	1.80

Model performance is also evaluated for each year's simulation during calibration and validation period. The NSE value varies from 0.45 to 0.94 whereas R² ranges from 0.48 to 0.96. Percent bias value is in the range of 0±25 percent with significantly low (0.0 - 1.0) RSR index value during calibration and validation period in both watersheds.

Table 4.7 Annual model performance indices during calibration and validation period

Basin	Model Run	Year	R ²	bR ²	NSE	PBIAS	RSR
Hare	Calibration	1995	0.94	0.90	0.94	0.52	0.06
		1996	0.94	0.90	0.93	3.86	0.07
		1997	0.86	0.67	0.85	2.71	0.15
		1998	0.51	0.34	0.46	1.54	0.54
		1999	0.88	0.81	0.82	-16.10	0.18
	2000	0.94	0.97	0.85	14.75	0.15	
	Validation	2003	0.48	0.35	0.45	1.25	1.08
		2004	0.96	0.88	0.73	26.58	0.27
		2005	0.66	0.65	0.30	11.98	0.68
		2006	0.75	0.86	0.50	2.99	0.50
Bilate		Calibration	1992	0.82	0.87	0.81	25.12
	1993		0.84	0.92	0.76	-0.33	0.24
	1994		0.97	0.97	0.92	22.69	0.08
	1995		0.87	0.65	0.78	22.93	0.22
	1996		0.96	0.87	0.96	5.81	0.04
	Validation	1998	0.57	0.42	0.50	13.83	0.50
		1999	0.80	0.71	0.75	-12.75	0.25
		2000	0.73	0.65	0.68	13.96	0.32
		2001	0.84	0.75	0.82	-11.10	0.07
		2002	0.77	0.67	0.76	-3.44	0.24

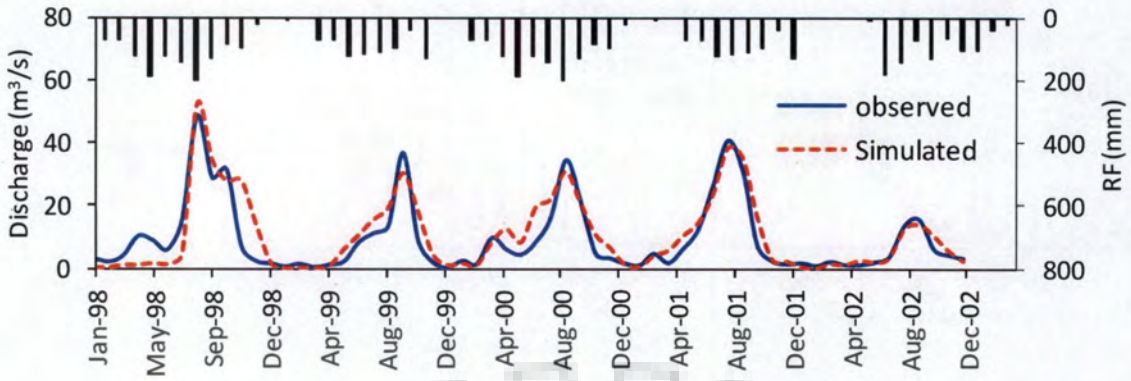


Fig. 4.19 Simulated runoff during model validation phase at Bilate watershed

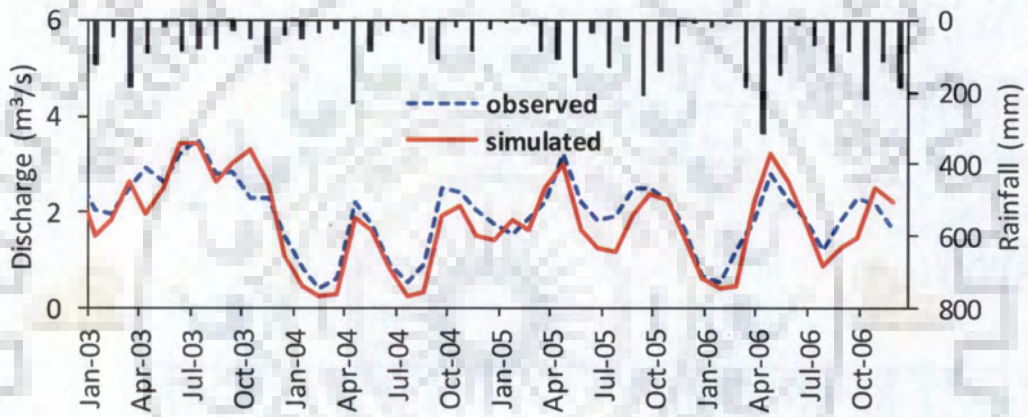


Fig. 4.20 Simulated runoff during model validation phase at Hare watershed

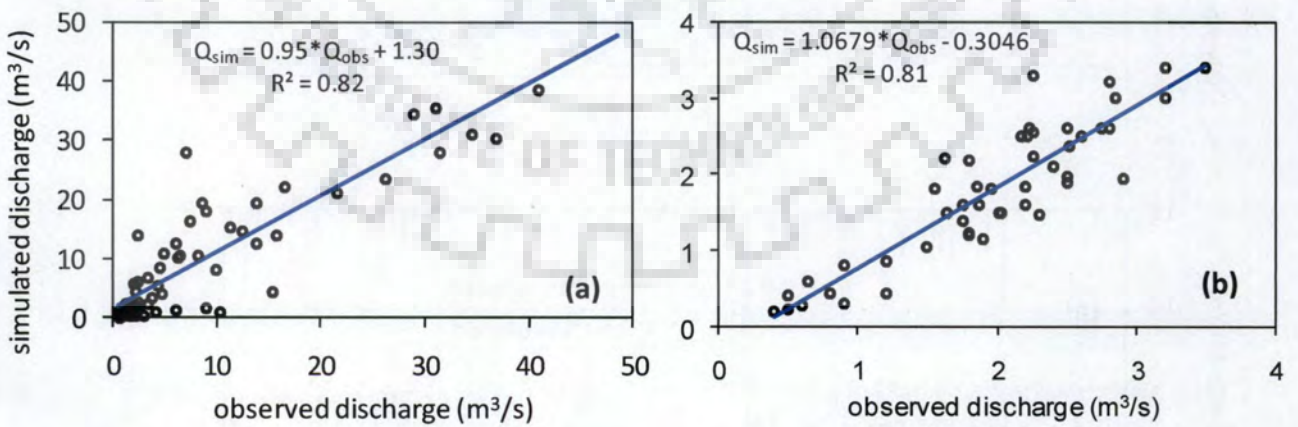


Fig. 4.21 Scatter plot of observed and simulated flow at Bilate (Fig. a) and Hare (Fig. b) watersheds for validation period

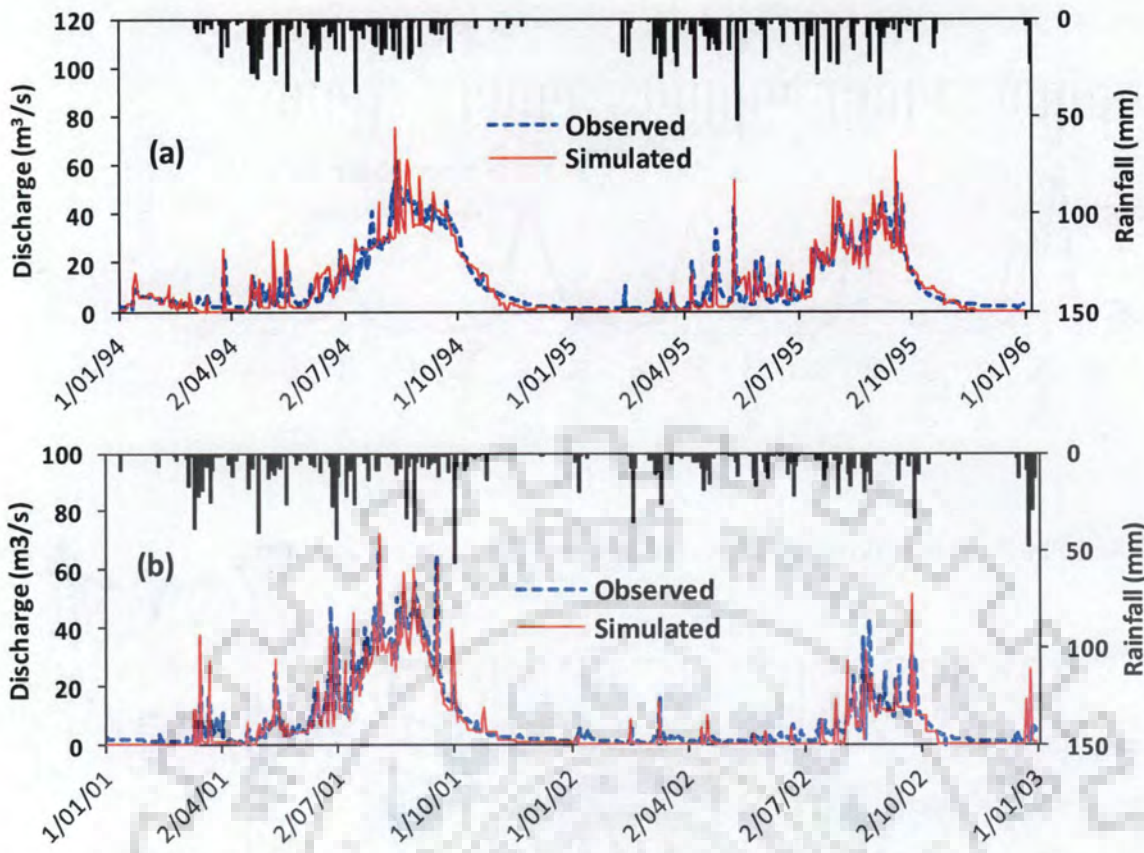


Fig. 4.22 Plots of model calibration (a) and validation (b) for daily series at Bilate watershed

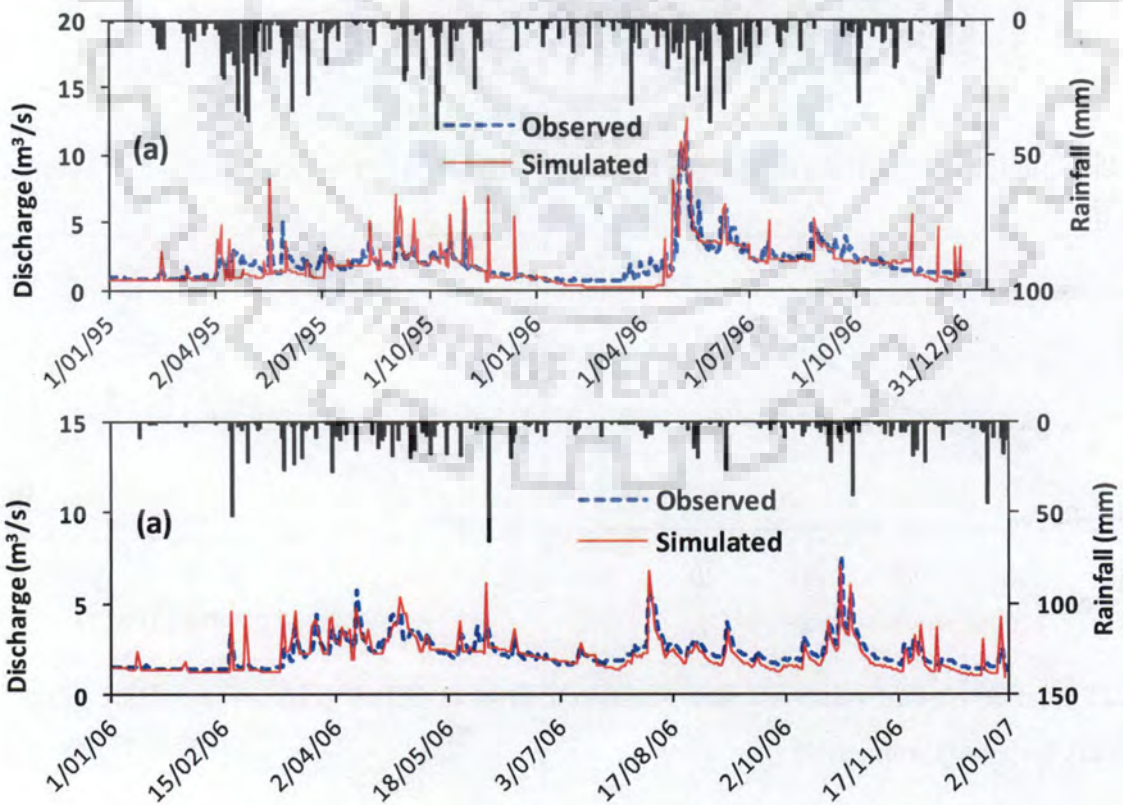


Fig. 4.23 Plots of model calibration (a) and validation (b) for daily series at Hare watershed

Table 4.8 Optimal model values after calibration at Bilate watershed

Parameter Name	Fitted Value (SUF12 output)	Corresponding Actual Parameter Value
v_RCHRG_DP.gw [-]	0.33	0.33
a_GWQMN.gw [mm]	367.73	368.27
r_CN2.mgt [-]	-14.56	48 to 61
v_ESCO.hru [-]	0.82	0.82
a_REVAPMN.gw [mm]	-10.82	-9.82
v_BLAI{1}.crop.dat [-]	0.53	0.53
v_CANMX.hru [mm]	0.50	0.5
r_SOL_AWC(1).sol [mm/mm]	34.07	0.2
r_SOL_K(1).sol [mm/hr]	-55.40	10.3
r_SOL_z(1).sol [mm]	1.50	505
a_GW_REVAP.gw [mm]	0.03	0.1

v = replace by value , a = add values , r =multiply by a relative change

Table 4.9 Optimal model values after calibration at Hare watershed

Parameter Name	Fitted Value (SUF12 output)	Corresponding Actual Parameter Value
a_GWQMN.gw [mm]	809.00	809
r_SOL_K().sol [mm/hr]	-21.12	3.95
r_SLOPE().hru [m/m]	8.55	0.28
v_ALPHA_BF.gw [days]	0.11	0.109
r_SOL_AWC().sol [mm/mm]	1.12	0.202
r_CN2.mgt [-]	-3.72	44 to 68
v_CANMX.hru [mm]	3.59	3.59
v_ESCO.hru [-]	0.05	0.05
v_BLAI{4}.crop.dat [-]	0.25	0.25
a_REVAPMN.gw [mm]	-74.07	0.00
r_SOL_Z().sol [mm]	10.88	554.4
a_GW_REVAP.gw [mm]	-0.02	0.02

v = replace by value , a = add values , r =multiply by a relative change

4.9.4 Groundwater (Baseflow) Contribution

The amount of water entering the sub-soil layer through infiltration, percolation and due to lateral and vertical movement of water from surface water bodies primarily fills the underground reservoir. Portion of such groundwater storage is joining the stream flow as baseflow. Uninterrupted flow in perennial streams is maintained through baseflow contribution. During dry periods, the surface runoff contribution to stream flow is negligible and appreciable amount of water is coming from the baseflow contribution. Observed from calibrated and validated model output, 70-87 % percent of annual water yield is dependent on

baseflow contribution. Figs. 4.24 and 4.25 show the relative contribution of groundwater to the total water yield at Bilate and Hare basins.

4.9.5 Simulated Total Water Yield of the Watersheds

Total water yield is estimated by deducting the transmission losses in the conveyance system from a sum of Surface flow (SUR Q), lateral soil flow (LAT Q) and shallow groundwater flow (GW Q). The simulated total water yield for each basin is compared against observed volume of flow in the basin to further examine the validity of model simulation. Average simulated annual water yield of 425Mm^3 against 411Mm^3 of observed volume at Bilate basin near Alaba Kulito during the calibration period is observed. In relatively small watershed of Hare, the simulated average annual water yield is 47.8Mm^3 whereas its corresponding observed average volume is 49.7Mm^3 . The residual error between simulated and observed water yields is less than $\pm 3.4\%$ during the calibration period at both basins. The monthly evapotranspiration amount exceeds rainfall during the driest months of November to March at Bilate and January to March at Hare watersheds during the calibration period. However, the total monthly rainfall exceeds evapotranspiration in the rest of the months. Average monthly basin values of water balance components for the study watersheds are presented in Table 4.10 and 4.11.

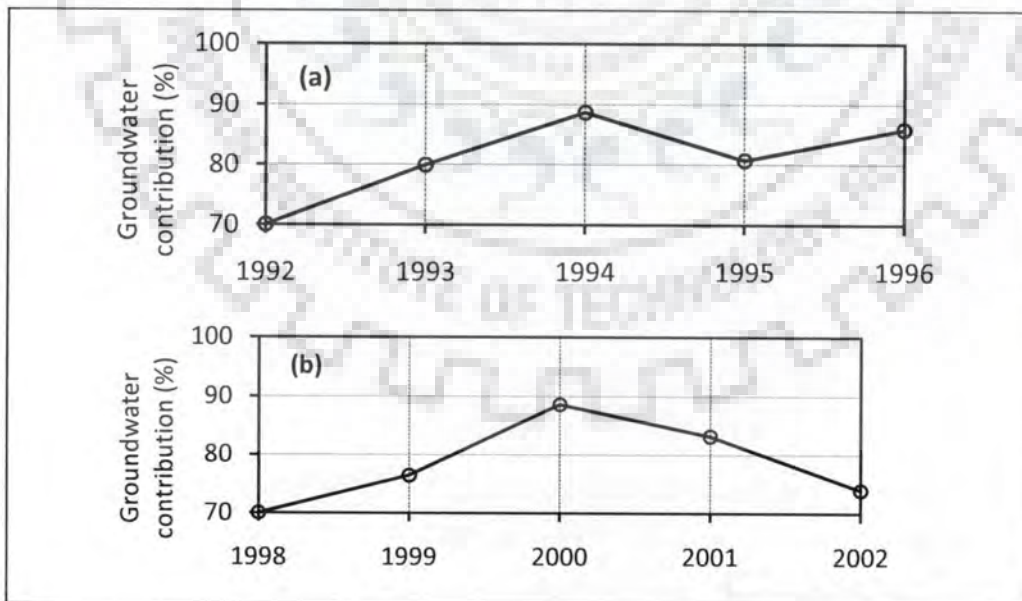


Fig. 4.24 Baseflow contribution as percentage of annual total water yield at Bilate watershed during calibration (a) and validation (b) period

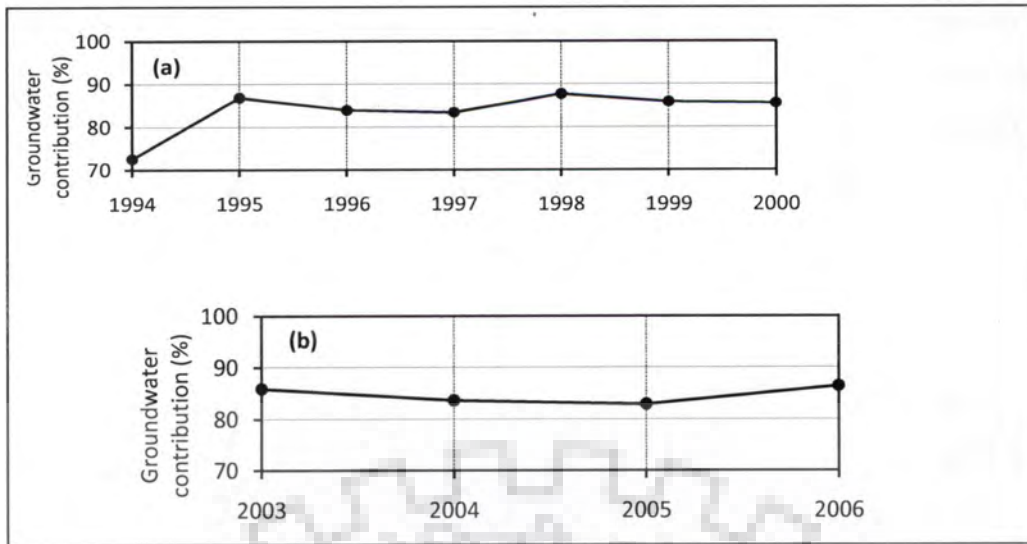


Fig. 4.25 Baseflow contribution as percentage of annual total water yield at Hare watershed during calibration (a) and validation (b) period

Table 4.10 Average monthly (1992-1996) basin values during calibration period at Bilate watershed

MONTH	WATER						
	RAIN (mm)	SURF Q (mm)	LAT Q (mm)	GW Q (mm)	YIELD (mm)	ET (mm)	PET (mm)
JAN	45.5	0.0	0.2	1.6	1.9	40.3	84.9
FEB	62.2	0.1	0.4	1.2	1.7	45.6	88.6
MAR	106.6	0.4	0.6	2.4	3.4	62.1	100.0
APR	147.8	1.2	1.0	7.3	9.5	64.0	82.7
MAY	130.6	1.5	1.4	18.0	20.8	60.6	79.3
JUN	128.3	0.7	1.4	26.6	28.8	46.2	71.8
JUL	96.3	0.4	1.1	31.0	32.5	43.5	75.1
AUG	121.4	1.3	1.3	31.0	33.5	45.7	77.4
SEP	68.0	0.0	0.9	27.3	28.2	42.0	76.2
OCT	77.5	3.0	1.0	22.2	26.2	35.6	74.2
NOV	28.3	0.0	0.5	15.5	16.0	26.5	77.6
DEC	7.2	0.0	0.2	7.2	7.5	18.1	68.1
Total	1019.7	8.7	10.0	191.3	210.0	530.0	955.8

Table 4.11 Average monthly (1994-2000) basin values during calibration period at Hare basin

MONTH	RAIN (mm)	SURF Q (mm)	LAT Q (mm)	GW Q (mm)	WATER		
					YIELD (mm)	ET (mm)	PET (mm)
JAN	26.7	0.0	2.2	16.6	18.81	40.2	67.1
FEB	26.8	0.0	1.2	5.3	6.44	32.7	66.3
MAR	59.1	0.0	1.0	1.5	2.47	50.9	80.7
APR	203.1	6.9	2.0	11.5	20.37	66.1	72.6
MAY	117.7	0.5	3.4	32.5	36.47	69.8	74.9
JUN	61.2	0.0	2.6	24.8	27.36	55.8	63.4
JUL	59.9	0.0	1.8	12.2	14.01	51.1	64.5
AUG	125.2	0.6	2.1	14.7	17.39	62.4	70.5
SEP	153.8	1.4	2.7	22.1	26.20	60.7	70.2
OCT	136.9	1.6	4.2	41.2	46.97	59.5	69.3
NOV	110.4	0.5	3.7	34.2	38.37	53.9	66.5
DEC	78.6	0.3	3.2	28.8	32.27	44.5	63.5
Total	1159.4	11.7	30.1	245.4	287.1	647.7	829.5

4.9.6 Manual Input-Output Sensitivity Analysis

SWAT model parameter sensitivity is associated to a range of climatic and hydrologic characteristics of watershed (Cibin et al., 2010). The relative influence of individual parameter on water yield is evaluated applying One-At-a-Time manual sensitivity analysis. Sensitive parameter value is either increased or decreased by prescribed amount within permissible parameter range maintaining all other parameters constant and corresponding change in water yield is estimated. Initial SCS curve number II (CN2.mgt), deep aquifer percolation fraction (RCHRG_DP.gw), threshold water depth in the shallow aquifer for flow (GWQMN.gw) and available water holding capacity (SOL_AWC.sol) have resulted in significant change in the water yield. The response of total water yield to change in baseflow alpha factor (ALPHA_BF.gw), groundwater delay (GW_DELAY.gw), saturated hydraulic conductivity (SOL_K.sol) and maximum canopy storage (CANMX.hru) is minimal. Percentage change in water yield is evaluated with reference to the calibration period. Relative increase in water yield as a function of change in input parameters for selected model parameters is summarized in Figs. 4.26 and 4.27.

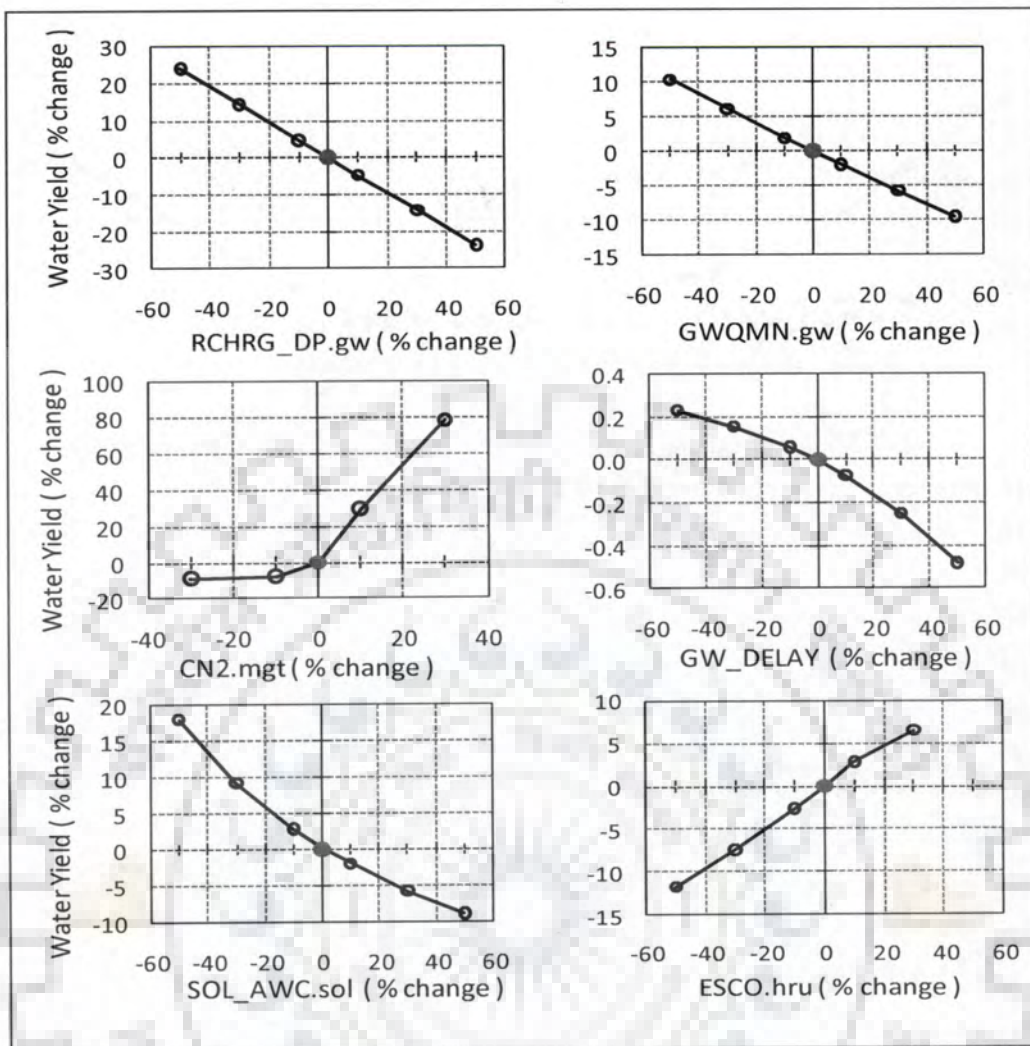


Fig. 4.26 Manual input-output sensitivity analysis result at Bilate watershed

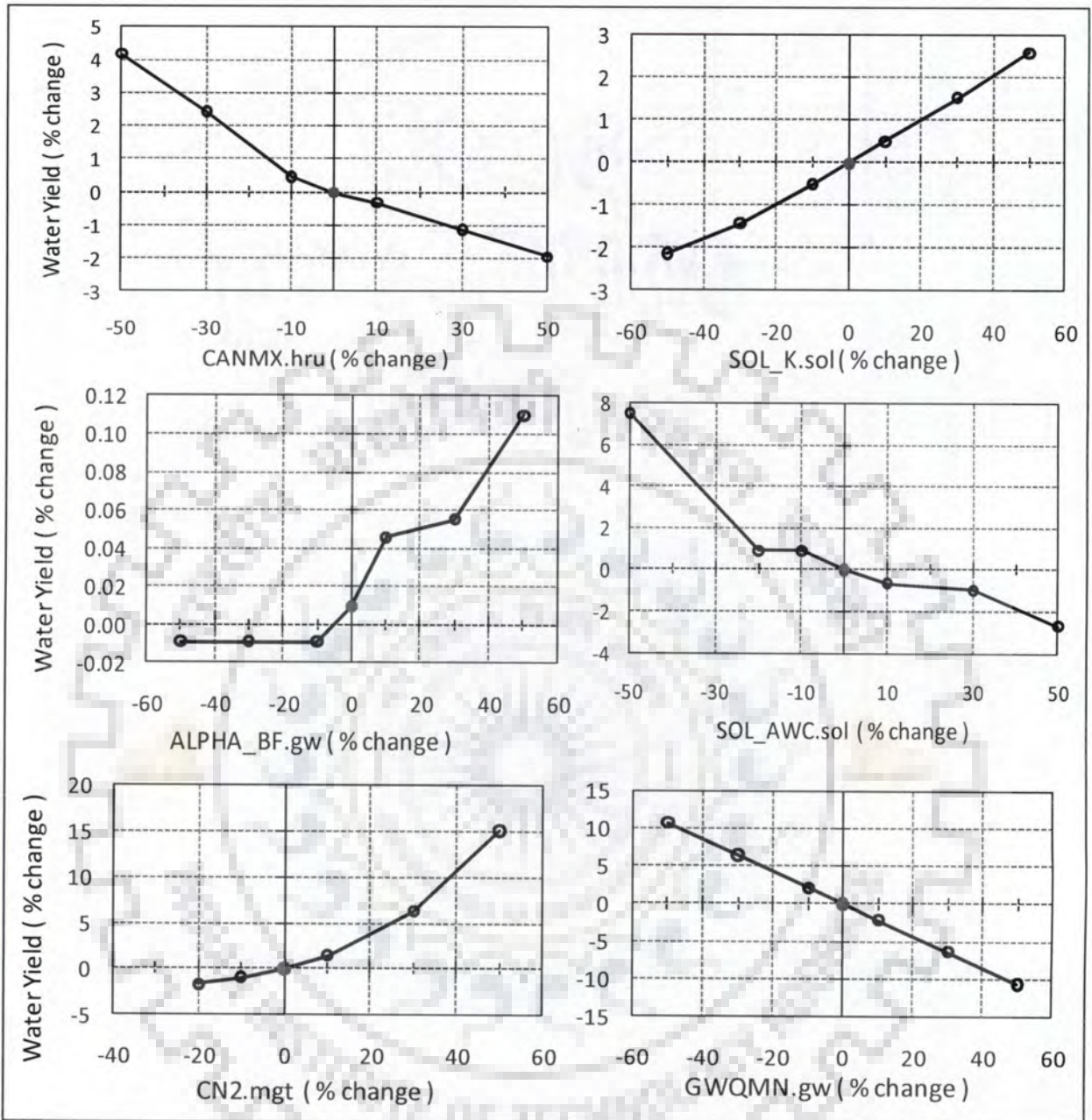


Fig. 4.27 Manual input-output sensitivity analysis result at Hare watershed

4.10 CONCLUSIONS

Watershed physiographic elements are extracted from 90m SRTM and 30m ASTER DEM data using ArcHydro and TOPAZ watershed delineation algorithms. It has been observed that 30m ASTER DEM resulted in spurious flow accumulation path that subsequently reduced the watershed area by 29% and affected other basin parameters at Hare watershed. However, 90m

DEM generated well patterned flow accumulation path conforming to existing watershed area and Landsat image derived flow paths. ArcHydro and TOPAZ watershed delineation algorithms failed to capture the actual flow path accurately in flat terrain of Bilate watershed. The main stream flow path deviates from surrogate Landsat (acquired for the year 2000) and Google Earth (2005/2006 image) extracted stream path by an average distance of 7.5 km in west-east direction for a total stream length of 30km at the lower foot.

SWAT model is calibrated and validated in two snow free agricultural watersheds in the Rift Valley lakes basin of Ethiopia. The impact of topographical, weather and catchment input parameters on runoff generation is investigated. In view of this, initial curve number for average soil moisture condition, deep aquifer fraction, minimum water depth in the shallow aquifer for flow and available soil water holding capacity parameters found to either attenuate or accentuate the resulting runoff more significantly than others in the watersheds. Model performance indices have shown that runoff at desired outlet is simulated at acceptable range of closeness to observations. The overall Nash-Sutcliffe and R^2 model performance indices range between 0.79 and 0.96 during calibration and validation period at both watersheds. Approximately 80% of measured data is bracketed by the 95 percent prediction uncertainty at both watersheds. It has been estimated that the simulated average annual water yield is 425 Mm^3 and 47.8 Mm^3 at Bilate and Hare gauge sites respectively. The simulated annual water yield is within $\pm 3.4\%$ error to the observed annual stream flow volume at the same outlet. Potential monthly evapotranspiration magnitude exceeds the total rainfall during critical soil moisture season (November – March) of the year.

DOWNSCALING GLOBAL CLIMATE MODEL OUTPUTS AND ASSESSMENT OF CLIMATE CHANGE IMPACTS ON RUNOFF GENERATION

5.1 GENERAL

The occurrence of frequent extreme precipitation and temperature events during last two decades signals key climate variability in Ethiopia and warns a future course of adaptive measures. Annual minimum and maximum temperature over the second half of twentieth century over the country shows an average increase of 0.4°/decade and 0.2°/decade respectively (Conway et al., 2004). However, precipitation does not exhibit a palpable increase over entire Ethiopia. The western, northern, southern and central part of the country are characterized by declining annual (1.5 - 9.9 mm/year) and seasonal rainfall trend over the second half of twentieth century (Cheung et al., 2008).

Region specific knowledge of the vulnerability associated to climate variability and possible adaptive measures to reduce the exacerbated impacts are an urgent course of actions to cope with such lingering condition. Ethiopian economy, which depends mostly on agriculture, is undoubtedly becoming a victim of this global challenge (Dercon, 2004; Conway and Schipper, 2011). More than 45 percent of the country's gross domestic product and 85 percent of the export revenue is directly linked to agricultural sector (MoFED, 2006; Byerlee et al., 2007; Yesuf et al., 2008; You and Ringler, 2010). The sector also employs 80 percent of the labour force and serves as a major source of subsistence and household income for the majority of rural population. Well motivated by the diverse impact of climate variability on water resources of a region, an attempt has been made to explore the impact of large-scale present and future climatic variables under different greenhouse gas forcings on local climate at Rift Valley lakes basin of Ethiopia.

To achieve the intended goals, this chapter is subdivided into the following major endeavours. Firstly, global and regional perspectives of climate change and hydrologic modeling in pursuit of changing climate condition are reviewed. Secondly, downscaling daily temperature and precipitation variables from large-scale atmospheric variables for current and

two future climate (A1B and A2) scenarios obtained from two GCMs is carried out. Thirdly, statistical behavior of downscaled and observed weather variables for current climate condition is explored and subsequent precipitation bias correction is undertaken. Fourthly, Soil and Water Assessment Tool (SWAT) hydrologic model is applied to simulate runoff at desired locations using bias corrected precipitation and temperature in two snow free, agricultural watersheds in the basin. Finally, on the premises of GCM outputs and predicted runoff, the likely future climate implications are discussed.

5.2 OVERVIEW OF GLOBAL CLIMATE CHANGE

Natural climate variability on daily, seasonal and inter-annual scale is perceived by human beings. Recently, this variability is becoming greater than the long term average magnitudes that were observed in decadal or centennial scale during the past. Global average sea and land surface temperature has increased by 0.6 ± 0.2 °C from 1860 to 2000 with much of the change occurring since 1976 (IPCC, 2001). IPCC's Fourth Assessment Report (IPCC, 2007a) further argues that the mean land and sea surface temperature change during 1906-2005 increased by a greater amount ($0.74^{\circ}\text{C} \pm 0.18^{\circ}\text{C}$) than it was in the second half of ninetieth century. The greatest temperature changes are observed in the mid and high latitudes of Northern Hemisphere. Increased precipitation in terms of frequency and intensity in the mid to high latitudes is discernible with palpable effects on the natural and human ecosystem (Karl and Night, 1998; Walther et al., 2002). If the increase in greenhouse gas concentration remains unabated, the predicted (1990-2100) global temperature would likely to rise between 1.4 and 5.8 °C (IPCC, 2001).

The tropical rainforest region of the globe is manifested by strong warming at a mean rate of $0.21\text{-}0.31^{\circ}\text{C}$ with contrasting decline of precipitation at the rate of 0.2-1.8 percent per decade since 1970s (Malhi and Wright, 2004; Conway et al., 2004; Kruger and Shongwe, 2004). The African continent is the most vulnerable region to climate change and arguably with least scientific research appraisals to cope with such adverse effects (Tadross et al., 2005; You and Ringler, 2010). The sub-Saharan region of Africa, in particular, has been challenged by natural and man-made stresses extending from flood and prolonged drought that put millions of lives at risk to poor economic and institutional developments. Currently, one-fourth of the population of Africa is facing high water stress and this magnitude is expected to increase two to three-fold in the next forty years (Boko et al., 2007). IPCC's Fourth

Assessment Report asserted that the adaptation mechanisms developed by African farmers are not sufficient enough to cope with current and future climate variability (IPCC, 2007b).

Global Climate Models (GCMs) are being applied in many parts of the world to study present and future climate variability and ensuing risks in agriculture (Yano et al., 2007; Kumar et al., 2010; Huda et al., 2010), water supply, hydropower (Harrison and Whittington, 2002; Schaepli et al., 2007) and overall livelihoods of the nation worldwide. However, these endeavours are very limited in developing countries like Ethiopia. Precipitation and runoff simulated from multiple GCMs realizations over Blue Nile basin of Ethiopia show significant variability across GCMs (Elshamy et al., 2009; Setegn et al., 2011; Block and Goddard, 2012). Notwithstanding the HadAM3 model could likely captures annual and seasonal rainfall variability over Ethiopia, it is associated with significant biases (Diro et al., 2011).

5.3 HISTORICAL EVIDENCES OF CLIMATE VARIABILITY OVER ETHIOPIA

Even though the scientific documentation of climate variability and ensuing impacts in Ethiopia is scarce till to-date, there were rich veins of historical evidences that give an aura of confidence to support the post-industrial era warming. Prolonged drought devoured crops and livestock as a consequence of which catastrophic famine and ecological disorder had become inevitable facets of the late ninetieth century.

Pankhurst (1966) discussed the 1888-1892 of Ethiopian Great Famine that resulted in complete sense of social, biological, economical and political disarray. Its ripple-effect over diverse environmental spectrum magnified the years in Ethiopian history and these events are locally known as '*Kifu Ken*' - the 'evil days' or 'harsh days'. The ultimate cause for such doom and gloom was natural calamity - prolonged drought that devoured harvest and cattle. Extended civil war feuding among the then rivalries for supremacy aggravated the situation.

Wood (1977) documented the major lean years in Ethiopian history between 1066 and 1975. The drought events were organized from royal chronicles, adventures nobles, societal repercussions and hydrological implications of declining water levels. These destructive drought events, occurred since 1066, were seemed to be influenced by solar cyclic activity. The absolute departure from sunspot minima is highly correlated to the drought episodes. The closet years to the sunspot minima were characterized by frequent drought events.

Degefu (1987) summarized the major historical drought events occurred in Ethiopia. The natural climate change in terms of prolonged drought in Ethiopia dated back to 250 BC. Since then, recurrent drought events of various magnitudes were inferred from the chronology of water levels records of river Nile and lake Rudolf. Some of these major droughts were culminated with famine in the second half of thirteenth and mid fifteenth century. However, the drought episodes became more frequent in the post-industrial era, particularly in the ninetieth and twentieth centuries, in Ethiopia.

The United Nations Environmental Programme and International Centre for Research in Agroforestry (UNEP and ICRAF, 2006) report provides a comprehensive overview of the Sahel drought. The Sahel region of Western Africa (10–20°N and 18°W–20°E), located at the southern edge of Sahara desert, is characterized by strong climatic variations. Rain-fed agriculture, livestock herding and fishing are among the mainstays of the population in the region. The region is affected by droughts of various degree of severity nearly in two out of five years. Three major drought episodes that overwhelmed the region during the 20th century are: 1910-1916; 1941-1945 and the desiccation period of 1970s and 1980s. The decreasing trend of Sahel rainfall is attributed to sustained climate change in the region manifested by a decline in boreal summer rainfall. The drought shock of 1970s and 80s in the Sahel region extended further to Eastern parts of Africa lying adjacent to the Sahel boundaries. The 1972-1973 and 1984-1985 droughts of Ethiopia were contemporary with Sahel region drought. The mid 1980s droughts were the second major natural disaster in Ethiopian history following the late ninetieth century drought-driven famine.

The beginning of the 21st century is marked by severe drought that have led to an utter bereft of hope in the Eastern Africa; namely Somalia, Djibouti, Kenya and Ethiopia. Prominent magazines and media outlets like *Telegraph*, *The Washington Post*, *BBC*, and *CNN* aired the recent protracted drought of the year 2010-2011 that jeopardized millions of lives in the Eastern Africa and judged as “the worst drought over the last 60 years in the Horn of Africa”. The United Nations (UN) described it as a “humanitarian emergency” or equivalently a “pre-famine” ordeal which is little less than the catastrophe.

Many of the early historical evidences of climate variability in Ethiopia are entirely founded on adverse environmental and societal implications. Little scientific appraisal has

been made to reinforce the accompanying variability and its direct and indirect causes. Scientific views based on historical hydro-climatic observations during the late twentieth century attempted to provide a wide picture of the calamities yet most of the studies culminated with regional scale assessments.

Notwithstanding the above limitations, it would be remiss of the author not to mention key contributions to African climate variability with the emphasis of GCMs applications. Hulme et al. (2001) used multiple GCMs simulations and demonstrated the present and future temperature and precipitation variability over African continents accounting country specific examples from Ethiopia, Senegal, Tunisia and Zimbabwe. It has been argued that the current climate of Africa is warmer than it was a century ago. This warming will remain more enhanced in the future and the warming could rise between 2 and 6 °C among different scenarios in the next 100 years. However, the magnitude and direction of future rainfall events remain variable and more uncertain. This is likely due to poor representation of ENSO-induced climate variability, dynamic land cover-atmospheric feedback and atmospheric aerosols in current GCMs. Similarly, couples of region specific studies such as Conway et al. (1996) in Egypt, Joubert et al. (1996), and Hewitson and Joubert (1998) in South Africa and Sun et al. (1999) in East Africa have applied the knowledge of GCMs to assess regional climate variability.

5.4 WATERSHED MODELLING IN PURSUIT OF CHANGING CLIMATE AND CATCHMENT CONDITIONS

Hydrologic models used to simulate the physical processes occurring in the catchment are very diverse. Singh and Frevert (2006) provided a comprehensive review of some of the popular hydrologic models being in use worldwide. It extends from an earlier empirical form of Rational Method (Mulvaney, 1851) to process oriented physical models like Système Hydrologique Européen (SHE) (Abbott et al., 1986a, b). A plethora of conceptual and process oriented hydrologic models have emerged since the establishment of Stanford Watershed Model (SWM) that could virtually model the entire hydrologic cycle occurring in the watershed (Crawford and Linsley, 1966).

With concise understanding of the retrospective and present climate and catchment pattern, prognoses of future hydrologic condition can be reached. Hydrologic responses to climate and catchment dynamics could be analyzed using physics based distributed models,

lumped conceptual approaches or employing empirical relationship where output is correlated to input through transfer function or statistical regression model.

Distributed hydrologic models become advantageous over lumped models as the later fail to adequately capture the spatial variability of various hydrologic responses under complex catchments where there are significant slope, land use and soil variability. Even though plethora of hydrologic models are being in use to estimate the response of catchment with respect to changing climate and catchment conditions, lack of direct relationship among the mathematical models involved and physical process occurring in the catchment, uncertainties generated due to the inherent behavior of models and use of point measurements to represent catchment scale behavior while deriving relationship remain challenges in quantifying the runoff process.

The response of land use/land cover dynamics and climate change could be evaluated using hydrologic modeling whereas statistical time series models are employed to assess the short and long-term time dependence of hydro-climatic variables (Refsgaard et al., 1989).

The top-bottom approach where the outputs from GCMs are used to address impact of climate change on global and regional water resources using hydrologic models is commonly applied approach in recent years. Some of such attempts over the recent decade are discussed herein.

Menzel and Burger (2002) applied a semi-distributed, conceptual hydrologic model (HBV-D) to simulate discharge in the Mulde catchment of Germany using GCM outputs from ECHAM4/OPYC3. An increase in simulated future temperature accompanied by decreased precipitation magnitude subsequently reduced mean future discharge in the basin.

Arnell (2003) assessed the implication of future climate change on runoff through multiple GCMs across the globe. He simulated streamflow at spatial scale of $0.5^{\circ} \times 0.5^{\circ}$ based on emission scenario for about 1200 catchments using catchment scale hydrologic model. The climate models produced increased runoff at high latitudes, East Africa, South and East Asia, and decreased runoff in parts of Europe, North, Central and Southern Africa, the Middle East, and most parts of North and South America. However, this study is based on global scale and local climate variability might influence the future runoff.

Andersson et al. (2006) investigated impact of climate change and development scenario on flow patterns in the Okavango River of Southern African regions. The sensitivity of hydrologic model to GCMs being a major constraint, the simulated mean flow for 2050-2080 and 2070-2099 time slices shows decrease in magnitude compared to the present condition.

Fujihara et al. (2008) used dynamical downscaling method to reduce large scale atmospheric variables into local level and explored the potential impacts of climate change on the hydrology and water resources of the Seyhan River Basin in Turkey. Bias corrected GCMs simulated the hydrology of the basin effectively and resulted in increased projected temperature, and decreased future rainfall, evapotranspiration and runoff.

Guo et al. (2008) examined the effects of climate and land-use and land-cover on hydrology and streamflow in the Xinjiang River basin of the Poyang Lake using SWAT model. Climate effect is dominant on annual streamflow whereas land use changes strongly affects seasonal streamflow variability and alters the annual hydrograph.

Li et al. (2009) assessed the impact of land use change and climate variability on hydrologic components of a watershed in Loess Plateau of China using SWAT model. It has been argued that the combined effect of land use change and climate variability in the catchment reduced the runoff, soil water and evaporation magnitude.

Tu (2009) analyzed the combined effect of land use and climate change on streamflow and water quality in Eastern Massachusetts, USA through GIS based watershed simulation approach. The impact was more profound on seasonal distribution of streamflow and nutrient load than average annual amounts.

Ficklin et al. (2009) modeled hydrological response to variations of atmospheric CO₂, temperature and precipitation based on IPCC climate change projections at agricultural San Joaquin watershed in California using SWAT model. Increasing CO₂ concentration and temperature decreased basin-wise average evapotranspiration that ultimately resulted in increased water yield and streamflow compared to the present- day climate.

Moradkhani et al. (2010) applied SWAT model to simulate streamflow for future climate scenario using daily downscaled precipitation and temperature input data over the Lower Tualatin basin in the Pacific Northwest US. The projected 50-year recurrence interval

streamflow will decrease for low and middle emission scenario whereas it will increase for high emission scenario condition.

Boyer et al. (2010) used multiple GCMs under two emission scenario (A2 and B2) conditions to examine climate change impacts on hydrology of the St. Lawrence tributaries in Canada. The study showed that most of the future hydrological simulations are characterized by increased winter and decreased spring discharges.

Taye et al. (2011) assessed climate change impacts on hydrological extremes of Nile river basin using multiple GCMs outputs. Future runoff simulated using conceptual hydrologic models for A1B and B2 emission scenario shows increased mean and extreme runoff at Nyando catchment of Kenya, however, impalpable pattern is detected at lake Tana catchment of Ethiopia despite better definition of hydrologic regime in the later case. Couples of climate change impacts assessment endeavours (Elshamy et al., 2009; Diro et al., 2011; Setegn et al., 2011) on hydrological regime of Ethiopian catchments are carried out during the beginning of 2010s.

5.5 DOWNSCALING GCM OUTPUTS

Information on local climate can be derived from GCM outputs through either statistical (Frost et al., 2008) or dynamical (McGregor, 1997) downscaling. The later involves nesting a higher resolution regional climate models on coarse resolution GCMs to reduce large-scale atmospheric variables into local (regional) level. Statistical downscaling model (SDSM) develops a statistical relationship between large-scale atmospheric variables and observed climatology so that the resulting relationship is further extended to extract future climatic variables from GCMs (Wilby et al., 2001). SDSM is public domain software available for rapid assessment of localized climate change impacts. It has an advantage over other methods in resolving large-scale atmospheric variables into localized (station) weather information with finer temporal (daily and sub-daily) resolution. Stochastic weather generators, transfer functions and weather typing are the broad classes where many of statistical downscaling techniques fall under.

Recent studies support the use of SDSM tool as an alternative approach to reduce large-scale atmospheric variables into localized weather variables. In the study conducted in the

northern part of China, Chen et al. (2010) asserted that SDSM performs better than the support vector machine based regression and multivariate analysis. Harpham and Wilby (2005) exhaustively examined the relative merit of SDSM to that of artificial neural network (ANN) based precipitation outputs and argued that SDSM simulated daily precipitation magnitudes show stronger inter-site correlations, however ANN method is more skilful in modelling the occurrence of certain attributes at individual sites. The fully deterministic forcing of amounts in ANN method attributed to the overestimated inter-site correlations. In contrast, the stochastic nature of SDSM contributed to heterogeneous response surfaces that ultimately resulted in realistic inter-site correlations. Khan et al. (2006) assessed uncertainty generated in downscaled daily precipitation, maximum and minimum temperature using SDSM, Long Ashton Research Station Weather Generator (LARS-WGEN) and ANN models and concluded that SDSM is the most capable of reproducing statistical characteristics of observed data in the corresponding downscaled variables.

The use of various forms of statistical downscaling approach to study the impact of global climate change on regional or watershed hydrology is growing in recent years. Mehrotra and Sharma (2008) assessed climate change impacts through non-parametric stochastic downscaling framework that combines atmospheric circulation and time-lagged wetness indicators. Daily rainfall is simulated for multiple sites to study catchment scale climate impacts. Fistikoglu and Okkan (2011) used large-scale atmospheric variables such as surface temperature and geopotential height at different pressure levels and sea level pressure to downscale monthly precipitation in Tahtali River Basin of Turkey. Statistical regression analysis is employed to develop statistical relationship between these large-scale explanatory variables (predictors) and station precipitation (predictand) magnitudes. Eum et al. (2010) applied the K-nearest neighbor weather generator models combined with the outputs of GCMs (CSIRO-MK3.0 and MIROC3) to provide future weather pattern in Nakdong river basin of Korea. The generated meteorological datasets are further used to simulate streamflow using rainfall-runoff models.

5.6 STUDY AREA AND CLIMATE DATASETS

5.6.1 The Study Area

The present study concentrates on Bilate and Hare watersheds of the Rift Valley lakes basin described in section 4.6.

5.6.2 Climate Datasets

The impact of global climate change on local or basin wise water resources is diverse and requires multitudes of datasets to adequately address the interactions. The raw datasets and subsequent methodologies utilized to extract the relevant information are presented in the subsequent sections.

Three major categories of climate datasets are used. These include observed daily precipitation and temperature data from 1980-2009, daily Global Climate Models (GCMs) output for current climate (1971-1999) and daily GCM output for future climate condition (2081-2090) for A1B and A2 scenarios. Observed station data from 5-stations (Alaba Kulito, Bilate Farm, Hawassa, Chenchu and Arba Minch Farm) at central and southern Rift Valley lakes basin is obtained from regional and national meteorological agencies. The location of respective meteorological stations is shown in Fig. 4.2 of previous chapter. Observed streamflow at Alaba Kulito of Bilate and near Arba Minch of Hare watersheds are used for subsequent analysis. Observed data is checked for quality in terms of inter-site comparison for consistency as described previously.

Daily GCM outputs for current and future climate conditions are obtained from World Climate Research Program's (WCRP's) Coupled Model Intercomparison Project phase-3 (CMIP3) multi-model dataset (<https://esgcet.llnl.gov:8443/index.jsp>). CMIP3 datasets have recently got growing demands by scientific community to study global climatology and regional or local climate change impact assessment (Kim et al., 2008; Karpechko et al., 2009; Straub et al., 2010; Kim et al., 2011). IPCC, Fourth Assessment Report (IPCC, FAR) approved climate models with respective atmospheric and oceanic resolutions are listed in Table 5.1 for easy references.

The climate experiments selected for present analysis includes current climate condition where experiment runs with greenhouse gases increasing as observed through twentieth-century and two future climate scenario experiments (A1B and A2). A1B scenario experiment is a medium forcing case where CO₂ concentration of about 720 ppm by the year 2100 is assumed whereas the A2 scenario is characterized by high forcing with CO₂ concentration of 820 ppm by 2100 (Meehl et al., 2007). The current and future climate scenario time span is selected based on the following limiting criteria. (1) Availability of observed data for the study area (2) availability and accessibility of refined large-scale current climate predictors and (3) accounting a future climate experiment that is sufficiently long enough to reflect the cumulative past and present climate signal. The impacts of large-scale current and future atmospheric-oceanic perturbations could modestly be captured from far long climate experiments. This is because large-scale future climate impacts are better resolved in the span of two to three climate periods in which each timeline preferably assumed to be a length of thirty years.

According to Special Report on Emission Scenario (SRES), the four major emission scenario storylines (A1, A2, B1, B2) are subdivided into six scenario families (A1F1, A1T, A1B, A2, B1 and B2) (Meehl et al., 2007). This classification is primarily based on demographic change, social, economical and broad technological developments that the earth-atmosphere-oceanic environment faces. However, the present analysis is limited to the current climate, A1B and A2 scenarios. The A1B scenario family describes a future world of very rapid economic growth, global population that peaks in mid-century and declines thereafter with rapid introduction of new and efficient technologies symbolized by a convergent world. The technological change in energy system is balanced across all forms of energy sources. The A2 scenario is characterized by a heterogeneous world with continuously increasing population, regionally oriented economic developments and more fragmented technological changes. Thus, here it has been emphasized to explore how the medium (A1B) and high (A2) emission scenario conditions affect the future water resources management. The medium emission scenario provides an average future climate situation whereas the high emission scenario helps us to examine the future climate condition as a result of worst combination of demographic, technological and environmental aspects that might affect the future environment conspicuously.

Prior to downscaling, preliminary model evaluation is required to identify a GCM that could probably reproduce the synoptic scale climatic behavior of a region of interest. The

available meteorological observatories are very sparse, in most cases, and accompanying spatial correlation between GCM grid points and station data could not be adequately established. Therefore, reanalysis climatic dataset available at regular intervals are useful to establish such statistical relationships for preliminary model evaluation. Furthermore, the reanalysis datasets are extracted from in-situ historical observations and real-time satellite captured climatologies and hence reflects most of the physical processes involved in the GCMs.

Gridded monthly temperature data covering the entire Ethiopia is accessed from Japanese 25-year reanalysis (JRA-25) data archive (http://jra.kishou.go.jp/JRA-25/index_en.html). JRA-25 temperature dataset extends from 1979-2004 and has horizontal resolution of approximately 1.2° (Onogi et al., 2007). Improved quality of gauge measurements and access to sparse ocean areas through satellite data have contributed to consistent reanalysis data since 1979. Gridded monthly precipitation data (Adler et al., 2003) for the same geographical coverage is extracted from Global Precipitation Climatology Project Version 2.2 (GPCPV2.2) data archive (<http://www.esrl.noaa.gov/psd>) that extends from 1979 to present time.

Spatial correlation coefficient (Scorr) and root mean square error (RMSE) between reanalysis and GCM simulated temperature and precipitation is computed. The spatial correlation provides a measure of variance as a function of distance between data points. Monthly reanalysis temperature and precipitation datasets during June to August are used to develop statistical relationship to corresponding model outputs.

Daily temperature is characterized by modestly good spatial correlation with RMSE ranging from 1.1-2.5 $^{\circ}\text{C}$. However, precipitation variables are characterized by RMSE values varying approximately between 1.5mm/day to 2.5mm/day. Fig. 5.1 presents a plot of model indices between reanalysis and model output temperature and precipitation variables analyzed for 1981-2000. Among IPCC- FAR approved GCMs listed in Table 1, model No. 3, 5, 10, 11, 19, 21 and 24 have showed relatively better spatial correlation and less RMSE value for temperature and precipitation (Fig. 5.1) variables. The model evaluation indices are based on June-July-August season climate dataset. However, subsequent statistical downscaling approach and runoff simulations are limited to model No. 3 and 5 for their relatively better correlation and availability of time coinciding GCMs outputs for present and future climate conditions.

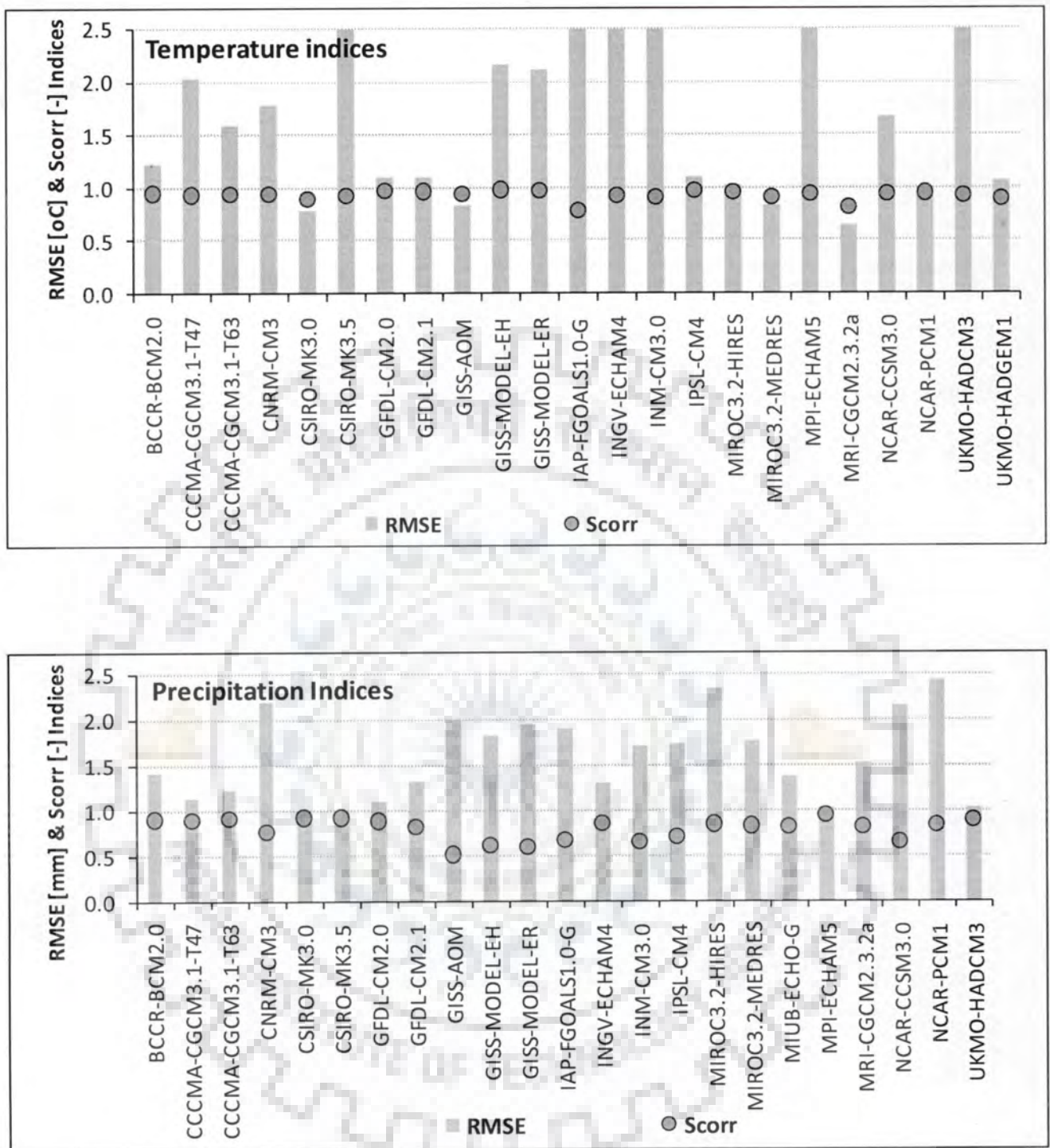


Fig. 5.1 Preliminary model evaluation indices (RMSE and Scorr) between reanalysis temperature and precipitation gridded dataset covering entire Ethiopia and GCMs output during 1981-2000

Table 5.1 IPCC Forth Assessment Report (IPCC-FAR) approved climate models and respective atmospheric and oceanic resolutions

Model No.	Model Acronym	Model Origin	Atmospheric Resolution	Oceanic Resolution
1	MPI-ECHAM5	Max Plank Institute for Meteorology , Germany	1.9°x1.9° (L31)	1.5°x1.5° (L40)
2	CSIRO-MK3.5	Commonwealth Scientific and Industrial Research Organization , Australia	1.9°x1.9° (L18)	0.8°x1.9° (L31)
3	BCCR-BCM2.0	Bjerknes Center for Climate Research, Norway	1.9°x1.9° (L31)	0.5°-1.5°x1.5° (L35)
4	INGV-ECHAM4	Max Plank Institute for Meteorology , Germany	2.8°x 2.8° (L19)	0.5°-2°x1.5° (L19)
5	CSIRO-MK3.0	Commonwealth Scientific and Industrial Research Organization , Australia	1.9°x1.9° (L18)	0.9°x1.9° (L31)
6	UKMO-HADCM3	Hadley Centre for Climate Prediction and Research/ Meteorological Office , UK	2.5°x3.75° (L19)	1.25°x1.25° (L20)
7	CCCMA-CGCM3.1-T47	Canadian Centre for Climate Modelling and Analysis, Canada	2.8°x2.8° (L31)	1.9°x1.9° (L29)
8	CCCMA-CGCM3.1-T63	Canadian Centre for Climate Modelling and Analysis, Canada	1.9°x1.9° (L31)	0.9°x1.4° (L29)
9	CNRM-CM3	Centre National de Recherches Meteorologiques, France	1.9°x1.9° (L45)	0.5°-2°x2° (L31)
10	GFDL-CM2.0	NOAA/Geophysical Fluid Dynamics Laboratory, USA	2.0°x 2.5° (L24)	0.3°-1.0°x 1.0°
11	GFDL-CM2.1	NOAA/Geophysical Fluid Dynamics Laboratory, USA	2.0°x 2.5° (L24)	0.3°-1.0°x 1.0°
12	GISS-AOM	NASA/Goddard Institute for Space Studies, USA	3°x 4° (L12)	3°x 4° (L16)
13	GISS-MODEL-EH	NASA/Goddard Institute for Space Studies, USA	4°x 5° (L20)	2°x 2° (L16)
14	GISS-MODEL-ER	NASA/Goddard Institute for Space Studies, USA	4°x 5° (L20)	4°x 5° (L13)
15	IAP-FGOALS1.0-G	National Key laboratory of Numerical Modeling for Atmospheric Sciences and Geophysical Fluid Dynamics (LASG)/Institute of Atmospheric Physics , China	2.8°x 2.8° (L26)	1°x1° (L16)
16	INM-CM3.0	Institute for Numerical Mathematics, Russia	4°x 5° (L21)	2.0°x 2.5° (L33)
17	IPSL-CM4	Institut Pierre Simon Laplace, France	2.5°x3.75° (L19)	2°x2° (L31)
18	MIROC3.2-HIRES	Center for Climate System Research, National Institute for Environmental Studies and Frontier Research Center for Global Change , Japan	1.1°x 1.1° (L56)	0.2°x 0.3° (L47)
19	MIROC3.2-MEDRES	Center for Climate System Research, National Institute for Environmental Studies and Frontier Research Center for Global Change , Japan	2.8°x 2.8° (L20)	0.5°-1.4°x1.4° (L43)
20	MIUB-ECHO-G	Meteorological Institute of the University of Bonn, Meteorological Research Institute of the Korea Meteorological Administration and Model and Data Group, Germany/Korea	3.9°x 3.9° (L19)	0.5°-2.8°x1.4° (L20)
21	MRI-CGCM2.3.2a	Meteorological Research Institute, Japan	2.8°x 2.8° (L30)	0.5°-2.0°x2.5° (L23)
22	NCAR-CCSM3.0	National Centre for Atmospheric Research , USA	1.4°x 1.4° (L26)	0.3°-1.0°x1.0° (L40)
23	NCAR-PCM1	National Centre for Atmospheric Research , USA	2.8°x 2.8° (L26)	0.5°-0.7°x1.1° (L40)
24	UKMO-HADGEM1	Hadley Centre for Climate Prediction and Research / Meteorological Office, UK	1.3°x 1.9° (L38)	0.3°-1.0°x1.0° (L40)

L() indicates number of vertical levels and resolutions are given as latitude by longitude.

The current and future climate scenario predictors are accessed from Bjerknæs Center for Climate Research Version 2.0 (herein after, BCM2.0) of Norway and Commonwealth Scientific and Industrial Research Organization of Australia (herein after, MK3.0). The BCM2.0 model has an atmospheric resolution of T63 (1.9°x1.9°) and oceanic resolution of 0.5°-1.5° x 1.5°. The model is initiated from the climate of twentieth century experiment with varying forcing agents like carbon dioxide, methane, nitrogen oxide, chlorofluorocarbons and sulphate aerosols. Solar irradiance (1368 w/m²), black carbon, sea salt and desert dust are assumed to be fixed in the model experiment. In this model the pressure at the top of the atmosphere is fixed at 10 hPa and no adjustment for surface momentum, volcanic aerosols, heat or freshwater fluxes (Deque et al., 1994 ; Bleck et al., 1992 ; Furvevik et al., 2003) is made. The MK3.0 GCM output has the same atmospheric spectral resolution to that of BCM2.0 but with oceanic resolution of 0.9°x1.9° (Gordon et al., 2002).

5.7 METHODS USED

Statistical downscaling method has the capability to develop statistical relationships in terms of correlation matrix between large-scale predictors and local or station level predictands. Regression analysis, simple quantile plots, quantile-quantile plot , scatter plot and analysis of above and below threshold magnitude of precipitation and temperature are some of major statistical components in SDSM tool to evaluate the stochastic behavior of observed and downscaled weather variables. The observed daily precipitation, maximum and minimum temperature values covering recent 30 years (1980-2009) are used to develop statistical relationship with predictor variables. Downscaling phase is calibrated for the year 1980-1989 and validated for 1990-1999. The closeness of simulated present and future weather variables to observed values are also examined in terms of regression coefficient. Quantile-quantile plot of observed and downscaled datasets is used to evaluate whether the two dataset stem from the same type of probability distribution. If the variables stem from the same distribution, such as normal distribution, the quantile-quantile plot reasonably fit into a straight line.

The f-quantile, $q(f_i)$, indicates that the data value below which approximately a decimal fraction f of the data is found. Let the time series x_i of length n be sorted from smallest to largest values such that the sorted values have rank, $i = 1, 2, \dots, n$, then the f_i for each observation is computed following Cleveland (1994) as:

$$f_i = \frac{i - 0.5}{n} \quad (5.1)$$

The corresponding data value of f quantile, $q(f_i)$ is given as:

$$q [f_i] = q \left[\frac{(i - 0.5)}{n} \right] = x_i \quad (5.2)$$

5.7.1 Temperature Downscaling

Weather variables, such as precipitation and temperature used for future climate impact assessment, can be extracted from large-scale atmospheric-oceanic variables, known as predictors, through appropriate bias correction. In the present study, the predictor variables used for statistical downscaling are specific humidity (S_{hum}), zonal wind velocity (U_x), meridonal wind velocity (V_x), geo-potential height at 500 hPa (Z_{500}) and 850 hPa (Z_{850}) pressure level and mean sea level pressure (P_{sl}). Among others U_x , V_x , S_{hum} and P_{sl} variables become better predictors of temperature and precipitation variables for the region under consideration.

Statistically downscaled daily temperature for current climate exhibits strong agreement to observed series. Fig. 5.2 presents the association of simulated maximum temperature of current and future climate scenario for BCM2.0 model to observed series. The coefficient of determination (R^2) is strong for current climate condition and modest enough for future scenarios. Similar level of association is also observed for MK3.0 model, yet not demonstrated here graphically. Quantile and quantile-quantile plots of observed and simulated temperature dataset fit well into straight line (Fig. 5.3 and Fig. 5.4). The quantile plots in Fig 5.3 are S-shaped and are characteristic example of bell-shaped distribution. This phenomenon is attributed to the characteristic property of simulated series for current and future climate condition stem from similar probability distribution to that of observed series.

Extreme daily temperature events from both GCM realizations exceed that of observed series for future climate events. It could be well inferred from the plot of probability of non-exceedance (quantile plot) in Fig. 5.3 that daily temperature magnitude below 30°C accounts large proportion of observed series. However, the same magnitude is characterized by lesser fractions of future scenario daily temperature events in both models.

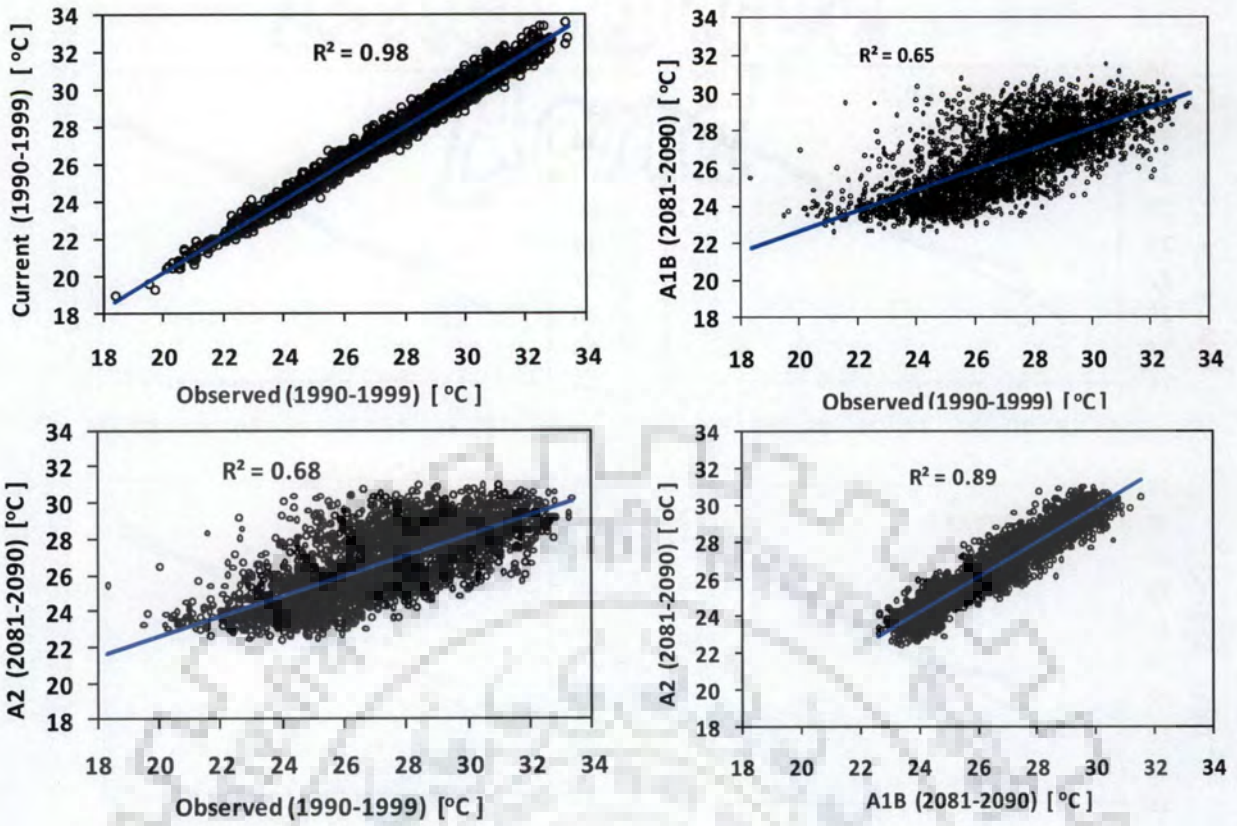


Fig. 5.2 Observed versus downscaled maximum temperature for BCM2.0 model at Alaba Kulito station

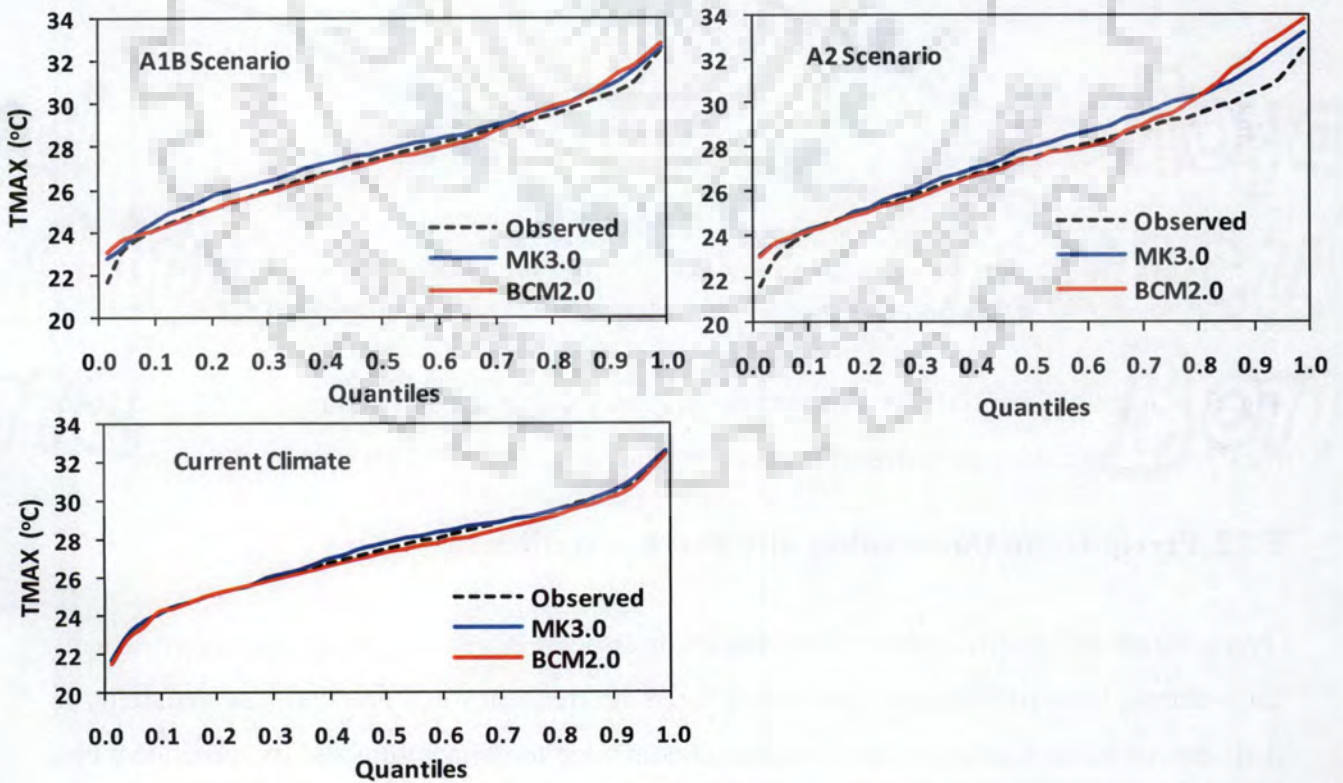


Fig. 5.3 Quantile plots of observed and downscaled maximum temperature at Alaba Kulito for current (1990-1999) and future (2081-2090) climate condition

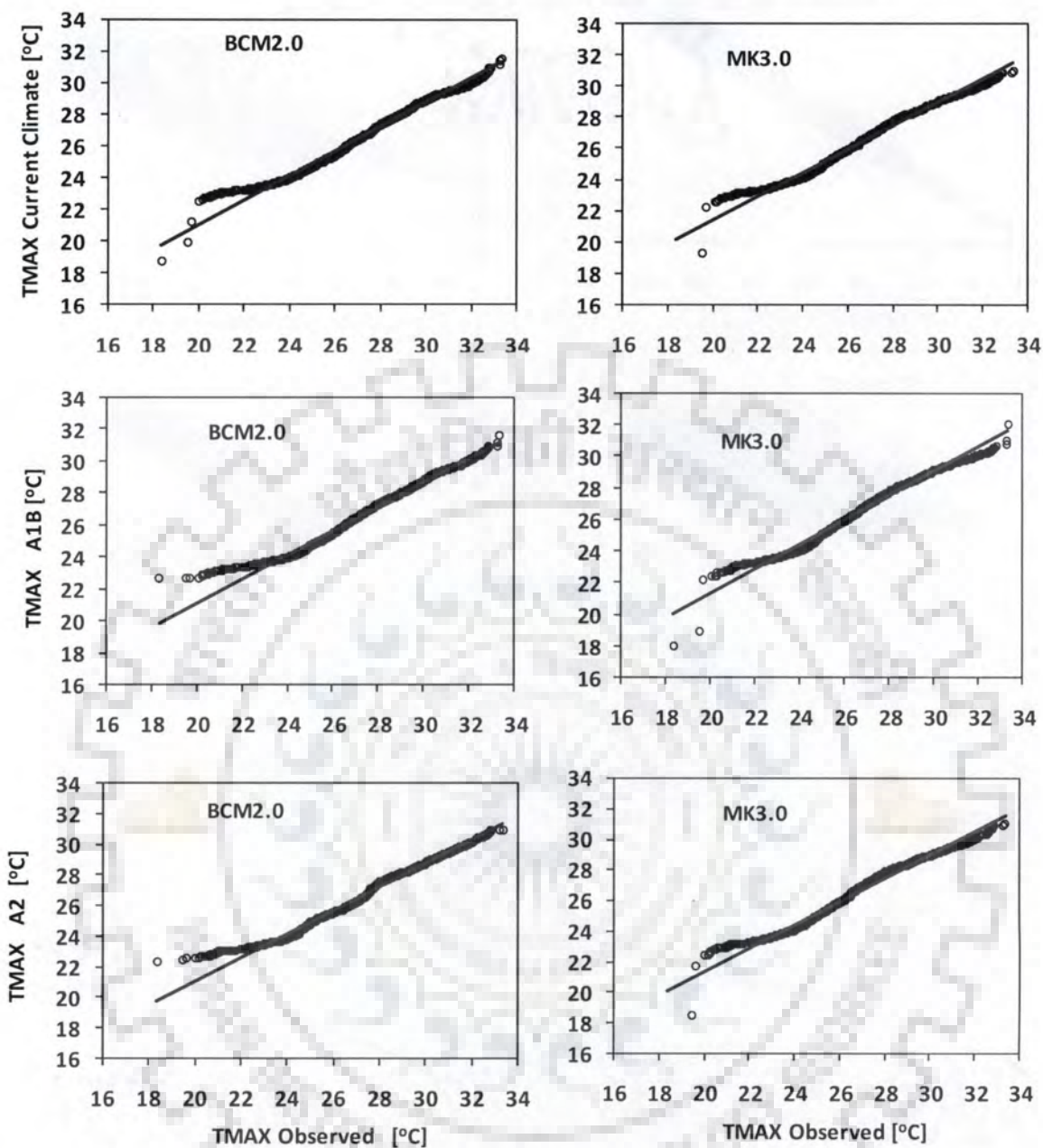


Fig. 5.4 Quantile-Quantile plot of observed (at Alaba Kulito station) and raw GCMs outputs of maximum temperature for current (1990-1999) and future (2081-2090) climate scenarios

5.7.2 Precipitation Downscaling and Bias Correction

Precipitation downscaled from GCM outputs or disaggregated from reanalysis results usually carry certain level of biases that ultimately alters its frequency and amount. The variability in daily precipitation amount is more significant compared to temperature and its subsequent bias correction technique requires an in-depth skill of time evolution of such variables. Some of the commonly employed precipitation bias correction methods include linear scaling, power

transformation (Shabalova et al., 2003; Leander and Buishand, 2007), gamma-gamma transformation (Ines and Hansen, 2006), delta change approach (Hay et al., 2000), multiple linear regression (Hay and Clark, 2003), analogue method (von Storch and Navarra, 1999; Moron et al., 2008), local intensity scaling (Widmann et al., 2003; Schmidli et al., 2007) and quantile mapping (Panofsky and Brier, 1968).

In the present study, both linear and non-linear precipitation bias correction methods are used to correct statistically downscaled daily precipitation values. The linear correction applies a scaling factor to transform raw precipitation to corrected precipitation magnitude. It is a linear transformation of state variable (precipitation) in such a way that both the mean and standard deviation are re-scaled by the same factor as to the individual daily records. Leander and Buishand, 2007 used the ratio between average observed and GCM output precipitation for every 5-days interval of the year including 30-days before and after the 5-days run to obtain the scaling factor. Using this 5-days ratio, the raw daily precipitation is rescaled. In linear correction method, the mean value of the variable is adjusted while the coefficient of variation remains unaffected as both the mean and standard deviation are rescaled by the same factor.

The non-linear correction follows a power transformation rule between raw and observed precipitation series.

$$P_C = aP_o^b \quad (5.3)$$

where P_C is bias corrected daily precipitation; P_O is original or uncorrected daily precipitation ; a and b are parameters. The parameters a and b are estimated using either of the following two approaches. In the first approach, the parameter b is estimated by identifying a point where the coefficient of variation of corrected daily precipitation matches to that of observed precipitation whereas parameter a is determined by obtaining a point where the mean of the transformed daily precipitation corresponds to that of observed daily records. This approach compares linearly rescaled series to that of the observed series to obtain the power transformation parameters a and b . In the second method, the parameters a and b can easily be estimated from logarithmic transformation using two matching quantile estimates of observed and uncorrected GCM scenario output precipitations.

$$P_{1,R} = aP_{1,O}^b \quad (5.4)$$

$$P_{2,R} = aP_{2,O}^b \quad (5.5)$$

Where $P_{1,R}$ and $P_{2,R}$ are raw precipitation values at two different quantiles 1 and 2 ; $P_{1,O}$ and $P_{2,O}$ are observed precipitation values at corresponding quantiles. Applying logarithmic transformation and solving eqns. (5.4) and (5.5) simultaneously b can be estimated as:

$$b = \frac{\log\left(\frac{P_{2,O}}{P_{1,O}}\right)}{\log\left(\frac{P_{2,R}}{P_{1,R}}\right)} \quad (5.6)$$

Finally, a is estimated from eqn. (5.4) or (5.5) by simple substitution. However, there are multiples of matching quantile estimates that yield to different a and b values. To fix the parameters, logarithmic regression is applied to matching quantile estimates where the slope and intercept of best fit line are associated to the parameters b and a respectively.

Statistically downscaled daily precipitation is corrected applying both linear and power transformation methods for current (1990-1999) and two future (A1B and A2) climate scenarios running from 2081-2090.

5.8 SIMULATION OF RUNOFF FOR CURRENT AND FUTURE CLIMATE

ArcGIS supported Soil and Water Assessment Tool (ArcSWAT 2009) described previously is utilized to simulate runoff at Bilate and Hare watersheds using downscaled and bias corrected daily precipitation and temperature variables as weather input parameters to the model. SWAT has the capability to twin up multiples of weather and spatial input variables into numerical hydrologic modelling so that runoff is generated at desired locations on daily or sub-daily basis (Arnold et al., 1998). Spatial and temporal datasets required to run SWAT model, model calibration and validation phases are briefly presented with explanatory details in Chapter 4. In this section, bias corrected daily precipitation and temperature datasets for current and future climate conditions are used to simulate runoff.

5.9 RESULTS AND DISCUSSION

5.9.1 Statistical Downscaling Model

Large-scale atmospheric variables called predictors are used to downscale precipitation and temperature variables using observed station precipitation and temperature variables at Bilate and Hare watersheds. Surface humidity (S_{hum}), zonal wind velocity (U_x), meridonal wind

velocity (V_x), geo-potential height at 500 hPa (Z_{500}) and 800 hPa (Z_{850}) pressure level and mean sea level pressure (P_{sl}) are large-scale atmospheric predictors used in statistical downscaling. U_x , V_x , S_{hum} and P_{sl} variables become better predictors of temperature and precipitation variables for region under consideration. Significant amount of variability is observed in downscaled precipitation for current climate condition when compared to the observed series while the associated variability for temperature is very less.

5.9.2 Precipitation Bias Correction

Atmospheric-Oceanic General Circulation Models (AOGCMs) are less accurate and characterized by significant spatial variability for monthly or daily precipitation magnitudes at regional level. The spatial variability of precipitation is more significant in tropical regions where precipitation varies greatly over small range of latitude and longitude (Covey et al., 2003). AOGCMs without flux adjustments are susceptible to such variability (Dai, 2006) and associated to certain level of biases. Sharma et al. (2011) argues that even regional climate models are susceptible for bias and need further correction in order to provide consistent prediction in timings and magnitude of prevailing climate change. Due to such deriving forces, examination of downscaled precipitation variable for possible biases and applying artificial correction to maintain the parent population distribution pattern is vital.

Daily precipitation, downscaled from large-scale variables for future climate scenario, is significantly higher than the corresponding observed mean monthly records. It is noticed that during the rainy seasons (March-April-May and July-August-September), the variability becomes more profound (Fig. 5.5). Higher precipitation events in terms of frequency and amount dominated the future climate scenario as a consequence of increased future extreme temperature events. The quantile plot in Fig. 5.3 shows that large fraction of extreme temperature ($>30^\circ\text{C}$) events are eminent for future climate scenarios. This Increased future temperature causes higher evapotranspiration rate that may ultimately enhances the rate of near atmospheric condensation process. The mean and coefficient of variation (CV) of uncorrected daily precipitation for current climate is in close agreement to its corresponding historical observation while the variability in mean and CV for future climate conditions (A1B and A2 scenarios) is significant. Bias correction employed to daily precipitation of the control period significantly reduced the CV.

The non-linear (power transformed) bias correction parameters a and b are estimated using arbitrarily selected matching quantile estimates of daily precipitation. The values of ‘ a ’ and ‘ b ’ are fixed through logarithmic regression for arbitrarily selected matching quantiles. In view of this, logarithmically fitted parameter (a , b) values for BCM2.0 model are (0.56, 1.14) and (0.35, 1.3) for A1B and A2 scenario respectively. The A1B and A2 scenarios parameter values of (1.7, 0.82) and (1.8, 0.8) removed most of the extreme biases in MK3.0 model. The uncorrected precipitation values for two future emission scenarios exhibit higher extreme events than the observed ones (Fig. 5.5). However, the bias correction improved both the mean and CV to a reasonable degree. Downscaled and subsequently bias corrected precipitation is aggregated to mean monthly values for easy examination of the variability for two GCM realizations under different scenarios (Fig. 5.6 to Fig. 5.8).

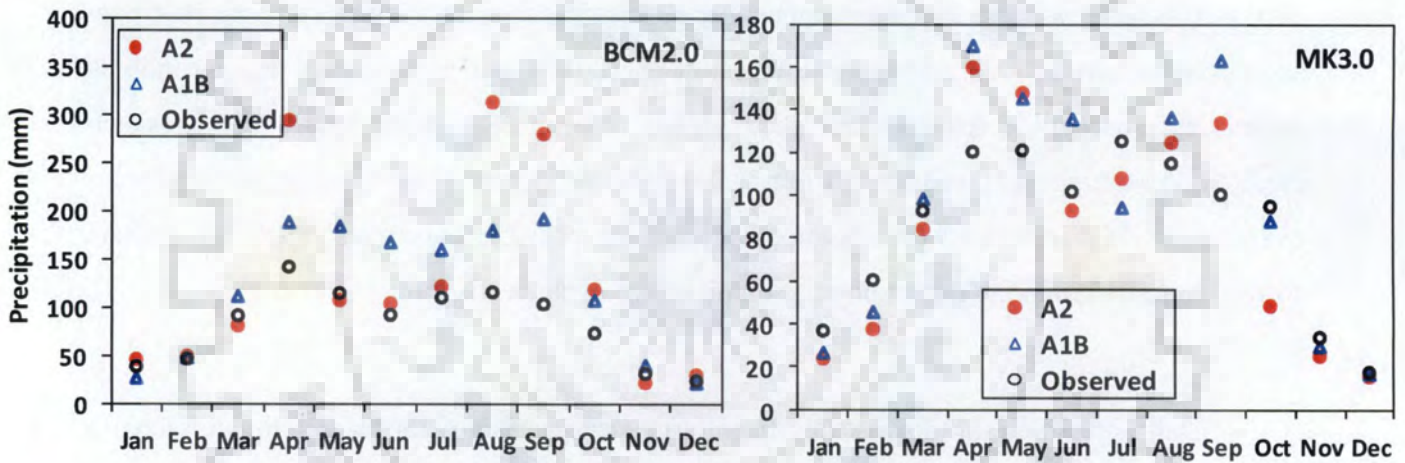


Fig. 5.5 Average monthly future scenario (2081-2090) precipitation variability for two different GCM realizations. The observed station (Alaba Kulito) precipitation spans from 1990-1999

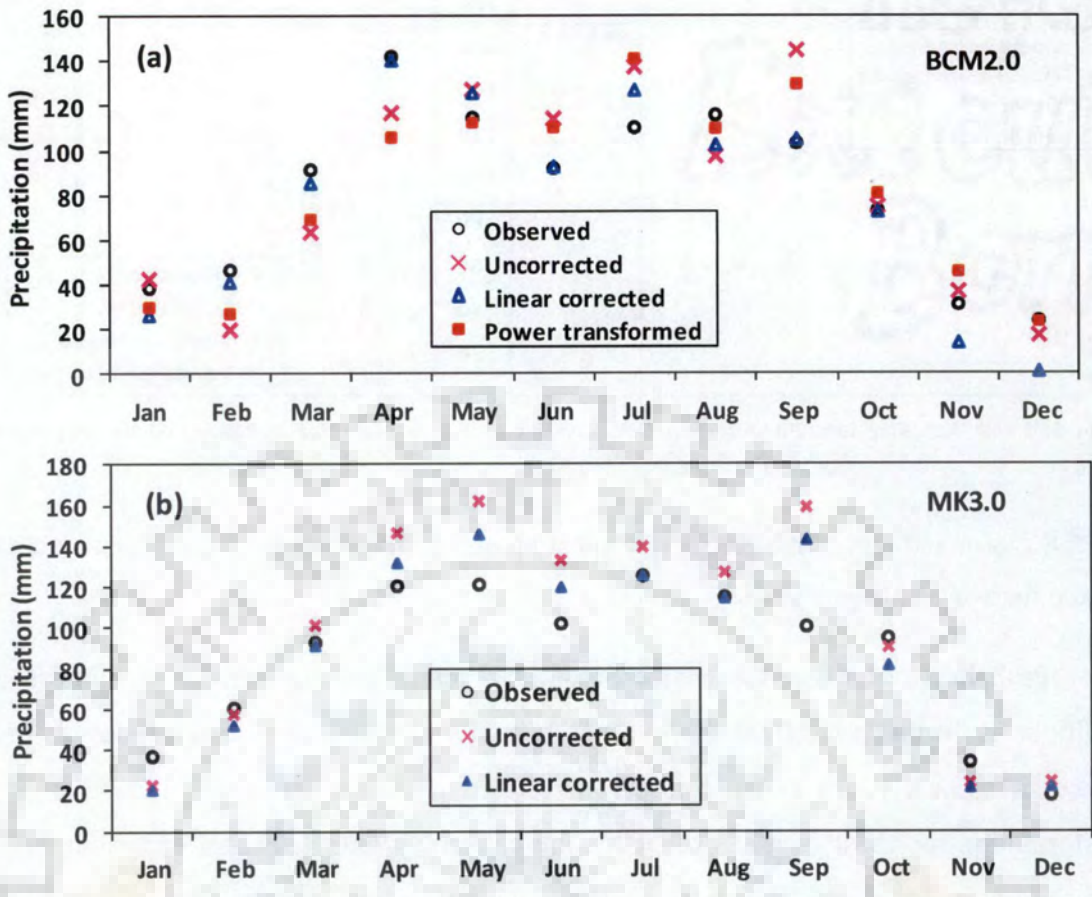


Fig. 5.6 Linear and power transformed bias correction of precipitation for current climate condition for BCM2.0 (a) and MK3.0 (b) GCMs

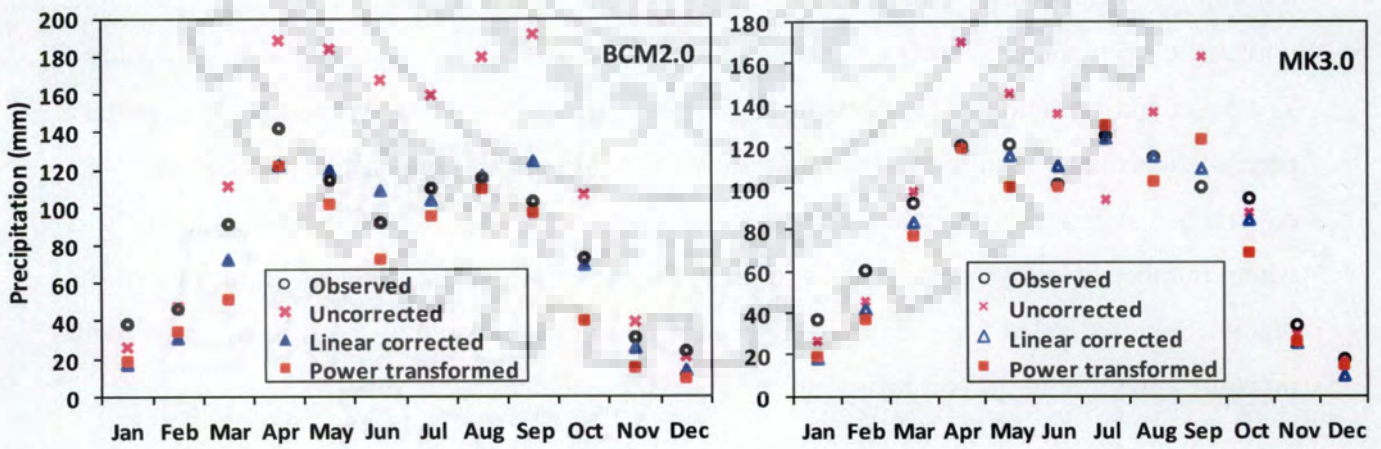


Fig. 5.7 Linear and power transformed precipitation bias corrections for A1B greenhouse gas emission scenario for two GCMs realizations

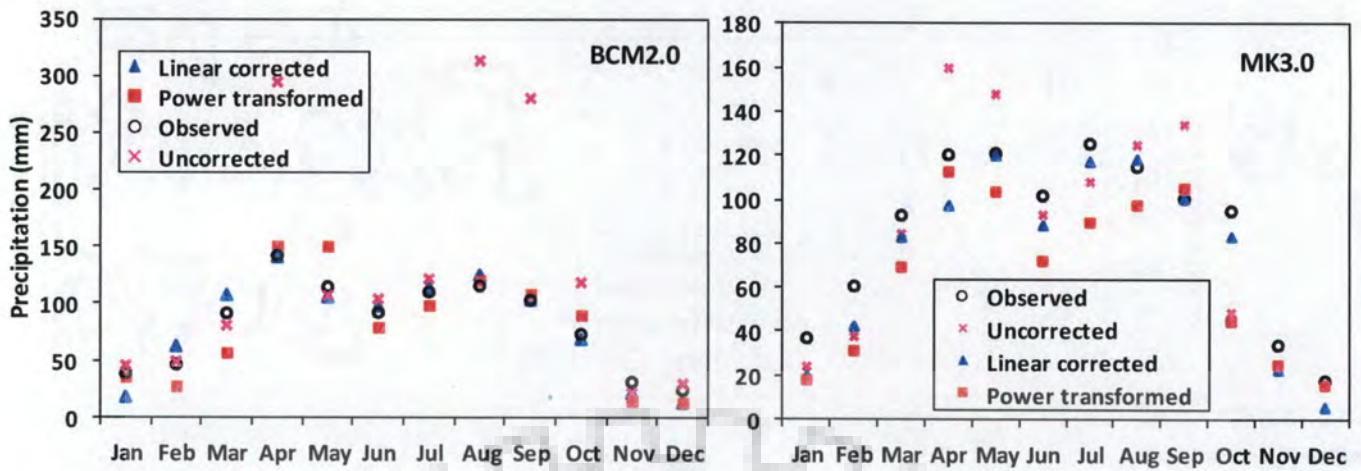


Fig. 5.8 Linear and power transformed precipitation bias corrections for A2 greenhouse gas emission scenario for two GCMs realizations

Probability of exceedance plot of daily precipitation for current and future climate conditions is further investigated to compare respective percentile magnitudes. It has been noticed that linearly rescaled precipitation resulted in better agreement than that of power transformation for most dataset except for the extreme higher tails that experience deviation from the observed values (Fig. 5.9). The extreme values in the right tails of the exceedance probability curves are as a result of extreme observed rainfall records in the years 1993 and 1998. An attempt has been made to explore the variability between single and multiple run (ensemble) mean daily precipitation. Ensemble mean of 20 runs ultimately produced unrealistic simulations in such a way that all days of the year are characterized by rainy days. The onset and cessation of precipitation days vary among ensembles. These lags in important precipitation events resulted in extended rainy days (almost all days of the year become wet-days) when averaged out through the ensembles on daily basis. Thus, in precipitation analysis where number of rainy/dry days is of interest, the ensemble mean produces an artifact of the reality. Such extended rainy days over the analysis period, resulted in sufficient antecedent moisture condition in the soil layers and subsequently yielded higher runoff.

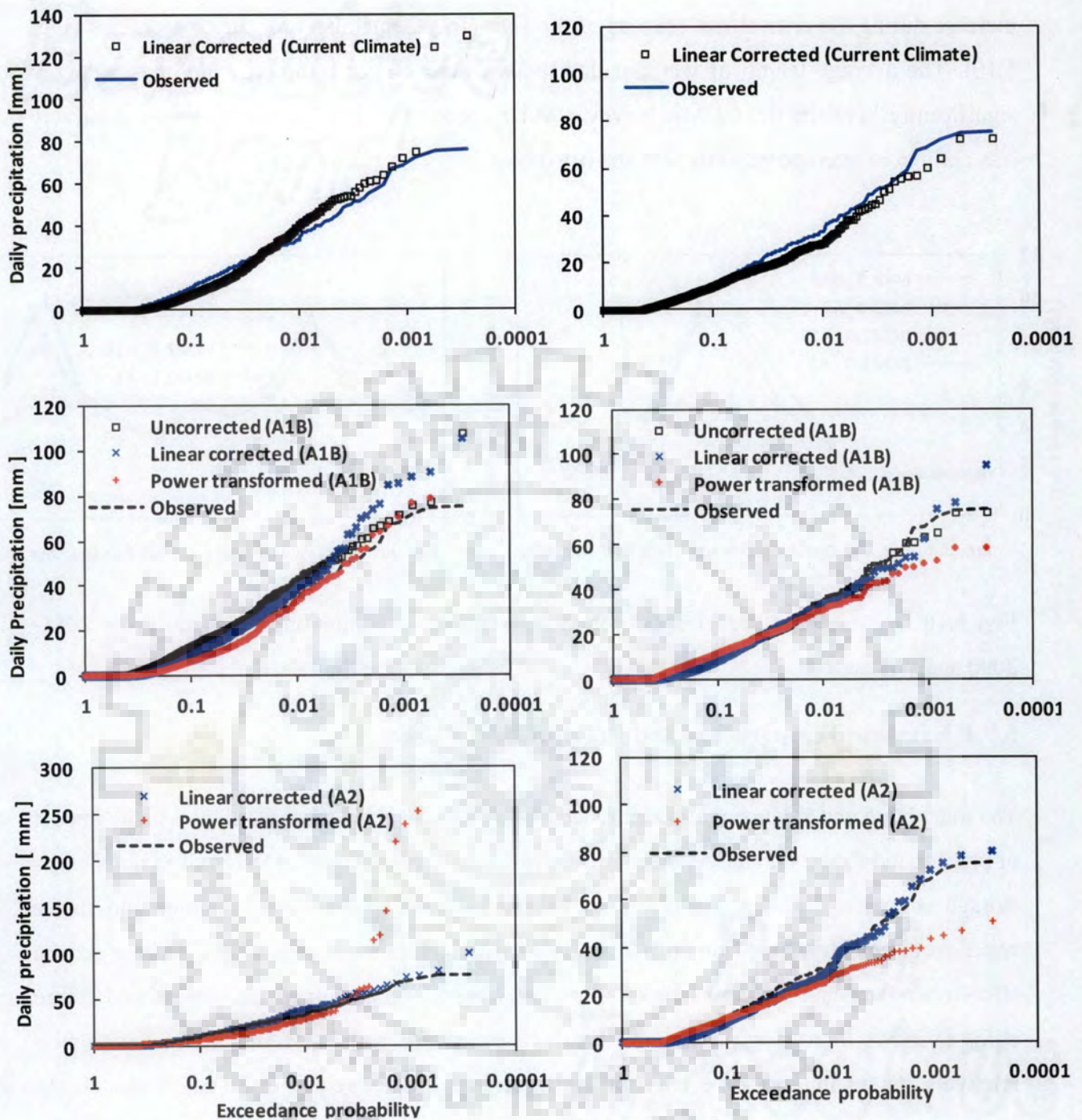


Fig. 5.9 Probability of exceedance of daily precipitation for current and future climate conditions for BCM2.0 (left panels) and MK3.0 (right panels) GCMs

5.9.3 Dry-/Wet-Spell Analysis

Increased extreme precipitation and temperature events prevail for future scenarios. Average dry-spell length found to increase between October and February whereas it remains stable from March-September months for both emission scenarios. The wet-spell length shows an

increase during the critical wet seasons of the year (July-September) for future scenarios (Fig. 5.10). The average length of wet and dry spells examined for future climate does not vary significantly between the GCMs, however, A1B scenario of MK3.0 model shows relatively less number of average monthly wet and dry days.

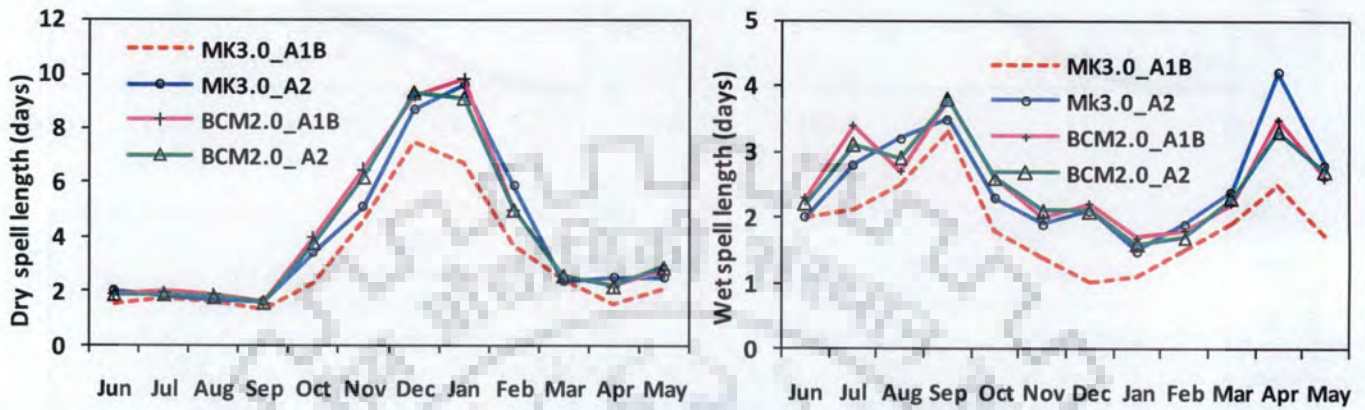


Fig. 5.10 Dry- and wet-spell lengths for future scenario precipitation predicted during 2081-2090 analysis period

5.9.4 Extreme Temperature and Precipitation Events

The magnitude and frequency of occurrence of extreme events is essential to assess the impact of present and future climate on basin's water resources management. Design of various water storage structures, flood management of coastal and susceptible inland regions and future water requirement is based on sufficient knowledge of future extreme events. Winter season (December-January-February) temperature exceeding 25°C , examined for current and future climate, shows increasing peaks over threshold events for both A1B and A2 scenarios with relatively higher number of events for A1B scenario. Observed from BCM2.0 model, the average monthly above threshold events lies between 27.7 and 29.9 days per month for observed series while the same event varies from 27.7 to 30.9 for future scenarios during winter months. Above threshold ($>25^{\circ}\text{C}$) temperature days increased by 11.6 (10.5) and 8.8 (6.7) percents in December and January months for A1B (A2) scenario respectively when compared against observed events. However, the total number of extreme temperature events assessed for MK3.0 events shows less variability. In comparison to BCM2.0, above threshold MK3.0 future temperature events are better approximated to the current climate events. Bias corrected current and future daily precipitations are characterized by few extreme events. The extreme events, in the present context, are defined arbitrarily as daily precipitation magnitude

exceeding 50mm. Linear bias corrected A2 scenario precipitation produced very few extreme rainfall events while A1B scenario is characterized by higher number of extreme daily precipitation. The percentage increase in extreme precipitation events of BCM2.0 model, relative to the observed series during the same analysis window, is 2.5 and 7 percent for A2 and A1B scenario simulated precipitation respectively (Fig. 5.9). Such extreme events are associated to the main rainy seasons, particularly April and September months. Therefore, it is imperative to deduce from such extreme events that the predictor variables reproduced significant number of extreme future precipitation. There is no well-defined pattern of changes in predicted future annual precipitation.

5.9.5 Runoff Generated

Before attempting to simulate runoff for future scenarios at desired locations, the SWAT model is intended to be calibrated and validated using observed streamflow data at both watersheds. Streamflow, land use management, soil and groundwater parameters governing the runoff process are calibrated for the years 1992-1996 and 1995-2000 at Bilate and Hare watersheds respectively. Respective validation phases run from 1998-2002 and 2003-2006 at both watersheds. Details in model sensitivity analysis, model calibration and validation are covered in section 4.9. The catchment condition is under dynamic state and respective hydrologic model parameters also vary over time. However, it is difficult to forecast such model parameters for future climate condition. Therefore, it has been assumed that SWAT model parameters calibrated and subsequently validated for current climate condition remain valid for future climate condition.

Current and future climate based weather input data series is used to simulate daily runoff at two independent watersheds debouching into terminal Lake, Abaya. Runoff is simulated at outlets where observed streamflow data is available. This helps in exploring the relative variability of streamflow under present and future climate conditions to observed series. Daily runoff is further reduced to monthly magnitudes for ease of comparison. Simulated monthly runoff for current climate condition (1990-1999) using downscaled and bias corrected precipitation and temperature variables modestly reproduced effects similar to that of observed values in both watersheds (Fig. 5.11). The average simulated annual water yield for current climate is characterized by a positive deviation from the observed counterpart at both watersheds. It varies from 8-10 % at Hare and 4-12% at Bilate basins between the two

GCMs utilized for present analysis (Table 5.2). This variability might be attributed to local weather influences and highly sensitive catchment behavior in response to precipitation. Simulated average annual water yield shows slight variation between GCMs. It lies within $\pm 10\%$ at Bilate basin and ranges from -17% to 12% at Hare basin. Fig. 5.12 presents simulated monthly runoff based on MK3.0 and BCM2.0 GCMs output for two future climate scenarios at Bilate and Hare watersheds. Future climate scenarios are characterized by highly extreme runoff events. The A1B scenario weather variables predicted higher runoff for MK3.0 model than BCM2.0 at both watersheds. The BCM2.0 model is characterized by relatively higher extreme runoff events for A2 emission scenario.

Average simulated monthly runoff for current and future climate condition during analysis period is summarized in Fig. 5.13. The plot compares observed streamflow against model predicted runoff magnitudes. The main rainy seasons i.e., April and May of the first rainy season and July to September of the summer rainy seasons are marked by highly variable runoff magnitudes during the analysis period. The difference in minimum and maximum runoff simulated during the ten years analysis period is significant during such wet seasons. The variability is much lower for other driest and limited rainfall seasons.

The gross annual water yield simulated for current and future climate scenarios for two climate scenarios is further compared to the average observed runoff in the respective watersheds. It has been noted that the simulated runoff varies from -3.5% to 18% at Hare watershed and is within the range of -4% and 14% at Bilate watershed. The simulated current and future runoff is featured with higher number of extreme events. Figs. 5.14 and 5.15 present percentile magnitudes of simulated monthly runoff at Bilate and Hare watersheds for future scenarios from two GCM realizations. The box plot illustrates a linear scale of the lowest, upper most and the intermediate (25%, 50%, and 75%) percentile runoff values. It is noticed from the plot that Inter-monthly runoff variability is significant during the wet seasons. The range of monthly runoff magnitude is sufficiently large enough during rainy seasons of March-May and July-September. However, the variability is modest over the other months of the year. A polynomial fitted to the average monthly runoff for future scenarios during the analysis period shows that significant portion of the runoff volume is exhibited during the summer rainy season (Figs. 5.14 and 5.15). Excessive peaks in the percentile plots are associated to extreme daily runoff events simulated during the rainy seasons.

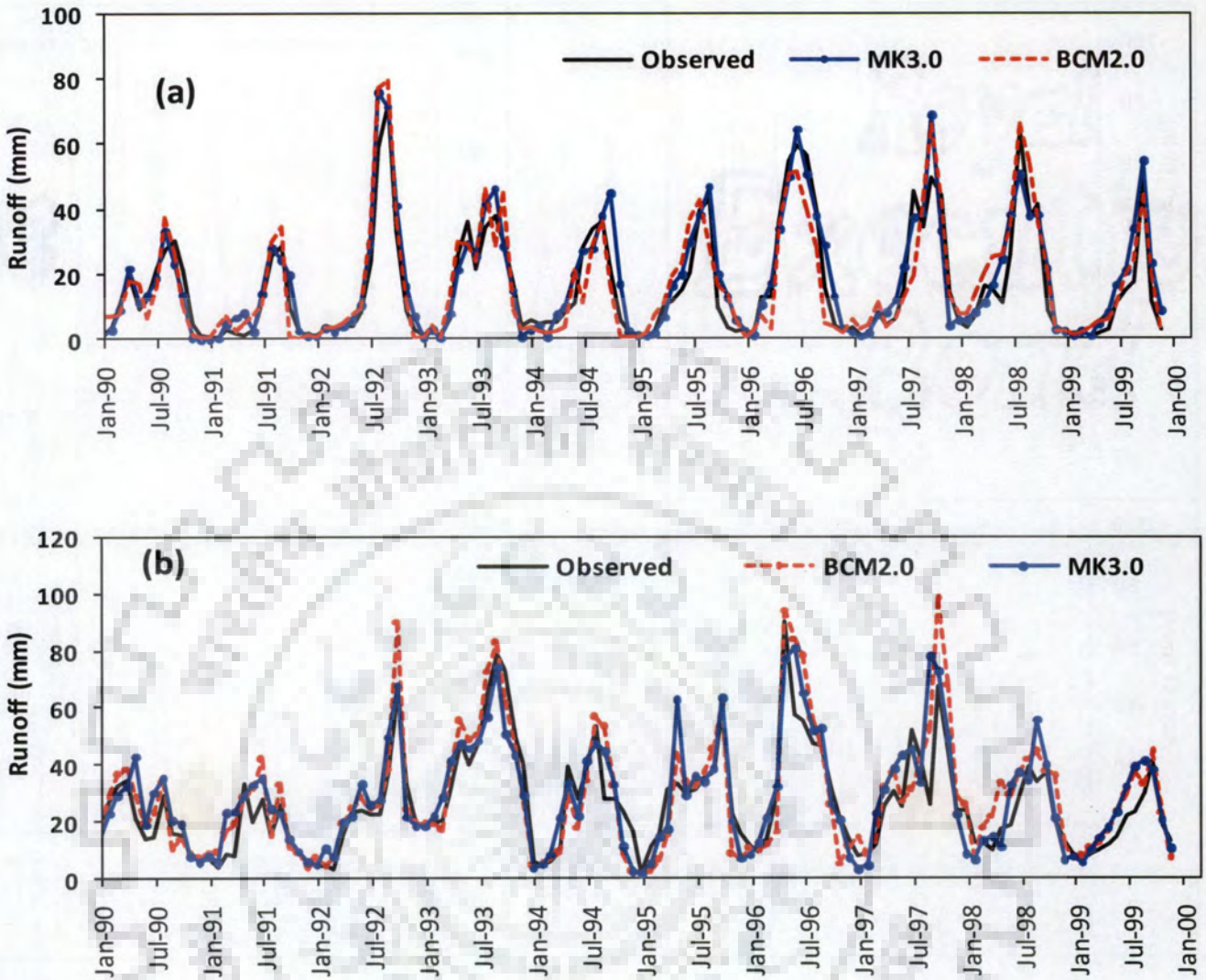


Fig. 5.11 Observed and simulated monthly runoff for current climate from two GCMs at Bilate (a) and Hare (b) watersheds

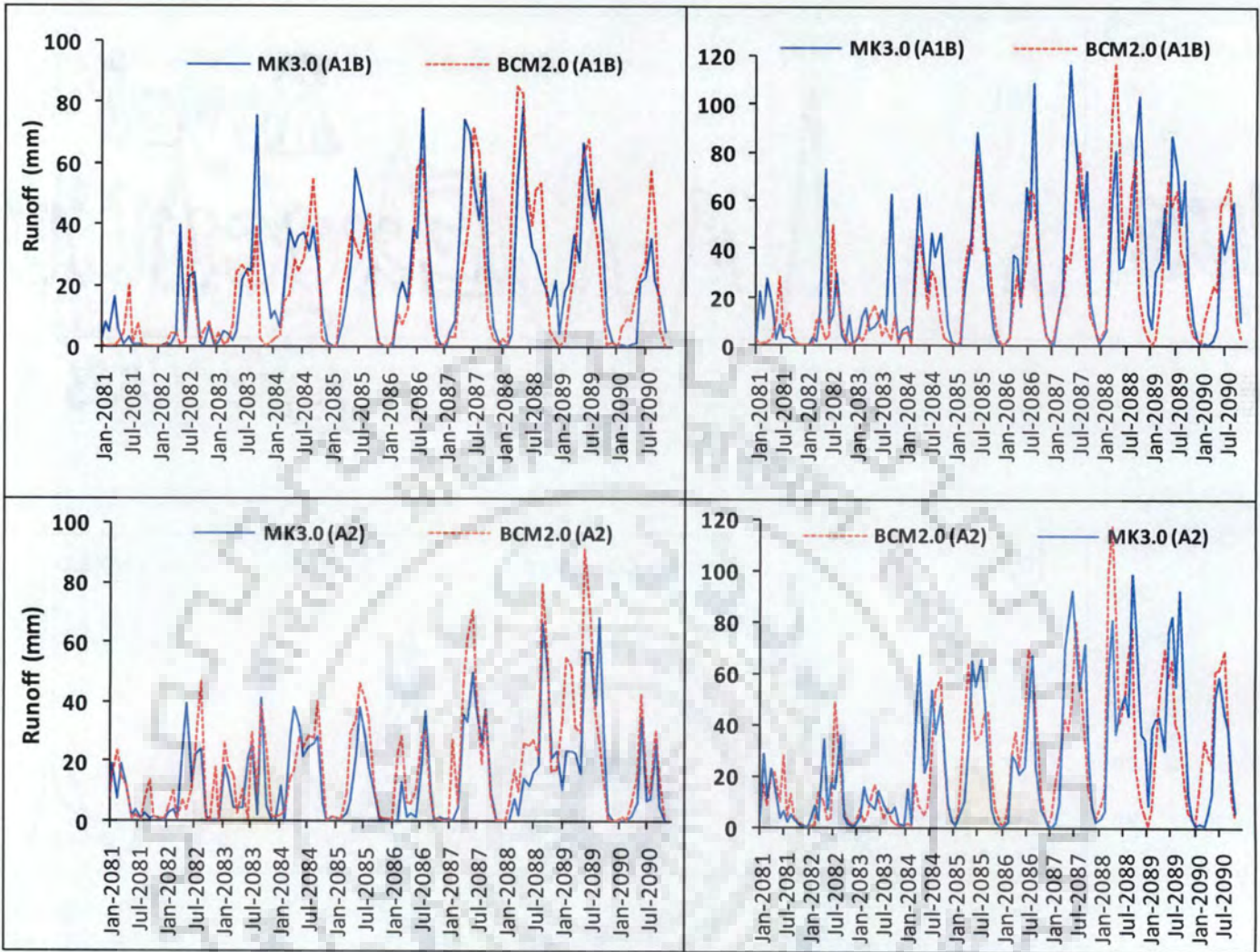


Fig. 5.12 Runoff simulated for future climate scenario at Bilate (left panels) and Hare (right panels) from two GCMs

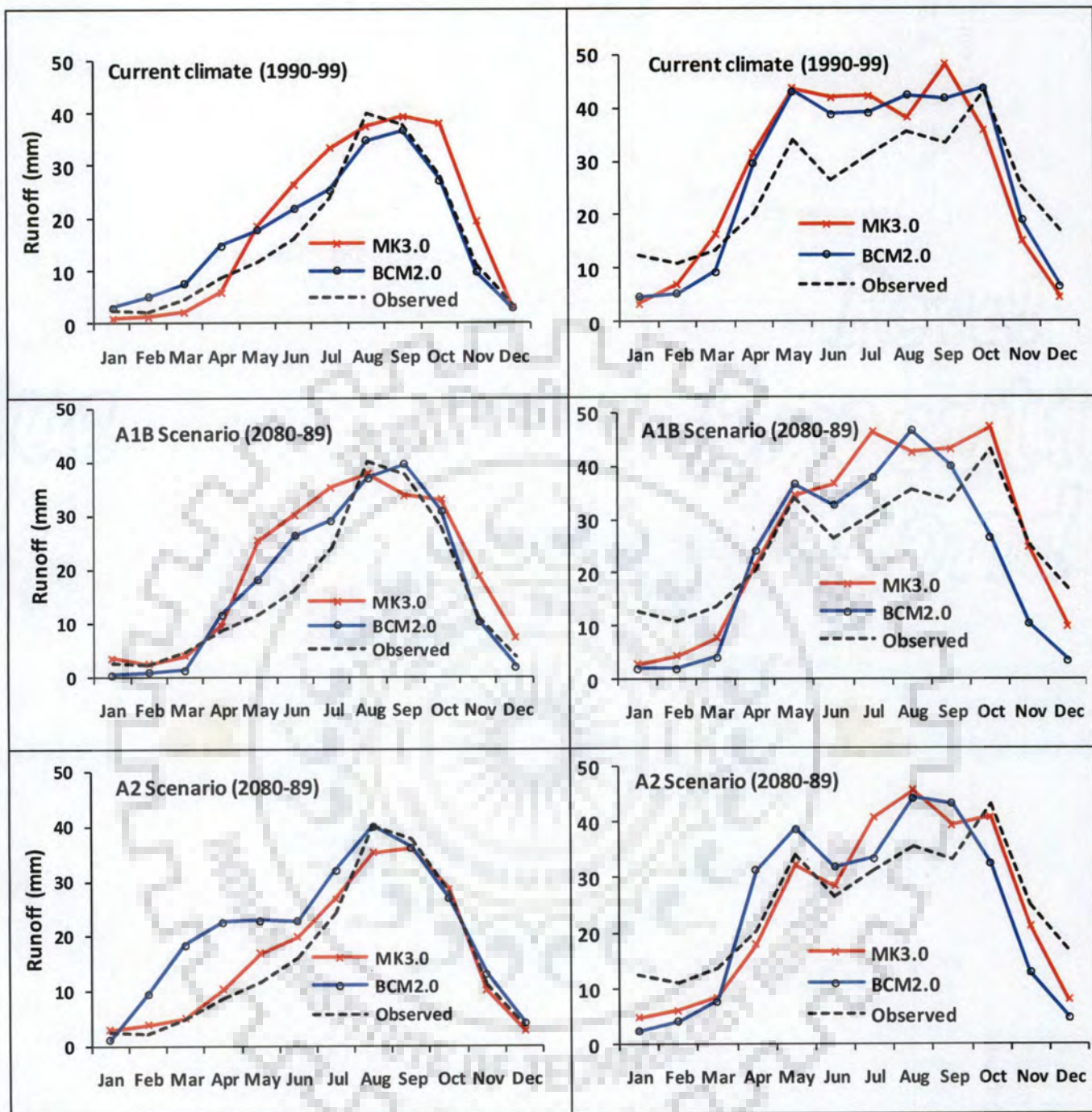


Fig. 5.13 Average monthly runoff simulated for current and future climate (A1B and A2 scenarios) conditions at Bilate (left panels) and Hare (right panels) watersheds

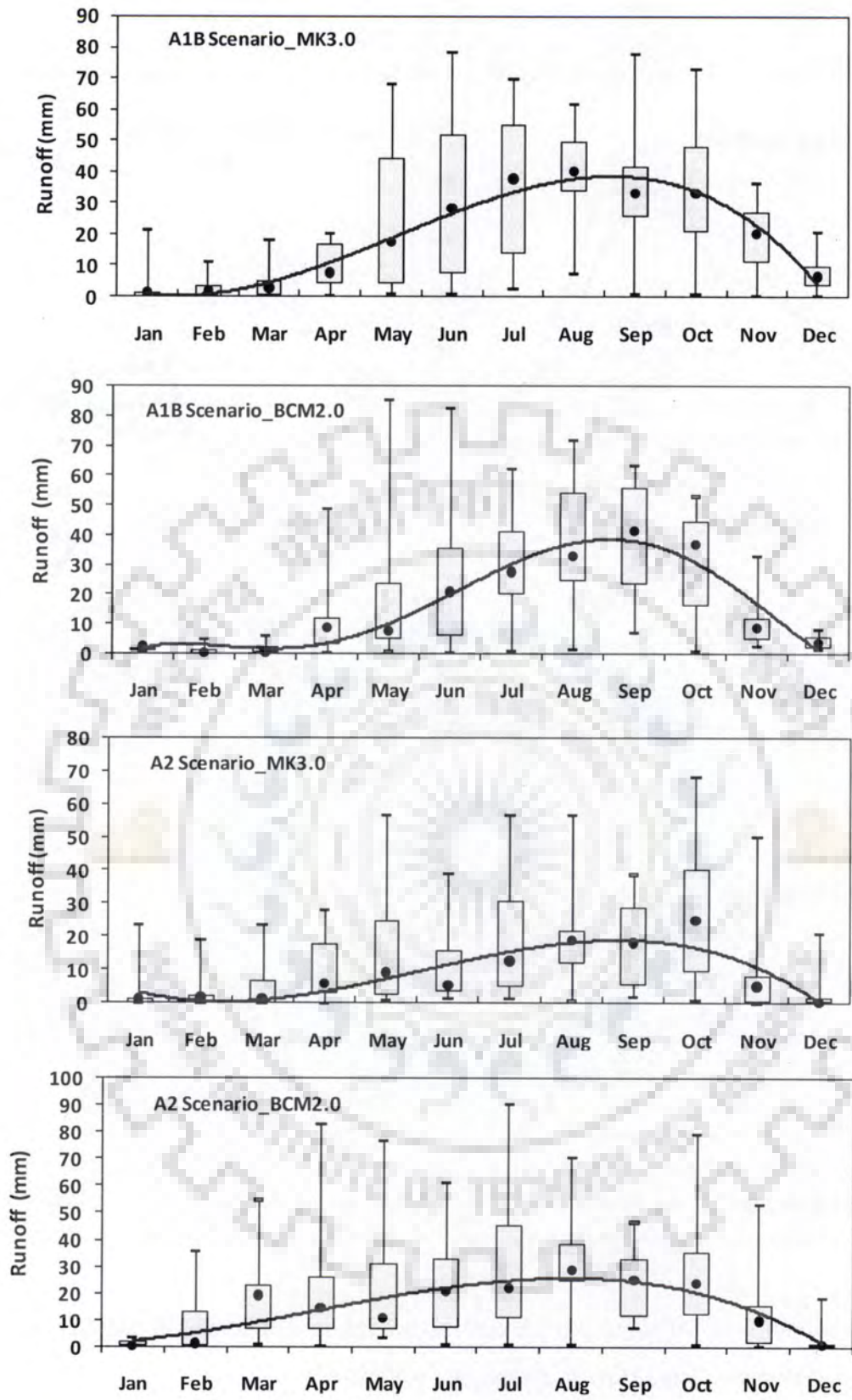


Fig. 5.14 Box plots of percentile (lowest, first quarter, median, third quarter and upper most) monthly runoff simulated for future climate scenarios at **Bilate watershed**

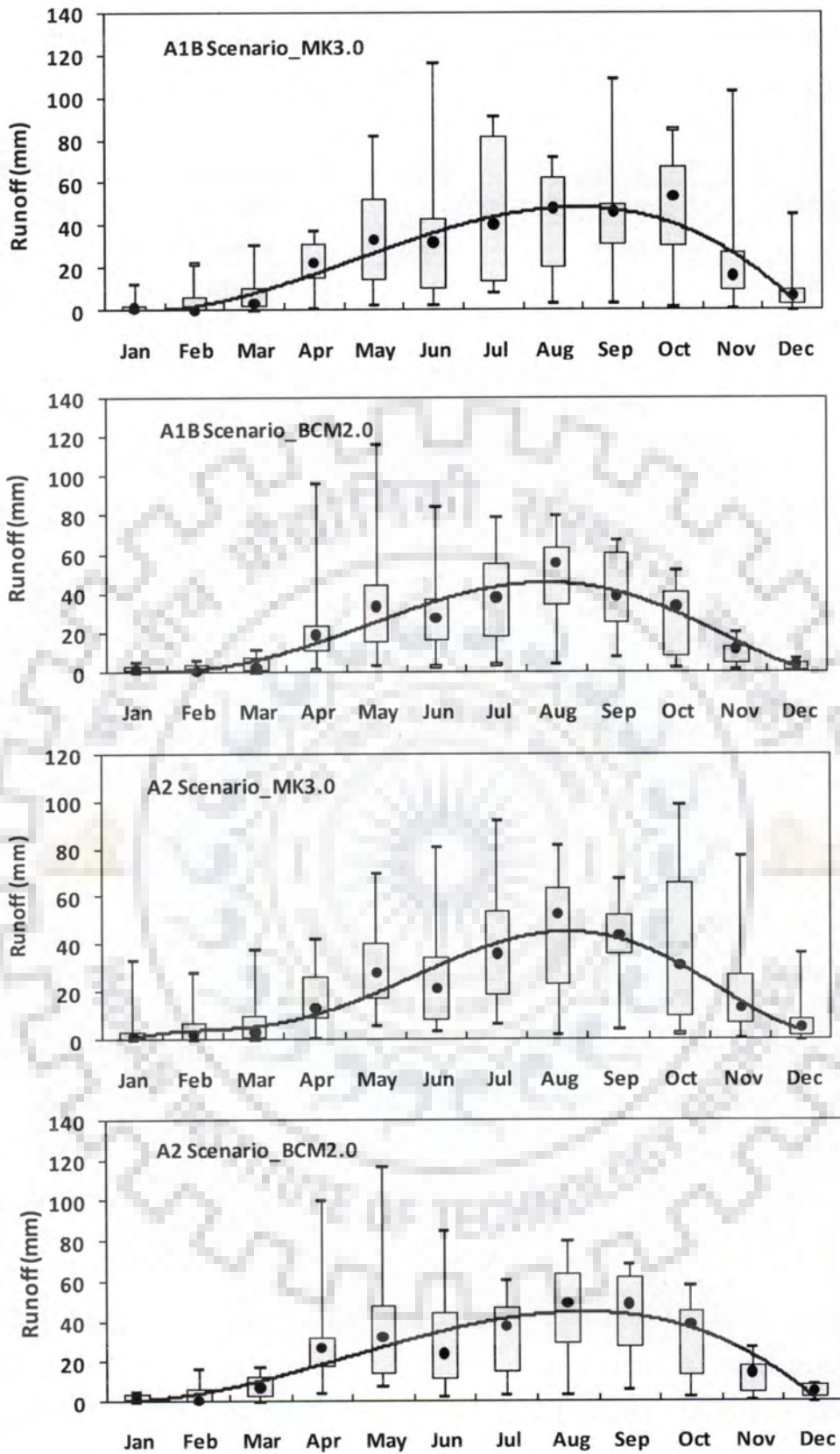


Fig. 5.15 Box plots of percentile (lowest, first quarter, median, third quarter and upper most) monthly runoff simulated for future climate scenarios at **Hare watershed**

Table 5.2 simulated average runoff depths for different climate scenarios and corresponding percentage change with respect to observed series

Climate Scenarios	Runoff depth (mm) at Hare Basin		Runoff depth (mm) at Bilate Basin	
	Observed (1990-1999) = 288		Observed (1990-1999) = 203	
	Simulated	% change*	Simulated	% change*
CSIRO- MK3.0_Current	315	9.4	211	3.9
CSIRO Mk3.0_A1B	314	9.0	221	8.9
CSIRO MK3.0_A2	290	0.7	210	3.4
BCM2.0_Current	312	8.3	228	12.3
BCM2.0_A1B	278	-3.5	195	-3.9
BCM2.0_A2	340	18.1	231	13.8

* percentage change is relative to the average observed runoff depth over 1990-1999 in respective watersheds

5.10 CONCLUSIONS

Potential impacts of climate change on runoff generation from two watersheds of Rift Valley lakes basin of Ethiopia are discussed. Statistically downscaled and subsequently bias corrected precipitation and temperature variables from two GCMs scenarios are used to simulate daily runoff. Statistical downscaling, followed by bias correction, effectively reproduced the current weather variables. Its effectiveness is evaluated using statistical comparison of downscaled variables and observed series.

Bias corrected current and future daily precipitations are characterized by few extreme events. Such extreme events are associated to the main rainy seasons, particularly April and September months. Winter and summer seasons are characterized by longer dry and wet days for future scenarios. There is no well-defined pattern of changes in predicted future annual precipitation.

The runoff simulated at both watersheds indicates potential variability of future climate. Simulated future scenario runoff at both watersheds is marked by increased daily extreme events that ultimately results in increase in the gross annual water yield of the basins. The simulated runoff varies from -4% to 18 % at Hare watershed and is within the range of -4 % and 14 % at Bilate watershed. Future water resources planning and management could likely be affected by such variability and hence existing design methods could expand their scope to account for these extreme events.

Further noticed is that there is obvious inter-annual variability in runoff magnitude during the analysis period. Simulated average annual water yield shows slight variation between GCMs. It lies within $\pm 10\%$ at Bilate basin and ranges from -17% to 12% at Hare basin. The use of multiple GCMs while predicting future climate condition and ensuing impacts could help to capture key climate features that are not well explained by one of the models. Hence, future attempts for the region could rely on realizations from multi-models.



IMPACT OF CATCHMENT DYNAMICS ON RUNOFF GENERATION

6.1 GENERAL

The response of a catchment is time and space variant and influenced by anthropogenic and climatic factors. A drop of water falling in the form of precipitation usually traverses long path until it reaches the main stream. This long journey is dominantly accelerated or decelerated by land cover, soil, rainfall intensity and catchment geomorphologic parameters (Tiwari et al., 2006).

This chapter deals with review of catchment dynamics on runoff generation; extraction of land use/land cover and other spatial input data for hydrologic modeling; watershed modelling of varied land use /land cover conditions and statistical analysis of streamflow trends. Finally, based on the results obtained from subsequent analysis and discussion, conclusions are drawn.

6.2 OVERVIEW OF IMPACT OF CATCHMENT DYNAMICS ON TOTAL WATER YIELD OF A WATERSHED

In most parts of the globe, significant areas of pristine ecosystems with lush vegetation have been converted to other forms of land use practices. Conversion of forest cover and dense naturally vegetated area to arable land and cattle grazing field has modified bulk water yield from the watersheds (Angelsen, 1999; Barbier, 2004). Land use change has been strongest in tropical regions and its contribution to global runoff outweighs that of climate change (Piao et al., 2007). The world's largest natural tropical rain forest of Amazon is currently experiencing a large-scale deforestation due to increasing number of cattle herds in the region that ultimately requires substantial pasturelands (Chaves et al., 2008).

The scientific understanding of the influence of forest cover and land use changes on water yield of the basin dates back to the early 20th Century during which advanced computational power to handle spatial data was almost none-existent. In 1911, the Wagon Wheel Gap experimental watershed in central Colorado and the Priest river experimental forest

in northern Idaho of USA were established to study forest associated influences on streamflow and erosion. Similar attempts were further extended to Europe (Hegg et al., 2006), Southern and Eastern parts of Africa (Wight, 1940; 1943; Dagg and Blackie, 1965) during later years. Field experiments and catchment studies conducted in multiple watersheds across the globe show that forest reduction increases water yield (Hibbert, 1967; Edwards and Blackie, 1981; Bosch and Hewlett, 1982; Fohrer et al., 2001; Hundecha and Bardossy, 2004; Yu et al., 2008) and sediment load (Alansi et al., 2009) from the catchment.

Effect of land use /land cover on runoff and sediment yield from the catchment is investigated following different approaches worldwide. The classical hydrologic models of a pair catchment consideration i.e., control and treatments (Bates, 1921; Bates and Henry, 1928; Nemeč et al., 1967) are in vogue to simulate the effect of land cover on watersheds. However, the areal extent of a control watershed is usually very small (Troendle and King, 1987; Hessling, 1999; Iroume et al., 2005; Hegg et al., 2006) and hence the physical relationship developed between the two watersheds is usually influenced by the watershed geomorphological parameters.

Mati et al. (2008) investigated the response of land cover changes at Mara Basin of Eastern Africa and observed significant increase in runoff over less than a couple of decade time span. Forest cover is reduced by approximately 70% over the years 1971-2000 in the Upper Gilgel Abbay catchment of the Blue Nile basin of Ethiopia (Rientjes et al. 2011). Reduced forest cover induced contrastingly variable streamflow trend in two neighbouring catchments of Blue Nile basin. Increased deforestation and intensified cultivation due to burgeoning population accelerated soil degradation rate and increased surface runoff at Ethiopian highlands (Hurni et al., 2005).

Study of catchment response with respect to vegetation cover and land use management are documented in many literatures (Dunford and Fletcher, 1947; Bari and Smettem, 2004; Shi et al., 2007; Yang and Tian, 2009; Li et al., 2010; Seibert and McDonnell, 2010; Greenwood et al., 2011). Many streamflow variability analyses in literature rely on independent treatment of statistical time series analysis and watershed modelling. However, urban and rural watersheds are under temporally varying vegetation cover condition and hence time series models alone can not capture runoff variability as a consequence of diminishing or expanding plantation.

Refsgaard et al. (1989) provides a comprehensive guide to distinguish between man-induced influences and natural climate variability on hydrological regimes of catchments. It is

suggested that joint application of statistical tests and watershed modelling approach to detect the prevailing variability in the catchment. Even though the scientific merits of the methods suggested by Refsgaard et al. (1989) are appealing, studies reported based on similar notions (Lorup et al., 1998; Li et al., 2012) are scanty. Couples of studies attempted to explore the impacts of altered land use/land cover condition on hydrological regimes of Ethiopian watersheds (Zelege and Hurni, 2001; Legesse et al., 2003; Gebresamuel et al., 2010).

Computational advancements coupled with availability of satellite data to extract valuable spatial information provide an aura of confidence to analyze watershed hydrologic processes critically; however, limited spatial and temporal datasets available to characterize the watershed processes besetting the endeavor of scientific communities in the developing countries. The Rift Valley lakes basin of Ethiopia is one among which access to real-time hydro-meteorological data and spatial information is scarce.

The present study concentrates on examining the response of a catchment to runoff for temporally varied land use/land cover conditions using physically based distributed hydrologic modelling. The catchment response is investigated by simulating runoff for temporally varied land use/land cover conditions over the last quarter of twentieth century. Finally, statistical analysis (trends, double mass curve and flow duration curves) of observed streamflow and rainfall is carried out to investigate the behavior of associated time-trend with respect to the prevailing land use/land cover conditions.

6.3 THE STUDY AREA

The impact of land use dynamics is investigated in two rural watersheds (Bilate and Hare) in the Rift Valley lakes basin of Ethiopia. Detailed description of study watersheds is given in section 4.6.

6.4 DATA USED AND METHODOLOGY

6.4.1 Data Used

The datasets utilized to investigate the impact of land use/land cover changes on runoff generation at agricultural watersheds include time variant landsat imageries, DEMs, soil and hydro-meteorological dataset. Table 6.1 provides details of orthorectified four band Multi-Spectral Scanner (MSS) LandSat-4, Thematic Mapper (TM) and seven band Enhanced

Thematic Mapper Plus (ETM+) land cover imageries acquired from Global Land Cover Facility archives (<http://glcf.umiacs.umd.edu/data/landsat>) for the present study.

Table 6.1 Orthorectified landsat images used for land use/land cover classification

Landsat Image ID	Sensor Type	Date Acquired	Path/Row	Producer	watershed Associated
029-736	MSS	Jan. 31, 1973	181/055	Earthsat	Bilate
044-075	MSS	Jan. 25, 1976	181/056	Earthsat	Hare
012-383	TM	Nov. 22, 1984	169/055	Earthsat	Bilate
012-382	TM	Nov. 22, 1984	169/054	Earthsat	Bilate
012-371	TM	Jan. 21, 1986	168/055	Earthsat	Bilate
012-384	TM	Jan. 28, 1986	169/056	Earthsat	Hare
037-658	ETM+	Nov. 26, 2000	169/055	Earthsat	Bilate
037-883	ETM+	Feb. 05, 2000	168/055	Earthsat	Bilate
037-659	ETM+	Jan. 27, 2000	169/056	Earthsat	Hare

Enhanced 90 m x 90 m longitudinal resolution processed Shuttle Radar Topographic Mission DEM data version 4.1 (Jarvis et al., 2008) was accessed from International Centre for Tropical Agriculture (CIAT) online source (<http://srtm.csi.cgiar.org>). Soil feature classes and respective physical properties for the study watersheds are customized from World Food and Agricultural Organization (FAO) soil map. Required weather data to run hydrologic model were obtained from regional and national meteorological offices. Daily rainfall, maximum and minimum temperature, wind speed, sun shine hours and relative humidity for five nearby stations for a record length between 1980 and 2009 were collected for subsequent analysis. Table 6.2 describes details of weather input data available for analysis. Daily streamflow records are collected from Ministry of Water Resources (MoWR) hydrological data archives of Ethiopia. Standard preliminary data analysis for consistency is conducted. Spatial and temporal datasets used to run SWAT model are briefly described in section 4.7. Temporal land use/land cover dataset and respective classes are discussed in the following section.

Table 6.2 Details of hydro-meteorological dataset used for analysis

Hydrometeorological Data/Stations	Alaba Kulito	Hawassa	Bilate Farm	Arba Minch Farm	Chencha
Daily weather data					
Rainfall	✓	✓	✓	✓	✓
Max. and Min. Temperature	✓	✓	✓	✓	✓
Wind Speed	✓	✓		✓	
Sunshine Hours	✓	✓		✓	
Relative Humidity	✓	✓		✓	
Record Length	1980-2009	1980-2009	1980-2009	1980-2009	1970-2006
Daily streamflow					
Bilate at Alaba Kulito (1971-2006)	✓				
Hare near Arba Minch (1980-2006)				✓	

6.4.2 Temporal Land Use/Land Cover Conditions

Temporal landsat images (1973/76, 1984/86 and 2000) acquired from Global Land Cover Facility archives have been further processed to extract required land use information. The temporal scales are sufficiently long enough to observe the expected land use changes and respective catchment responses. Geometrically corrected landsat images are processed using ERDAS Imagine image analysis facilities. Supervised and unsupervised image classification is applied to enjoy the benefit of both approaches and further assimilated based on land use class similarity. Classified land use map units are also verified against coarser resolution land use maps developed by the Ministry of Water Resources (MoWR) of Ethiopia. The present classification is based on small spatial scale and hence more land use classes than the existing broad classification were identified. The land use management classes for the study area were defined as per Anderson et al. (2001) land use/land cover classification as follows.

Agricultural lands: These include diverse class of cultivated land, plots covered by food and commercial crops (croplands) and land units covered by residuals after immediate harvest.

Forest lands: Forest lands have usually tree-crown areal density capable of modulating the micro climate and water holding capacity of watershed. It ranges from densely populated tall trees of tropical rain forest used for timbering to moderately grown green forest. This could be evergreen, deciduous or mixed forest land.

Range lands: These are land cover units typical to arid and semi-arid regions characterized by xerophytic vegetation and transition zones from forest land to sparse woodlands.

Grass lands: These are land units where the potential natural vegetation is predominantly grasses and grass like plants. It is dominated by naturally occurring grasses as well as those areas of actual rangeland that have been modified to include grasses.

Water and marshy land: Area that remains water logged and swampy throughout the year, and rivers are categorized into this class.

Barren land: Land of limited ability to support life and in which less than one-third of the area has vegetation or other cover. It is an area of thin soil, sand or rocks and the areal coverage of available vegetation is much less than that of range land.

The major land use/land cover units identified for the study watersheds are dense forest, woodland, shrub land, pasture, green vegetation, cultivated land, settlements and water body.

6.4.3 Watershed Modelling Under Changing Land Use/Land Cover Conditions

Physically based distributed hydrologic models have the ability to synthesize various spatial information and weather data to predict catchment responses. SWAT model (Arnold et al., 1993; 1998) has got growing demand among watershed modelers due to its capability to model the watershed responses at very small spatial scale characterized by unique land use, soil and slope attributes called hydrologic response units (HRUs). It is a physically based distributed hydrologic model developed to predict the impact of land use management practices on water, sediment, agricultural chemical yields from large and complex watersheds with varying degree of spatial information over long period of time.

In the present study, SWAT model is used to analyze the impact of change in land use/land cover on runoff generation in study basins. The ArcHydro module of the ArcSWAT model delineates the watershed boundary and generates prevailing stream network from available digital elevation model with assigned draining area threshold magnitude. The smaller the draining area threshold the denser the stream network. This helps in capturing the spatial variability of a channel network at very small areal extent. Runoff is generated from individual HRUs and routed to form the main channel flow.

Land use/land cover information separated by moderately sufficient time events (1976/1986/2000) are used as input dataset to the watershed modelling. Other spatial input parameters such as soil, slope and weather information are organized to suit SWAT modelling. Runoff simulation in the watersheds is carried out on daily basis. The model is calibrated using the year 2000 land use/land cover information for both watersheds. The model parameters are further utilized to simulate runoff at desired temporal and spatial scale for the years 1976 and 1986. In SWAT model, the bulk simulated water yield is comprised of surface runoff (SUR Q), lateral flow (LAT Q) and groundwater flow (GW Q). The model has the capability to separate each component independently so that the relative response of catchment to individual components can easily be evaluated. Catchment morphometric parameters and spatial variables such as soil and land covers affect the partition of liquid mass flow into the corresponding components. Attempted here is that, being all other factors held constant, how the land use/land cover has either enhanced or retarded the quick surface flow component.

6.4.4 Land Use/Land Cover Change and Streamflow Trend

To enhance the justification from watershed modelling, the behavior of observed streamflow and rainfall in the study watersheds is examined. Detection of monotonic trends and abrupt changes are assessed using statistical trend analysis and rainfall-runoff double mass curve analysis. The behaviour of historical streamflow is further examined from flow duration curve analysis for time-segmented series.

Climate change and anthropogenic disturbances have been influencing the hydrologic regime of rivers. Man-induced disturbances (land use/ land cover changes, river regulation mechanisms, water abstraction for various purposes, continuous groundwater recharging or discharging) alter the watershed behavior significantly. Possible monotonic and step changes in annual and daily extreme streamflow magnitude are examined applying the commonly used Mann-Kendall (MK) (Mann, 1945; Kendall, 1975) and Mann-Whitney-Pettitt's (MWP) (Pettitt, 1979; Zhang and Lu, 2006) change detection approaches. The MK test statistic is explained in section 2.5.2.3 and hence a concise statistical background of MWP is presented in this section.

The MWP change detection method is a non-parametric test that can be used to analyze data from two independent groups when measurement is ordinal. It analyzes the degree of separation or overlap between the two groups. For a sequence of random variables X_1, X_2, \dots ,

X_T which have a change point at $\tau (X_t)$ for $t = 1, 2, \dots, \tau$ have a common distribution function $F1(x)$ and X_t for $t = \tau + 1, \dots, T$ have a common distribution function $F2(x)$ where $F1(x) \neq F2(x)$ (Pettitt, 1979). The null hypothesis (H_0) assumes that the two set of scores are samples from the same population (no change) and the alternative hypothesis ($H1$) is that the two sets of scores differ systematically (there is change).

The test statistic is:

$$K_T = \max_{1 \leq t \leq T} |U_{t,T}| = \max(K_T^+, K_T^-) \quad (6.1)$$

where
$$U_{t,T} = \sum_{i=1}^t \sum_{j=t+1}^T \text{sgn}(X_i - X_j) \quad (6.2)$$

and
$$\text{sgn}(\theta) = \begin{cases} 1 & \text{if } \theta > 0 \\ 0 & \text{if } \theta = 0 \\ -1 & \text{if } \theta < 0 \end{cases} \quad (6.3)$$

For changes in one direction i.e, for downward (K_T^+) or upward shift (K_T^-), K_T is given as:

$$K_T^+ = \max_{1 \leq t \leq T} U_{t,T} \quad \text{and} \quad K_T^- = -\min_{1 \leq t \leq T} U_{t,T} \quad (6.4)$$

The significance level associated to K_T is estimated by:

$$\rho = \exp\left(\frac{-6K_T^2}{T^3 + T^2}\right) \quad (6.5)$$

If the magnitude of ρ is smaller than the specific significance level (for example $\alpha = 0.05$) the null hypothesis is rejected. The time t when K_T occurs is the change point time.

6.5 RESULTS AND DISCUSSION

6.5.1 Land Use/Land Cover Dynamics in the Study Watersheds During 1973-2000

The ever growing demand for food crops, eventually emerging market for commercial crops, timbering and local energy consumption largely transformed the natural forest cover over Ethiopia. The 1985 official document of Ethiopian Relief and Rehabilitation Commission asserts that the country's forest cover was 44% in 1885, 16% in 1950 and 4% in 1985 (McCann, 1997).

The Rift valley lakes basin has also undergone similar level of forest cover decline over the last century. Dense forest and riparian woodlands of the Rift Valley lakes basin eventually converted to open woodland and rangelands. Major fraction of riparian forest that cover in the fertile delta region underwent clearcutting for cultivation. Temporal land use/land cover map developed from satellite imageries for three different time spans (1973/76, 1986 and 2000) shows major transformation of land cover and land use management over the last quarter of twentieth century.

A phenomenal increase in cultivated land and settlement area over the analysis period is observed at both watersheds. Forest cover decreased by 34.5% and 50.7% during 1976/86 and 1986/2000 time period respectively at Bilate watershed (Fig. 6.1). The total area covered by cultivated land, settlement area and barren land increased by 30.9% and 23.4 % for corresponding period. Range and shrubland show alternating trends over the years in such a way that an increase in any one of them result in decrease in the other land cover unit. However, on aggregate the rangelands increased by 26.7% whereas the pasture land units decreased by 43.8%. The decrease in pasture land might be the result of the growing demand of arable land for crop cultivation in most parts of the watershed. Land units that lost its fertile top soil formation due to excessive erosion and weathering activities are commonly located as small patches in the middle and lower Bilate basin.

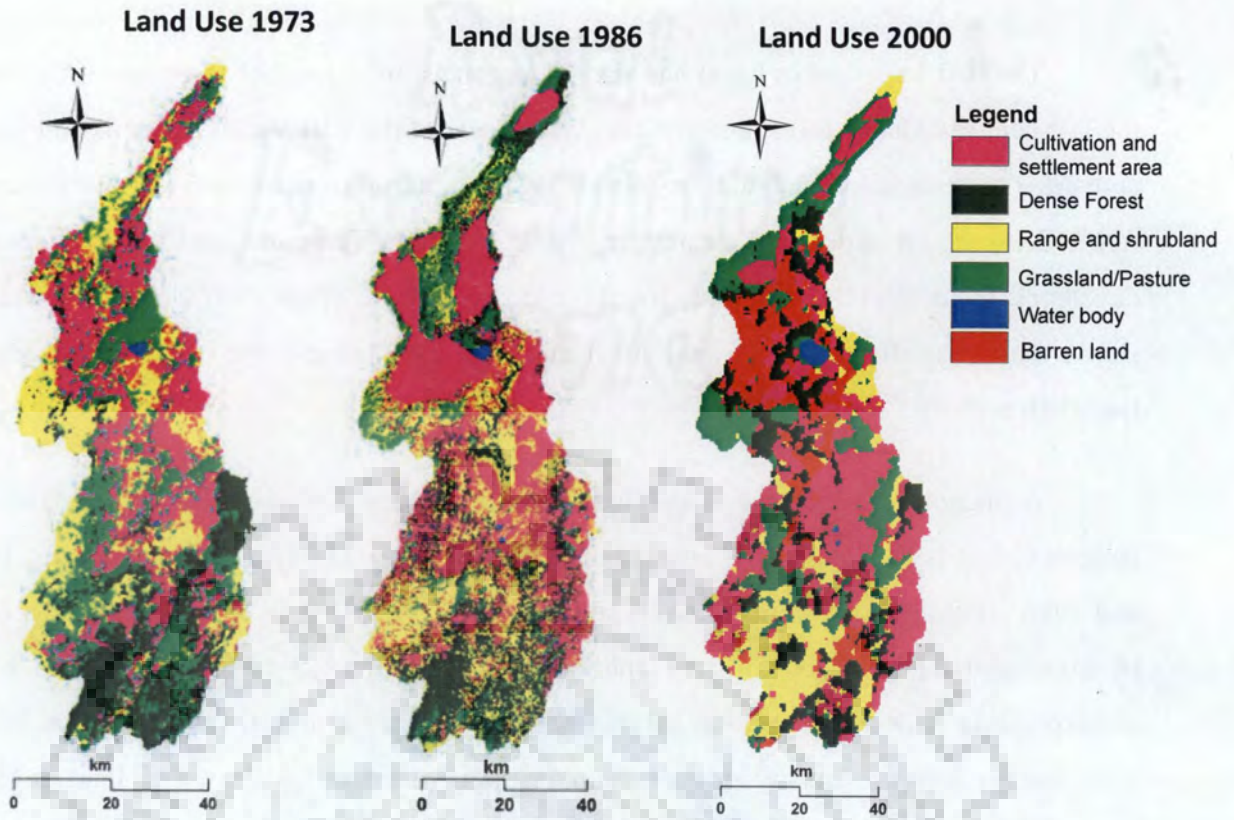


Fig. 6.1 Reclassified land use/land cover classes for use in hydrologic modelling at Bilate watershed

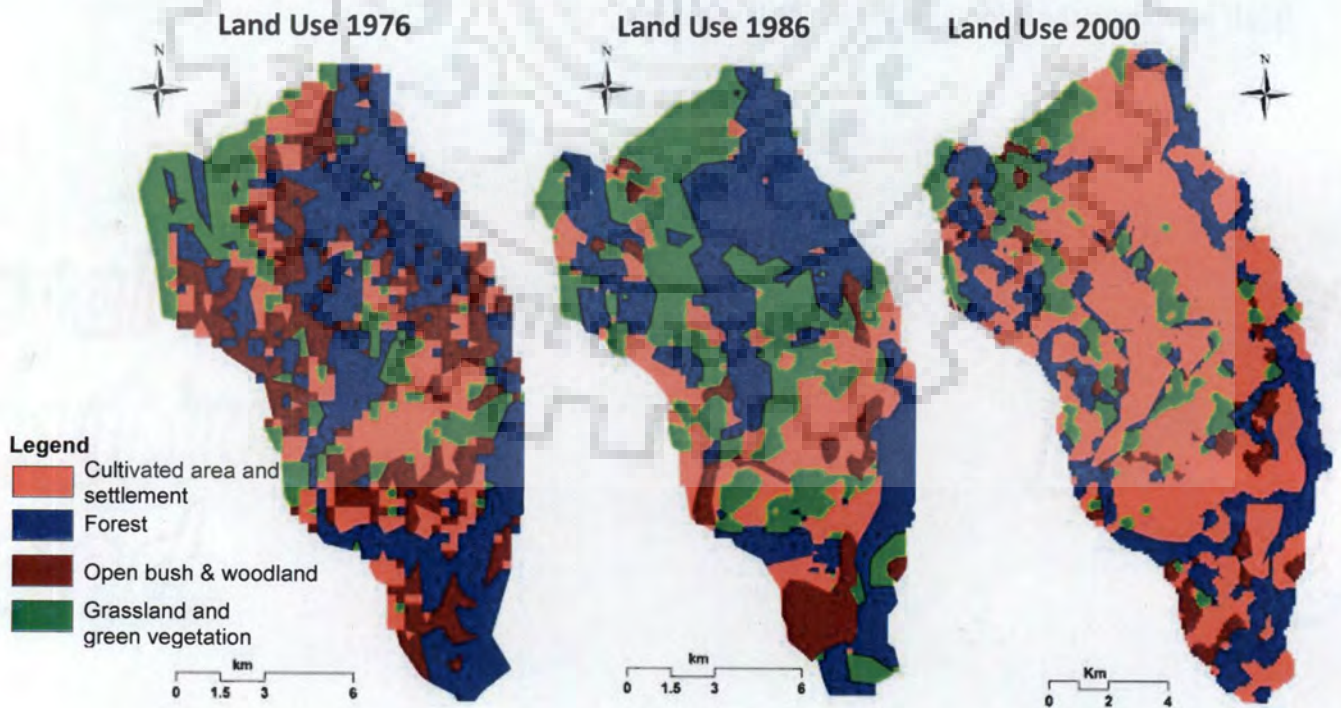


Fig. 6.2 Reclassified land use/land cover classes for use in hydrologic modelling at Hare watershed

The land use/land cover condition at Hare basin follows similar temporal trend to that of Bilate basin. An aggregate increment of 60% in cultivated land and rural settlement whereas 40% decrement in forest cover is identified during 1976-2000 analysis period (Fig. 6.2). Area under pasture and rangeland found to decrease during the same period. Table 6.3 provides major land use /land cover conditions and respective percentage changes over the time period 1976/1986/2000 at Bilate and Hare watersheds of the Rift Valley lakes basin of Ethiopia. The major fraction of land use/land cover is occupied by cultivation, settlement and forest cover during 1970s, however, the forest cover eventually reduced during the last two decades of twentieth century (Fig. 6.3). The upstream riverine course of Hare watershed is commonly growing an evergreen bamboo plantation. Its dense and fibrous roots have soil gripping capability hence minimizes erosion of top soil layers. Studies report that bamboo grass is capable to sequester more CO₂ and generate sufficiently larger fraction of oxygen compared to other young forests.

Table 6.3 Areal coverage of reclassified land use /land cover condition for study watersheds

Land use/land cover class	Percentage land use/land cover			Percentage change		
	1976	1986	2000	1976-1986	1986-2000	1976-2000
Bilate Watershed						
Cultivation and Settlement	36.1	47.2	58.3	30.9	23.4	61.6
Forest-mixed	26.5	17.4	8.6	-34.5	-50.7	-67.7
Range and shrubland	17.2	24.8	21.8	44.0	-12.0	26.7
Pasture	20.2	10.6	11.4	-47.4	6.7	-43.8
Hare watershed						
Cultivation and Settlement	29.65	36.38	47.4	22.7	30.3	59.9
Forest-mixed	30.23	25.32	18.2	-16.2	-28.1	-39.8
Rangeland	24.26	27.2	24.2	12.1	-11.0	-0.2
Pasture	15.86	11.1	10.2	-30.0	-8.1	-35.7

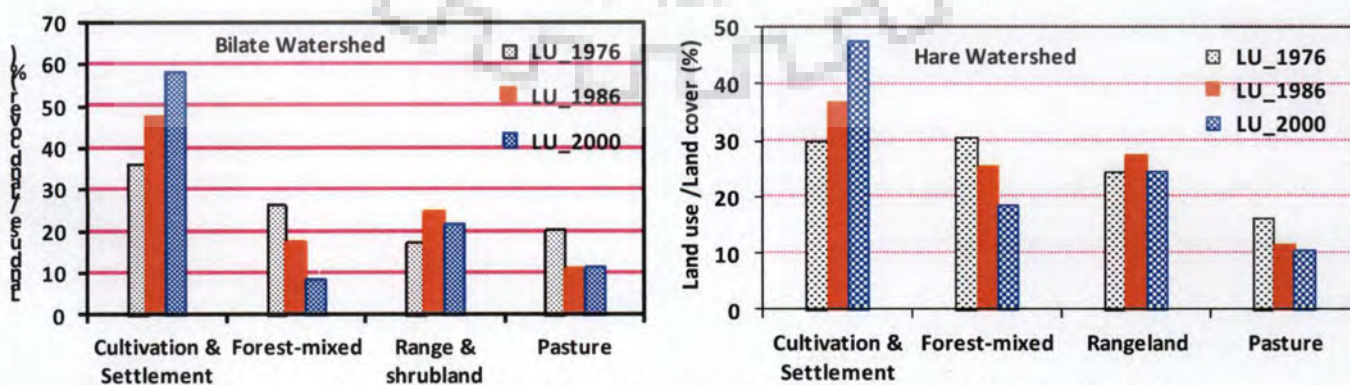


Fig. 6.3 Temporal variation of dominant land use/land cover proportion in the study watersheds

6.5.2 Land Use/Land Cover Dynamics and Hydrologic Modelling

Land use/land cover affects runoff in the form of initial abstraction due to canopy cover and enhanced or reduced infiltration rate (Jinno et al., 2009) due to surface cover that subsequently affects lateral flow. The surface runoff component is separated from the total water yield of a catchment to assess its variability due to altered land use/land cover conditions. SWAT model is calibrated for the year 2000 land use condition and subsequently utilized to predict runoff for 1976 and 1986 land use conditions. SWAT model calibration and validation is covered widely in previous works for the study watersheds. Other input variables such as weather, soil and catchment morphologic parameters remain constant for each simulation. This enables us to identify the catchment response uniquely to land use changes.

SWAT model disaggregates the output into surface runoff component, lateral flow and shallow aquifer flow. The response of a catchment as a result of land use change is evaluated in terms of simulated surface runoff component. It is observed that the surface runoff component increases progressively since mid 1970s at both watersheds. The rate of change of runoff with respect to the base period (1976) is more significant during wet years. This is due to high intensity and extended duration of rainfall events that are more likely to produce runoff immediately with minimal travel time. Moreover, availability of sufficient antecedent moisture condition in the soil retards infiltration rate and accelerates overland flow.

Catchment geomorphologic factors also attributed to varying rate of change of surface runoff magnitude. In steep and smaller size Hare watershed the rate of change is more profound. The catchment response is significant during wet years of the analysis period. The land use condition in the year 2000 increased annual surface runoff by 10-23 % at Bilate watershed with respect to 1976 reference line. The rate of change is higher at smaller size Hare watershed. The increment extends from 16% to more than 100% during the very wet years. Fig. 6.4 presents the relative proportion of simulated surface runoff component for three different land use conditions at two watersheds maintaining all other factors constant throughout the three simulations.

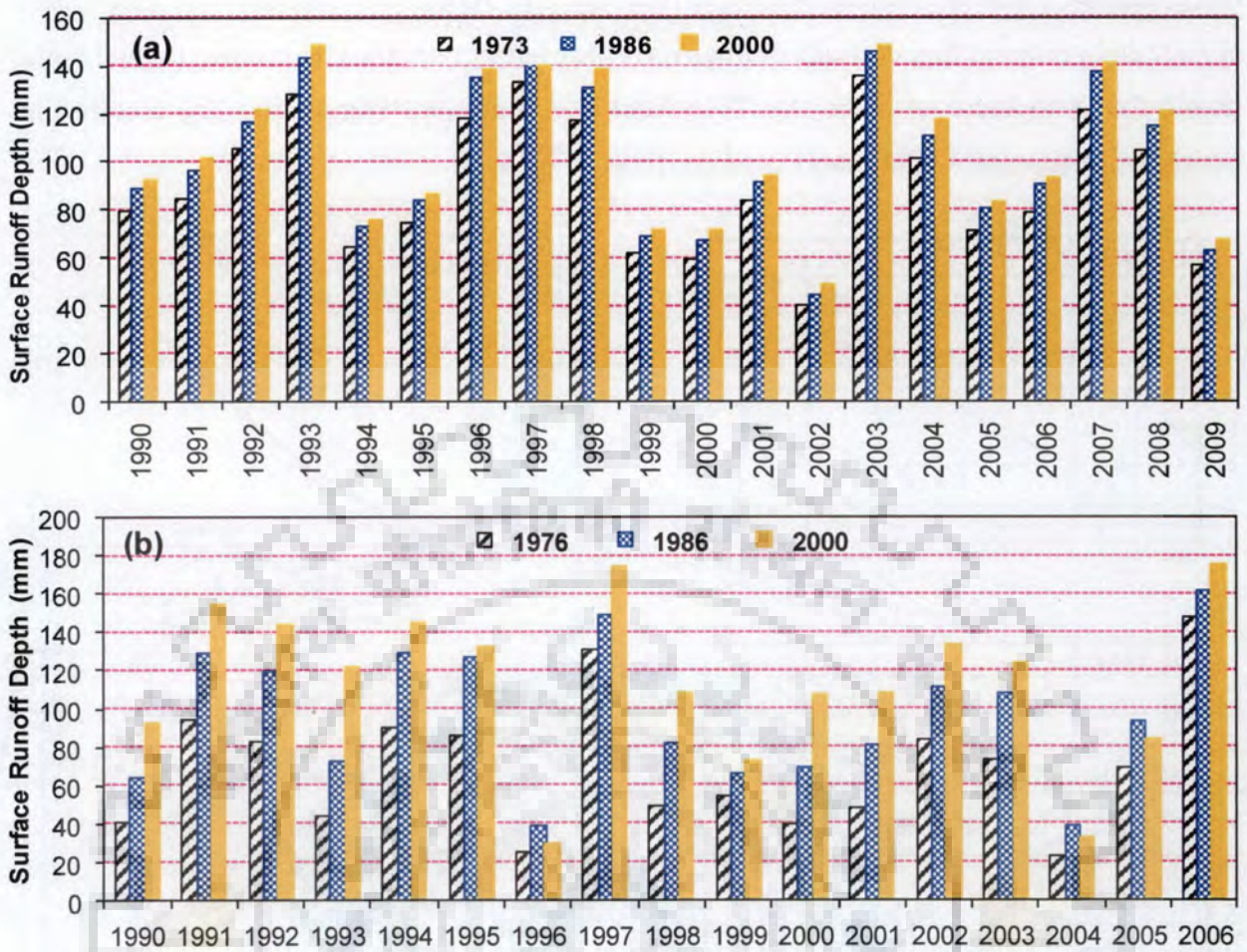


Fig. 6.4 Simulated surface runoff component for different land use/land cover condition during the analysis period

Average monthly predicted surface runoff is compared against respective rainfall in the watersheds during the analysis period. The surface runoff component shows better agreement to respective rainfall for all simulations. The coefficient of determination (R^2) ranges from 0.85 to 0.96. A better correlation ($R^2 = 0.91-0.96$) is observed at Hare watershed where the statistical relationship follows an exponential law (Fig. 6.5). Intercomparison of simulated annual surface runoff to corresponding annual rainfall clearly shows increasing runoff magnitude since 1976 land use condition at both watersheds. Simulations for specific land use conditions are approximated by a lower order polynomial and exponential curves where simulations for recent land use conditions are modestly lying above the early ones (Fig. 6.6).

Summer monsoon season rainfall dominates at Bilate watershed and subsequently yielded substantial amount of total water yield during June-October months. However, bimodal rainfall pattern at Hare watershed produced alternating raised hydrograph limbs during the

rainy seasons. The major rainfall season at Hare extends from mid of March to the first decade of June and produced higher peaks during April-May heavy rainfall. The average monthly total runoff found to increase since the 1976 land use condition. During the dry months the variability in simulated total runoff is insignificant (Fig. 6.7).

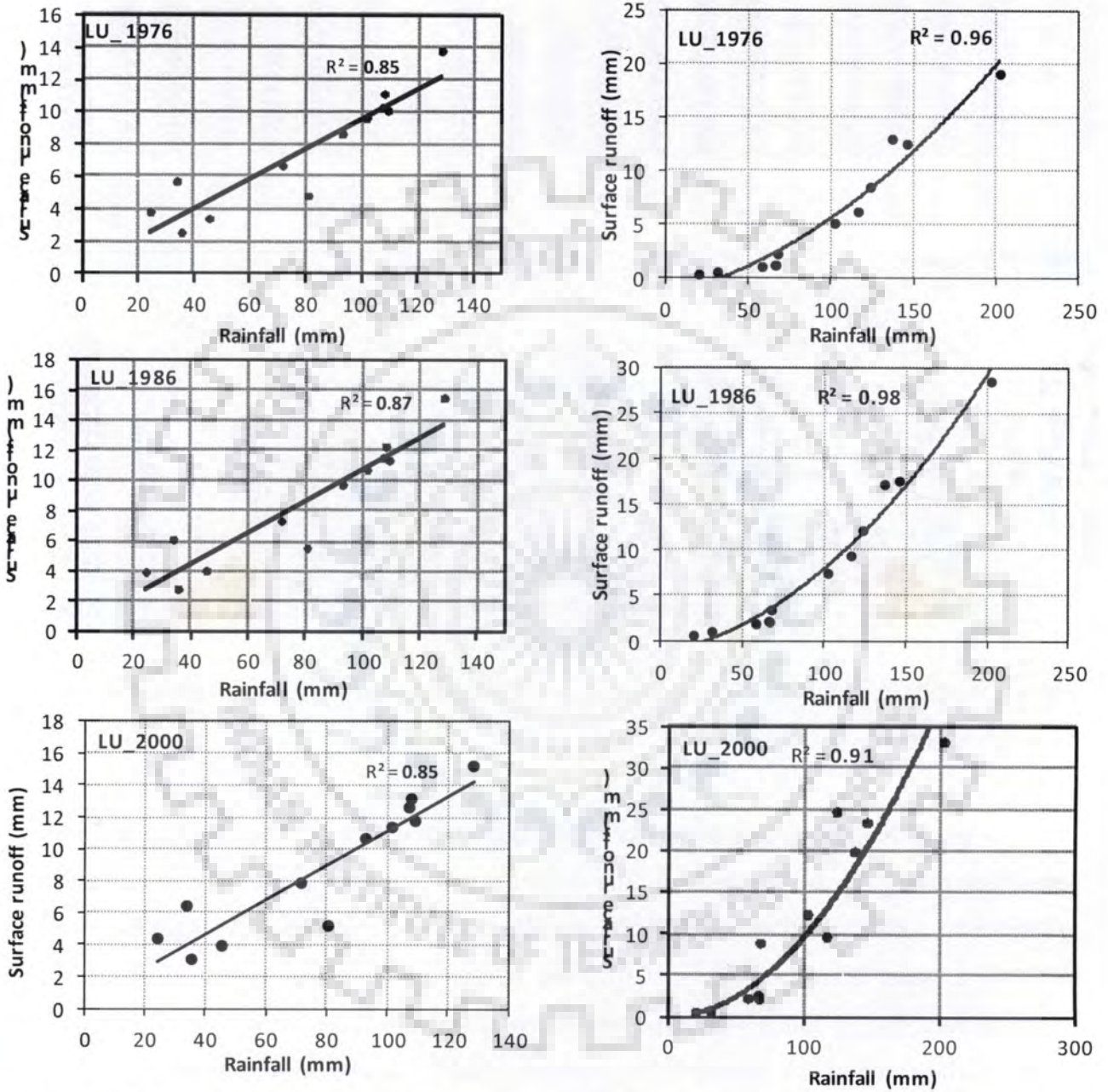


Fig. 6.5 Average monthly simulated surface rainfall-runoff relationship for different land use condition at Hare (left column) and Bilate (right column) watersheds

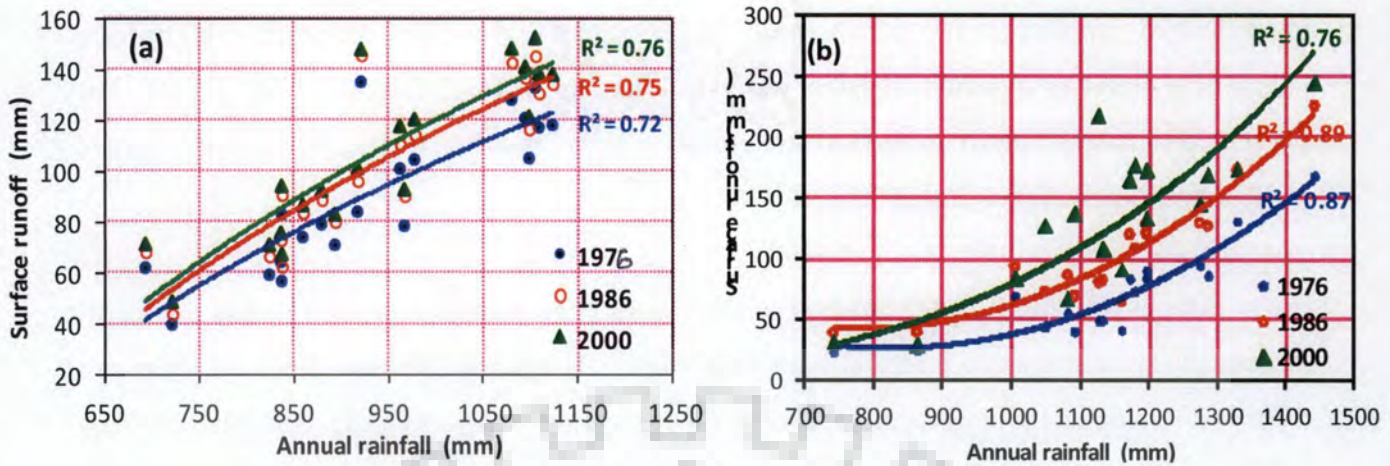


Fig. 6.6 Average annual simulated surface runoff and rainfall relationship for three (1976, 1986 and 2000) land use/land cover conditions at Bilate (a) and Hare (b) watersheds

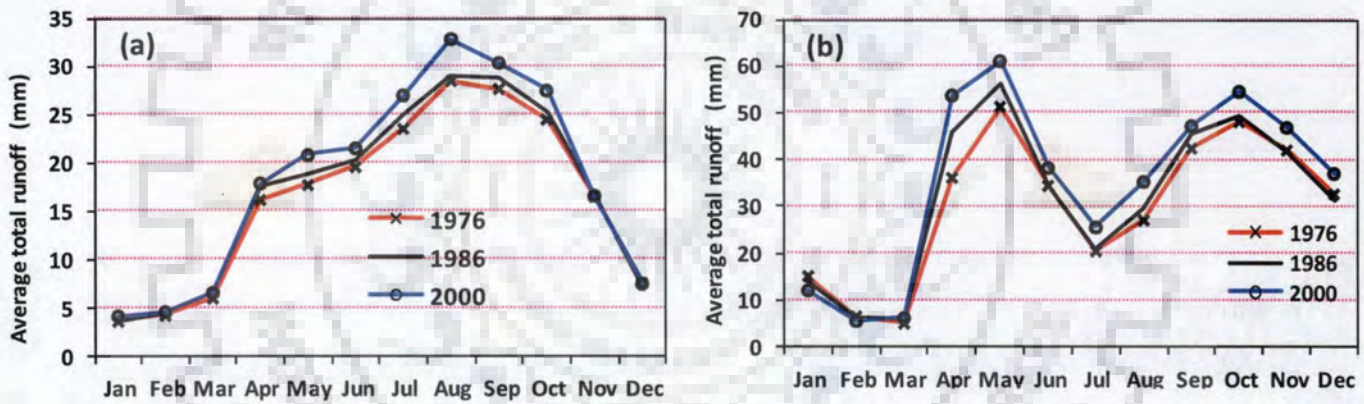


Fig. 6.7 Simulated average monthly total water yield for three (1976, 1986, 2000) land use/land cover conditions at Bilate (a) and Hare (b) watersheds. The simulation is averaged for 1990-2009 at Bilate and 1990-2006 at Hare watersheds

6.5.3 Streamflow Trend Analysis

Statistical trend analysis to detect possible monotonic trends and step changes is conducted for annual and extreme daily streamflow events at Bilate (1971-2005) and Hare (1970-2007) watersheds. We further examined the historical variability of observed streamflow at Alaba Kulito using flow duration curve (FDC). Mann-Kendall (MK) trend analysis is conducted both for original and prewhitened series to account for the effect of significant serial correlation while detecting possible trends. MK-trend analysis for original and prewhitened series reveals that annual streamflow shows insignificant monotonic trend at both watersheds. However,

daily extreme (daily maximum and minimum) streamflow events at Bilate basin are characterized by increasing trends at 5% significance level. No statistically significant streamflow trend is detected at Hare watershed for annual and extreme daily events. The prewhitened series of daily minimum streamflow of Hare is characterized by increasing trend at 10% significance level (Table 6.4).

Mann-Whitney-Pettitti's method employed for step change detection shows couple of statistically weaker change points at both watersheds. The years 1999 and 1992 are estimated to be with statistically significant yet weak change points at Bilate basin whereas the years 1990 and 1986 are detected as possible change points at Hare watershed. The change points detected at two neighbouring watersheds show that the magnitude and temporal location of change points vary slightly. The change points are noticeable in the mid of 1980s and 1990s. These change points are associated to low annual rainfall years. Minor seasonal water abstraction and other unspecified catchment condition that are not quantified in the present context might have attributed to this recurrent and statistically weak change points. The observed land use changes in the watersheds are not dramatic but they have been developed gradually over the years.

Cumulative mass analysis of rainfall and runoff provides statistical information regarding the underlying input-output relationship. When there is no significant alteration in rainfall and runoff pattern due to various circumstances, the data points in the double mass curve fit into a straight line with uniform slope. However, sudden break in slope line of the mass curve is eminent when either or both of the variables undergo localized or long term deviations from the preceding values.

Double mass curve analysis of observed annual streamflow and rainfall conducted in the study watershed shows slight deviation in slope line of the double mass curve around the year 1992 (Fig. 6.8). Even though the change in slope after the break point is small (0.005 MCM/mm at Bilate and 0.012 MCM/mm at Hare watersheds), yet it is indicative of increased runoff in recent years.

Contrary to insignificant annual rainfall in the study watersheds, the maximum daily streamflow at Alaba Kulito of Bilate basin follows statistically increasing trend since 1980. However, average annual streamflow at both watersheds does not reveal statistically significant

on the total record length (n-values) utilized for FDC construction. Average monthly streamflow records are divided into segments of preferably ten years and FDCs are constructed for each segment. The intent of sub-segmented FDC is to study the relative variability in the behavior of streamflow over three decades; namely, 1970s, 1980s and 1990s. Our analysis of FDC is limited to Bilate streamflow with relatively long and uninterrupted flow records. The corresponding average monthly streamflow at Bilate in the 1990s are positioned at higher level than that of 1970s and 1980s for the same level of exceedance probability. The transition segment i.e. 1980s is characterized by slightly wiggling FDCs (higher quantile estimates during the high flow period and lower estimates during the low flow period) that lies between the 1970s and 1990s (Fig. 6.9). The decadal variability in streamflow could be inferred from such short segmented FDCs which otherwise could not be captured from long term time-trend analysis.

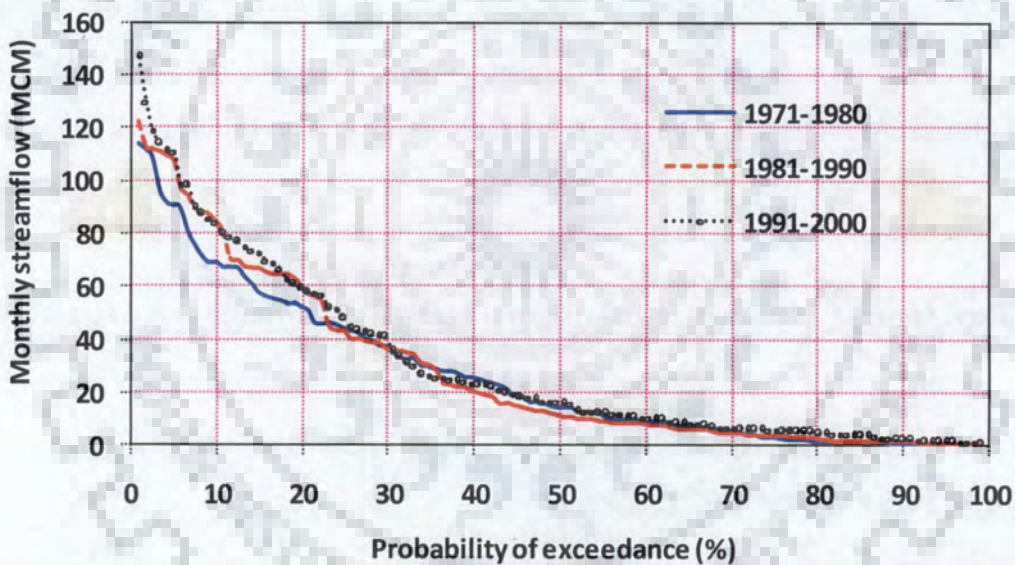


Fig. 6.9 Flow Duration Curves (FDCs) for various segments of average monthly streamflow records of Bilate river at Alaba Kulito station

Results from twin consideration of watershed modeling for temporally varied land use/land cover condition and statistical time series analysis of streamflow are in close agreement to each other. The annual runoff simulated for recent land use/land cover conditions, maintaining all other factors constant, are greater than the preceding cases. The effect of climate variables on streamflow variability that is not explained by watershed modeling is captured through streamflow time-trend, double mass curve and FDC analysis.

The results obtained from these multiple statistical analysis approve the modestly increasing trend of streamflow at Bilate watershed. It has been discussed in chapter 3 that despite annual and monthly rainfall remain without significant trend during the analysis period, the streamflow and lake levels in the watersheds investigated show increasing trend. Such attribution is likely associated to the land use/land cover dynamics in the watersheds.

6.6 CONCLUSIONS

The study watersheds are under intensive catchment modification since the 1970s. Substantial fraction of riparian forest and pristine vegetation cover were converted to agricultural land and grazing field. Compared to its 1976 reference period, the percentage of forest cover declined by 68% and 40% at Bilate and Hare watersheds respectively. Meanwhile, the gross area of agricultural land, permanent settlements and barren land were collectively expanded by approximately 60 % of its baseline proportion at both watersheds during the same period.

The response of a catchment as a result of changing land use/land cover condition is modeled using SWAT for three different (1976/1986/2000) temporal land use conditions. The SWAT model separates overland flow component from total catchment water yield. The simulated surface runoff component increases progressively since 1970s. Percentage annual surface runoff varies from 10 to 23% at Bilate, and 16% to over twofold at Hare watersheds. Statistical time-trend analysis reveals that annual streamflow do not show significant monotonic trend, however, extreme daily streamflow at Alaba Kulito of Bilate catchment is characterized by increasing trend during the analysis period. Recurrent yet statistically weaker step change points are observed in the years 1986, 1990, 1992 and 1999 in the watersheds. The change point years are independent of each other in two watersheds and hence they are governed by land use attributes unique to respective watersheds that influence overland flow. Slightly rising slope of rainfall-runoff double mass curve during post-1992 and 1994 period at Bilate and Hare watersheds respectively supports the subtle increasing trend of streamflow that is not fully explained by time-trend analysis. Time-segmented FDCs of monthly streamflow at Bilate shows increased quantile estimates of high flows for similar level of exceedance probability for recent years.

The attribution of land use/land cover to inter-annual streamflow variability is clearly demonstrated in the present analysis. The increasing trend of observed daily maximum flow at Alaba Kulito and slightly raised slope of rainfall-runoff double mass curve since 1992 supports

the attribution of climate induced changes at Bilate catchment. There are an obfuscated time-trend responses for other variables such as average annual and daily minimum flow at both catchments, but not justified statistically. Annual rainfall time-trend analysis in the study watersheds is marked by statistically insignificant trends. This has been covered by previous studies of the authors. Therefore, joint application of statistical methods and watershed modelling has an advantage to distinguish the underlying variability between climate change and catchment dynamics. The effect of catchment dynamics is modeled by watershed model and accompanying long term climate variability, if any, is explained by statistical tests. This avoids the propensity to associate the resulting variability to either of the two (natural climate variability and land use changes).



CONCLUSIONS AND SCOPE FOR FURTHER WORK

7.1 GENERAL

In the present study, an attempt has been made to explore the impact of climate change and catchment dynamics on runoff generation at Rift Valley lakes basin of Ethiopia. Joint application of statistical time-trend analysis in hydro-climatic variables and process oriented watershed modeling to characterize the prevailing climate and catchment dynamics in the watersheds is carried out. The natural fluctuation in hydro-climatic variables caused by climatic and catchment conditions is detected by hydrologic models and the remaining unexplained variability is manipulated through statistical time series analysis.

Time series analysis of rainfall, streamflow and lake level is investigated through statistical models pertinent to short-term and long-term persistence. Process oriented Soil and Water Assessment Tool is applied to explore the impact of weather and catchment parameters on runoff at Bilate (5330 km²) and Hare (166.5 km²) watersheds. The impact of large-scale atmospheric variables on runoff generation in the watersheds is explored using outputs from Global Climate Models (GCMs). Downscaled and bias corrected daily precipitation and temperature variables are used to simulate runoff for present and future climate conditions for two greenhouse gas emission scenarios. Finally, the impacts of temporal land use/land cover dynamics on runoff generation in the watersheds is investigated through watershed modeling.

7.2 MAJOR FINDINGS OF THE STUDY

The major findings of the study are summarized under the following five categories.

i) Spatila and Temporal Variability of Annual and Seasonal Rainfall Over Ethiopia

The main summer season and annual rainfall exhibit significant decreasing trend in northern, north-western and western part of Ethiopia. In most other parts of the country (approximately 77% of geographical coverage), the annual rainfall series remained without significant trend

for the second half of 20th century. Based on the Moran's spatial analysis, annual rainfall for the total sampling points (381 grid stations) is divided into four zones of annual rainfall spatial similarity. Regions with high annual and seasonal rainfall distribution exhibit high indices of temporal (r_1 and r_2) and spatial (Moran index) autocorrelation coefficients. Atlantic Multidecadal Oscillation and annual rainfall indices over the last half century reveal modestly good correlation in the northern region whereas the association is weakly developed in other parts of the country.

ii) Short and Long-Term Time Dependence of Hydro-climatic Variables

Despite less statistically significant trends in seasonal and annual rainfall events and number of rainy days within the catchment, streamflow and lake levels have showed significant increasing trends for more than 75 percent of events investigated. This observed non-stationarity is variable across hydro-climatic elements that could likely be attributed to the combined effect of global climatic variability on local climate and altered catchment condition over the years. The estimated Hurst's coefficient (H) is greater than 0.5 for all events of streamflow and lake level, which suggests a likely evidence of long term persistence in hydrologic variables. The average stations total rainfall is better correlated to summer season (June-September) nearby Indian Ocean SST whereas the association becomes weak for annual average SST.

iii) Application SWAT model to Investigate the Impacts of Weather and Catchment Input Parameters on Runoff Generation

The impact of topographical (30m ASTER and 90m SRTM DEM), weather and catchment input parameters on runoff generation are investigated. Contrary to 90m SRTM DEM, the 30m ASTER DEM resulted in spurious flow accumulation path that subsequently reduced the watershed area by 29% and affected other basin parameters at Hare watershed. Soil and Water Assessment Tool effectively captured the underlying hydrologic processes in the watershed while simulating runoff at both watersheds. The simulated annual water yield is within $\pm 3.4\%$ error to the observed series. Initial curve number for average soil moisture condition, deep aquifer fraction, minimum water depth in the shallow aquifer for flow and available soil water holding capacity parameters are found to either attenuate or accentuate the resulting runoff more significantly than other parameters in the watersheds.

iv) Impact of Large-scale Atmospheric Variables (GCM Outputs) on Present and Future Runoff

Statistically downscaled and subsequently bias corrected precipitation and temperature variables from BCCR-BCM2.0 of Norway and CSIRO-MK3.0 GCMs of Australia are used to simulate daily runoff at Bilate and Hare watersheds. Runoff is predicted for present and two future (A1B and A2) greenhouse gas emission scenarios. Since GCMs are operating at coarser scales, the statistical downscaling model (SDSM) is employed to reduce large-scale atmospheric variables to local level weather condition. SDSM, followed by bias correction, effectively reproduced the current climate (1990-1999) conditions. Simulated future runoff events are characterized by increased extreme events that ultimately resulted in increase in the gross annual runoff volume from the watersheds. The simulated runoff varies from -4% to 18 % at Hare watershed and is within the range of -4 % and 14 % at Bilate watershed. Bias corrected current and future daily precipitations are characterized by few extreme events. Such extreme events are associated to the main rainy seasons, particularly April and September months. There is no well defined future precipitation pattern is observed from both GCM outputs. Future water resources planning and management could likely be affected by such variability and hence existing design methods could expand their scope to account for these extreme events.

v) Impact of Catchment Dynamics on Runoff

Joint analysis of watershed modeling for temporally varying land use/land cover information and statistical time-trend analysis of streamflow is undertaken to explore the impact of altered land use/land cover condition on runoff generation at two watersheds. The method detected the underlying variability efficiently. The percentage of forest cover declined substantially at Bilate and Hare watersheds during 1976/2000 analysis period. The simulated surface runoff component increases progressively since 1970s. Percentage annual surface runoff varies from 10 to 23% at Bilate, and 16% to over twofold at Hare watersheds. The increasing trend of observed daily maximum flow at Alaba Kulito and slightly raised slope of rainfall-runoff double mass curve since 1992 supports the attribution of climate induced changes at Bilate catchment.

7.3 LIMITATIONS OF THE STUDY AND SCOPE FOR FURTHER WORK

The present study has the following limitations.

- Spatio-temporal analysis of annual and seasonal rainfall pattern covers entire Ethiopia whereas other parts of present study is limited to Bilate and Hare watersheds at Rift Valley lakes basin of Ethiopia.
- Time series analysis is better resolved when available data for analysis is sufficiently long enough. However, limited length data, in present case, constrains the investigations and conclusions drawn might result in biases if extrapolated for extended time period.
- The Rift Valley lakes basin embraces many perennial and ephemeral streams other than Bilate and Hare which otherwise are not accounted during this study.
- Predicted future runoff is based on the assumption that the present catchment conditions and respective hydrologic model parameters remain valid in future too. However, the catchment condition may vary and model parameters would also be affected accordingly.

No scientific study is ever complete, so is true for this case as well. Therefore, the future studies should be undertaken to overcome the limitations of the present study.

REFERENCES AND BIBLIOGRAPHY

- Abbaspour, K. C. (2009) SAWT-CUP2 calibration and uncertainty program user manual version 2. Eawag: Swiss Federal Institute of Aquatic Science and Technology.
- Abbott, M. B. and Refsgaard J. C. (1996) Distributed hydrological modelling. Kluwer Academic Publisher.
- Abbott, M. B., Bathurst, J. C., Cunge, J. A., O'Connell, P. E. and Rasmussen, J. (1986a) An introduction to the European Hydrological System- Syst`eme Hydrologique Europ`een, "SHE", 2: History and philosophy of a physically-based, distributed modelling system. *Journal of Hydrology*, 87, 45-59.
- Abbott, M. B., Bathurst, J. C., Cunge, J. A., O'Connell, P. E., and Rasmussen, J. (1986b) An introduction to the European Hydrological System - Syst`eme Hydrologique Europ`een, "SHE", 2: Structure of a physically-based, distributed modelling system. *Journal of Hydrology*, 87, 61-77.
- Adamowski, J. F. (2008) Development of a short-term river flood forecasting method for snowmelt driven floods based on wavelet and cross-wavelet analysis. *Journal of Hydrology*, 353, 247-266.
- Adler, R. F., Huffman, G. J., Chang, A., Ferraro, R., Xie, P., Janowiak, J., Rudolf, B., Schneider, U., Curtis, S., Bolvin, D., Gruber, A., Susskind, J. and Arkin, P. (2003) The Version 2 Global Precipitation Climatology Project (GPCP) monthly precipitation analysis (1979-Present). *Journal of Hydrometeorology*, 4, 1147-1167.
- Alansi, A. W., Amin, M. S. M., Halim, G. A., Shafri, H. Z. M., Thamer, A. M., Waleed, A. R. M., Aimrun, W. and Ezrin, M. H. (2009) The effect of development and land use change on rainfall-runoff and runoff-sediment relationships under humid tropical condition: Case study of Bernam watershed, Malaysia. *European Journal of Scientific Research*, 31, (1) 88-105.
- Almedeij, J. and Al-Ruwaih, F. (2006) Periodic behavior of groundwater level fluctuations in residential areas. *Journal of Hydrology*, 328, 677-684.
- Anderson, J. R., Hardy, E. E., Roach, J. T. and Witmer, R. E. (2001) A land use and land cover classification system for use with remote sensor data. Geological Survey Professional Paper, 964, first printing in 1976.
- Anderson, R. L. (1942) Distribution of the serial correlation coefficient. *Annals of Mathematical Statistics*, 13, 1-13.

- Andersson, L., Wilk, J., Todd, M. C., Hughes, D. A., Earle, A., Kniveton, D. Layberry, R. and Savenije, H. H. G. (2006) Impact of climate change and development scenarios on flow patterns in the Okavango River. *Journal of Hydrology*, 331, 43-57.
- Andreo, B., Jimenez, P., Duran, J. J., Carrasco, F., Vadillo, I. and Mangin, A. (2006) Climatic and hydrological variations during the last 117-166 years in the south of the Iberian Peninsula, from spectral and correlation analyses and continuous wavelet analyses. *Journal of Hydrology*, 324, 24-39.
- Angelsen, A. (1999) Agricultural expansion and deforestation: Modelling the impact of population, market forces and property rights. *Journal of Development Economics*, 58, 185-218.
- Anselin, L. (1988) *Spatial econometrics: Methods and models*. Dordrecht, The Netherlands, Kluwer Academic.
- Anselin, L. (1995) Local Indicators of Spatial Association- LISA. *Geographical Analysis*, 27, (2), 93-115.
- Arnell, N. W. (2003) Effects of IPCC SRES emission scenario on river runoff: A global perspective. *Hydrology and Earth System Sciences*, 7, (5), 619-641.
- Arnold, J. G., Allen, P. M. and Bernhardt, G. (1993) A comprehensive surface-groundwater flow model. *Journal of Hydrology*, 142, 47-69
- Arnold, J. G., Allen, P.M., Muttiah, R. S. and Bernhardt, G. (1995) Automated baseflow separation and recession analysis techniques. *Groundwater*, 33, (6), 1010-1018.
- Arnold, J. G., Srinivasan, R., Muttiah, R. S. and Williams, J. R.(1998) Large area hydrologic modeling and assessment. Part 1: Model Development. *Journal of American Water Resources Association*, 34, (1), 73-89.
- Bae, D. H., Jung, W. and Lettenmaier D. P. (2011) Hydrologic uncertainties in climate change from IPCC AR4 GCM simulations of the Chungju Basin, Korea. *Journal of Hydrology*, 401, 90-105.
- Baigorria, G. A., Jones, J. W. and O'Brien, J. J. (2007) Understanding rainfall spatial variability in southeast USA at different timescales. *International Journal of Climatology*, 27,749-760.
- Barbier E. B (2004) Explaining agricultural land expansion and deforestation in developing countries. *American Journal of Agricultural Economics*, 86, (5), Proceedings Issue, 1347-1353.

- Bari, M. and Smettem, K. R. J. (2004) Modeling monthly runoff generation processes following land use changes: Groundwater-surface water interactions. *Hydrology and Earth System Sciences*, 8, (5), 903-922.
- Barnett, T. P., Adam, J. C. and Lettenmaier, D. P. (2005) Potential impacts of a warming climate on water availability in snow-dominated regions. *Nature*, 438, 303-309.
- Bartels, R. (1982) The rank version of Von Neumann's ratio test for randomness. *Journal of the American Statistical Association*, 77, 40-46.
- Bates, C. G. and Henry, A. J. (1928) Forest and streamflow experiments at Wagon Wheel Gap, Colorado. U.S. Weather Bureau Monthly weather review, Suppl. No. 30. 79 pp.
- Bates, C. G. (1921) First results in the streamflow experiment, Wagon Wheel Gap, Colorado. *Journal of Forestry*, 19, (4), 402-408.
- Bayazit, M. and Onoz, B. (2004) Comment on Applicability of prewhitening to eliminate the influence of serial correlation on the Mann-Kendall test by Sheng Yue and Chun Yuan Wang. *Water Resources Research*, 40, W08801.
- Beck, C., Grieser, J. and Rudolf, B. (2005) A new monthly precipitation climatology for the global land areas for the period 1951 to 2000. *Climate status report 2004*, German Weather Service, Offenbach, Germany, 181-190.
- Bekele, S. (2001), Investigation of water resources aimed at multi- objective development with respect to limited data situation. The case of Abaya-Chamo Basin, Ethiopia, Ph.D. thesis, University of Dresden, Germany.
- Belete, A. B. (1999) To upgrade the hydrometeorological networks in Ethiopia. 25th WEDC Conference, Addis Ababa, Ethiopia, 211-214.
- Betrie, G. D., Mohamed, Y. A., van Griensven, A. and Srinivasan, R. (2011) Sediment management modelling in the Blue Nile basin using SWAT model. *Hydrology and Earth System Sciences*, 15, 807-818, 2011.
- Beven, K., Calver, A. and Morris, E. M. (1987). The Institute of Hydrology distributed model. Institute of Hydrology Report 98. Wallingford, UK.
- Beven, K. J. (2001) *Rainfall-runoff modelling -The primer*. John Wiley and Sons Ltd, New York.
- Bhang, K. J. and Schwartz, F. (2008) Limitations in the hydrologic applications of C-Band SRTM DEMs in low-relief settings. *IEEE Geosciences and Remote Sensing Letters*, 5, (3), 497-501.
- Blackman, R. B. and Tukey, J. W. (1958) *The measurement of power spectra from the point of view of communication engineering*. Dover Publications.

- Bleck, R., Rooth, C., Hu, D. and Smith, L. T. (1992) Salinity-driven thermocline transients in a wind- and thermohaline-forced isopycnic coordinate model of the North Atlantic. *Journal of Physical Oceanography*, 22, 1486-1505.
- Block, P. and Goddard, L. (2012) Statistical and dynamical climate predictions to guide water resources in Ethiopia. *Journal of Water Resources Planning and Management*, 138, (3), 287-298.
- Boer, G. J., McFarlane, N. and Lazare, M. (1992) Greenhouse gas-induced climate change simulated with the CC second-generation general circulation model. *Journal of Climatology*, 5, 1045-77.
- Boko, M., Niang, I., Nyong, A., Vogel, C., Githeko, A., Medany, M., Osman-Elasha, B., Tabo, R. and Yanda, P. (2007) Africa. *Climate Change 2007: Impacts, adaptation and vulnerability*. Contribution of working group II to the Fourth Assessment Report of the Intergovernmental Panel on Climate Change. Cambridge University Press, Cambridge UK, 433-467.
- Bolzan, M. J. A. and Vieira, P. C. (2006) Wavelet analysis of the wind velocity and temperature variability in the Amazon forest. *Brazilian Journal of Physics*, 36, (4A), 1217-1222.
- Bosch, J. M. and Hewlett, J. D. (1982) A review of catchment experiments to determine the effect of vegetation changes on water yield and evapotranspiration. *Journal of Hydrology*, 55, 3-23.
- Box, G. E. P. and Jenkins, G. M. (1970) *Time series analysis, forecasting and control*. Holden Day, San Francisco.
- Boyer, C., Chaumont, D., Chartier, I. and Roy, A. G. (2010) Impact of climate change on the hydrology of St. Lawrence tributaries. *Journal of Hydrology*, 384, 65-83.
- Berndtsson, R., Sivakumar, B., Olsson, J. and Graham, L. P. (2009) Climate variability and its effects on regional hydrology: a case study for the Baltic Sea drainage basin. 18th World IMACS / MODSIM Congress, Cairns, Australia, 3893-3899.
- Brillinger, D. (1994) Some river wavelets. *Environmetrics*, 5, 211-220.
- Burn, D. H., Sharif, M. and Zhang, K. (2010) Detection of trends in hydrological extremes for Canadian watersheds. *Hydrological Processes*, 24, 1781-1790.
- Byerlee, D., Spielman, D. J., Alemu, D. and Gautam, M. (2007) Policies to promote cereal intensification in Ethiopia: A review of evidence and experience. International Food Policy Research Institute, Development Strategy and Governance Division, Discussion Paper, 0707.

- Cai, X. and Wang, D. (2006) Spatial autocorrelation of topographic index in catchments. *Journal of Hydrology*, 328, 581–591.
- Carl, G. and Kuhn, I. (2007) Analyzing spatial autocorrelation in species distributions using Gaussian and logit models. *Ecological Modeling*, 207, 159–170.
- Cermak, R. J., Feldman A. D. and Webb, R. P. (1979) Hydrologic land use classification using LandSat. US Army Corps of Engineers, Institute of Water Resources, HEC.
- Chaplot, V. (2005) Impact of DEM mesh size and soil map scale on SWAT runoff, sediment, and NO₃-N loads predictions. *Journal of Hydrology*, 312, 207–22.
- Chaplot, V., Saleh, V. A. and Jaynes, D. B. (2005) Effect of the accuracy of spatial rainfall information on the modeling of water, sediment, and NO₃-N loads at the watershed level. *Journal of Hydrology*, 312, 223–234.
- Chatfield, C. (1981) *Statistics for technology: A course in Applied Statistics*. Bath University, England, Chapman and Hall, London.
- Chaubey, I., Haan, C. T., Grunwald, S. and Salisbury, J. M. (1999) Uncertainty in the model parameters due to spatial variability of rainfall. *Journal of Hydrology*, 220, 48–61.
- Chaves, J., Neill, C., Germer, S., Neto, S. G., Krusche, A. and Elsenbeer, H. (2008) Land management impacts on runoff sources in small Amazon watersheds. *Hydrological Processes*, 22, 1766–1775.
- Chen, S. T., Yu, P. S. and Tang, Y. H. (2010) Statistical downscaling of daily precipitation using support vector machines and multivariate analysis. *Journal of Hydrology*, 385, 13–22.
- Cheung, W. H., Senay, G. B. and Singh, A. (2008) Trends and spatial distribution of annual and seasonal rainfall in Ethiopia. *International Journal of Climatology*, DOI: 10.1002/joc.1623.
- Chow, V. T. (1959) *Open Channel Hydraulics*. McGraw-Hill, New York.
- Christensen, J. H., Hewitson, B., Busuioc, A., Chen, A., Gao, X., Held, I., Jones, R., Koli, R. K., Kwon, W. T., Laprise, R., Rueda, V. M., Mearns, L., Menéndez, C. G., Räisänen, J., Rinke, A., Sarr, A. and Whetton, P. (2007) Regional climate projections. *Climate Change 2007: The Physical Science Basis. Contribution of Working Group I to the Fourth Assessment Report of the Intergovernmental Panel on Climate Change*, Cambridge University Press, Cambridge, 847–940.
- Cibin, R., Sudheer, K. P., Chaubey, I. (2010) Sensitivity and identifiability of stream flow generation parameters of the SWAT model. *Hydrological Processes*, 24, (9), 1133–1148.

- Clarke, R. T. (1973) *Mathematical models in hydrology*. FAO Consultant, Institute of Hydrology, Wallingford, UK. Published as FAO of the United Nations series, Rome.
- Cleveland, W. S. (1994). *The Elements of Graphing Data*. Hobart Press, ISBN 0-9634884-1-4.
- Cliff, A. D. and Ord, J. K. (1969) The problem of spatial autocorrelation. In: Scott, A. J., Editor, *London Papers in Regional Science, and Studies in Regional Sciences*. vol. 1, Pion, London, 25–55.
- Cliff, A. D. and Ord, J. K. (1973) *Spatial autocorrelation*, Pion, London.
- Cliff, A. D. and Ord, J. K. (1981) *Spatial Processes: models and applications*. Pion, London.
- Conway, D. and Schipper, E. L. F. (2011) Adaptation to climate change in Africa: Challenges and opportunities identified from Ethiopia. *Global Environmental Change*, 21, 227-237.
- Conway, D., Krol, M., Alcamo, J. and Hulme, M. (1996) Future water availability in Egypt: The interaction of global, regional and basin-scale driving forces in the Nile basin. *Ambio*, 25, 336-342.
- Conway, D., Mould, C. and Bewket, W. (2004). Over one century of rainfall and temperature observations in Addis Ababa, Ethiopia. *International Journal of Climatology*, 24, 77-91.
- Covey, C., AchutaRao, K. M., Cubasch, U., Jones, J., Lambert, S. J., Mann, M. E., Phillips, T. J. and Taylor, K. E. (2003). An overview of results from the Coupled Model Intercomparison Project. *Global Planetary Change*, 37, (1–2), 103–133.
- Crawford, N. H., and Linsley, R. K. (1966) *Digital simulation in hydrology: Stanford Watershed Model IV*, Technical Report 39, Dept. of Civil Eng., Stanford University, California.
- Cunderlik, J. M. and Burn, D. H (2004) Linkages between regional trends in monthly maximum flows and selected climatic variables. *ASCE Journal of Hydrologic Engineering*, 9, (4), 246-256.
- Dagg, M. and Blackie, J. R. (1965) Studies of the effects of changes in land use on the hydrological cycle in East Africa by means of experimental catchment areas. *International association of scientific hydrology, bulletin*, 10, (4), 63-75.
- Dai, A. (2006) Precipitation characteristics in eighteen coupled climate models. *Journal of Climate*, 19, 4605-4630.
- Degefu, W. (1987) Some aspects of meteorological drought in Ethiopia. Chapter 2, in: *Drought and Hunger in Africa - Denying famine a future* (Glantz, M. H., ed.). Cambridge University Press , 223-226.

- Deque, M., Drevet, C., Braun, A., and Cariolle, D. (1994) The ARPEGE/IFS atmosphere model: A contribution to the French community climate modeling. *Climate Dynamics*, 10, 249-266.
- Dercon, S. (2004) Growth and shocks: Evidence from rural Ethiopia. *Journal of Development Economics*, 74, 309-329.
- Dinpashoh, Y., Jhajharia, D., Fakheri-Fard, A., Singh, V. P. and Kahya, E (2011) Trends in reference crop evapotranspiration over Iran. *Journal of Hydrology*, 399, 422-433.
- Diro, T. G., Toniazzo, T. and Shaffery, L. (2011) Ethiopian rainfall in climate models: William C. J. R and Kniveton, D. R. (eds.) In *African Climate and Climate Change. Advances in Global Climate Research*, 43, DOI 10.1007/978-90-481-3842-5_3.
- Dore, M. I. (2005) Climate change and changes in global precipitation patterns: What do we know? *Environment International*, 31, 1167-1181.
- Douglas, E. M., Vogel, R. M. and Kroll, C. N. (2000) Trends in floods and low flows in the United States: The impact of spatial correlation. *Journal of Hydrology*, 240 (1-2), 90-105.
- Dunford, E. G. and Fletcher, P. W. (1947) Effect of removal of stream-bank vegetation upon water yield. *Transactions of American Geophysical Union*, 28, (1), 105-110.
- Easterling, D. R., Evans, J. L., Groisman, P. Y., Karl, T. R., Kunkel, K. E. and Ambenje, P. (1999) Observed variability and trends in extreme climate events: A brief review. *Bulletin of the American Meteorological Society*, 81, 417- 425.
- Edwards, K. A. and Blackie, J. R. (1981) Results of the East African catchment experiments 1958-1974. *Tropical Agricultural Hydrology* edited by Lal, R. and Russel, E. W., John Wiley and Sons Ltd.
- Ehsanzadeh, E. and Adamowski, K. (2010) Trends in timing of low stream flows in Canada: Impact of autocorrelation and long term persistence. *Hydrological process*, 24, 970-980.
- Elshamy, M. E., Seierstad, I. A. and Sorteberg, A. (2009) Impacts of climate change on Blue Nile flows using bias-corrected GCM Scenarios. *Hydrology and Earth System Sciences*, 13, 551-565.
- Emanuel, K. A. (2005) Increasing destructiveness of tropical cyclones over the past 30 years, *Nature*, 436, 686-688.
- EM-DAT. (2010) Emergency events database. Brussels, Belgium: Center for Research on the Epidemiology of Disasters, Université Catholique de Louvain, Belgium. <<http://www.emdat.be/>>. Accessed August 27, 2010.

- Enfield, D. B., Mestas-Nuñez, A. M. and Trimble, P. J. (2001) The Atlantic multidecadal Oscillation and its relationship to rainfall and river flows in the continental US. *Geophysical Research Letters*, 28, 2077-2080.
- Eum, H. Simonovic, S. P. and Kim, Y. (2010) Climate change impact assessment using K-nearest neighbor weather generator: Case study of the Nakdong river basin in Korea. *Journal of Hydrologic Engineering*, 15, (10), 772-785.
- Fact Sheet (2010) A climate trend analysis of Kenya: Famine early warning systems network informing climate change adaptation series. Fact Sheet, August, 3074.
- FAO (1997) Land and water bulletin 4. Food and Agriculture Organization of the United Nations Land & Water Development Division, ISBN 92-5-103966-6, Rome, Italy.
- Ficklin, D. L., Luo, Y., Luedeling, E. and Zhang, M. (2009) Climate change sensitivity assessment of a highly agricultural watershed using SWAT. *Journal of Hydrology*, 374, 16-29.
- Fistikoglu, O. and Okkan, U. (2011) Statistical downscaling of monthly precipitation using NCEP/NCAR reanalysis data for Tahtali river basin in Turkey. *Journal of Hydrologic Engineering*, 16, (2), 157-164.
- Fohrer, N., Haverkamp, S., Eckhardt, K. and Frede, H. G. (2001) Hydrologic response to land use changes on the catchment scale. *Physics and Chemistry of the Earth (B)*, 26, (7-8), 577-582.
- Folland, C. K., Palmer, T. N. and Parker, D. E. (1986) Sahel rainfall and worldwide sea surface temperature 1901-1985. *Nature*, 320.
- Frost, A., Mehrotra, R. Sharma, A. and Srikanthan, R. (2009), Comparison of statistical downscaling techniques for multi-site daily rainfall conditioned on atmospheric variables for the Sydney region. *Australian Journal of Water Resources*, 13, (1), 1-15.
- Fujihara, Y., Tanaka, K., Watanabe, T., Nagano, T., and Kojiri, T. (2008) Assessing the impacts of climate change on the water resources of the Seyhan River basin in Turkey: Use of dynamically downscaled data for hydrologic simulations. *Journal of Hydrology*, 353, 33-48.
- Furevik, T., Bentsen, M., Drange, H., Kindem, I. K. T., Kvamstø, N. G. and Sorteberg, A. (2003) Description and validation of the Bergen Climate Model: ARPEGE coupled with MICOM. *Climate Dynamics*, 21, 27-51.
- Gallant, J. C. and Wilson J. P. (1996) TAPES-G: A grid based terrain analysis program for the environmental analysis. *Computers and Geosciences*, 22, (7), 713-722.

- Galván, L., Olías, M., Fernandez de Villarán, R., Domingo Santos, J. M., Nieto, J. M., Sarmiento, A. M. and Cánovas, C. R. (2009) Application of the SWAT model to an AMD-affected river (Meca River, SW Spain): Estimation of transported pollutant load. *Journal of Hydrology*, 377, 445–454.
- Garbrecht, J. and Martz, L. W. (1997) TOPAZ Version 1.20: An automated digital landscape analysis tool for topographic evaluation, drainage identification, watershed segmentation and subcatchment parameterization - Overview. Grazinglands Research Laboratory, USDA, Agricultural Research Service, El Reno, Oklahoma.
- Gauchere, C. (2002) Use of wavelet transform for temporal characterization of remote watersheds. *Journal of Hydrology*, 269, 101-121.
- Gebresamuel, G., Singh, B. R. and Dick, O. (2010) Land-use changes and their impacts on soil degradation and surface runoff of two catchments of Northern Ethiopia, *Acta Agriculturae Scandinavica, Section B, Soil and Plant Science*, 60, (3), 211-226.
- Ghosh, S., Luniya, V. and Gupta, A. (2009) Trend analysis of Indian summer monsoon rainfall at different spatial scales. *Atmospheric Sciences Letters*, 10, 285-290.
- Gibbons, R., Bhaumik, D. and Aryal, S. (2009) *Statistical methods for groundwater monitoring*. John Wiley and Sons Inc., Hoboken, New Jersey.
- Giles, B. D. and Flocas, A. A. (1984) Air temperature variation in Greece, Part-I: Persistence, trend and fluctuations. *International Journal of Climatology*, 4, 531-539.
- Gissila, T., Black, E., Grimes, D. I. F. and Slingo, J. M. (2004) Seasonal forecasting of the Ethiopian summer rains. *International Journal of Climatology*, 24, 1345-1358.
- Gonfa, L. (1996) *Climate classification of Ethiopia*. Meteorological Research Report Series, No. 3, NMSA, Addis Abeba, Ethiopia.
- Gonzalez, R. C. and Woods, R. E. (2002) *Digital image Processing*. Second eds., Prentice Hall, New Jersey.
- Goodchild, M. F. (1986) *Spatial autocorrelation: Concepts and techniques in modern Geography*, ISBN 0-86094-223-6, Geo Books, Norwich.
- Gordon, H. B., Rotstayn, L. D., McGregor, J. L., Dix, M. R., Kowalczyk, E. A., O'Farrell, S. P., Waterman, L. J., Hirst, A. C., Wilson, S. G., Collier, M. A., Watterson, I. G. and Elliott, T. I. (2002) *The CSIRO-MK3.0 climate system model*. Aspendale, CSIRO Atmospheric Research technical paper, no. 60, 130 pp.
- Green, W. H., and Ampt, G. A. (1911) Studies on soil physics, part I; The flow of air and water through soils. *Journal of Agricultural Sciences*, 4, (1), 1-24

- Greenwood, A. J. B., Benyon, R. G. and Lane, P. N. J. (2011) A method for assessing the hydrological impact of afforestation using regional mean annual data and empirical rainfall-runoff curves. *Journal of Hydrology*, 411, 49-65.
- Grunsky, E. C. and Agterberg, F. P. (1991) SPFAC: A FORTRAN-77 program for spatial factor analysis of multivariate data. *Computers and Geosciences*, 17, (1), 133-160.
- Guo, H., Hu, Q. and Jiang, T. (2008) Annual and seasonal streamflow responses to climate and land-cover changes in the Poyang Lake basin, China. *Journal of Hydrology*, 355, 106-122.
- Gupta, H. V., Sorooshian, S. and Yapo, P. O. (1999) status of automatic calibration for hydrologic models: Comparison with multilevel expert calibration. *Journal of Hydrologic Engineering*, 4, (2), 135-143.
- Hamed, K. H. (2009) Enhancing the effectiveness of prewhitening in trend analysis of hydrologic data. *Journal of Hydrology*, 368, 143-155.
- Hamed, K. H. and Rao, A. R. (1998) A modified Mann-Kendall trend test for autocorrelated data. *Journal of Hydrology*, 204, 182-196.
- Harpham, C. and Wilby, R. L. (2005). Multi-site downscaling of heavy daily precipitation occurrence and amounts. *Journal of Hydrology*, 312, 235-255.
- Harrison, G. P. and Whittington, H. W. (2002) Susceptibility of the Batoka Gorge hydroelectric scheme to climate change. *Journal of Hydrology*, 264, 230-241.
- Hay, L. E. and Clark, M. P. (2003) Use of statistically and dynamically downscaled atmospheric model output for hydrologic simulations in three mountainous basins in the western United States. *Journal of Hydrology*, 282, 56-75.
- Hay, L. E., Wilby, R. L. and Leavesley, G. H. (2000). A comparison of delta change and downscaled GCM scenarios for three mountainous basins in the United States. *Journal of American Water Resources Association*, 36, 387-398.
- Hegg, C. McArdell, B. W. and Badoux, A. (2006) One hundred years of mountain hydrology in Switzerland by the WSL. *Hydrological Processes*, 20, 371-376.
- Hepple, L. W. (1991) Testing for spatial autocorrelation in simultaneous equation models. *Computers, Environment and Urban Systems*, 21, (5), 307-315.
- Hessling, M. (1999) Hydrological modelling and a pair basin study of Mediterranean. *Physics and Chemistry of the Earth (B)*, 24, (1-2), 59-63.
- Hewitson, B. C. and Joubert, A. (1998) Climate downscaling: current South African projections. Available online at <http://www.egs.uct.ac.za/fccc/>.

- Hibbert, A. R. (1967) Forest treatment effects on water yield. In *Forest Hydrology*, Sopper, W. E. and Lull, H. W. (eds.), Pergamon, Oxford, 813 pp.
- Hirsch, R. M., Helsel, D. R., Cohn, T. A. and Gilroy, E. J. (1993) Statistical analysis of hydrologic data. *Handbook of Hydrology* (ed. by D. R. Maidment), Ch. 17, 17.11-17.37. McGraw-Hill, New York, USA.
- Huda, S., Mehrotra, R. and Sharma, A. (2010), *Adaptation Strategies in Coping with Climate Change Impacts for Improved Crop Health and Sustainable Food Production*, in *Climate Change, Food Security, Sea Level Rise and the Environment*, edited by R. Lal, pp. 325-342, Springer.
- Hulme, M., Doherty, R., Ngara, T., New, M. and Lister, D. (2001). African climate change: 1900-2100. *Climate Research*, 17, 145-168.
- Hundecha, Y. and Bardossy, A. (2004) Modeling of the effect of land use changes on the runoff generation of a river basin through parameter regionalization of a watershed model. *Journal of Hydrology*, 292, 281-295.
- Hurni, H., Tato, K. and Zeleke, G. (2005) The implication of changes in population, land use and land management for surface runoff in the upper Nile basin area of Ethiopia. *Mountain Research and Development*, 25, (2), 147-154.
- Hurst, H. R. (1951) Long-term storage in reservoirs. *Transactions of American Society of Civil Engineers*, 116, 770-799.
- Ines, A. V. M. and Hansen, J. W. (2006) Bias Correction of daily GCM rainfall for crop simulation studies. *Agriculture and Forest Meteorology*, 138, 44-53.
- IPCC (2001) *Climate change 2001: the scientific basis: Contribution of Working Group I to the third assessment report of the Intergovernmental Panel on Climate Change*. Houghton, J. T., Ding, Y., Griggs, D. J., Noguer, M., van der Linden, P. J. and Xiaosu, D. (eds.) Cambridge University Press, Cambridge.
- IPCC (2007a) *Climate change 2007: The physical Sciences basis. In contribution of working group I to the Forth Assessment Report of the Intergovernmental Panel on Climate Change*, Solomon, S., Qin, D., Manning, M., Chen, Z., Marquis, M., Averyt, K. B., Tignor, M. and Miller, H. L. (eds.). Cambridge University Press, Cambridge, United Kingdom and New York, NY, USA, 996.
- IPCC (2007b) *Climate Change 2007: Impacts, Adaptation and Vulnerability. Summary for policy makers*. Available online at <http://www.ipcc.cg/SPM13apr07.pdf>
- Iroume, A., Huber, A., Schulz, K. (2005) Summer flows in experimental catchments with different forest covers, Chile. *Journal of Hydrology*, 300, 300-313.

- Jain, S. K and Sudheer, K. P. (2008) Fitting of hydrologic models: A close look at the Nash–Sutcliffe index. *ASCE Journal of Hydrologic Engineering*, 13, (10), 981-986.
- Jarvis, A., Reuter, H. I., Nelson, A. and Guevara, E. (2008) Hole-filled seamless SRTM data V4. International Centre for Tropical Agriculture, available from <http://srtm.csi.cgiar.org>.
- Jhajharia, D., Dinpashoh, Y., Kahya, E., Singh V. P. and Fakheri-Fard, A. (2012) Trends in reference evapotranspiration in the humid region of northeast India. *Hydrological Processes*, 26, 421-435.
- Jhajharia, D. and Singh, V. P. (2011) Trends in temperature, diurnal temperature range and sunshine duration in Northeast India. *International Journal of Climatology*, 31, 1353–1367.
- Jhajharia, D., Shrivastava, S. K., Sarkar, D. and Sarkar, S. (2009) Temporal characteristics of pan evaporation trends under the humid conditions of northeast India. *Agriculture and Forest Meteorology*, 149, 763-770.
- Jinno, K., Tsutsumi, A., Alkaeed, O., Saita, S. and Berndtsson, R. (2009) Effects of land-use change on groundwater recharge model Parameters. *Hydrological Sciences Journal*, 54, (2), 301-315.
- Joubert, A. M., Hewitson, B. C. (1997) Simulating present and future climates of Southern Africa using general circulation models. *Progress in Physical Geography*, 21, 51-78.
- Joubert, A. M., Mason, S. J. and Galpin, J. S. (1996) Droughts over southern Africa in a doubled-CO₂ climate. *International Journal of Climatology*, 16, 1149-1156.
- Jury, M. L. (2010) Ethiopian decadal climate variability. *Theoretical and Applied Climatology*, 101, 29-40.
- Kahya, E. and Kalayci, S. (2004) Trend analysis of streamflow in Turkey. *Journal of Hydrology*, 289, 128–144.
- Kampata, J. M., Parida, B. P. and Moalafhi, D. B. (2008) Trend analysis of rainfall in the headstreams of the Zambezi River Basin in Zambia. *Physics and Chemistry of the Earth*, 33, 621–625.
- Kang, S. and Lin, H. (2007) Wavelet analysis of hydrological and water quality signals in an agricultural watershed. *Journal of Hydrology*, 338, 1-14.
- Kannan, N., White, S. M., Worrall, F. and Whelan, M. J. (2007) Hydrological modelling of a small catchment using SWAT-2000 - Ensuring correct flow partitioning for contaminant modeling. *Journal of Hydrology*, 334, 64-72.
- Kaplan, A., Cane, M. A., Kushnir Y. and Clement, A. C. (1998) Analysis of global sea surface temperatures 1856-1991. *Journal of Geophysical Research*, 103, 18567-18589.

- Karl, T. R., Knight, R. W. (1998) Secular trends of precipitation amount, frequency, and intensity in the United States. *Bulletin of the American Meteorological Society*, 79, 231-241.
- Karpechko, A. Y., Gillett, N. P., Marshall, G. J. and Screen, J. A. (2009) Climate impacts of the southern annular mode simulated by the CMIP3 models. *Journal of Climate*, 22, (13), 3751-3768.
- Kendall, M. G. (1975) Rank correlation methods. Charles Griffin, London.
- Kendall, M. G. and Stuart, A. (1968) The advance theory of statistics. Vol. Griffin, London.
- Khan, M. S., Coulibaly, P. and Dibike, Y. (2006) Uncertainty analysis of statistical downscaling methods. *Journal of Hydrology*, 319, 357-382.
- Kim, H. J., Wang, B. and Ding, Q. (2008) The Global Monsoon Variability Simulated by CMIP3 coupled climate models. *Journal of Climate*, 21, (20), 5271-5294.
- Kim, H. J., Takata, K., Wang, B., Watanabe, M., Kimoto, M., Yokohata, T. and Yasunari, T. (2011) Global monsoon, El Niño, and their interannual linkage simulated by MIROC5 and the CMIP3 CGCMs. *Geophysical Research Abstracts*, 13, 2351-2351.
- Koenig, W. D. (1999) Spatial autocorrelation of ecological phenomena. *Trends in Ecology and Evolution*, 14, (1), 22-26.
- Koirala, S. R., Gentry, R. W., Mulholland, P. J., Perfect, E. and Schwartz, J. S. (2010) Time and frequency domain analyses of high-frequency hydrologic and chloride data in an east Tennessee watershed. *Journal of Hydrology*, 387, 256-264.
- Korecha, D. and Barnston, A. (2007) Predictability of June-September rainfall in Ethiopia. *American Meteorological Society*, 135, 625-650.
- Kottegoda, N. T. (1980) Stochastic water resources technology. Dept. of Civil Engineering, University of Birmingham, John Wiley and Sons, New York.
- Koutsouris, A., Destouni, G., Jarsjö, J. and Lyon, S. (2010) Hydro-climatic trends and water resource management implications based on multi-scale data for the Lake Victoria region, Kenya. *Environmental Research Letters*, 5.
- Koutsoyiannis, D. (2003) Climate change, the Hurst phenomenon, and hydrological statistics. *Hydrological Sciences Journal*, 48, (1), 3-24.
- Kruger, A. C. and Shongwe, S. (2004) Temperature trends in South Africa: 1960-2003. *International Journal of Climatology*, 24, 1929-1945.
- Kulkarni, A. and von Storch, H. (1995) Monte Carlo experiments on the effect of serial correlation on the Mann-Kendall test of trend. *Meteorologische Zeitschrift*, 4, (2), 82-85.

- Kumar, G., Chakravarty, N. V. K., Kurothe, R. S., Sena, D. R., Tripathi, K. P., Adak, T., Halder, D. and Anuranjan (2010) Effect of projected climate change on mustard (*Brassica juncea*). *Journal of Agrometeorology*, 12, (2), 168-173.
- Labat, D. (2005) Recent advances in wavelet analyses: Part1. A review of concepts. *Journal of Hydrology*, 314, 275-288.
- Labat, D., Ronchail, J. and Guyot, J. (2005) Recent advances in wavelet analyses: Part 2- Amazon, Parana', Orinoco and Congo discharges time scale variability. *Journal of Hydrology*, 314, 289– 311.
- Lau, K. M. and Weng, H. (1995) Climate signal detection using wavelet transform: How to make a time series sing. *Bulletin of American Meteorological Society*, 76, 2391–2404.
- Leander, R. and Buishand, T. (2007) Resampling of regional climate model output for the simulation of extreme river flows. *Journal of Hydrology*, 332, 487-496.
- Leclerc, M. and Ouarda, T. B. M. J. (2007) Non-stationary regional flood frequency analysis at ungauged sites. *Journal of Hydrology*, 343, 254-265.
- Legates, D. R. and McCabe, G. J. (1999) Evaluating the use of "goodness-of-fit" measures in hydrologic and hydroclimatic model validation. *Water Resources Research*, 35, (1), 233-241.
- Legesse, D., Vallet-Coulomb, C., Gasse, F. (2003) Hydrological response of a catchment to climate and land use changes in Tropical Africa: Case study South Central Ethiopia. *Journal of Hydrology*, 275, 67-85.
- Li, H., Zhang, Y., Vaze, J. and Wang, B. (2012) Separating effects of vegetation change and climate variability using hydrological modelling and sensitivity-based approaches. *Journal of Hydrology*, 403–418.
- Li, Q., Cai, T., Yu, M., Lu, G., Xie, W. and Bai, X. (2010) Investigation into the impacts of land-use change on runoff generation characteristics in the upper Huaihe river basin, China. *ASCE Journal of Hydrologic Engineering*, doi:10.1061/(ASCE)HE.1943-5584.0000489.
- Li, Z., Liu, W. Z., Zhang, X. C. and Zheng, F. L. (2009) Impacts of land use change and climate variability on hydrology in an agricultural catchment on the Loess Plateau of China. *Journal of Hydrology*, 377, 35-42.
- Loaiciga, H. A., Valdes, J. B., Vogel, R. M., Garvey, J. and Schwarcz, H. (1996) Global warming and hydrologic cycle. *Journal of Hydrology*, 174, 83-127.

- Lorup, J. K., Refsgaard, J. C. and Mazvimavi, D. (1998) Assessing the effect of land use change on catchment runoff by combined use of statistical tests and hydrological modelling: Case studies from Zimbabwe. *Journal of Hydrology*, 205, 147-163.
- Mair, A. and Fares, A. (2010) Assessing rainfall data homogeneity and estimating missing records in Makaha Valley, O'ahu Hawai'i. *Journal of Hydrologic Engineering*, 15, (1), 101-106.
- Makin, M. J., Kingham, T. J., Waddams, A. E., Birchel, C. J. and Tefera, T. (1975) Development prospects in the Southern Rift Valley of Ethiopia, Land Resources Division, Ministry of Overseas Development No. 21, UK.
- Malamud, B. D. and Turcotte, D. L. (1998) Self-affine time series: measures of weak and strong persistence. *Journal of Statistical Planning and Inference*, 80, 173-196.
- Malhi, Y., and Wright, J. (2004) Spatial patterns and recent trends in the climate of tropical rainforest regions. *Philosophical Transactions of the Royal Society Lond. B.*, 359, 311-329.
- Mallat, S. G. (1989) A theory for multiresolution signal decomposition: the wavelet representation. *IEEE Transactions on Pattern Analysis and Machine Intelligence*, 11, (7), 674-693.
- Mandelbrot, B. B. and Wallis, J. R. (1968) Noah, Joseph and operational Hydrology. *Water Resources Research*, 4, (5), 909-918.
- Mann, H. B. (1945) Nonparametric tests against trend. *Econometrica*, 13, 245-259.
- Markgraf, V., Baumgartner, T. R., Bradbury, J. P., Diaz, H. F., Dunbar, R. B., Luckman, B. H., Seltzer, G. O., Swetnam, T. W. and Villalba, R. (2000) Paleoclimate reconstruction along the Pole-Equator-Pole transect of the Americas (PEP 1). *Quaternary Sciences Reviews*, 19, 125-140.
- Marshall, M. H., Lamb, H. F., Huws, D., Davies, S. J., Bates, R., Bloemendal, J., Boyle, J., Leng, M. J., Umer, M. and Bryant, C. (2011) Late Pleistocene and Holocene drought events at lake Tana, the source of the Blue Nile. *Global and Planetary Change*, 78, 147-161.
- Martz, L. W., and Garbrecht, J. (1998) The treatment of flat areas in depressions in automated drainage analysis of raster digital elevation models. *Hydrological Processes*, 12, 843-855.
- Matalas, N. C., Sankarasubramanian, A. (2003) Effect of persistence on trend detection via regression. *Water Resources Research*, 39, (12), 1342.

- Mati, B. M., Mutie, S., Gadain, H., Hame, P., and Mtaló, F. (2008) Impacts of land-use/cover changes on the hydrology of the transboundary Mara River, Kenya/Tanzania, Lakes Reservoirs. *Resources Management*, 13, (1), 169-177.
- McCann, J. C. (1997) The Pillow and the forest: Narratives of deforestation in Ethiopia, 1840-1992. *Environmental History*, 2, (2), 138-159.
- McCuen, R. H. (2003) Modeling hydraulic change: Statistical methods. Dept. of Civil and Environmental Engineering, University of Maryland, Lewis Publishers.
- McGregor, J. J. (1997) Regional climate modelling. *Meteorology and Atmospheric Physics*, 63, 105-117.
- McGuffie, K. and Henderson-Sellers, A. (2005) A climate modeling primer (Third edition), John Wiley and Sons, Ltd., West Sussex, England.
- Mckay, M. D. (1988) Sensitivity and uncertainty analysis using a statistical sample of input values. In: *Uncertainty analysis*, Y. Ronen, (ed.) CRC Press, Inc. Boca Raton, Florida, 145-186.
- Meehl, G. A., Covey, C., Delworth, T., Latif, M., Mcavaney, B., Mitchell, J. F. B., Stouffer, R. J. and Taylor, K. E. (2007) The WCRP CMIP3 multi-model dataset: A new era in climate change research. *American Meteorological Society*, 88, (9), 1383-1394.
- Mehrotra, R., and Sharma, A. (2011), Impact of atmospheric moisture in a rainfall downscaling framework for catchment scale climate change impact assessment, *International Journal of Climatology*, 31, (3), 431-450.
- Menzel, L. and Burger, G. (2002) Climate change scenarios and runoff response in the Mulde catchment (Southern Elbe, Germany). *Journal of Hydrology*, 267, 53-64.
- Mielniczuk, J. and Wojdyłłoa, P. (2007) Estimation of Hurst exponent revisited. *Computational Statistics and Data Analysis*, 51, 4510-4525.
- Milly, P. C. D., Betancourt, J., Falkenmark, M., Hirsch, R. M., Kundzewicz, Z. W., Lettenmaier, D. P. and Stouffer, R. J. (2008) Stationarity is dead: Whither water management? *Science*, 319.
- MoFED (2006) Survey of the Ethiopian Economy. Ministry of Finance and Economic Development (MoFED), Addis Ababa, Ethiopia.
- Moradkhani, H., Baird, R. G. and Wherry, S. A. (2010) Assessment of climate change impact on floodplain and hydrologic ecotones. *Journal of Hydrology*, 395, 264-278.
- Moran, P. A. P. (1950) Notes on continuous stochastic phenomena. *Biometrika*, 37, 17-23.

- Moreda, F. and Bauwens, W. (1998) Influences of variability of rainfall on flow regimes in Central Ethiopia: Water resources variability in Africa during the XXth century. (Proceedings of Abidjan '98 Conference) IAHS Publication No. 252.
- Moriasi, D. N., Arnold, J. G., Van Liew, V. W., Bingner, R. L., Harmel, R. D. and Veith, T. L. (2007) Model evaluation guidelines for systematic quantification of accuracy in watershed simulations. *American Society of Agricultural and Biological Engineers*, 50, (3), 885-900.
- Moron, V. (1998) Trend, decadal and interannual variability in annual rainfall of Subequatorial and Tropical North Africa. *International Journal of Climatology*, 17, 785-805.
- Moron, V., Robertson, A. W., Ward, M. N. and Ndiaye, O. (2008) Weather types and rainfall over Senegal. Part II: Downscaling of GCM simulations. *Journal of Climatology*, 21, 288-307.
- Mulvaney, T. J. (1851) On the use of self-registering rain and flood gauges in making observations of the relations of rainfall and flood discharges in a given catchment. *Transactions of the Institute of Civil Engineers of Ireland*, IV, (II), 19-33.
- Mwale, D., Gan, T. Y., Shen, S. S. P. (2004) A new analysis on variability and predictability of seasonal rainfall of central southern Africa. *International Journal of Climatology*, 24, 1509-1530.
- Nash, J. E. and Sutcliffe J. V. (1970) River flow forecasting through conceptual models: Part 1. A discussion of principles. *Journal of Hydrology*, 10, (3), 282-290.
- Neitsch, S. L., Arnold J. G., Kiniry J. R. and Williams, J. R. (2005) Soil and Water Assessment Tool theoretical documentation, Version 2005.
- Nemec, J., Pasak, V. and Zeleny, V. (1967) Forest hydrology research in Czechoslovakia. In Sopper, W. E. and Lull, H. W. (Eds): *International Symposium on Forest Hydrology*. Pergamon Press, New York, pp. 31-33.
- Ntale, H. K., Gan T. Y. (2003) Drought indices and their application to East Africa. *International Journal of Climatology*, 23, 1335-57.
- O'Callaghan, J. F., Mark, D. M. (1984) The extraction of drainage networks from digital elevation data. *Computer Vision, Graphics and Image Processing*, 28, 323-344.
- Oeurng, C., Sauvage S. and Sánchez-Pérez J. (2011) Assessment of hydrology, sediment and particulate organic carbon yield in a large agricultural catchment using the SWAT model. *Journal of Hydrology*, 401, 145-153.
- Onogi, K., Tsutsui, J., Koide, H., Sakamoto, M., Kobayashi, S., Hatsushika, H., Matsumoto, T., Yamazaki, N., Kamahori, H., Takahashi, K., Kadokura, S., Wada, K., Kato, K.,

- Oyama, R., Ose, T., Mannoji, N. and Taira, R. (2007) The JRA-25 reanalysis. *Journal of Meteorological Society of Japan*, 85, (3), 369-432.
- Orlandini, S., Moretti G., Franchini M., Aldighieri B., and Testa B.(2003) Path-based methods for the determination of nondispersive drainage directions in grid-based digital elevation models, *Water Resources Research*, 39, (6), 1144.
- Otache, M. Y., LI Zhijia and Bakir, M. (2008) Analysis of long-term dependence phenomenon in Benue River flow process and its hypothesis testing. *Chinese Journal of Oceanology and Limnology*, 26, (3), 313-322.
- Pandey, V. K., Panda, S. N., Raghuvanshi, N. S. and Sudhakar, S. (2006) Delineation and parameterization of Banikdih watershed using remote sensing and AVSWAT model. *Journal of Indian society of Remote Sensing*, 34, (2), 143-152.
- Pankhurst, R. (1966) The great Ethiopian famine of 1888-1892: A new assessment. *Journal of History of Medicine and Allied Sciences*, 21, 95-124.
- Panofsky, H. A. and Brier, G. W. (1968) *Some Applications of Statistics to Meteorology*. The Pennsylvania State University Press, 224 pp.
- Partal, T. and Kahya, E. (2006) Trend analysis in Turkish precipitation data. *Hydrological Processes*, 20, 2011-2026.
- Partal, T. and Kucuk, M. (2006) Long-term trend analysis using discrete wavelet components of annual precipitations measurements in Marmara region (Turkey). *Physics and Chemistry of the Earth*, 31, 1189-1200.
- Parthasarathy, B. and Dhar, O. N. (1975) Trend analysis of annual Indian rainfall. *Hydrological Sciences Bulletin*, 20, (2), 257-260.
- Patra, J., Mishra, A., Singh, R. and Raghuvanshi, N. S. (2012) Detecting rainfall trends in twentieth century (1871-2006) over Orissa State, India. *Climate Change*, 111, (3-4), 801-817.
- Peel, M. C., Finlayson, B. L. and McMahon, T. A. (2007) Updated world map of the Koppen-Geiger climate classification. *Hydrology and Earth System Sciences*, 11, 1633-1644.
- Pettitt, A. N. (1979) A non-parametric approach to the change point problem. *Applied Statistics*, 28, 126-135.
- Piao, S., Friedlingstein, P., Ciais, P., de Noblet-Ducoudre, N., Labat, D., and Zaehle, S. (2007) Changes in climate and land use have a larger direct impact than rising CO₂ on global river runoff trends. *Proceedings of the National Academy of Sciences*, 104, (39), 15242-15247.

- Ping, J. L., Green, C. J., Zartman, R. E. and Bronson, K. F. (2004) Exploring spatial dependence of cotton yield using global and local autocorrelation statistics. *Field Crops Research*, 89, 219-236.
- Pryde, J. K., Osorio, J., Wolfe, M. L., Heatwole, C., Benham, B. and cardenas, A. (2007). Comparison of watershed boundaries derived from SRTM and ASTER digital elevation datasets and from a digitized topographic map. American Society of Agricultural and Biological Engineers, Annual International Meeting. Minneapolis Convention Center, Minneapolis, Minnesota, USA.
- Quinn, W. H. and Neal, V. T. (1987) El Niño occurrences over the past four and half centuries. *Journal of Physical Research*, 92, 14449-14461.
- Rahman, M. M., Arya, D. S., Goel, N. K. (2010) Limitation of 90 m SRTM DEM in drainage network delineation using D8 method - a case study in flat terrain of Bangladesh. *Applied Geomatics*, 2, 49-58.
- Rajeevan, M., Bhate, J., Kale, J. D. and Lal, B. (2006) High resolution daily gridded rainfall data for the Indian region: Analysis of break and active monsoon spells. *Current Science*, 91, (3), 296-306.
- Rao, A. R., Hamed, K. H. and Chen, H. L. (2003) Nonstationarities in Hydrologic and Environmental time series. Kluwer Academic Publishers, The Netherlands, pp 362.
- Rao, R. and Bhattacharya, D. (1999) Hypothesis testing for long-term memory in hydrologic series. *Journal of Hydrology*, 216, 183-196.
- Read, J. M. and Lam, S. N. (2002) Spatial methods for characterizing land cover and detecting land-cover changes for the tropics. *International Journal of Remote Sensing*, 23, (12), 2457-2474.
- Refsgaard, J. C., Alley, W. M. and Vuglinsky, V. S. (1989) Methodology for distinguishing between man's influence and climatic effects on the hydrologic cycle. Technical Document in Hydrology, International Hydrological program, UNESCO, Paris.
- Reynolds, R. W. and Smith, T. M. (1995) A high-resolution global sea surface temperature climatology. *Journal of Climatology*, 8, 1571-1583.
- Rientjes, T. H. M., Haile, A. T., Mannaerts, C. M. M., Kebede, E., Habib, E., Steenhuis, T. S. (2011) Changes in land cover and stream flows in Gilgel Abbay catchment, Upper Blue Nile basin - Ethiopia. *Hydrology and Earth System Sciences*, 15, 1979-1989.
- Sakalauskiene, G. (2003) The Hurst phenomena in Hydrology. *Environmental Research, Engineering and Management*, 3, (25), 16-20.

- Salas, J. D., Delleur, J., Yeyjevich, V. and Lane, W. (1980) Applied modeling of hydrologic time Series. Water Resources Publication, Littleton, Colorado.
- Schaefli, B., Hingrey, B. and Musy, A. (2007) Climate change and Hydropower production in the Swiss Alps: Quantification of potential impacts and related model ling uncertainties. *Hydrology and Earth System Sciences*, 11, (3), 1191-1205.
- Schmidli, J., Goodess, C. M., Frei, C., Haylock, M. R., Hundecha, Y., Ribalaygua, J., and Schmith, T. (2007) Statistical and dynamical downscaling of precipitation: An evaluation and comparison of scenarios for the European Alps. *Journal of Geophysical Research*, 112, doi:10.1029/2005JD007026 D04105.
- Schuol, J., Abbaspour K. C., Srinivasan R. and Yang H. (2008) Estimation of freshwater availability in the West African Sub-continent using SWAT hydrologic model. *Journal of Hydrology*, 352, 30-49.
- Segele, Z. T. and Lamb, P. J. (2005) Characterization and variability of Kiremt rainy season over Ethiopia. *Meteorology and Atmospheric Physics*, 89, 153-180.
- Seibert, J. and McDonnell, J. J. (2010) Land-cover impacts on streamflow: a change-detection modelling approach that incorporates parameter uncertainty. *Hydrological Sciences Journal*, 55, (3), 316-332.
- Seibert, J. and McDonnell, J. J. (2010) Land-cover impacts on streamflow: a change-detection modeling approach that incorporates parameter uncertainty. *Hydrological Sciences Journal*, 55, (3).
- Seleshi, Y. and Demaree, G. R. (1995) Rainfall variability in the Ethiopian and Eritrean highlands and its links with the Southern Oscillation Index. *Journal of Biogeography*, 22, 945-952.
- Seleshi, Y. and Zanke, U. (2004) Recent changes in rainfall and rainy days in Ethiopia. *International Journal of Climatology*, 24, 973-983.
- Sen, P. K. (1968) Estimates of the regression coefficient based on Kendall's tau. *Journal of the American Statistical Association*, 63, 1379-1389.
- Setegn, S. G., Rayner, D., Melesse, A. M., Dargahi, B. and Srinivasan, R. (2011) Impact of climate change on the hydroclimatology of Lake Tana Basin, Ethiopia. *Water Resources Research*, 47, W04511.
- Setegn, S. G., Srinivasan, R. and Dargahi, B. (2008) Hydrological Modelling in the Lake Tana Basin, Ethiopia using SWAT Model. *The Open Hydrology Journal*, 2, 49-62.
- Sharma, M., Coulibaly, P. and Dibike, Y. (2011) Assessing the need for downscaling RCM data for hydrologic impact study. *Journal of Hydrologic Engineering*, 16, (6), 534-539.

- Sharpley, A. N. and Williams, J. R. (1990) EPIC-Erosion Productivity Impact Calculator, 1. Model documentation. U.S. Department of Agriculture, Agricultural Research Service, Technical Bulletin, 1768.
- Shabalova, M. V. van Deursen, W. P. A. and Buishand, T. A. (2003) Assessing future discharge of the river Rhine using regional climate model integrations and a hydrological model. *Climate Research*, 23, 233-246.
- Shi, P. J., Yuan, Y., Zheng, Z., Wang, J. A., Ge, Y., and Qiu, G. Y. (2007) The effect of land use/cover change on surface runoff in Shenzhen region, China. *Catena*, 69, 31-35.
- Siegel, S., and Castellan, N. J. (1988) *Nonparametric statistics for the behavioral sciences* (Second edition). McGraw Hill, New York, pp. 399.
- Singh, P. and Kumar, N. (1997) Impact assessment of climate change on the hydrological response of a snow and glacier melt runoff dominated Himalayan river. *Journal of Hydrology*, 193, 316–350.
- Singh, V. P. (1997) Effect of spatial and temporal variability in rainfall and watershed characteristics on stream flow hydrograph. *Hydrological Process*, 11, 1649-1669.
- Singh, V. P. and Frevert, D. K. (2006) *Watershed Models*. CRC Press, Taylor & Francis Group, USA.
- Singh, J., Knapp, H. V. and Demissie, M. (2005) Hydrologic modeling of the Iroquois river watershed using HSPF and SWAT. *Journal of American Water Resources Association*, 41 (2), 361-375.
- Smith, M. B., Koren, V. I., Zhang, Z., Reed, S. M., Pan, J. J. and Moreda, F. (2004) Runoff response to spatial variability in precipitation: An analysis of observed data. *Journal of Hydrology*, 298, 267–286.
- Sridhar, V. and Nayak, A. (2010) Implications of climate-driven variability and trends for the hydrologic assessment of the Reynolds Creek Experimental Watershed, Idaho. *Journal of Hydrology*, 385, 183–202.
- Srinivasan, R., Zhang, X. and Arnold, J. (2010) SWAT ungauged: hydrological budget and crop yield predictions in the upper Mississippi river basin. *The American Society of Agricultural and Biological Engineers*, 53, (5), 1533-1546.
- Steel, E. A. and Lange, I. A. (2007) Using wavelet analysis to detect changes in water temperature regimes at multiple scales: Effects of multi-purpose dams in the Willamette river basin. *River Research and Application*, 23, 351–359.

- Steele-Dunne, S., Lync, P., McGrath, R., Semmler, T., Wang, S., Hanafin, J. and Nolan, P. (2008) The impacts of climate change on hydrology in Ireland. *Journal of Hydrology*, 356, 28-45.
- Straub, K. H., Haertel, P. T. and Kiladis, G. N. (2010) An analysis of convectively coupled Kelvin waves in 20 WCRP CMIP3 Global Coupled Climate Models. *Journal of Climate*, 23, (11), 3031-3056.
- Sun, L. Q., Semazzi, F. H. M., Giorgi, F., Ogallo, L. (1999) Application of the NCAR Regional Climate Model to Eastern Africa-2. Simulation of interannual variability of short rains. *Journal of Geophysical Research*, 104, 6549-6562.
- Tadele (2009) Watershed hydrological responses to changes in land use and land cover and management practices at Hare watershed. Ph.D. Thesis, Siegen University, Germany.
- Tadross, M., Jack, C. and Hewitson, B. (2005) On RCM-based projections of change in southern African summer climate. *Geophysical Research Letter*, 32, (23), L23713.
- Tarboton, D. G. (1997) A new method for the determination of flow directions and upslope areas in grid digital elevation models. *Water Resources Research*, 33, (2), 309-319.
- Taye, M. T. and Willems, P. (2012) Temporal variability of hydroclimatic extremes in the Blue Nile basin. *Water Resources Research*, 48, W03513, doi:10.1029/2011, WR011466.
- Taye, M. T., Ntegeka, V., Ogiramoi, N. P., and Willems, P. (2011) Assessment of climate change impact on hydrological extremes in two source regions of the Nile River Basin, *Hydrology and Earth System Sciences*, 15, 209-222.
- Theil, H. (1950) A rank-invariant method of linear and polynomial regression analysis, III. *Nederlands Akad. Wetensch. Proceedings*, 53, 1397-1412.
- Tiwari, S. P. and Kurothe, R. S. (2006) Effect of vegetative barriers on soil and nutrients losses at 2% slope on agricultural lands of reclaimed Mahi ravines. *Indian Journal of Soil Conservation*, 34, (1), 37-41.
- Torrence, C. and Compo, G. P. (1998) A practical guide to wavelet analysis. *Journal of American Meteorological Society*, 79, (1), 61-78.
- Trenberth, K. E. and Shea, D. J. (2006) Atlantic hurricanes and natural variability in 2005. *Geophysical Research Letters*, 33, L12704.
- Trenberth, K. E., Jones, P. D., Ambenje, P., Bojariu, R., Easterling, D., Klein Tank A., Parker, D., Rahimzadeh, F., Renwick, J. A., Rusticucci, M., Soden, B. and Zhai, P. (2007) Observations: Surface and atmospheric climate change. *Climate Change 2007: The Physical Science Basis. Contribution of Working Group I to the Fourth Assessment*

- Report of the Intergovernmental Panel on Climate Change, Cambridge University Press, Cambridge, 235-336.
- Tripathi, M. P., Raghuwanshi, N. S. and Rao, G. P. (2006) Effect of watershed sub-division on simulation of water balance components. *Hydrological Processes*, 20, (5), 1137-1156.
- Troendle, C. A. and King, R. M. (1987) The effect of partial and clearcutting on streamflow at deadhorse creek, Colorado. *Journal of Hydrology*, 90, 145-157.
- Tsegay, W. (1998) El Niño and drought early warning in Ethiopia. *Internet Journal of African Studies*, No. 2. (available online at <http://ccb.colorado.edu/ijas/ijasno2/georgis.html>).
- Tu, J. (2009) Combined impact of climate and land use changes on streamflow and water quality in eastern Massachusetts, USA. *Journal of Hydrology*, 379, 268-283.
- UNEP and ICRAF (2006) Climate change and variability in the Sahel region: Impacts and adaptation strategies in the agricultural sector. Kandji, S. T., Verchot, L., Mackensen, J., (eds.). Nairobi, Kenya, pp. 48.
- USDA-SCS (1972) National Engineering Handbook Section 4, Hydrology. USDA-SCS, Washington DC, USA.
- Uvo, C. V. and Berndtsson, R. (2002) North Atlantic Oscillation; a climatic indicator to predict hydropower availability in Scandinavia. *Nordic Hydrology*, 33, (5), 415-424.
- van Griensven, A. and Bauwens, W. (2001) Integral modeling of catchments. *Water Science and Technology*, 43, (7), 321-328.
- Vaze, J., Post, D. A., Chiew, F. H. S., Perraud, J. M., Viney, N. R. and Teng, J. (2010) Climate non-stationarity-Validity of calibrated rainfall-runoff models for use in climate change studies. *Journal of Hydrology*, 394, 447-457.
- Vitousek, P. M. (1994) Beyond global warming: Ecology and global change. *Ecology*, 75, (7), 1861-1876.
- Vitousek, P. M., Mooney, H. A., Lubchenco, J. and Melillo, J. M. (1997) Human domination of Earth's ecosystems. *Science*, 277.
- von Neumann J. (1941) Distribution of the ratio of the mean square successive difference to the variance. *Annals of Mathematical Statistics*, 13, 367-395.
- von Storch, H. and Navarra, A. (1999) Analysis of climate variability: Applications of statistical techniques. Springer Verlag, Second updated extended edition, ISBN 3-540-66315-0, 342 pp.
- Wallis, J. R. and O'Connell, P. E. (1973) Firm reservoir yield - How reliable are historic hydrological records? *Hydrological Sciences, Bulletin*, XVIII, 39.

- Walther, G. R., Post, E., Convey, P., Menzel, A., Parmesan, C., Beebee, T. J. C., Formentin, J. M., Hoegh-Guldberg, O. and Bairlein, F. (2002) Ecological responses to recent climate change. *Nature*, 416, 389-395.
- Wang, W. and Ding, J. (2003) Wavelet network model and its application to the prediction of Hydrology. *Nature and Science*, 1, (1), 67-71.
- Widmann, M. M., Bretherton, C. S., Salathe, E. P. (2003) Statistical precipitation downscaling over the North-western United States using numerically simulated precipitation as a predictor. *Journal of Climate*, 16, 799-816.
- Wight, C. L. (1940) A preliminary account of rainfall in Jonkershoek. *Transactions of the Royal Society of South Africa*, 28, (2), 161-73.
- Wight, C. L. (1943) Determination of the effects of watershed management on mountain streams. *American Geophysical Union Transactions*, 2, 594-608.
- Wilby, R. (2007) Decadal climate forecasting techniques for adaptation and development planning: A briefing document on available methods, constraints, risks and opportunities. Department of Geography, Lancaster University & Science Department, Environment Agency of England and Wales, UK.
- Wilby, R. L., Dawson, C. W. and Barrow, E. M. (2001) SDSM - a decision support tool for the assessment of regional climate change impacts. *Environmental Modelling and Software*, 17, 147-159.
- Williams, J. R. and Hann, R. W. (1973) HYMO: Problem oriented computer language for hydrologic modeling. USDA ARS-S-9, US Government Printing Office.
- Wood, C. A. (1977) A preliminary chronology of Ethiopian droughts: In drought in Africa -2, African Environmental Special Report 6 (eds.). Dalby, D., Church, R. J. H. and Bezzaz, F., pp. 68-73, International African Institute, London.
- Wu, K. and Johnston, C. A. (2007) Hydrologic response to climatic variability in a Great Lakes Watershed: A case study with the SWAT model. *Journal of Hydrology*, 337, 187-199.
- Xu, Z. X., Takeuchi, K. and Ishidaira, H. (2003) Monotonic trend and step changes in Japanese precipitation. *Journal of Hydrology*, 279, 144-150.
- Yang, Y. and Tian, F. (2009) Abrupt change of runoff and its major driving factors in Haihe river catchment, China. *Journal of Hydrology*, 374, 373-383.
- Yano, T., Aydin, M., and Haraguchi, T. (2007) Impact of climate change on irrigation demand and crop growth in a Mediterranean environment of Turkey. *Sensors*, 7, 2297-2315.

- Yesuf, M., Di Falco, S., Deressa, T., Ringler, C. and Kohlin, G. (2008) The impact of climate change and adaptation on food production in low-income countries: Evidence from Nile basin of Ethiopia. IFPRI Discussion Paper, 00828, Addis Ababa, Ethiopia.
- You, G. J. Y. and Ringler, C. (2010) Hydro-economic modeling of climate change impacts in Ethiopia. IFPRI Discussion Paper No. 960, International Food Policy Research Institute, Washington, DC.
- Yu, D. S., Shi, X. Z., Wang, H. J., Zhang, X. Y. and Weindorf, D. C. (2008) Functions of soils in regulating rainwater in Southern China: Impacts of land uses and soils. *Pedosphere*, 18, (6), 717-730.
- Yue, S., Pilon, P., Phinney, B. and Cavadias, G. (2002) The influence of autocorrelation on the ability to detect trend in hydrological series. *Hydrological Processes*, 16, 1807-1829.
- Zelege, G. and Hurni, H. (2001) Implications of land use and land cover dynamics for mountain resource degradation in the northwestern Ethiopian highlands. *Mountain Research and Development*, 21, (2) 184-191.
- Zhang, S. and Lu, X. X. (2006) Long-term water and sediment change detection in a small mountainous tributary of the lower pearl river, china. *Advances in Geosciences*, Vol. 6, Hydrological Science (eds.) Namsik Park et al., 97-108,
- Zhang, X., Harvey, K. D., Hogg, W. D. and Yuzyk, T. R. (2001) Trends in Canadian streamflow. *Water Resources Research*, 37, (4), 987-998.
- Ziervogel, G., Cartwright, A., Tas, A., Adejuwon, J., Zermoglio, F., Shale, M. and Smith, B. (2008) Climate change and adaptation in African agriculture. Technical paper prepared for Rockefeller Foundation, Stockholm Environment Institute, Sweden.

Lists of publications from present study are given as follows.

1. Wagesho, N., Goel, N. K. and Jain, M. K. (2012) Investigation of non-stationarity in hydro-climatic variables at Rift Valley lakes basin of Ethiopia. *Journal of Hydrology*, (444–445), 113–133 (**Paper Published**).
2. Wagesho, N., Goel, N. K. and Jain, M. K. (2012) Temporal and Spatial Variability of Annual and Seasonal Rainfall over Ethiopia. *Hydrological Sciences Journal*, Ms ID: HSJ-2011-0197.R1 (**Paper Accepted**).
3. Wagesho, N., Jain, M. K. and Goel, N. K. (2012) Impact of Climate Change on Runoff Generation: An Application to Rift Valley Lakes Basin of Ethiopia. *ASCE, Hydrologic Engineering Journal*, Ms ID: HEENG-1409.R2 (**Paper Accepted**).
4. Wagesho, N., Jain, M. K. and Goel, N. K. (...) Assessment of Impact of Terrain, Weather and Catchment input parameters on Runoff Generation in Rift Valley Lakes Basin of Ethiopia. *Water Resources Management Journal*, Ms ID: WARM 2576 (**Paper Under Review**).